University of Southampton

MATRIX ISOLATION AND MASS SPECTROMETRIC STUDIES ON SOME ASPECTS OF FISSION PRODUCT CHEMISTRY

A thesis submitted for the
Degree of Doctor of Philosophy

by

Nigel Andrew Young

Department of Chemistry
Southampton

- July 1988 -

UNIVERSITY OF SOUTHAMPTON

ABSTRACT

FACULTY OF SCIENCE

CHEMISTRY

Doctor of Philosophy

MATRIX ISOLATION AND MASS SPECTROMETRIC STUDIES ON SOME ASPECTS OF FISSION PRODUCT CHEMISTRY

By Nigel Andrew Young

The work in this thesis is concerned with some specific aspects of fission product chemistry encountered in a severe reactor accident. The fission products selected for this study were iodine, caesium and tellurium. Considerable emphasis is also placed on the involvement of structural materials such as boric acid in determining the fate of the fission products. Matrix isolation infrared spectroscopy and mass spectrometry were the techniques chosen to investigate the chemistry.

The vapour above orthoboric acid has been studied by both mass spectrometry and matrix isolation infrared spectroscopy and found to consist of monomeric H_3BO_3. As a result of extensive isotope labelling it is possible to verify that molecular orthoboric acid has C_{3h} symmetry. Estimates of the inactive frequencies have been made by a partial normal co-ordinate analysis. The reaction of boric acid with caesium iodide has been investigated and it is shown that the volatile iodine species produced is hydrogen iodide. A semi-quantitative study has shown that between 1% and 10% of the available iodine is transported as hydrogen iodide and that under some circumstances the yield may be quantitative.

Aspects of the fission product chemistry of tellurium under both reducing and oxidising steam conditions are considered. A matrix infrared study of hydrogen telluride and its deuterated analogues has been carried out. From this study the stretching frequencies have been resolved and assigned for the first time. The co-deposition of tellurium dioxide with potassium in nitrogen matrices has resulted in the identification of the new $KTeO_2$ species.

Also included, as an example of how matrix isolation and mass spectrometry can be used to investigate new high temperature species, is the identification of caesium thiotungstate, Cs_2WS_4, as the first ternary metal sulphide to be stable in the vapour phase.

To

Mum and Dad
who made it possible

and

Rachel
who made it worthwhile

"The world little knows how many of the thoughts and theories which have passed through the mind of a scientific investigator have been crushed in silence and secrecy by his own severe criticism and adverse examination; that in the most successful instances not a tenth of the suggestions, the hopes, the wishes, the preliminary conclusions have been realised."

Michael Faraday

ACKNOWLEDGEMENTS

My thanks first and foremost must go to Dr Steve Ogden whose experience, ability and enthusiasm has trained me so well in the art of matrix isolation and the science of vibrational spectroscopy. Thanks are also due to Dr Brian Bowsher who as industrial supervisor has kept a watchful, but distant eye on the proceedings at Southampton. Professor Ian Beattie is thanked for his interest, comments and patience whilst this thesis went through a prolonged gestation period.

The many people who made me so welcome in Southampton as an interloper from London are much appreciated, and in particular Alan Brisdon, Robin Gomme and David Wild. Pete Jones is especially thanked for his concern and many fatherly conversations over a pint of 'Pedigree' at the Brook.

The financial assistance of the SERC and AEE Winfrith was very welcome, nay vital, as was the production of this thesis at Winfrith.

Last but no least I would like to thank my wife, Rachel, for putting up with the odd hours, peculiar smells and most especially the paper chase that must have seemed omnipresent during the writing of this thesis.

CONTENTS

CHAPTER ONE

INTRODUCTION

The study of high temperature vapour phase species is fundamental from an academic point of view, especially with respect to bonding theories. It is also of great interest industrially where the nature of the corrosion of gas turbines and steam generating plants by hot gases is of prime importance. This thesis however covers another area of vital concern, namely the determination of the chemical species evolved from the core of a nuclear reactor under severe accident conditions. The extent of any release from a damaged core depends on the plant design, burn-up history of the fuel and the accident sequence. Whether any of the fission products are released into the environment depends upon their interaction with the fuel rods, control rods, primary circuit pipework and the containment building. The identification of the products formed from these interactions is therefore important in assessing the amount and nature of release of material into the environment resulting from a severe accident.

The reactor and its chemistry considered is the pressurised water reactor (PWR). In a PWR the fuel is in the form of 2-3% ^{235}U enriched UO_2 in Zircaloy tubes. When this ^{235}U undergoes fission it produces neutrons and fission products. The neutrons so produced are then used to initiate further fission reactions in the other ^{235}U nuclei in the fuel rod. On average 2.5 neutrons are produced in each fission reaction and therefore to avoid an exponential increase in the rate of fission something needs to be used to absorb the excess 1.5 neutrons. In the case of the PWR, control rods made of a silver alloy containing 15% indium and 5% cadmium encased in stainless steel are used, and these are lowered and raised between the fuel rods to control the rate of fission.

The reactivity is also controlled by a 0.025 molar solution of boric acid in the light water used for cooling. In order to maximise the cross-section for fission, which is greatest for low energy or thermal neutrons, the neutrons need to be slowed down or "moderated" by something that elastically scatters them, but has a low neutron absorption coefficient. The material normally used for this purpose is the light water in the cooling circuits.

Although the fissile material splits into roughly equal parts the range of possible fission products is large, and for each fission product there may be a range of isotopes present. The fission product inventory(1) of a 1000 MW(e) PWR after full power operation for a three year cycle (average burn-up 2.9%) is given in Table 1. Those nuclides that are considered to be radiologically important(1) are given in Table 2 along with their half lives. It is obviously important to know the chemical state of the fission products within the fuel rod since these factors define the starting point for considering fission product chemistry. Table 3 groups together the fission products according to their chemical properties and proposed chemical forms within the fuel(1).

The oxygen potential of the system is one of the most important factors in determining the chemistry in the fuel rod because of the large quantity of urania present. As the fissioning takes place the oxygen which was associated with the uranium partitions itself amongst the fission products to generate the oxides that have the lowest oxygen potential. Some of these oxides are soluble in the UO_2 lattice (eg lanthanides, niobium and some molybdenum and zirconium oxides), however some are insoluble (eg BaO, SrO). Other fission products remain in their elemental form whilst in the fuel pellets but as they diffuse along the grain boundaries or to the fuel-clad gap they may react to form chemical compounds, eg caesium and iodine to give caesium iodide. The noble gases (Xe, Kr) are insoluble and either form bubbles within the fuel or diffuse to the fuel-clad gap.

TABLE 1

Fission Product Inventory

Element	Atom %	Decay Heat (MW)
Ga	3.67×10^{-9}	4.3×10^{-5}
Ge	9.87×10^{-5}	1.1×10^{-3}
As	3.33×10^{-5}	5.7×10^{-3}
Se	0.01	2.5×10^{-3}
Br	5.43×10^{-3}	2.2×10^{-2}
Kr	0.09	0.61
Rb	0.08	0.56
Sr	0.21	1.58
Y	0.11	2.60
Zr	0.76	1.53
Nb	0.01	2.35
Mo	0.64	0.57
Tc	0.17	0.13
Ru	0.41	0.94
Rh	0.11	0.54
Pd	0.13	2.4×10^{-2}
Ag	2.74×10^{-3}	4.5×10^{-2}
Cd	5.77×10^{-3}	6.1×10^{-3}
In	4.93×10^{-4}	4.9×10^{-3}
Sn	6.79×10^{-3}	5.7×10^{-3}
Sb	2.68×10^{-3}	0.35
Te	0.07	0.57
I	0.03	6.01
Xe	0.60	0.91
Cs	0.53	0.21
Ba	0.19	0.79
La	0.18	4.41
Ce	0.39	0.89
Pr	0.15	1.41
Nd	0.48	0.22
Pm	0.05	0.19
Sm	0.07	1.9×10^{-2}
Eu	8.83×10^{-3}	2.8×10^{-2}
Gd	2.66×10^{-3}	7.8×10^{-4}
U	93.86	2.99
Np	0.02	
Pu	0.60	
Am	4.55×10^{-3}	
Cm	1.15×10^{-3}	

TABLE 2

Radiologically Important Nuclides

Isotope	Half-Life (d)
Iodine 131	8.05
Iodine 132	0.096
Iodine 133	0.875
Iodine 135	0.280
Caesium 134	750.0
Caesium 137	11,000.0
Strontium 90	11,030.0
Ruthenium 106	366.0
Tellurium 132	3.25
Barium 140	12.8
Cerium 144	284.0
Plutonium 238	32,500.0
Plutonium 239	8.9×10^6
Plutonium 240	2.4×10^6
Plutonium 241	5,350.0
Curium 242	163.0
Curium 244	6,630.0

TABLE 3

Fission Product Classification and Chemical State in Irradiated UO_2

Class	Fission Products	Chemical State
1	Xe, Kr	Elemental
2	I, Br	Single phase halide solution CsI, I, I_2
3	Cs, Rb	CsI, $Cs_2UO_{3.56}$, Cs_2UO_4, Cs_2Te, Cs_2MoO_4
4	Te, Se	Single phase chalcogenide solution Cs_2Te
5	Ba, Sr	Oxides which can dissolve to some extent in the fuel and form separate phases BaO, $Ba_2(Zr-U-Pu)O_3$
6	Mo	Single phase metallic alloy, MoO_2, Cs_2MoO_4
7	Tc, Ru, Rh, Pd	Single phase metallic alloy
8	La, Y, Zr, Nb, lanthanides, actinides	Oxides which dissolve in fuel
9	Ag, Cd, In, Sn, Sb	Ag (fission yield low)

Under normal operating conditions the fission products remain within the fuel rod and slight pressure fluctuations, (eg Kr, Xe formation) are absorbed by the fuel-clad gap and the spring loading mechanisms within the rod. However under accident conditions the fission products could diffuse through the fuel pellets and it is postulated (1) that they can be released in one of four ways:

(i) fuel-clad gap release on breaching of the Zircaloy cladding;

(ii) diffusional release from exposed fuel pellets;

(iii) melt release;

(iv) aqueous leaching of quenched fuel.

Estimates(1) of the quantities of fission products released during these stages are given in Table 4.

If the fission products are released from the core they may then interact with the surrounding structure materials and Table 5 lists the amounts and properties of these structural materials that are present in a PWR core(1).

Despite the fact that there are a range of possible accident scenarios on which the fission product release is dependent the temperature of the core is one of the key parameters in quantifying releases. The effect of the core temperature on behaviour of the fission products is summarised in Table 6(1).

The determination of the fission product chemistry within the fuel and primary circuit is therefore dependent on understanding and establishing the following:

TABLE 4

Estimated Fission Product Release During the Course of a Severe Accident

Class	Fission Products	Release (%)				Balance in Fuel (%)
		Gap	Diff	Melt	Leach	
1	Xe, Kr	0.5	99.5	-	-	-
2	I, Br	0.5	99.5	-	-	-
3	Cs, Rb	0.5	99.5	-	-	-
4	Te, Se	5×10^{-4}	35.0	60	1	4
5	Ba, Sr	$5\ z\ 10^{-6}$	5.0	15	20	60
6	Mo	5×10^{-6}	5.0	15	20	60
7	Tc, Ru, Rh, Pd	-	0.3	3	2	95
8	La, Y, Zr, Nb, lanthanides, actinides	-	0.3	3	2	95
9	Ag, Cd, In, Sn, Sb	5×10^{-4}	35.0	60	1	4

TABLE 5

Amounts and Properties of Structural Materials in a PWR Core

Material	Components		Aerosol Species			
	Element	Weight (kg)	Possible Form	MP (°C)	BP (°C)	Vp at 2400°C (atm)
Control Rod	Ag	2,260	Ag	961	2210	2.5
	In	425	In	156	2080	4.5
			In_2O_3	-	850	-
	Cd	142	Cd	321	765	850
			$Cd(OH)_2$	d 300	-	-
			CdO	1500	d 1000	-
Boric Acid	B	120*	H_3BO_3	169→HBO_2	-	-
			HBO_2	300→B_2O_3	-	-
			B_2O_3	450	1860	9.0
Borosilicate Glass	B	82	As above	-	-	-
	Si	64	SiO_2	1700	2230	0.8
Zircaloy-4	Zr	16,200	Zr	1852	4380	2×10^{-5}
			ZrO_2	2700	5000	-
	Sn	240	Sn	232	2270	1.5
Stainless Steel	Fe	1,360	Fe	1535	2750	0.2
			FeO	1370	-	-
			Fe_2O_3	1565	-	-
			Fe_3O_4	1595	-	-
	Cr	380	Cr	1860	2670	0.6
			Cr_2O_3	2270	4000	-
	Ni	200	Ni	1455	2730	0.1
			NiO	1984	-	-
	Mn	40	Mn	1244	1962	4.1
			MnO	-	-	-
			Mn_2O_3	1080	-	-
			Mn_3O_4	1564	-	-
Urania Fuel	U	10^5	UO_2	2880	-	0.002

* Boric acid present in primary circuit cooling water only (in a severe accident a maximum of 39 tonnes of boric acid could be delivered to the core).

d Decomposes.

TABLE 6

Summary of Core Behaviour During Severe Accidents

Core Temperature (°C)	Sequence of Events
$\sim$325	Normal operation.
700-750	Borosilicate glass starts to soften.
830	Melting of Ag-In-Cd control alloy inside stainless steel cladding (Cd vapour pressure 0.2 MPa).
700-980	Monoclinic zirconia, relatively slow oxidation rate (parabolic or cubic rate law).
$\geqslant$780	Possible clad ballooning and rupture - gap release of fission products (Xe, Kr).
980-1500	Monoclinic zirconia, increasing rate of oxidation and hydrogen generation accelerating fuel rod temperature rise.
1005-1155	Relatively slow oxidation of stainless steel.
1155-1400	More rapid rate of oxidation of stainless steel (parabolic law).
1430	Failure of stainless steel control rod cladding. Depending on accident sequence, formation of Cd-dominant aerosol; Ag-In alloy ejected and flows downwards, Ag-Zr eutectic formation (mp 1500 K). Borosilicate glass also flows downwards.
$\geqslant$1430	Liquid formation due to Inconel-Zircaloy reaction and UO_2-Zircaloy reaction at inner cladding surface.
$\geqslant$1430-$\sim$2300	Major diffusional release of fission product from fuel.
$\geqslant$1430	Molten stainless steel foams during oxidation - reaction kinetics not understood, Mn-based aerosol may be significant.
1430-1580	Tetragonal zirconia, very rapid reaction (rectilinear) provided steam flow sufficient to sustain reaction.
1580-1850	Cubic zirconia, rapid oxidation, increased fuel rod heat-up rate.
1860-1960	Zircaloy melts: subsequent behaviour governed by thickness of ZrO_2 layer (a function of heat-up rate and steam supply). For a thin oxide layer molten Zircaloy flows down fuel rod and dissolves UO_2. If oxidation is more extensive, internal Zircaloy may be protected. As Zircaloy melts formation of Sn aerosols may be significant.
$\sim$2400	α Zr(O)/UO_2 monotectic temperature. UO_2 solubility in molten Zircaloy increases from $\sim$22 to $\geqslant$90 mol%.
2700	ZrO_2 melts.
$\sim$2830	UO_2 melts - core completely molten with enhanced release of fission products. Core slump processes not well understood.

(i) accurate knowledge of the chemical forms of the fission products within the fuel;

(ii) determining the nature and extent of any chemical reactions between the fission products out of the fuel;

(iii) determining the nature and extent of any reactions of the fission products with the structural and control materials.

These interactions fall into five different categories:

(i) vapour-vapour;
(ii) vapour-aerosol;
(iii) vapour-surface;
(iv) aerosol-aerosol;
(v) aerosol-surface.

At present there are two main strategies for investigating these problems. The first of these relies on the use of thermodynamic data to model both normal and accident situations using a variety of computer programs. This approach is very attractive because it allows predictions to be made over a wide range of pressure temperatures and elemental composition. The flexibility of this approach is illustrated by Garisto's recent work (2). This approach is severely hampered however, if the thermodynamic data are not available or are inaccurate. If the chemistry is poorly understood because of the presence of unexpected species, or because gross assumptions are made, then the results may also be dubious.

The second approach is to study the high temperature systems in situ using either small scale irradiated fuel pellets or simulant fission products. This is not as straightforward as first appears because of the problems of carrying out high temperature spectroscopy as outlined in

Appendix A. This experimental approach is often used to test the predictions of the computer programs.

The work described in this thesis utilises this second approach and concentrates upon some of the fission product chemistry of iodine, caesium and tellurium. These three were chosen because of their high fission product yield, radiobiological toxicity and volatility. There is also considerable emphasis on the role of boric acid in modifying the nature of any iodine release.

In Chapter 2 the experimental techniques and requirements of matrix isolation infrared spectroscopy and mass spectrometry are considered. As these are the spectroscopic methods used exclusively in this thesis to characterise vapour phase species some of the other physical methods available are given in Appendix A. The Wilson FG method of analysing the vibrational data to determine the molecular shape of the vapour phase species is described in Chapter 3.

The identification and partial characterisation of the first stable vapour phase ternary metal sulphide is outlined in Chapter 4. Although this has more relevance to the fossil fuel plants it is included here to demonstrate the utility of the powerful combination of matrix isolation and mass spectrometry.

Some aspects of tellurium reactor chemistry in both oxidising and reducing steam conditions are discussed in Chapter 5 along with the characterisation of hydrogen telluride and the identification of a new potassium-tellurium-oxygen compound.

The characterisation of vapour phase molecular monomeric boric acid is presented in Chapter 6 and this chapter illustrates how isotopic substitution and normal co-ordinate analysis can be used to determine not only the molecular shape, but also give reasonable values for the vibrational frequencies that cannot be observed using infrared spectroscopy. The new vibrational frequencies have been used to determine thermodynamic parameters which should be more accurate than those presently available.

The possible interaction between caesium iodide and boric acid has been a source of considerable debate and study. In Chapter 7 this reaction is studied in some detail and the volatile iodine reaction products identified. A semi-quantitative analysis has also been carried out to determine the extent of the release of volatile iodine species from this reaction.

Chapter 8 contains some concluding remarks and observations. As mentioned previously Appendix A compares the various physical methods for the study of non-trivial vapours. Appendix B is a worked example of how to derive $\underline{F}$ and $\underline{G}$ matrix elements and Appendix C makes use of these principles for the analysis carried out in Chapter 6. The last appendix is a flow diagram and listing of the program used in Chapter 6.

Throughout this thesis 'vapour' implies that the species is in some sort of equilibrium with either its liquid or solid phase, 'gas' implies that this is the only form present, and 'aerosol' means a suspension of particulate material in a gas or vapour. Where the infrared spectra are labelled as high resolution, the stated instrument resolution was greater than 1.5 cm^{-1}, medium or moderate resolution was between 1.5 and 2.5 cm^{-1} and in survey spectra the resolution was less than 4 cm^{-1}. The compounds used were all general purpose reagents (GPR) unless specified otherwise.

References

1. Bowsher B.R.
   Prog. Nucl. Energy, 20, 199, 1987.

2. Garisto F.
   AECL - 7782, 1982.

CHAPTER TWO

EXPERIMENTAL TECHNIQUES

1. Introduction

In this chapter the experimental and theoretical background to matrix isolation infrared (ir) spectroscopy and quadrupole mass spectrometry will be considered in detail. The theoretical approach to interpreting the ir spectra will be discussed in the following chapter.

2. Matrix Isolation Infrared Spectroscopy

Matrix isolation is a widely used method for stabilising reactive and unstable species (as well as stable species) so that they can be characterised by a variety of spectroscopic techniques. A summary of these techniques and the information each can yield is given in Appendix A. The most popular of these is vibrational spectroscopy and infrared in particular. It is therefore worth considering why this is so.

a) The lifetimes of the trapped species can be extended almost indefinitely because the matrix cage restricts bimolecular collisions and reactions. Hence species that may only have a very transient existence under normal conditions can be studied at leisure. The results of photolysis and photochemical reactions are also easily followed.

   The lifetimes are also extended because the cryogenic temperatures employed means that only reactions with very low activation energies (typically 3 $kJmol^{-1}$) can take place and thus unimolecular decomposition is largely avoided.

b) Because matrix isolation is an accumulative technique, compounds with low vapour pressures can be studied. The vapour pressure required for spectral observation will usually be less than that required for closed cell or molecular beam studies and thus the temperature required to obtain this vapour pressure will also be lower.

c) The ir spectra of matrix isolated samples are different to those of a gas phase spectrum, the principal difference being that the matrix spectrum consists of a number of sharp bands (typically 1 cm^{-1} full width at half maximum (fwhm)) whereas one would expect the gas phase spectrum to be made up of a large number of vibration rotation bands, which if unresolvable would result in broad absorptions. This sharpening of the bands is principally for three reasons:

i) because the matrix and its trapped species are at cryogenic temperature all the molecules will be in their (vibrational) ground states and thus no hot bands will be observed;

ii) the rigidity of the cage restricts, and usually prevents the rotation of the trapped species in the matrix. (The exceptions to this are small molecules, such as H_2O(1) and hydrogen halides(2) in rare gas matrices). The lack of rotational fine structure means that all direct moment of inertia data (and hence structural data) are lost. This however leads to a sharpening of the vibrational absorptions to the extent that near coincidental (~ 2 cm^{-1} apart) fundamentals can be resolved. This sharpening of the bands also enables isotopomeric splitting to be resolved. Indeed this is one of the reasons why ir is so popular, because isotopic substitution experiments are used extensively to gain structural information via normal co-ordinate analysis(3);

iii) the bands are also sharp because of the lack of interaction with other molecules.

d) If the matrix is warmed up so that it loses some of its rigidity then the trapped species can diffuse through it and undergo polymerisation and agglomeration reactions. When these reactions are followed spectroscopically it is possible to identify the features in a spectrum that are due to polymers or aggregates.

e) In closed cell experiments, containing the hot reactive species in a spectroscopically compatible vessel is often a major problem. In matrix experiments these problems are almost completely solved as only the furnace (sample holder) has to withstand both the high temperatures and the reactive sample. The rest of the apparatus can usually be constructed out of conventional materials.

f) Ir spectrometers are widely available at modest cost and are easily used. Therefore the information gleaned to cost outlay ratio is very favourable.

As with all beds of roses there are a number of prickly and thorny parts that need to be understood in order to appreciate the whole. The main disadvantage of matrix isolation is that all matrices perturb the energy levels of the trapped species to a certain extent. The extent of this perturbation can vary widely but generally manifests itself as matrix frequency shifts of the order of 0.5 - 1.0% and the observation of more bands than expected. Some of its effects are discussed in detail later.

In order to be able to carry out matrix experiments one needs to choose a material, or materials that are suitable as the matrix cage . The criteria for this choice are summarised below.

a) Purity - if the matrix is not pure then non-reproducible spectra may result because of the absorptions of the impurities. The species of interest may also react with the impurities(8).

b) Transparency - the matrix should ideally be spectroscopically transparent in the region of interest, and certainly not have absorptions which coincide directly with the trapped species. A glassy matrix is usually more transparent than a crystalline one because it scatters the incident radiation less.

c) Rigidity - since the raison d'etre of matrix isolation is to study isolated, non-interacting species, the rigidity of the cage is of paramount importance. If the matrix is not sufficiently rigid then diffusion of the solute (isolated) molecules can take place through the solvent (matrix) leading to recombinations in free radical studies and aggregation and polymers in the study of stable molecules.

A good indication of matrix rigidity is the melting point T_m(in K), and in general it has been found that the melting point of the matrix gas must be at least double the temperature at which it is to be used. Several workers(4,5) however, have found that diffusion can occur below these limits. To prevent diffusion on deposition it is therefore advisable to operate at the lowest temperature attainable. If this results in badly scattering crystalline matrices, then they can be annealed gently afterwards.

d) Volatility and vapour pressure - in order to be able to obtain a good matrix, the flow rate of the matrix material needs to be easily and carefully controlled. This therefore restricts the choice to gases or highly volatile liquids at room temperature unless elaborate heated systems are constructed. At the pressures (10^{-6}

torr) and temperatures (10K) conventionally employed in matrix studies, the matrix itself must have a vapour pressure lower than 10^{-3} torr, in order that it does not boil off. This therefore rules out helium, and also in practice neon and hydrogen.

The upper temperature limit is usually determined by rigidity considerations rather than those of vapour pressure.

e) Inertness - the matrix should ideally be inert with respect to the isolated species unless some interaction is anticipated[8].

f) Latent heat of fusion - the latent heat of fusion, L_f, is an important parameter because it is a measure of the amount of heat that has to be removed from the cold support on condensation of the gases to form the matrix. The amount of heat that has to be carried away is proportional to the depositon rate, and if this exceeds the cooling capacity of the cryostat its temperature will rise and diffusion is likely to occur.

g) Lattice energy - the lattice energy, U_o, is the energy required to form a lattice at 0K, and is important in assessing the rate of deposition. It also relates to the energy required to remove a molecule from its site in the lattice and gives an indication of the ease of diffusion of the isolated species.

h) Thermal conductivity - the thermal conductivity, λ, of the matrix material is of considerable practical importance. When the matrix is condensed on the cold support, heat has to be dissipated. Initially this is done directly through the cold support; however, as the layer of matrix grows, the heat that the cryostat needs to remove to maintain the rigidity of the matrix has to be conducted through the previously deposited layers of the matrix. Therefore, if the thermal conductivity of the matrix material is poor, the outer edge of the matrix will suffer local heating and the possibility of aggregation and polymerisation occurs. This parameter obviously affects not only the rate of depositon but also the total deposition time that can be used for a given matrix material.

A detailed listing of these thermal properties of matrix materials is given in refs 6 and 7.

As a result of the above criteria, the most widely used matrix gases are the rare gases and nitrogen. Helium is non-condensable under matrix conditions and for neon and hydrogen one needs to use liquid helium cryostats (4K) rather than the popular closed cycle Displexes. Xenon produces matrices which are notoriously bad scatterers unless deposited above 50K. Argon and krypton therefore emerge as those that can be regarded as inert, nitrogen is an equally good matrix, but one needs to exercise some care and caution in the interpretation of nitrogen matrix spectra because it is able to co-ordinate to some trapped species(8,24). It should be borne in mind that the matrix can give rise to structural perturbations(9). Other materials such as CO(10,11), CO_2(11), CH_4(10,11,12), CF_4(11,12), SF_6(11,12), C_2H_4(11), O_2(10), F_2(10,13), OCS(14), NH_3(15) have found occasional use. They are however usually employed as either reactive materials(12,13,14) or for probing the effect on the spectra of varying the matrix environment(10,11).

The interpretation of matrix isolation ir spectra is based on the assumption that the trapped species is essentially a free entity restrained in an inert and non-perturbing cage, and that it closely resembles the species in the gas phase. As has been noted earlier, this approximation is not entirely valid because of perturbations the matrix exerts on the trapped species energy levels. Normally matrix isolation is used to study species that cannot be investigated by more conventional methods. Therefore it is important to consider how good this approximation is and where it breaks down in the case of stable well characterised molecules.

In order to understand the effects the matrix can have on the trapped species, it is necessary to have a knowledge of the geometrical structure of the cage and hence the crystal properties of the matrix gas.

The rare gases, because of their spherical nature, crystallise in one of the close packed structures. By so doing they maximise the number of nearest neighbours(12) and hence their intermolecular van der Waals forces. This close packed structure is usually the face centred cubic structure (fcc) but argon can in the presence of impurities (eg, N_2, O_2, or CO) assume a hexagonal close packed structure (hcp). Both of these structures utilise 74% of the available volume and the remainder is taken up by interstitial holes. If these interstices have four adjacent atoms they are known as tetrahedral holes, whereas if they have six they are known as octahedral holes. The sizes of these holes vary between the rare gases and are listed(2,4) in Table 1. (There is a slight increase on warming to 20K).

From this table it can be seen that the tetrahedral holes are too small to accommodate even isolated atoms, whilst the octahedral holes will probably accommodate small atomic species. If these were the only sites available, then one would be very restricted to the number of compounds that could be studied.

However if one of the host (matrix) atoms or molecules is replaced in the lattice by a guest (trapped) species this then becomes a substitutional site and from Table 1 it can

TABLE 1

Mean Site Diameters in Commonly used Matrix Materials

Solid (4K)	Tetrahedral Hole Å	Octahedral Hole Å	Substitutional Hole Å
Ne	0.71	1.31	3.16
Ar	0.85	1.56	3.75
Kr	0.91	1.65	3.99
Xe	0.97	1.80	4.34
CH_4	0.94	1.73	4.147
CF_4			4.76
N_2			4.52 x 3.42 x 3.42
O_2			4.18 x 3.20 x 3.20
CO			4.61 x 3.48 x 3.48
CO_2			5.32 x 3.0 x 3.0

be seen that these are much larger than the interstitial sites. If the guest molecule is too large for a single substitutional site then it can be accommodated by introducing strain in the lattice. This is done either by trapping in a multiple vicinal vacancy or by making use of the lattice imperfections such as edge or screw dislocations. These dislocations will be present in the lattice because of the way in which it is formed, ie, rapid condensation of a gas onto a cold surface. They can not only act as extra trapping sites but also as pathways for diffusion.

Although nitrogen is non-spherical it too crystallises in a fcc structure below 35K. Above this temperature it will crystallise in a hcp structure in which the molecules can freely rotate. The result of this is that at temperatures above 35K diffusion will proceed very rapidly, so any annealing of the matrix should be carried out at temperatures below this. The other main difference between nitrogen and the rare gases is that in nitrogen the site will not be symmetrical.

From these geometrical considerations it would seem that the observed matrix spectra would be very complicated as a result of the guest molecule occuping a number of different sites, each with a different potential, leading to a large number of bands. However, in practice, it is usually found that the bands are sharp (~ 1 cm^{-1} fwhm) and the spectra very reproducible. This indicates that the guest molecules are trapped in similar sites each time and there is a large degree of homogeneity of the matrix itself, or that the differences between sites cannot be detected by ir spectroscopy.

The main complications are that in nitrogen the spectra can be more complex than anticipated because the unsymmetrical site can lift the degeneracy of some modes, whereas in argon the complexity is usually due to there being more than one type of trapping site. It is therefore advisable to carry out matrix experiments in several different matrices to check and confirm spectral observations.

The perturbation of the matrix upon the trapped species usually manifests itself as vibrational shifts and more bands observed than anticipated.

The shift in vibrational frequencies ($\Delta\nu = \nu_{matrix} - \nu_{gas}$) can be considered to arise from 1st and 2nd order perturbation of the Hamiltonian of the free molecule. The first order perturbation results from the electrostatic charge distribution of the host and that of the guest molecules. For noble gases this is zero, whilst for nitrogen it is non-zero because of the quadrupole moment. The second order perturbations arise from inductive and dispersive interactions. The former is the result of the interaction between the permanent charge distribution of one molecule and the charge distribution in the other molecule (eg, dipole-induced dipole and quadrupole induced quadrupole interactions). The dispersive interaction is caused by the attraction between the instantaneous charge distribution of the two molecules. Although the average moment is zero, it is a net attractive force because the fluctuating charge distribution in one molecule and the induced moment in the other are always in phase with each other.

These considerations are modified from those applied to solutions, but for solid cages one needs to include repulsive interactions, which are caused by the overlap of the electronic distributions of the host and guest. In addition to these static contributions one also needs to consider a dynamic contribution to the frequency shift to take account of the constrained translational motion of the guest. This is however small when compared to the static effects.

Calculations of the inter-molecular potential energy of stable molecules such as diatomics (eg, hydrogen halides) using the relevant physical constants have been carried out(16), allowing the evaluation of frequency shifts. For non-polar spherical cavities (eg, rare gases) the correlation between theory and experiment is reasonable, but for polar non-spherical cavities the agreement is very poor. For polyatomic guest molecules the situation becomes much more complicated and the quantitative evaluation of frequency shifts becomes impractical.

As a general rule the bond stretching modes in polyatomics are red shifted ($\Delta\nu$ negative) but examples of blue shifted compounds do exist (eg, HI in nitrogen(17)). The case for angle bending and other deformations is much more complicated, and no general rule can be applied, but often they are blue shifted ($\Delta\nu$ positive). A recent review by Jacox(18) compares the vibrational data for diatomic molecules in the gas phase and in inert solid matrices. She found that the matrix shifts for diatomic molecules tended to increase in the order $Ne \leqslant Ar \leqslant Kr \leqslant Xe \leqslant N_2$ and that the matrix shifts for most diatomics were less than 2% in argon. The notable exceptions to this were the alkali metal halides with red shifts of up to 24.5% (LiBr in N_2) or weakly bound species which often have large blue shifts. The former is probably due to large molecular dipole moments whereas the latter is attributed to the introduction of a potential barrier to dissociation in the matrix. Therefore force constant and thermodynamic parameters derived from matrix data can usually be used as the data for free molecules without introducing too large an error, comparable to anharmonic corrections and solvent shifts.

The observation of multiple bands where group theoretical considerations dictate that only one should be observed can arise for several reasons as listed below.

a) There may be two distinct species in the matrix with near coincident absorptions. This problem can usually be resolved by varying the deposition conditions.

b) Multiple trapping sites: the majority of isolated species are trapped in substitutional sites of one form or another. If there exists within the lattice several different forms of site, each with a different potential surface, then when a guest is isolated in these it will sense a different inter-molecular potential for each site. This will give rise to different frequency shifts and hence a multiplet in the spectrum. Multiplets arising form multiple trapping sites can usually be identified because their relative intensity is unaffected by change in concentration. When the matrix is annealed the guest molecules tend to selectively diffuse into only one site. If the site in which the guest is located is asymmetrical this can be classed as a multiple site if the molecule can sense it. For example, in a low symmetry species such as HDTe all the fundamentals are split into doublets, whereas in the higher symmetry H_2Te and D_2Te species only one band for each fundamental is observed(19) in nitrogen matrices.

c) Polymerisation and aggregation: extra bands may be observed due to the presence of polymeric forms of the guest molecule. These can be identified by comparison of relative intensities before and after annealing (or diffusion) is carried out. If molecules do not form polymeric species, but are located close to each other, as in aggregation, then they can interact which will also give rise to multiplet features. In both of these cases the bands are usually broader than matrix isolated monomeric species.

d) Rotation: the vast majority of solute molecules are held so rigidly in the matrix cage that they are unable to rotate. Small molecules such as hydrogen halides, water, ammonia and methane have been found to rotate(1,2) in spherical sites, as in rare gas matrices. Multiplets due to rotation can be identified because the features should have a reversible temperature dependence. Rotation has been confirmed using far infrared and Raman spectroscopy for matrices with spherical cavities(20). There is no firm evidence however for rotation in matrices with unsymmetrical cavities, such as nitrogen (20).

e) Lifting of degeneracy: More bands than anticipated can be observed if the degenerate modes of the guest molecule are susceptible to splitting as a result of the perturbation of the matrix cage. This can only happen if the trapped molecule has at least a C_3 axis. The degeneracy can be lifted if the symmetry of the trapping site is lower than that of the trapped species. Thus a doubly degenerate "E" mode may be split into two bands, whilst a triply degenerate "T" mode may be resolved into 2 or 3 bands depending on the exact nature of the perturbation. Eg in SeO_3(21), the E' stretching mode at 1007 cm^{-1} is split into two components separated by ~2 cm^{-1}. In a similar manner low site symmetry can result in the observation of bands which are theoretically inactive.

g) The final reason for the observation of more bands than expected is due to the breakdown in the assumption that the matrix is non-interacting. Recent elegant work by Beattie et al(9,10) has shown that despite Perutz's statement(22) that there are "no convincing cases in which molecular symmetry differs in gas and matrix phases", the matrix does have an appreciable effect upon the molecular geometry. For example, it is found that for $ThCl_4$ and UCl_4(9) the matrix ir spectra in argon and nitrogen can be explained in terms of a C_{2v} structure, whilst neon matrices appear to give rise to spectra that can be assigned to a T_d species. They have also found that the mode of co-ordination of the alkali metal in hexafluoroanions and perchlorates(10) is critically dependant on the matrix gas used. In matrices with a weak guest-host interaction (eg Ne, Ar) the spectra were interpreted in terms of a C_{3v} structure where the cation was facially bound. In matrices with stronger host-guest interactions (eg N_2, CO) a C_{2v} structure with the cation edge co-ordinated was found. The interaction was found to increase as Ne $\leqslant$ Ar $\leqslant$ O_2 $\leqslant$ F_2 $\leqslant$ Kr $\leqslant$ Xe $\leqslant$ N_2 $\leqslant$ CO. For Xe (and to a lesser extent Kr) features arising from both C_{2v} and C_{3v} species were observed. For this latter example it cannot be considered that these results are different from the gas phase as the bonding there is almost certainly polytopic(23). A polytopic bond is defined as having essentially the same energy when it connects atoms in very different positions.

Despite all the problems and complications, matrix isolation ir remains a very convenient (and in some cases the only viable) means for the characterisation of unknown, high temperature, highly reactive or highly unstable compounds and systems.

3. Experimental Arrangement For Matrix Isolation Infrared Spectroscopy

In a typical study the species of interest are vaporised, travel a distance of 10-20 cm in a high vacuum and are then co-condensed with a large excess of the matrix gas onto the cryogenically cooled deposition window. The sample temperature is crucial to the success of the experiment in as much that the vapour pressure needs to be controlled so that the sample is isolated monomerically. Vapour pressure data are available for some systems but for the majority they are not. In these latter cases one has to increase the sample temperature slowly and monitor the spectrum until bands are observed. If the vapour pressure at room temperature is too high then it can be controlled by taps or valves but more often it is convenient to use liquid nitrogen/solvent slush baths. If the vapour pressure at room temperature is not sufficient to obtain a spectrum then the sample needs to be heated.

Recent work by Ogden and Wyatt(24) has shown that the method of vaporisation has a strong effect on the species volatilised. When vaporisation of $CrCl_3$ took place from a 6mm silica tube the matrix ir spectrum was significantly different to that from a tube of 1-2mm diameter. The former approximates to Langmuir free evaporation and it was found that the predominant vapour phase species was $CrCl_3$ whilst the latter approaches Knudsen effusion and the principal vapour species was found to be $CrCl_4$.

In this work either resistive or inductive heating was used. For the former, nichrome wire was used as the heating element and this was usually wrapped onto a pyrex or silica former which was slipped over the sample holder. The heating power was controlled by a Variac and monitored with a chromel-alumel thermocouple. Resistive heating can be used up to ~ 450°C if the sample holder is pyrex or as high as 1000°C if it is silica. However one has trouble controlling the vaporisation at these temperatures as the sample will condense on any part that is cooler than the point of sublimation and it is possible to see the sample shuttle from one end of the tube to the other with very little being deposited on the window. At these elevated temperatures nichrome is unusable and there is also the increased possibility of the silica tube failing and hence leading to a catastrophic pressure rise. Figure 1(a) shows the conventional pyrex/silica sample holders used.

Therefore, in general, for temperatures exceeding 600-700°C induction heating was used. The susceptor can either act as the sample holder (eg, graphite, molybdenum or stainless

(a) SILICA / PYREX
(b) SILICA FORMER
(c) NICHROME WIRE FURNACE
(d) CHROMEL - ALUMEL THERMOCOUPLE

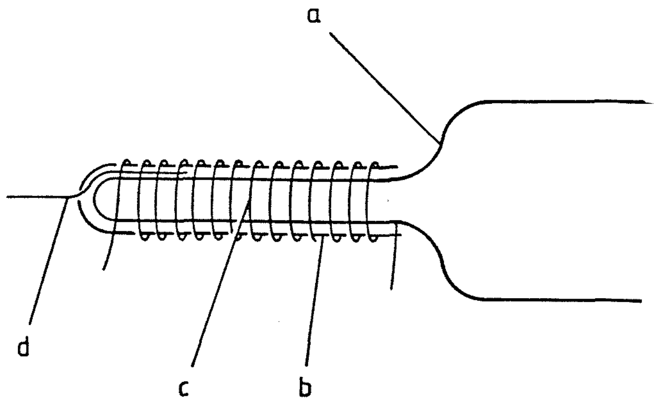

a) RESISTIVE HEATING

(e) ALUMINA TUBE
(f) CEMENT
(g) ALUMINA ROD
(h) TANTALUM SUSCEPTOR
(i) VACUUM JACKET
(j) INDUCTION COIL
(k) YOUNG'S GREASELESS CONE

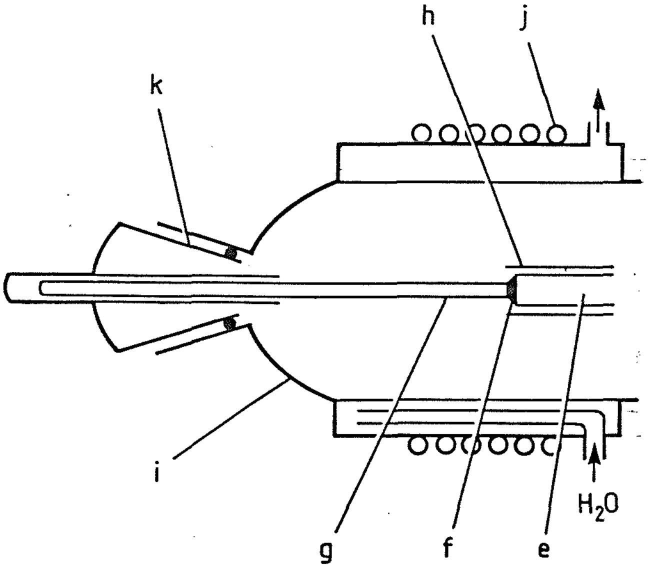

b) INDUCTION HEATING

FIG. 1 SAMPLE HOLDERS AND VAPORISATION APPARATUS steel) or if a more inert material such as silica or alumina is used as the sample holder then the susceptor, usually tantalum foil, is wrapped around this. In general, the latter proves more convenient to use.

Figure 1(b) shows the experimental arrangement most commonly used for induction heating of samples. The sample is loaded into a platinum boat which is then placed in an alumina tube (e). This is connected to an alumina rod (g) by cement (f); the rod (g) is located in a sealed Young's greaseless cone (k) which in turn is sealed in a water-cooled vacuum jacket (i). The sample is heated inductively by the tantalum sleeve (h) suscepting with the copper water-cooled induction coils (j). The estimation of temperature in these experiments is difficult because thermocouples can also suscept and give rise to inaccurate temperature readings. The method usually employed in estimating temperature is to gauge the temperature from the susceptor colour using optical pyrometry.

More elaborate vaporisation techniques can be used and these include sputtering(9) and laser vaporisation(26).

The sample holders are connected to the vacuum shroud (h) shown in Figure 2 by a brass ring (i) and an 'O' ring to ensure a vacuum-tight seal. The subliming vapours are co-condensed with the matrix gas from the spray-on line (j) which is fitted with a needle valve (k) to control the rate of deposition onto the central caesium iodide window (e). This window is mounted in a copper holder (d) which is attached to the cold end of the cryostat (b) with an indium gasket (e) to maintain good thermal contact. A radiation shield (f) maintained at ~ 50-70K is used both to protect the window during degassing and also to prevent it warming up due to the radiation from the hot sample holder.

The outer windows (g) need to be transparent to ir radiation and caesium iodide is usually used for this

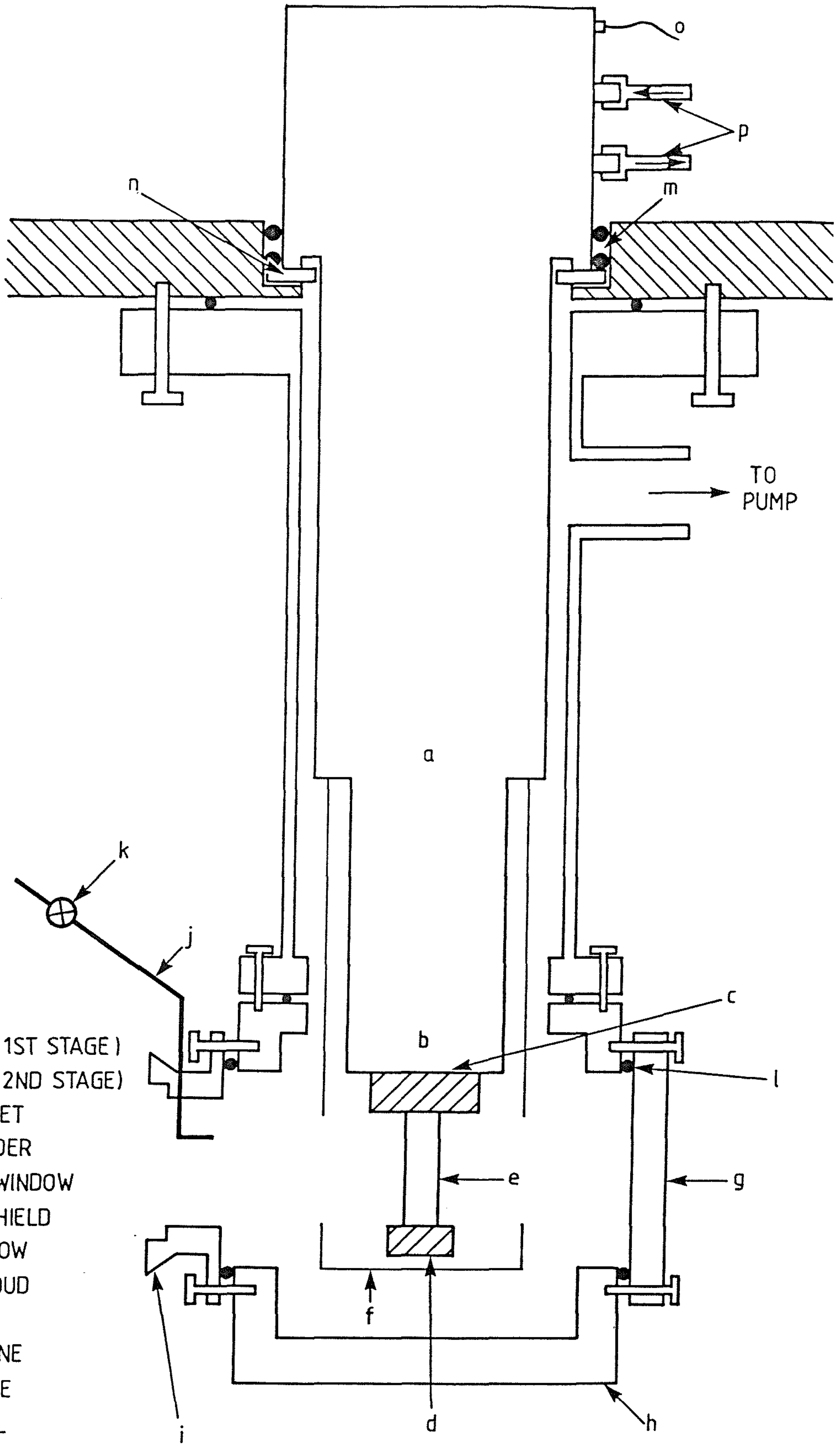

a EXPANDERS (1ST STAGE)
b EXPANDERS (2ND STAGE)
c INDIUM GASKET
d COPPER HOLDER
e DEPOSITION WINDOW
f RADIATION SHIELD
g OUTER WINDOW
h VACUUM SHROUD
i BRASS RING
j SPRAY-ON LINE
k NEEDLE VALVE
l 'O' RING SEAL
m DOUBLE 'O' RING SEAL
n TEFLON GASKET
o ELECTRICAL CONNECTION TO COMPRESSOR UNIT
p HIGH PRESSURE HOSES TO AND FROM COMPRESSOR

FIG. 2 VACUUM SHROUD, CRYOSTAT AND DEPOSITION WINDOW purpose. The spectrometer beam passes through the vacuum shroud perpendicular to the sample holder. The double 'O' ring seal (m) ensures a good vacuum seal when the window and cryostat need to be rotated between deposition and spectral recording positions. The traditional deposition window has been one piece of flat caesium iodide crystal held in a copper holder. Therefore as Figure 3 shows it needs to be rotated between deposition (a) and recording positions (b). This means that it is hard to monitor the spray on as it is happening and even if the window is held at 45° (to both the beam and sample) there is the possibility that a higher proportion of the sample will not "stick" to the window. To try to overcome these problems a 'V' shaped window has been developed for the study of these systems. This is basically an equilateral triangle with CsI windows on two faces and the front face is left open for the sample deposition as shown in Figure 3(c). Although the transmission through the assembly is less due to scattering and absorbance by the additional CsI, it does have the advantage that if a sample molecule bounces off one window it will then stick to the other one, or bounce off back to the original window. This set up has proved very successful in the study of highly volatile, reactive species such as H_2Te(19) and platinum metal oxyfluorides(25). It has also proved invaluable for determining the appropriate temperature at which a spectrum can be obtained. Usually this 'V' shaped window is used for the first few experiments to determine the conditions and then the more conventional setup is used due to its higher transmission characteristics which enables one to obtain higher quality spectra.

The window is maintained at the necessary cryogenic temperatures to condense the matrix gases by an Air Products CS202 Water-cooled Displex, closed cycle refrigerator. This employs a modified Solvay cycle using helium as the working medium. The cooling is achieved by allowing the helium to expand into a volume and to work

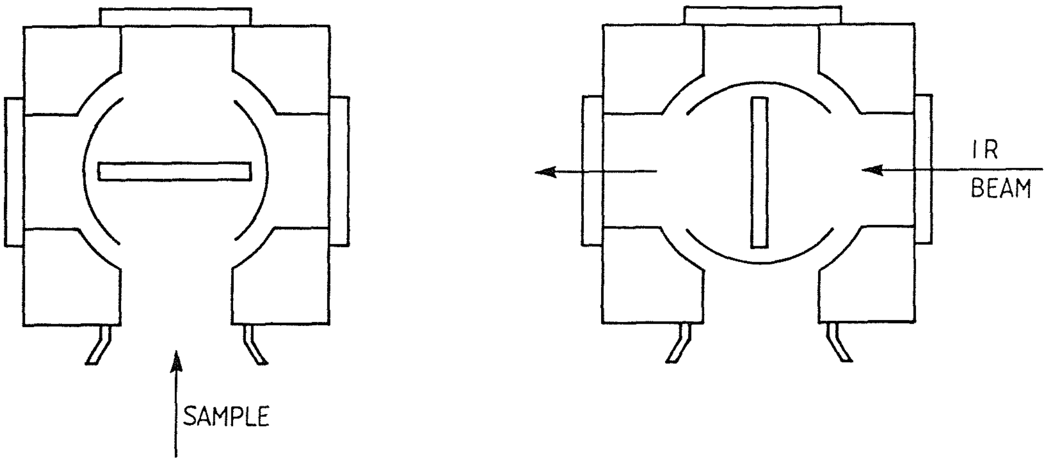

a) SAMPLE DEPOSITION

b) SPECTRAL RECORDING

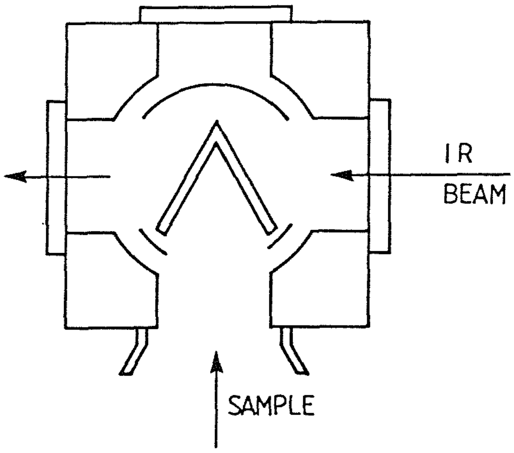

c) SIMULTANEOUS SAMPLE DEPOSITION AND SPECTRAL RECORDING

FIG. 3 METHODS OF SAMPLE DEPOSITION AND SPECTRAL RECORDING against a piston. As the gas expands it cools and so the energy for this expansion comes from the surroundings, ie the deposition window. Therefore the window temperature decreases with every cycle. It is not possible however to use just one expander to obtain the necessary cryogenic temperatures and two expanders are used end to end with the cold end of the first stage (~ 50-70K) being the warm end of the second stage expander (10-14K). These are shown as (a) and (b) respectively in Figure 2, the electrical connections and high pressure hoses are shown as (o) and (p) respectively.

If lower temperatures than this (10-14K) are needed (eg, for neon or hydrogen matrices) then one has to use either liquid helium flow or dewar systems, or the recently introduced Air Products Heliplex, which is a 3 stage closed cycle cryostat capable of reaching 3.6K.

The tip and window temperature can be monitored by either thermocouples or hydrogen vapour bulbs (up to 24K) and diffusion and annealing experiments can be carried out by use of tip heaters.

The high vacuum necessary to avoid the build up of atmospheric gases on the window was achieved and maintained by the use of a pumping unit comprising an Edwards Diffstak, a liquid nitrogen trap and a rotary pump.

The spectrometers used were a Perkin Elmer 983G interfaced to a model 3600 Perkin Elmer Data station, and a Perkin Elmer 225. Both of these were fitted with dry air purgers to remove absorptions due to water vapour in the spectrometer. The data station was used to store spectra and also for procedures such as spectral smoothing and the subtraction of background features which may obscure genuine absorptions. A few experiments were carried out on an FTIR machine (Bruker IFS 113V) at AEE Wifrith and the results were found to be comparable to those obtained on the grating machines at Southampton.

These spectrometers were calibrated(27) using residual water and carbon dioxide and gas cells of hydrogen chloride and carbon monoxide in the conventional manner.

The matrix gases were supplied by BOC and were high purity grade argon (99.999%), 'white spot' nitrogen, and research grade krypton.

4. Mass Spectrometry

Mass spectrometry is a very valuable tool for identifying the species present in a vapour above a (heated) solid. This information is obtained by measuring the mass/charge ratios of the ions and then attempting to assign them to parent and daughter species. There are currently four main ways of measuring these mass/charge ratios

(i) separation of the ions by a magnetic field in a sector instrument(28),

(ii) separation of the ions by velocity in a time of flight instrument(29),

(iii) separation of the ions in an ion cyclotron resonance cell in a Fourier Transform Mass Spectrometer(30),

(iv) separation of the ions by oscillating radio frequency (rf) fields in a quadrupole mass analyser.

It is the last method that has been used (almost) exclusively in this work. For a very entertaining and pertinent review of the various mass spectrometric techniques see reference 31.

5. Quadrupole Mass Spectrometry

In the system employed in these studies the sample vapour pressure was controlled by rf heating, resistance heating or nitrogen slush baths as in the matrix experiments. The vapour was ionised by electron bombardment generated by thermionic emission of a heated tungsten filament. The energy of these electrons was varied by altering the accelerating potential between the filament and the ion source cage that also acts as the electron trap. The resultant ions were then injected through a pair of focussing plates into the quadrupole analyser itself, in the form of a beam with circular cross section. The potential of these focussing plates is variable and is used to trade off sensitivity and resolution. For example, the lower the potential of the plates, the fewer ions will be injected into the analyser, but they will have a lower velocity which results in an increase in resolution because the rf and dc fields can have a much greater effect upon them.

The quadrupole mass spectrometer or mass filter was invented by Paul and co-workers(32,33) in 1953 and a schematic view of one is shown in Figure 4. The mass spectrometer itself consists of four parallel hyperbolic rods and to these is applied an rf voltage of peak amplitude V superimposed on a dc voltage U. The potential of the field is given by:

$$\Phi = (U + V\cos \omega t) \, . \, (x^2 - y^2)/r_0^2$$

where $\omega = 2\pi f$ (f is the radiofrequency) and x, y and r_0 are defined as in Figure 4. Therefore in the xz plane the rods have a positive potential, whereas in the yz plane they have a negative potential.

For the following equations and description to be rigorously correct the rods need to be hyperbolic; however,

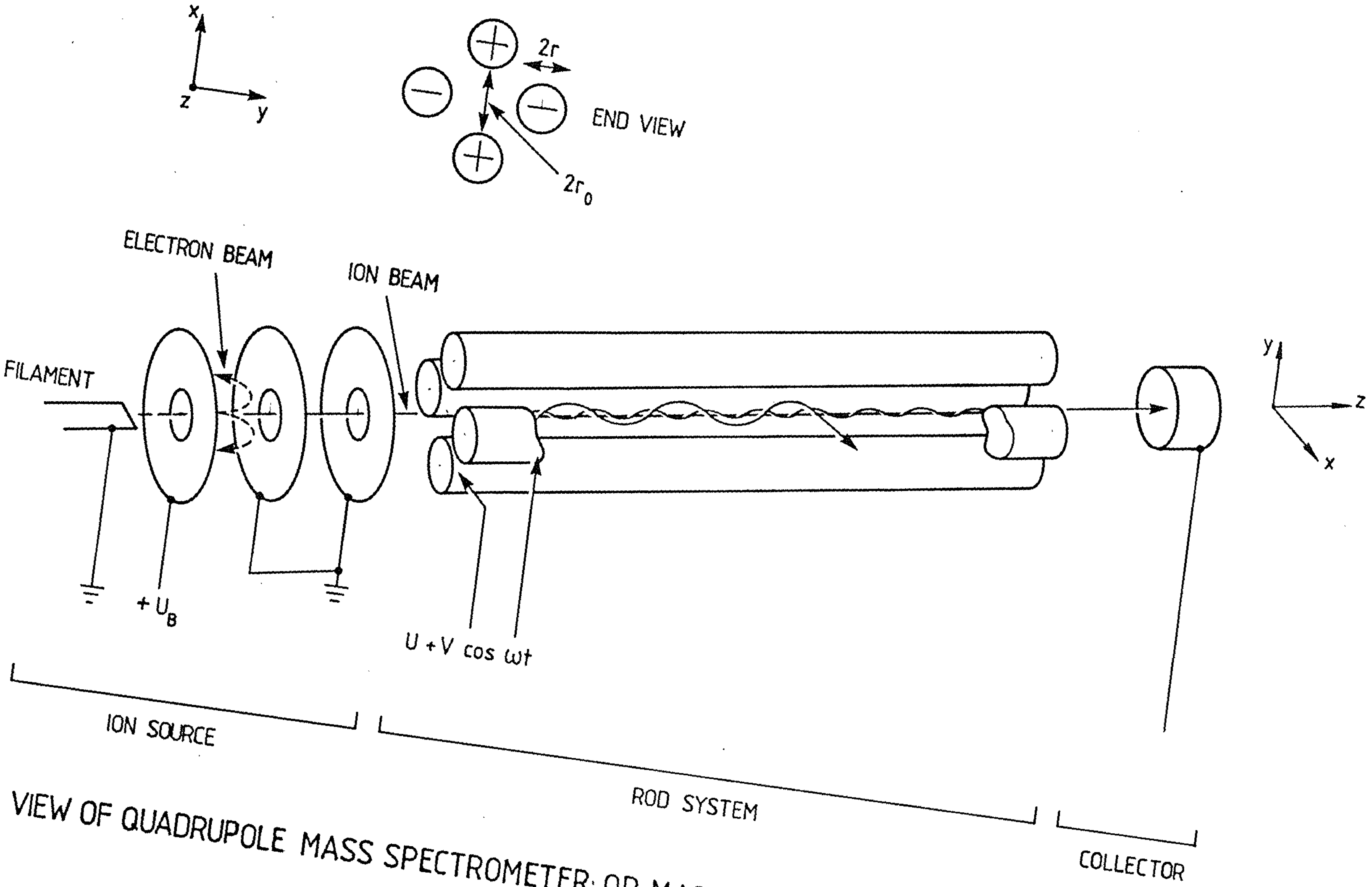

FIG. 4 SCHEMATIC VIEW OF QUADRUPOLE MASS SPECTROMETER OR MASS FILTER

in practice most rods are cylindrical (due to relative ease of manufacture) and by the use of an r/r_o ratio of 1.1468 a good approximation to an exact quadrupole field is obtained.

The trajectory of the ions in the quadrupole field can be described by the following equations of motion.

$$m\ddot{x} + 2e(U + V\cos \omega t) \,.\, x/r_0{}^2 = 0$$

$$m\ddot{y} - 2e(U + V\cos \omega t) \,.\, y/r_0{}^2 = 0$$

$$m\ddot{z} = 0$$

By use of the following transformation parameters:

$$2\zeta = \omega t$$

$$a = \frac{8eU}{mr_0{}^2\omega^2}$$

$$q = \frac{4eV}{mr_0{}^2\omega^2}$$

the Matthieu differential equations below can then be derived:

$$\ddot{y} + (a + 2q\cos 2\zeta).x = 0$$

$$\ddot{x} - (a + 2q\cos 2\zeta).y = 0$$

The solution of these equations reveals that an ion injected into the analyser along the z axis will perform oscillations perpendicular to this axis. The ion will either undergo stable oscillations which will result in it emerging from the quadrupole to be detected, or unstable oscillatory motion with rapidly rising amplitude so that it hits the rods and is neutralised.

A qualitative explanation of these processes can be made by separating out the trajectories in the xz and yz planes. As noted previously the rods in the xz plane are at a positive potential and hence a positive ion lies in a dc potential well. This ion is then excited into oscillation by the applied rf field. The average force and energy gained from these oscillations increases with mass. This means that the heavier ions will have a larger amplitude of oscillation than the lighter ions with the result that the heavier ions are more likely to strike one of the electrodes and be neutralised. Therefore in this plane the analyser is acting as a low mass pass filter.

In the negative potential plane (yz), the positive ion lies on a potential hill. The ion is attracted to the electrodes but the rf field gradients near to the electrodes exert a focussing force on the ion. This force also increases with mass and means that the higher masses are affected more than the lighter masses resulting in the lighter masses hitting the electrodes. Hence in this plane the quadrupole is behaving as a high mass pass filter.

By suitably adjusting the parameters the low and high mass pass filters can be made to overlap and hence the overall quadrupole analyser is a band pass mass filter.

From the previous equations it can be seen that the variable parameters are V, U and ω, because r_0 is set in any given system and m/e is the parameter analysed for. In Paul's development work(32,33) he chose to vary the frequency of the rf field. This however is not the method chosen for commercial machines because the mass scale is linearly dependent on the V/U ratio. As the radiofrequency is kept constant the parameters that are varied are U and V.

The stability diagram (Figure 5) shows pictorially how both the m/e ratios are scanned and the resolution varied. The transformation parameters a and q are the ordinate and abscissa respectively. The shaded area corresponds to those values of a and q that give rise to the stable solutions outlined above, this region is therefore known as the stability area. The remaining area corresponds to the unstable solutions and will not concern us further. The ratio a/q and hence U/V (ie, the ratio of the dc voltage U and the superimposed rf voltage V) is kept constant and all the mass numbers lie on the straight line A, which intersects the origin. All the masses that lie on this line within the shaded area can undergo stable motion and therefore pass through the mass filter to be detected.

A range of masses is allowed through the filter because a and q are each proportional to two independent parameters, ie, U/m and V/m respectively. Therefore although U and V are fixed, there can be several values of a and q that give rise to stable solutions because of their dependence on 1/m. This range of solutions can be increased or decreased by varying the gradient of A and hence the U/V ratio. At higher ratios the resolution will be greater but with a concomitant loss in sensitivity. If the appropriate ratio is chosen (usually 6:1) then the shaded area can be made to represent only 1 mass unit and hence 1 amu resolution can be achieved.

The masses are scanned by increasing U and V in such a manner that U/V remains constant. The values of a and q which give rise to stable solutions remain the same for values of U and V, and therefore the value of m, which gives values of a and q which lie in the stability area, increases with U and V and successive masses pass through the quadrupole mass filter to be detected according to:

$$m = V/(7.219\ f^2 r_0{}^2)$$

and

$$m = U/(1.212\ f^2 r_0{}^2).$$

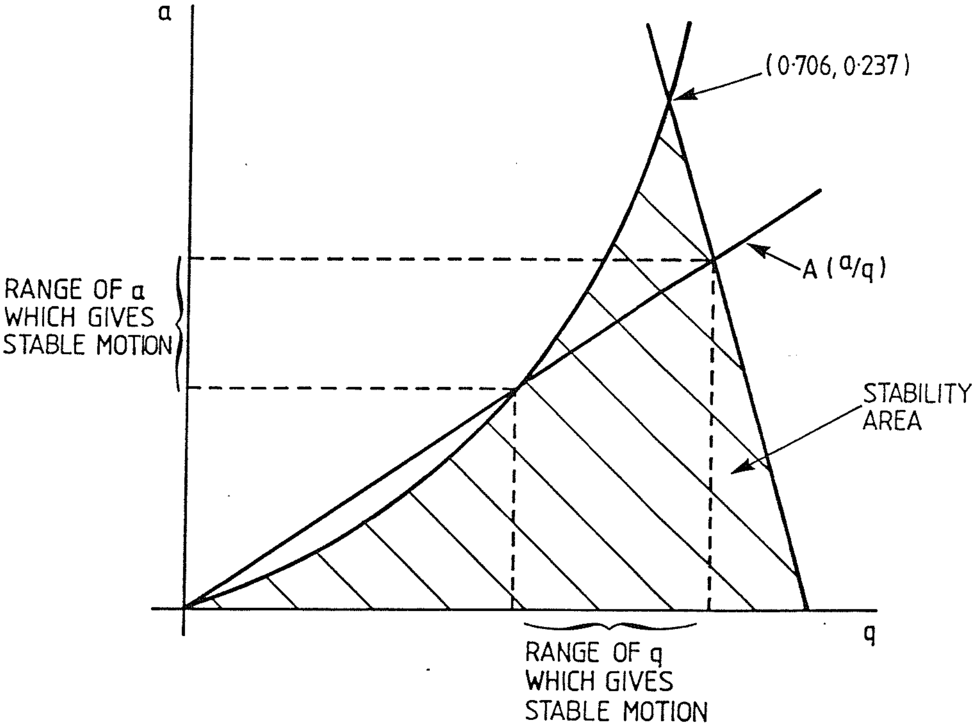

FIG. 5 STABILITY DIAGRAM FOR A QUADRUPOLE MASS SPECTROMETER

The ions that have undergone stable motion in the quadrupole are either detected by a Faraday plate collector or an electron multiplier tube. The Faraday plate has no means of signal amplification and is hence only used when it is inadvisable to use the multiplier (eg, when the pressure is greater than 10^{-4} torr). The electron multiplier employed is a wide bore channeltron multiplier. This consists of a curved funnel shaped piece of glass which is coated on the inside with a resistive coating. When the incident ions strike the mouth of the channeltron a number of electrons are liberated from the resistive coating. Because the mouth is held at a high negative potential (-3 kV), and the collector is held at ground level, the electrons flow down the potential gradient to be collected at the end of the tube. In passing down the tube they repeatedly collide with the resistive surface thus liberating more electrons and so increasing the collector current. The current that arrives at the collector is then fed to the amplifier and subsequently to the chart recorder or interfaced microcomputer. The channeltron is mounted off axis from the quadrupole rods and ion source so that the soft x-rays produced by the electron beam in the source do not enter the channeltron, which would increase the dark current of the multiplier and hence lower the signal/noise ratio.

Recently the mass spectrometer has been interfaced to a BBC microcomputer via the BBC's internal Analogue to Digital converter (ADC). This has allowed the development of a suite of programs that enables one to store, retrieve, view and manipulate spectra.

The spectra observed can be more complex than anticipated because of a number of complications such as fragmentation, multiply charged ions, ion rearrangement, metastable ions, or ions formed from ion-molecule reactions and the interaction of the sample with the spectrometer and filaments, etc(34). Some of these effects can be identified immediately whilst some are more pernicious. Fragmentation of the parent ion can sometimes lead to wrong assumptions being made, for example it is reported(35) that the MCl_6^+ and MCl_5^+ parent ions have only a very small relative intensity compared to their daughter ions MCl_5^+ and MCl_4^+ respectively. To try to remove the problems of fragmentation it has been suggested(36) that Angular Distribution Mass Spectrometry could be used. In this it is assumed that for a given system the angular distribution is unique for each vapour phase species effusing from a non-ideal orifice.

Conventional mass spectrometers require a high vacuum ($\sim 10^{-5}$ torr) in order to operate. However the use of molecular beam technology has enabled the sampling of systems at much higher pressure (typically several torr to atmospheres) to be studied(37,38).

In order for a system to be investigted by mass spectrometry, its components need to be vaporised. Initially this was done using Knudsen cells in conjunction with vapour pressure or transpiration studies. The methods available currently are much more diverse and include Fast Atom Bombardment (FAB), and laser vaporisation.

Once the components have been vaporised they need to be ionised so that the mass/charge ratio has a finite value. The conventional mean of ionisation is electron impact (EI) in which a stream of electrons is directed at the target gas. Other methods such as Secondary Ion Mass Spectrometry (SIMS) can also be used.

The energy of the bombarding electrons needs to reach a threshold (because of quantum mechanical considerations) before the molecule suffers electron loss and hence becomes a positive ion. The value of this threshold is called the

Appearance Potential (AP) and from its value one can often conclude whether the ion is a parent or due to fragmentation of another ion or molecule. Information can also be gleaned by plotting an "Ionisation Efficiency Curve" of intensity vs electron energy. Figure 6 shows some of the possible curves obtainable.

Figure 6(a) is by far the most typical of curves observed and is that for a conventional parent or daughter ion. Figure 6(b) has been observed(39) for the I_2^+ ion and indicates that at high electron energy the parent ion is being extensively fragmented. Figure 6(c) is a curve obtained(21,40) for SeO_3^+ and indicates that the ion is both a parent ion and also a daughter ion. The first step is ionisation of the SeO_3 parent molecule, whilst the step at higher electron energy arises from the fragmentation and ionisation of $(SeO_3)_4$.

The method of determining the APs in this work was by extrapolation of the linear part of the curve to the base line. A detailed account of the more sophisticated methods is given in refs 41, 42. The method used, often gives values which are too high compared to those given by the better routines. This discrepancy arises because of the tail at the beginning of the linear portion which itself is a result of the ionising electrons having a Maxwellian energy distribution. If the electrons were monoenergetic then a sharp cut off would be observed, as would fine structure on the curve itself. This fine structure is due to the population of vibrationally excited states and it is this that can be used to obtain thermodynamic and structural data(43).

6. Experimental Configuration For Quadrupole Mass Spectrometry

The vapour pressure in the mass spectrometric experiments usually needs to be higher than in the matrix ir

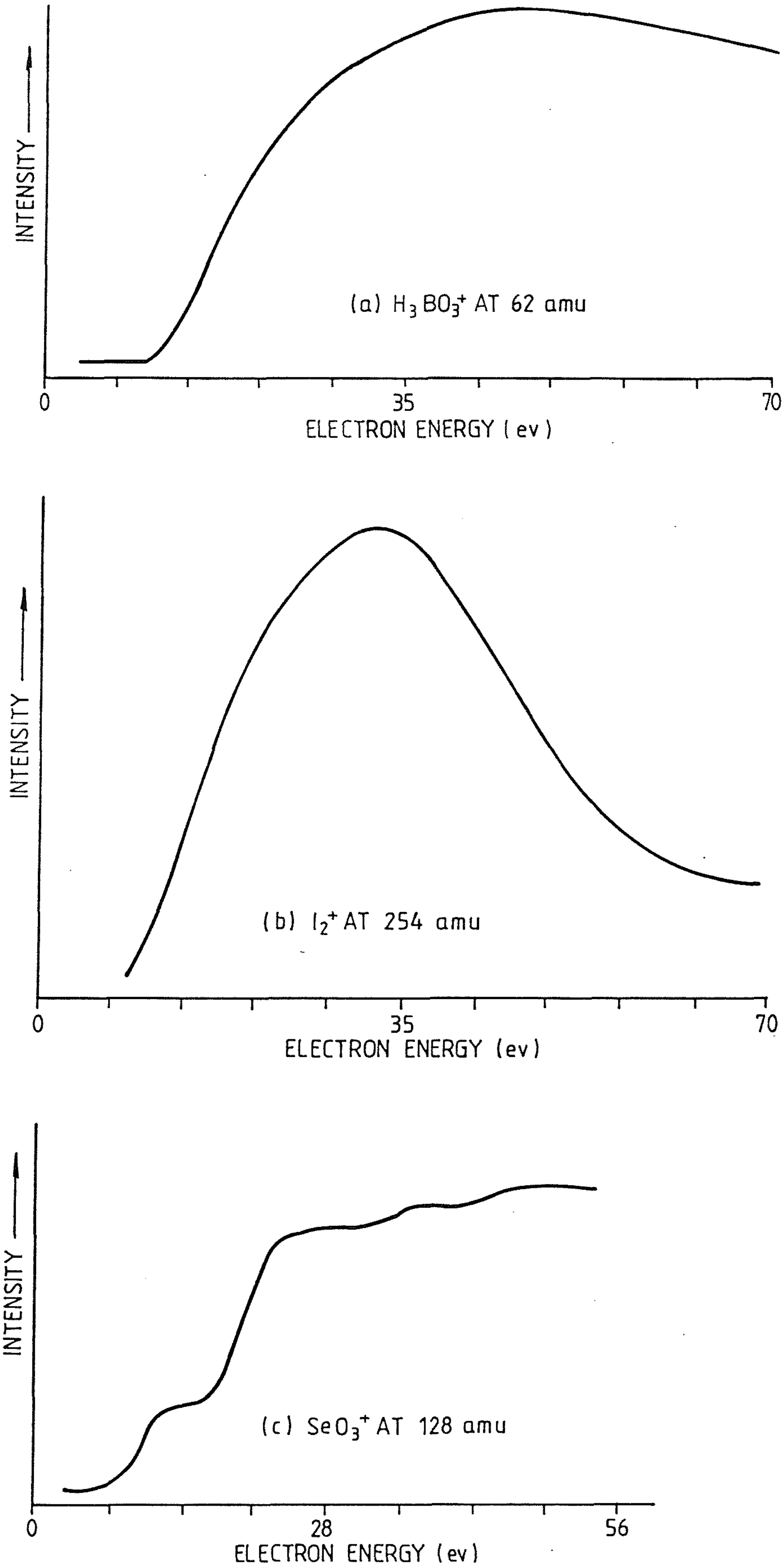

FIG. 6 REPRESENTATIVE IONISATION EFFICIENCY CURVES OBSERVABLE IN MASS SPECTROMETRY

experiments because it is not accumulative and also to discriminate against the background features.

The experimental arrangement of the VG SXP 400 quadrupole mass filter and spectrometer chamber is shown in Figure 7. The quadrupole analyser (a) is seated in the "dural" chamber (k) by means of a rotable double 'O' ring seal (d) and Teflon gasket (e). The radiation shield (c) is used to protect the delicate exposed parts from the high temperature vapours during degassing and spectral observation. The ion source (b) contains two tungsten filaments and is mounted perpendicular or "cross axis" to the sample molecular beam. The sample inlet ports (f) are identical to those used on the matrix rigs so that minimum contamination is caused on transfer of samples, especially of those isotopically enriched. The small port (g) is used for the admission of gaseous samples or the PFK standard (used for calibration) via needle valves. The perspex windows (h) allow the operator to align the ion source and sample holder to be in line of sight of each other to maximise sensitivity. The vacuum is monitored by a Penning gauge (j) and an ion gauge (i). The ion gauge also acts as the protection system in that if the pressure exceeds a pre-set limit (usually 1.5×10^{-5} torr) either because of a leak or rapid vaporisation of the sample, the entire quadrupole system is depowered. This thus protects both the filaments and the channeltron from serious degradation.

The necessary high vacuum was achieved by two Edwards Diffstacks backed by rotary pumps in conjunction with liquid nitrogen traps.

(a) QUADRUPOLE ASSEMBLY
(b) ION SOURCE CHAMBER
(c) RADIATION SHIELD
(d) DOUBLE 'O' RING SEAL
(e) TEFLON GASKET
(f) BRASS RING
(g) SECONDARY PORT
(FOR PFK CALIBRANT AND GAS SAMPLES)
(h) PERSPEX WINDOWS
(i) ION GAUGE HEAD
(j) PENNING GAUGE HEAD
(k) 'DURAL' VACUUM CHAMBER

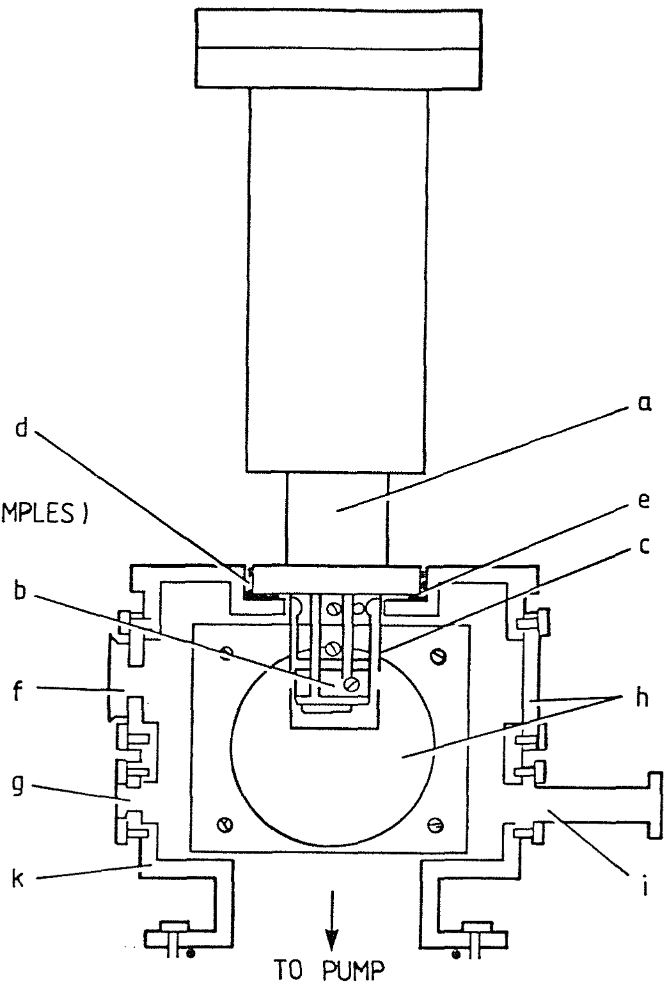

A. CROSS-SECTION OF QUADRUPOLE ANALYSER AND SPECTROMETER CHAMBER.

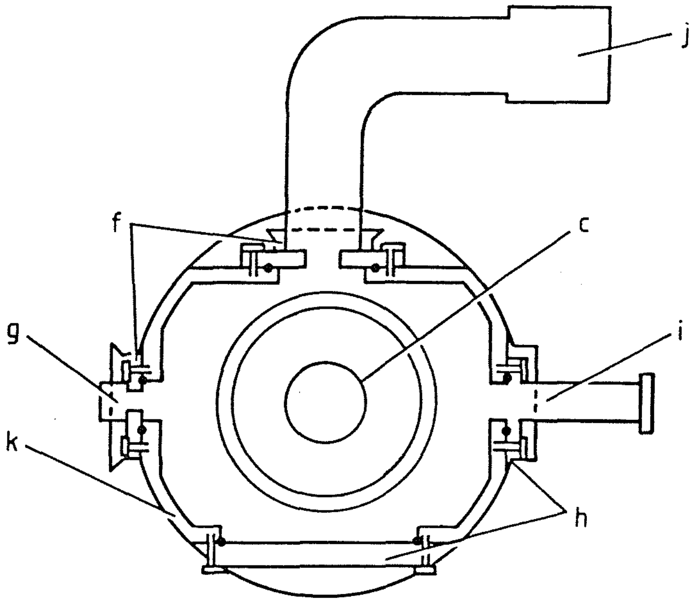

B. PLAN DIAGRAM OF SPECTROMETER CHAMBER FROM BELOW.

FIG. 7 ARRANGEMENT OF QUADRUPOLE MASS SPECTROMETER AND VACUUM CHAMBER.

7. References

1. Redington R.L. and Milligan D.E.
J. Chem. Phys., 39, 1276, 1963.

2. Hallam H.E.
"Vibrational Spectroscopy of Trapped Species",
Wiley, 1973.

3. See chapter 3.

4. Moscovits M. and Ozin G.A.
"Cryochemistry", Wiley, 1976.

5. Mile B., Angew. Chem., 7, 507, 1968.

6. p39 of ref 2.

7. p 24 of ref 4.

8. Beattie I.R. and McDermott S.D.
University of Southampton, Personal Communication, 1987.
Beattie I.R., Blayden H.E. and Ogden J.S.
J. Chem. Phys., 64, 909, 1976.
Beattie I.R., Blayden H.E., Hall S.M., Jenny S.N. and
Ogden J.S.
J. Chem. Soc. Dalton Trans., 1978, 666.
Lesiecki M.L. and Shirk J.S.
J. Chem. Phys., 56, 4171, 1972.

9. Beattie I.R., Jones P.J., Millington K.R. and
Willson A.D.
J. Chem. Soc. Dalton Trans., in press.

10. Beattie I.R. and Millington K.R.
J. Chem. Soc. Dalton Trans., 1987, 1521.

11. Barnes A.J., Hallam H.E. and Scrimshaw G.F.
Trans. Farad. Soc., 65, 3150, 1969.

12. Poliakoff M. and Turner J.J.
J. Chem. Soc. Dalton Trans., 1973, 1351.

13. Hauge R.H., Gransden S., Wang J. and Margrave J.L.
Ber. Buns., 82, 104, 1978.

14. De Vore T.C. and Franzen H.F.
High Temp. Sci., 7, 220, 1975.

15. Smyrl N. and Devlin J.P.
J. Phys. Chem., 77, 3067, 1973.

16. Barnes A.J.
Chapter 4 in ref 2.

17. See Chapter 7.

18. Jacox M.E.
J. Mol. Spect., 113, 286, 1985.

19. See Chapter 5.

20. Knozinger E. and Willengeck R.
Infra Red Phys., 24, 135, 1984.

21. Brisdon A.K. and Ogden J.S.
J. Mol. Struct.,
157, 141, 1987.

22. Perutz R.N.
Chem. Rev., 85, 77, 1985.

23. Clementi E., Kistermaeher H. and Popkie H.
J. Chem. Phys., 58, 2460, 1973.

24. Ogden J.S. and Wyatt R.M.
J. Chem. Soc. Dalton Trans., 1986, 859.

25. Hope E.G., Levason W. and Ogden J.S.
J. Chem. Soc. Dalton Trans., 1988, 61 and 997.

26. Knight L.R., Gregory B.W., Cograncki S.T., Feller D. and Davidson E.R.
J. Am. Chem. Soc., 109, 3521, 1987.

27. Cole A.R.H.
"Tables of Wavenumbers for the Calibration of Infrared Spectrometers". IUPAC. Pergamon 1977.

28. Errock G.A.
pl "Mass Spectrometry" Ed Reed R.I., Academic Press 1965.

29. Damoth D.C.
p67 in ref 28.

30. Creasey W.R., O'Keefe A. and McDonald J.R.
J. Phys. Chem., 91, 2848, 1987.

31. Brunne C.
J. Int. Mass Spec. and Ion Proc., 76, 125, 1987.

32. Paul W. and Steinwedel H.
Z. Naturforsch., 84, 448, 1953.

33. Paul W. and Raether H.
Z. Phys., 140, 262, 1955.

34. Litzow M.R. and Spalding T.R.
"Mass Spectrometry of Inorganic and Organometallic Compounds". Elsevier 1973.

35. Preiss H.
Z. Anorg. Allg. Chem., 389, 280, 1972.

36. Grimley R.T. and Forsman J.A.
NBS Special Report, 561/1, 211, 1978.

37. Stearns C.A., Kohl E.J., Fryberg G.G. and Miller R.A.
NBS Special Report, 561/1, 303, 1978.

38. Alexander C.A.
Columbus Battelle Labs., Personal Communication 1987.

39. See Chapter 7.

40. Brisdon A.K.
PhD Thesis, University of Southampton, 1988.

41. Wahrhaftig A.L.
p137 in ref 28.

42. Collin J.E.
p183 in ref 28.

43. Collin J.E.
p201 in ref 28.

CHAPTER THREE

VIBRATIONAL ANALYSIS AND MOLECULAR VIBRATIONS

1. Introduction

Once an infrared spectrum of a matrix isolated species has been recorded it needs to be interpreted and then used to characterise the trapped molecule. In the previous chapter it was shown how it is possible to identify the frequencies arising from monomerically trapped species. In this chapter it will be shown how the observed fundamentals and their relative intensities can give valuable structural information such as approximate bond angles and force constants.

This characterisation takes place in two distinct steps. The first step is qualitative, and makes use of group theoretical principles to determine the symmetry and hence shape of the molecule by comparing the number of observed fundamental frequencies with those predicted for model structures. The more complete characterisation takes place in the second step which uses normal co-ordinate analysis to relate the experimental frequencies and intensities to molecular parameters such as force constants and bond angles. Both stages of the analysis are enhanced enormously if isotopic substitution can be used. In this work, Wilson's GF method with a general valence force field (GVFF) or a simplified valence force field (SVFF) has been used.

2. Vibrations of a Diatomic Molecule

Although all the systems studied were polyatomic, it is instructive to look at the case for a diatomic species first, because of its simplicity. Quantum mechanical considerations reveal that the vibrations of two nuclei in a diatomic molecule can be reduced to the motion of a single particle of mass, μ, whose displacement q from its equilibrium position is equal to the change in the internuclear distance. The mass μ is known as the reduced mass and is given by

$$\mu = \frac{m_1 m_2}{m_1 + m_2}$$

where m_1 and m_2 are the masses of the two nuclei.

The kinetic energy (T) of the system is given by

$$T = \frac{1}{2}\mu\dot{q}^2 = \frac{p^2}{2\mu} \qquad (p = \mu\dot{q}) \qquad (1)$$

$$(\dot{q} = \frac{dq}{dt})$$

One usually assumes that the vibrations are harmonic and by doing so, can use Hooke's law for expressing the potential energy (V) thus

$$V = \frac{1}{2} Kq^2 \qquad (2)$$

where K is the force constant for the vibration.

This enables the Schrödinger equation to be written as

$$\frac{d^2\psi}{dq^2} + \frac{8\pi^2\mu}{h^2}(E - \frac{1}{2}Kq^2)\psi = 0 \qquad (3)$$

When this is solved using the usual quantum mechanical boundary conditions of ψ being single valued, finite and continuous, the eigenvalues (E_v) are given as

$$E_v = h\nu(v + \frac{1}{2}) \qquad (4)$$

where the frequency $\nu = \frac{1}{2\pi}\sqrt{(K/\mu)}$ (5)

v is the vibrational quantum number and can take the values 0, 1, 2, 3, etc. The eigenfunctions, ψ_v have been evaluated and take the form of Hermite polynomials.

The majority of infrared spectroscopists express the value of the fundamental transitions in reciprocal wavelengths or wavenumbers, $\tilde{\nu}$ in units of cm^{-1}. These are related to the frequency by $\tilde{\nu} = \nu/c$.*

As is well known the potential curve of a vibrating molecule is not harmonic and is better approximated by the addition of higher terms to the potential energy thus([1], [2]):

$$V = \tfrac{1}{2}Kq^2 - Gq^3 \quad (K \gg G) \qquad (6)$$

The eigenvalues are then given by

$$E_v = hc\omega_e\ (v + \tfrac{1}{2}) - hcx_e\omega_e\ (v + \tfrac{1}{2})^2 + \ldots . \qquad (7)$$

ω_e is the wavenumber corrected for anharmonicity and the $x_e\omega_e$ term indicates the magnitude of the anharmonicity ($\omega_e = 2x_e\omega_e + \tilde{\nu}$). The physical result of the above equation is that the energy levels of an anharmonic oscillator are not equally spaced, but that the separation decreases as v increases. It is the anharmonicity that is also responsible for overtones and combination vibrations, which are forbidden in the harmonic oscillator approximation.

The force constant K can be imagined to be a measure of the curvature of the potential well near the equilibrium position, ie,

---

* Although wavenumbers should be labelled $\tilde{\nu}$, in practice only ν is used and that is the convention adopted in the later chapters.

$$K = \left(\frac{d^2V}{dq^2}\right)_{q\to 0}$$

the depth of the well however is dependent on the dissociation energy D_e. Therefore a large force constant implies sharp curvature of the potential well, but does not necessarily indicate a deep well.

3. Polyatomic Systems

3.1 Normal Vibrations and Normal Co-ordinates

In polyatomic systems the situation is much more complex because in general all the nuclei undergo (periodic) oscillations simultaneously. This complexity can be reduced if one uses the concept of normal vibrations. It can then be shown that any of the extremely complicated vibrations of the molecule can be represented as a superposition of these normal vibrations. If the displacement of each nucleus is expressed in a rectangular co-ordinate system with the origin of the equilibrium position of each nucleus then the kinetic energy for an N atom molecule is given by:

$$T = \frac{1}{2}\sum_N m_N\left(\left(\frac{d\Delta x_N}{dt}\right)^2 + \left(\frac{d\Delta y_N}{dt}\right)^2 + \left(\frac{d\Delta z_N}{dt}\right)^2\right) \qquad (8)$$

this expression can be rewritten as:

$$T = \frac{1}{2}\sum_i^{3N} \dot{q}_i^2 \qquad (9)$$

if the mass weighted co-ordinates

$q_1 = \surd m_1\Delta x_1$, $q_2 = \surd m_1\Delta y_1$, $q_3 = \surd m_1\Delta z_1$, $q_4 = \surd m_2\Delta x_1$, etc are used.

The potential energy of the system is a function of the displacements and is hence a complicated function of the q's. If the displacements are small then the potential energy V may be expressed as a Taylor power series(³,⁴) in q_i, thus:

$$V(q_1 q_2 q_3 \cdots\cdots q_{3N}) = V_o + \sum_{i}^{3N} \left\{ \frac{\partial V}{\partial q_i} \right\}_0 q_i + \frac{1}{2} \sum_{i,j}^{3N} \left\{ \frac{\partial^2 V}{\partial q_i \, \partial q_j} \right\}_0 q_i q_j + \text{higher terms} \qquad (10)$$

The V_o term is taken as zero if the potential energy at $q_i = 0$, which is the usual convention. The $\left\{ \frac{\partial V}{\partial q_i} \right\}_0$ terms are also zero because V must be a minimum at $q_i = 0$.

Therefore V can be expressed as:

$$V = \frac{1}{2} \sum_{i,j}^{3N} \left\{ \frac{\partial^2 V}{dq_i \, dq_j} \right\}_0 q_i q_j = \frac{1}{2} \sum_{i,j}^{3N} b_{ij} q_i q_j \qquad (11)$$

if the higher order terms are neglected.

If it were not for the presence of the cross term products such as $q_i q_j$ then the problem could be solved directly using Lagrange's form of Newton's equation, ie,

$$\frac{d}{dt} \left\{ \frac{\partial T}{\partial \dot{q}_i} \right\} + \frac{\partial V}{\partial q} = 0 \quad i = 1,\ 2 \ldots\ldots \ 3N \qquad (12)$$

which in turn could be expressed as:

$$\ddot{q}_i + \sum_j b_{ij} q_j = 0 \quad j = 1,\ 2,\ \ldots\ 3N \qquad (13)$$

If $b_{ij} = 0$ for $i \neq j$ this then becomes:

$$\ddot{q}_i + b_{ii} \, q_i = 0 \qquad (14)$$

whose solution can be given as:

$$q_i = q_i^0 \sin(\sqrt{b_{ii}}t + \delta_i) \qquad q^0 = \text{amplitude} \qquad (15)$$

$$\delta_i = \text{phase constant}$$

However, this simplification is not usually possible, and the mass weighted co-ordinates q_i have to be transformed into a new set of normal co-ordinates Q_i,

where
$$q_1 = \sum_i B_{1i} Q_i$$

$$q_2 = \sum_i B_{2i}\ Q_i$$

$$\vdots \qquad (16)$$

$$q_k = \sum_i B_{ki} Q_i$$

If one chooses the coefficients of B_{ki} appropriately then the kinetic and potential energies can be written without any cross products thus

$$T = \frac{1}{2}\sum_i \dot{Q}_i^2 \qquad (17)$$

$$V = \frac{1}{2}\ \sum_i \lambda_i Q_i^2 \qquad (18)$$

If these equations are then combined with Newton's equation the following is found:

$$\ddot{Q}_i + \lambda_i Q_i = 0 \qquad (19)$$

and the solution is given by:

$$Q_i = Q_i^0 \sin\ (\sqrt{\lambda_i}t + \delta_i) \qquad (20)$$

The frequency ν_i is

$$\nu_i = \frac{1}{2\pi} \sqrt{\lambda_i} \tag{21}$$

The vibrations ν_i are the normal vibrations mentioned earlier.

In an N atom molecule there are 3N degrees of freedom, and in general there will be 3N-6 vibrational degrees of freedom. This is because 3 degrees of freedom are required to describe the translational motion of the molecule whilst another 3 are required for the rotational description. Thus the complex vibration is a superposition of the 3N-6 normal vibrations.

In order to obtain a physical picture of normal vibrations the case when only one such vibration is excited will be considered. The mass weighted co-ordinate q_k is related to the normal co-ordinate Q_i by

$$q_k = \sum_i B_{ki} Q_i \tag{22}$$

Because the normal vibrations are independent of one another the case when $Q_1^\circ \neq 0$ but $Q_2^\circ = Q_3^\circ = 0$ etc can be separated

$$\therefore\ q_k = B_{k1} Q_1 = B_{k1} Q_1^\circ \sin(\sqrt{\lambda_1} t + \delta_1) \tag{23}$$

$$= A_{k1} \sin(\sqrt{\lambda_1} t + \delta_1) \tag{24}$$

From this relation it can be seen that the excitation of one normal vibration (ν_1) of the system causes vibrations of all the nuclei in the system. Therefore in a normal vibration all the nuclei move with the same frequency and in phase with each other.

3.2 Spectroscopic Selection Rules

The normal frequencies described in the preceding section are simple harmonic and therefore the harmonic selection rule ($\Delta v = \pm 1$) is applicable. However, the infrared and Raman spectra of non-linear polyatomics do not in general show 3N-6 fundamentals because the occurrence of ir absorption is governed by another set of rules known as the symmetry selection rules.

The infrared selection rule can be expressed as "energy can only be absorbed or emitted if the change in vibrational state is accompanied by a change in the molecular dipole moment".

Quantum mechanically it can be shown(3,4) that the intensity of a vibrational transition (in the infrared region of the spectrum) is dependent upon the transition moments

$$
\begin{aligned}
[\mu_x]_{v'v''} &= \int \psi_{v'} \mu_x \psi_{v''} \, d\tau \\
[\mu_y]_{v'v''} &= \int \psi_{v'} \mu_y \psi_{v''} \, d\tau \qquad (25) \\
[\mu_z]_{v'v''} &= \int \psi_{v'} \mu_z \psi_{v''} \, d\tau
\end{aligned}
$$

where μ_x is the magnitude of the molecular dipole moment in the x direction, ψ is the vibrational eigenfunction and v' and v'' are the vibrational quantum numbers before and after the transition respectively.

These three equations can be expressed as:

$$\underline{\mu}_{v'v''} = \int \psi_{v'} \, \underline{\mu} \, \psi_{v''} \, d\tau \qquad (26)$$

where $\underline{\mu}$ is the vector representing the cartesian molecular dipoles.

At first sight this appears to imply that only molecules with permanent dipoles will have ir active vibrational modes. If this was the case the usefulness of vibrational spectroscopy would be very limited, but it is well known that molecules that do not have permanent dipoles, eg, CO_2, do have ir active fundamental frequencies. This can be explained if equation (26) is expanded in a Taylor series(³,⁴) thus

$$\underline{\mu}_{\underline{v}'\underline{v}''} = \underline{\mu}_0 \int \psi_{v'} \psi_{v''} \, d\tau + \sum_k \left(\left\{ \frac{d\underline{\mu}}{dQ_k} \right\}_0 \int \psi_{v'} Q_k \psi_{v''} \, d\tau \right) \qquad (27)$$

Because the wave functions ψ are orthogonal, the first integral vanishes unless v' and v'' are the same. This however corresponds to no transition. Therefore the permanent molecular dipole moment, $\underline{\mu}_0$, has no influence on the intensity of the vibrational transitions. (It does however determine the intensity of bands in pure rotational spectra.) If the second term is expanded then it is found that it is only non-vanishing if the following criteria are met.

(a) For all the modes except the k^{th}, the two states v' and v'' are identical and

(b) For the k^{th} mode the vibrational quantum number must only change by unity, ie, $\Delta v = \pm 1$.

It does not follow though that all such modes will in fact be active because the second term on the right hand side also includes the $\left\{ \frac{\partial \underline{\mu}}{\partial Q_k} \right\}_0$ terms. Hence a transition will only be ir active if $(\partial \mu_x / \partial Q_k)_0$, $(\partial \mu_y / \partial Q_k)_0$ or $(\partial \mu_z / \partial Q_k)_0$ are non zero. Therefore a transition between two vibrational levels is only ir active if there is a dipole change involved in the vibration and if the vibrational quantum number does not change by more than one.

It can be shown(2) that if v' = 0, (ie the vibrational ground state) then the simple harmonic wave functions are totally symmetric. If v'' = 1 (the first vibrationally exited state) then the wave functions belong to the same symmetry species as the vibrational mode. For one of the integrals to be non zero, it must then be invariant to all symmetry operations of the molecular point group. For this to happen the product $\mu\psi_{v'}$ must contain the totally symmetric species and this by consulting "direct product" tables implies that μ and ψ' must belong to the same irreducible representation. As μ_x, μ_y and μ_z transform as translations in the directions x, y and z then for a vibration to be infrared active its symmetry species must be the same as one of the components of the electric moment of the molecule.

Therefore from the above comments it can be seen that the number of ir active fundamentals in any given polyatomic molecule is intimately linked with the symmetry properties of that molecule and hence much valuable information can be gleaned by band counting. In order to determine how many of the 3N-6 normal vibrations will be ir active one needs to make use of Group theory.

3.3 The Symmetry and Number of Normal Modes

In this section the preceding ideas about normal vibrations will be used in order to fulfil the first stage in the characterisation of a species, ie. the determination of its shape by the use of group theory(4,5).

If the molecular formula of the species is known then one has to choose chemically sensible models and determine the number of ir active modes for each model. These can then be compared with the observed spectra and from this it is possible to choose one of the models as the probable shape.

If the molecular formula is not known, then models for a variety of formulae have to be chosen and in a similar manner it is possible to end up with a probable shape. One has to exercise some caution however, because group theory only predicts whether fundamental frequencies are ir active, but does not give any indication of the relative intensities. In some cases a fundamental may be technically ir active but have a very low intensity so that it cannot be observed above the noise level.

In order to illustrate the principles the YXY type molecule will be utilised as an example. This can be either bent or linear, the former having C_{2v} point group whilst the latter is $D_{\infty h}$. If the group symmetry operations of each molecular point group are applied to a set of 3N atomic cartesian displacement vectors or a set of 3N-6 internal co-ordinates and the appropriate equations (2,3,4,5) used, this then gives rise to what is termed an irreducible representation.

This irreducible representation (Γ_{3N}) is determined by considering the effect on the cartesian displacement co-ordinates of each of the symmetry operations of the molecular point group in turn. As can be imagined there are a number of short cuts available because the effect on the cartesian displacement co-ordinates by each operation is similar in each point group.

The most commonly used method, is to consider how many unshifted atoms there are after each of the symmetry operations has been carried out. To convert this into Γ_{3N}, these values need to be multiplied by a "contribution to character per unshifted atom", and these are widely listed (eg ref 6).

In order to get the vibrational irreducible representation, Γ_{vib}, one needs to subtract the rotational and translational irreducible representations (Γ_{rot} and Γ_{trans}) from Γ_{3N}. The separation of stretching and deformation (both in plane and out of plane) modes is achieved by using the number of unshifted bonds, bends, etc. under each symmetry operation to give Γ_{str} and Γ_{bend} etc.

If this is done for the two YXY cases then the following results.

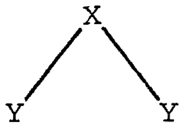

C_{2v}

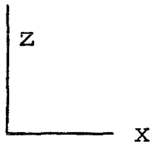

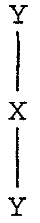

$D_{\infty h}$

$\Gamma_{3N} = 3A_1 + A_2 + 3B_1 + 2B_2$	$\Gamma_{3N} = \Sigma_g^+ + \Pi_g + 2\Sigma_u^+ + 2\Pi_u$
$\Gamma_{rot} = A_2 + B_1 + B_2$	$\Gamma_{rot} = \Pi_g$
$\Gamma_{trans} = A_1 + B_1 + B_2$	$\Gamma_{trans} = \Sigma_u^+ + \Pi_u$
$\therefore \Gamma_{vib} = 2A_1 + B_1$	$\Gamma_{vib} = \Sigma_g^+ + \Sigma_u^+ + \Pi_u$
ir active $= 2A_1 + B_1$	ir active $\Sigma_u^+ + \Pi_u$
$\Gamma_{str} = A_1 + B_1$	$\Gamma_{str} = \Sigma_g^+ + \Sigma_u^+$
$\Gamma_{bend} = A_1$	$\Gamma_{bend} = \Pi_u$

Therefore an ir spectrum of an YXY molecule containing 3 bands could be assigned to a C_{2v} structure whilst one containing only 2 bands could be assigned to a $D_{\infty h}$ structure. This approach begins to breakdown when the bond angle approaches 180° as the symmetric stretch will only have a low intensity. The use of isotopic data can make this assignment more rigorous especially if the substitution occurs at the Y atoms thus

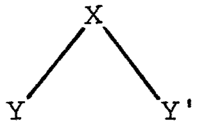

C_s

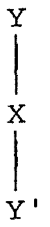

$C_{\infty v}$

$\Gamma_{vib} = 3A'$	$\Gamma_{vib} = 2A_1 + E_1$
ir active = $3A'$	ir active $2A_1 + E_1$

Hence in a bent molecule one would expect to see 9 bands, (3 from each isotopomer), whereas in a linear molecule only seven are anticipated to be observed.

A similar strategy can be used for other molecules where a variety of structures are possible

eg	XY_3	C_{3v} or D_{3h}
	XY_4	T_d or D_{4h}
	XY_5	D_{3h} or C_{4v}

If one is considering the mode of co-ordination of a cation to an anion(7), eg $M^+ReO_4^-$, then by calculating the expected number of bands for mono (C_{3v}) bi (C_{2v}) or tridentate (C_{3v}) co-ordination of the cation and comparing these to the number of bands observed, a structure can be inferred.

Therefore having decided upon a probable shape of the molecule by group theory and band counting a more quantitative approach such as normal co-ordinate analysis can be employed. This can be used to calculate force fields which in turn can be used to generate intensity patterns and isotopic frequencies, which can then be compared with the observed spectrum.

4. **Wilson's GF Method**

In the calculation of Γ_{vib} and its components Γ_{str} and Γ_{bend} use was made of the Y-X bond distance and the Y-X-Y bond angle as generators. These are known as internal co-ordinates and their use in normal co-ordinate analysis gives a much clearer physical meaning to the force constants obtained. In addition they do not contain any rotational and translational components.

As described previously the frequency of a normal vibration is determined by the kinetic and potential energies of the system. The kinetic energy is proportional to the masses of the atoms in the molecule and their geometrical arrangement. The potential energy however arises from the interaction between the individual atoms, and these interactions are usually described in terms of force constants. These force constants provide valuable data about the nature of interatomic forces and it is usually the practice to obtain values for them from the observed frequencies. Structural information can also be obtained, especially from isotopically substituted species and also by consideration of the relative intensities.

For the bent XY_2 molecule the following internal co-ordinates can be defined

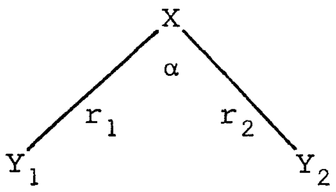

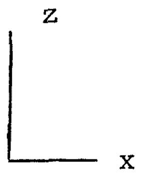

and hence the displacement co-ordinates are defined as Δr_1, Δr_2 and $\Delta\alpha$. Using these internal co-ordinates the potential energy can be written as

$$2V = \underline{\tilde{R}}\ \underline{F}\ \underline{R} \tag{28}$$

where $\underline{R}$ is of the form $\begin{bmatrix} \Delta r_1 \\ \Delta r_2 \\ \Delta\alpha \end{bmatrix}$ (29)

$\underline{\tilde{R}}$ is the transpose of $\underline{R}$, ie $[\Delta r_1,\ \Delta r_2,\ \Delta\alpha]$ (30)

and $\underline{F}$ is a matrix of force constants thus

$$\underline{F} = \begin{bmatrix} f_{11} & f_{12} & r_1 f_{13} \\ f_{21} & f_{22} & r_2 f_{23} \\ r_1 f_{31} & r_2 f_{32} & r_1 r_2 f_{33} \end{bmatrix} = \begin{bmatrix} F_{11} & F_{12} & F_{13} \\ F_{21} & F_{22} & F_{23} \\ F_{31} & F_{32} & F_{33} \end{bmatrix} \tag{31}$$

where f_{11} and f_{22} are the stretching force constants of the X-Y_1 and X-Y_2 bonds respectively, and f_{33} is the bending force constant of the Y_1-X-Y_2 angle. The other symbols represent interaction force constants between the stretching and stretching, or between the stretching and bending vibrations. In order to make the dimensions of all the force constants the same (mdyn/Å) f_{13} (or f_{31}) f_{23} (or f_{32}) and f_{33} need to be multiplied by r_1, r_2 and $r_1 r_2$ respectively.

The kinetic energy is not so easily expressed in terms of the same internal co-ordinates but Wilson(4), has shown that it can be written as

$$2T = \underline{\tilde{\dot{R}}}\ \underline{G}^{-1}\ \underline{\dot{R}} \qquad (32)$$

where $\underline{\dot{R}}$ is the derivative with respect to time of $\underline{R}$ and $\underline{G}^{-1}$ is the reciprocal of the $\underline{G}$ matrix which will be defined later.

If equations (28) and (32) are combined with Newton's equation in Lagranges' form (12)

$$\frac{d}{dt}\left\{\frac{\partial T}{\partial \dot{R}_k}\right\} + \frac{\partial V}{\partial R_k} = 0 \qquad (33)$$

then the following secular equation is obtained

$$\begin{vmatrix} F_{11} - (G^{-1})_{11}\ \lambda & F_{12} - (G^{-1})_{12}\ \lambda \ \cdots \\ F_{21} - (G^{-1})_{21}\ \lambda & F_{22} - (G^{-1})_{22}\ \lambda \ \cdots \\ \cdot & \cdot \\ \cdot & \cdot \\ \cdot & \cdot \\ \cdot & \cdot \end{vmatrix} = \left|\underline{F} - \underline{G}^{-1}\lambda\right| = 0$$

$$(34)$$

If this is multiplied through by the determinant of $\underline{G}$

ie
$$\begin{vmatrix} G_{11} & G_{12} & \cdots \\ G_{21} & G_{22} & \cdots \\ G_{31} & \cdots & \cdots \end{vmatrix} = \left|\underline{G}\right| \qquad (35)$$

this then gives equation (34) as

$$\begin{vmatrix} \sum G_{1t}F_{t1} - \lambda & \sum G_{1t}F_{t2} & \cdots \\ \sum G_{2t}F_{t1} & \sum G_{2t}F_{t2} - \lambda & \cdots \\ \cdot & \cdot & \\ \cdot & \cdot & \\ \cdot & \cdot & \\ \cdot & \cdot & \end{vmatrix} = \left| \underline{G}\ \underline{F} - \underline{E}\ \lambda \right| = 0 \qquad (36)$$

$\underline{E}$ is the identity matrix and λ is related to the wavenumber, $\tilde{\nu}$, by the relation $\lambda = 4\pi^2c^2\tilde{\nu}^2$ and $\tilde{\nu} = 1302.83\sqrt{\lambda}$. The order of the equation is equal to the number of internal co-ordinates used.

The $\underline{F}$ matrix is written by assuming a suitable set of force constants, it is however the $\underline{G}$ matrix that is more difficult to construct. If the $\underline{G}$ matrix elements are derived by the following method then by solving equation (36) the calculated vibrational frequencies are obtained.

If the $\underline{G}$ matrix is defined as:

$$\underline{G} = \underline{B}\ \underline{M}^{-1}\ \underline{\tilde{B}} \qquad (37)$$

Where $\underline{M}^{-1}$ is the diagonal matrix whose components are μ_i, the reciprocal masses of the ith atom. For a bent XY_2 molecule

$$M^{-1} = \begin{bmatrix} \mu_1 & 0 & 0 & & 0 \\ 0 & \mu_1 & 0 & \cdots\cdots & \\ 0 & 0 & \mu_1 & \cdots\cdots & \\ \cdot & \cdot & \cdot & \ddots & \\ \cdot & \cdot & \cdot & \mu_2 & \cdots \\ \cdot & \cdot & \cdot & & \ddots \\ 0 & \cdot & \cdot & & \mu_3 \end{bmatrix} \tag{38}$$

The $\underline{B}$ matrix is defined as

$$\underline{R} = \underline{B}\ \underline{X} \tag{39}$$

where $\underline{R}$ and $\underline{X}$ are column matrices whose components are the internal and rectangular co-ordinates respectively, ie. it is the matrix that converts the rectangular displacement co-ordinates to internal displacement co-ordinates. Having achieved the $\underline{B}$ matrix the individual elements of the $\underline{G}$ matrix are given by:

$$G_{tt'} = \sum_{i=1}^{3N} \mu_i \ B_{ti}\ B_{t'i} \tag{40}$$

5. The Use of Symmetry Properties to Reduce the Complexity of FG Analysis

In the bent XY_2 molecule the two X-Y bonds are equivalent and hence both the internal co-ordinates Δr_1 and Δr_2 will be equivalent. If a molecule possesses such symmetrically equivalent sets of internal co-ordinates it is possible to reduce the order of the $\underline{F}$ and $\underline{G}$ matrices and therefore the order of the secular equation by use of a co-ordinate transformation.

If the internal co-ordinate matrix, $\underline{R}$ is transformed by the transformation matrix $\underline{U}$ to the symmetry co-ordinate matrix $\underline{S}$ thus:

$$\underline{S} = \underline{UR}$$

Then: $$2T = \tilde{\dot{\underline{R}}}\ \underline{G}^{-1}\ \dot{\underline{R}} = \tilde{\dot{\underline{S}}}\ \tilde{\underline{U}}^{-1}\ \underline{G}^{-1}\ \underline{U}^{-1}\ \dot{\underline{S}}$$

$$= \tilde{\dot{\underline{S}}}\ \underline{G_s}^{-1}\ \dot{\underline{S}} \qquad (42)$$

where $\underline{G_s}^{-1} = \tilde{\underline{U}}^{-1}\ \underline{G}^{-1}\ \underline{U}^{-1}$

and $2V = \tilde{\underline{R}}\ \underline{F}\ \underline{R} = \tilde{\underline{S}}\ \tilde{\underline{U}}^{-1}\ \underline{F}\ \underline{U}^{-1}\ \underline{S}$

$$= \tilde{\underline{S}}\ \underline{F_s}\ \underline{S} \qquad (43)$$

and $\underline{F_s} = \tilde{\underline{U}}^{-1}\ \underline{F}\ \underline{U}^{-1}$ (44)

If $\underline{U}$ is an orthogonal matrix then equations (42) and (44) can be expressed as

$$\left.\begin{aligned} \underline{G_s} &= \underline{U}\ \underline{G}\ \tilde{\underline{U}} \\ \underline{F_s} &= \underline{U}\ \underline{F}\ \tilde{\underline{U}} \end{aligned}\right. \qquad (45)$$

It can be shown that $\left|\underline{G_s}\ \underline{F_s} - \underline{E}\ \lambda\right| = \left|\underline{G}\ \underline{F} - \underline{E}\ \lambda\right|$ (^{2,4}) and if a proper $\underline{U}$ matrix is chosen from symmetry considerations then it is possible to "block out" or factor the original $\underline{G}$ and $\underline{F}$ matrices into smaller ones. In the case of the bent XY_2 molecule the secular equation can be factored into A_1 and B_1 components and the order of secular equations has been reduced from one of the three to one of two (A_1) and one of one (B_1). This therefore makes the solution much easier, because only a quadratic and linear expression need to be solved instead of a cubic equation.

The $\underline{U}$ matrix is constructed by use of the following equation for Δr_1:

$$\underline{S} = N \sum_K \chi_i(K) . K(\Delta r_1) \qquad (46)$$

Here K is a symmetry operation, and the summation is made over all the symmetry operations of the point group to which the molecule belongs. $\chi_i(K)$ is the character of the representation to which S belongs. Δr_1 is known as a generator and is transformed by the symmetry operation K into $K(\Delta r_1)$ which is another co-ordinate of the same symmetrically equivalent set and N is a normalising factor.

For the bent XY_2 molecule in which $\Delta r_1 = \Delta r_2$ and by use of Δr_1 as a generator the following is obtained:

C_{2v}	E	$C_{2(z)}$	σ_{xz}	σ_{yz}
$K(\Delta r_1)$	Δr_1	Δr_2	Δr_1	Δr_2
$\chi_{A_1}(k)$	1	1	1	1
$\chi_{B_1}(k)$	1	-1	1	-1

Thus $S_{A_1} = N \sum \chi_{A_1}(K) . K(\Delta r_1) = 2N(\Delta r_1 + \Delta r_2)$

$$N = \frac{1}{2\sqrt{2}} \qquad \left((2N)^2 + (2N)^2 = 1\right)$$

$$\therefore \quad S_{A_1} = \frac{1}{\sqrt{2}} (\Delta r_1 + \Delta r_2)$$

and $S_{B_1} = \frac{1}{\sqrt{2}} (\Delta r_1 - \Delta r_2)$

the remaining symmetry co-ordinate $S_{A_1} = \Delta\alpha$

Therefore

$$\begin{bmatrix} S_{1}(A_1) \\ S_{2}(A_1) \\ S_{3}(B_1) \end{bmatrix} = \begin{bmatrix} 1/\sqrt{2} & 0 & 1/\sqrt{2} \\ 0 & 1 & 0 \\ 1/\sqrt{2} & 0 & -1/\sqrt{2} \end{bmatrix} \begin{bmatrix} \Delta r_1 \\ \Delta\alpha \\ \Delta r_2 \end{bmatrix} \qquad (47)$$

$$\underline{S} = \underline{U} \quad \underline{R}$$

For an XY_3 molecule where $r_1 = r_2 = r_3$ the symmetry co-ordinates S_i for the stretching modes are given by

$$S_1 = \frac{1}{\sqrt{3}} (\Delta r_1 + \Delta r_2 + \Delta r_3) \qquad A$$

$$\left.\begin{aligned} S_2 &= \frac{1}{\sqrt{6}} (2\Delta r_1 - \Delta r_2 - \Delta r_3) \\ S_3 &= \frac{1}{\sqrt{2}} (\Delta r_2 - \Delta r_3) \end{aligned}\right\} \qquad E$$

In this case, S_2 and S_3 are orthogonal and therefore represent a doubly degenerate mode. In a triply degenerate mode there will be three orthogonal symmetry co-ordinates.

These symmetry co-ordinates are not only useful in blocking out the secular equation, they also give an indication of which atoms are moving relative to each other in any vibrational mode. In the bent XY_2 case the A_1 stretching mode is represented by $S = \frac{1}{\sqrt{2}} (\Delta r_1 + \Delta r_2)$, therefore both the bond lengths are increasing and decreasing in phase whereas for B_1, $S = \frac{1}{\sqrt{2}} (\Delta r_1 - \Delta r_2)$ and this implies that one bond length is increasing whilst the other is decreasing.

6. The use of Isotopic Substitution in Normal Co-ordinate Analysis

As indicated earlier the use of isotopic substitution can greatly help in the process of band counting to assign the observed number of fundamentals to give a probable molecular shape. In normal co-ordinate analysis isotopic data can be used more rigorously than in the group theory approach. However before proceeding any further the assumptions that lie behind its use need to be noted. These are that the molecular geometry and force field are not altered upon isotopic substitution.

Because the frequency is proportional to $\sqrt{(\frac{1}{m})}$ it may be altered significantly upon substitution of m. The frequency shift is greatest for hydrogen-deuterium substitution and in the limiting case when only hydrogen atom motion is involved in a normal mode a shift of $(1/\sqrt{2})$ is expected. The shift obviously gets smaller as the change in mass decreases but in matrix isolated ir spectra, bands that are 2cm^{-1} apart can be observed, so that it is usually possible to detect the splitting arising from the natural isotope distribution of chlorine in transition metal chlorides.

There are two important rules that have been found to hold on isotopic substitution and these are known as the product rule and the sum rule respectively.

6.1 The Product Rule

If $\lambda_1, \lambda_2 \ldots \lambda_n$ are the roots of the secular equation $|\underline{GF} - \underline{E}\lambda| = 0$

Then $\lambda_1\lambda_2 \ldots \lambda_n = |\underline{G}|\,|\underline{F}|$ holds for a given molecule.

Since it is assumed that $|F| = |F'|$, (where the prime (') indicates the isotopically substituted molecule)

$$\lambda_1'\lambda_2' \; . \; . \; . \; \lambda_n = |\underline{G}'|\,|\underline{F}|$$

$$\therefore \quad \frac{\lambda_1\lambda_2\cdots\lambda_n}{\lambda_1'\lambda_2'\cdots\lambda_n'} = \frac{|\underline{G}|}{|\underline{G}'|} \tag{48}$$

where $|\underline{G}|$ is the determinant of the $\underline{G}$ matrix. Using the relationship $\tilde{\nu} = 1302.83\sqrt{\lambda}$ the following relationship can be derived:

$$\frac{\tilde{\nu}_1\tilde{\nu}_2 \cdots \tilde{\nu}_n}{\tilde{\nu}_1'\tilde{\nu}_2' \cdots \tilde{\nu}_n'} = \sqrt{\frac{|\underline{G}|}{|\underline{G}'|}} \tag{49}$$

This relationship only holds exactly for harmonic frequencies but as the ratio of anharmonic frequencies is approximately that for harmonic frequencies it is a widely used equation.

6.2 The Sum Rule

The second important rule for frequencies of isotopically substituted species is known as the sum rule. The basis of this rule is the fact that the sum of the squares of the frequencies is a linear function of the reciprocal masses of the atoms. If therefore, several isotopic molecules can be found and geometrically superimposed with appropriate signs in such a way that the atoms vanish at all positions, the corresponding linear combination, (ie superposition,) of all the frequency sums should vanish.

Thus if

$$\sigma = \sum_k \lambda_k = 4\pi^2 \sum_k \nu_k^2 \tag{50}$$

there exist sum rules of the form

$$\sigma(HOD) + \sigma(DOH) - \sigma(HOH) - \sigma(DOD) = 0$$

$$\text{or } \sigma(HOD) + \sigma(DOH) = 2\sigma(HOD) = \sigma(HOH) + \sigma(DOD) \qquad (51)$$

for water.

For more complex molecules the situation is not so simple and the reader is directed to the references in the bibliography (eg ref 4).

7. Solution of the Secular Determinat

The solution of $\left|\underline{FG} - \underline{E\lambda}\right| = 0$ can be carried out in two ways. One is to use a computer program to calculate the $\underline{G}$ matrix elements from cartesian co-ordinates. The secular equation is then solved and the calculated vibrational frequencies compared with the observed ones. The force constant matrix $\underline{F}$ is then perturbed iteratively until good correspondance is achieved(8). The other method is to derive the $\underline{G}$ matrix elements from first principles and then to solve the secular equation on a microcomputer or a calculator. Paradoxically it has been found that the former is better for small molecules, eg up to XY_4 whilst the latter is more satisfactory for larger molecules, eg $X(YZ)_3$. This surprising result is due to the fact that as one increases the number of atoms in a molecule then the number of force constants that need to be defined using a general valence force field rises dramatically.

eg	XY_2	4 force constants
	$X(YZ)_3$	32 force constants

The number of independant force constants are 4 and 20 respectively. (If some of the interaction force constants can be set to zero then a simple valence force field can be employed.)

In order to obtain a unique force field a very large number of frequencies is thus required and this can usually only be realised by the data from different isotopic species. At present the program SOTONVIBP([9,10]) is not configured to incorporate isotopic data directly.

With the "hand written" BASIC (or FORTRAN) programs, the programmer can choose to fix or vary parameters at will, and isotopic data can be incorporated at an early stage - in some cases before the molecular geometry is established.

For the solving of the highly complex $X(YZ)_3$ problem in boric acid a program has been developed that calculates the determinant $|\underline{GF} - \underline{E}\lambda|$ directly for any given frequency. As the frequency is swept through, those values that give a determinant of zero are recorded as the roots for the parameters initially set (eg bond lengths and angles or values of force constants). The frequency can then be swept with new values until a satisfactory fit is obtained. The inclusion of the isotopic data is relatively easy and identifies the fit more rigorously. The flow diagram and listing for this are given in Appendix D.

8. Intensities

In order to discuss infrared intensities reference needs to be made to section 3.2 and equation 27 where it was noted that the intensity was dependent on $\left(\frac{d\mu}{dQ_k}\right)_0$. Therefore the magnitude of the dipole changes needs to be established and this in turn requires a knowledge of vibrational amplitudes. The vibrational amptitudes are contained in the $\underline{L}$ matrix which Wilson([4]) has defined as

$$\underline{R} = \underline{L}\,\underline{Q} \qquad (52)$$

ie $R_1 = l_{11}\, Q_1 + l_{12}\, Q_2 + \ldots\ldots + l_{1n}\, Q_n$ etc

In a normal vibration the co-ordinate Q_n changes with frequency ν_n and all the internal co-ordinates $R_1, R_2 \ldots R_i$ change with the same frequency. The amplitude of oscillation for each internal co-ordinate is however different. The relative ratios of the amplitudes of the internal co-ordinates in a normal vibration associated with the normal co-ordinate Q_n are given by

$$l_{1n} : l_{2n} : \ldots : l_{in} \tag{53}$$

If these ratios of l's are written as a column matrix $\underline{l}_N$ then the following relationship is satisfied:

$$\underline{G}\ \underline{F}\ \underline{l}_N = \underline{l}_N\ \lambda_N \tag{54}$$

Therefore once the $\underline{G}$ and $\underline{F}$ matrices have been arrived at the $\underline{l}_N$ matrix can be calculated. If one uses an assembly by columns of the l elements obtained for each λ then the following holds:

$$\underline{G}\ \underline{F}\ \underline{L} = \underline{L}\ \underline{\Lambda} \tag{55}$$

where $\underline{L}$ is the assembly of $\underline{l}_N$ and $\underline{\Lambda}$ is a diagonal matrix whose elements consist of the values of λ.

The true integrated absorption co-efficient A_n of the N^{th} normal vibration is given by (^{2,4})

$$A_n = \frac{n\pi}{3c}\left(\left\{\frac{\partial\mu_x}{\partial Q_n}\right\}_0^2 + \left\{\frac{\partial\mu_y}{\partial Q_n}\right\}_0^2 + \left\{\frac{\partial\mu_z}{\partial Q_n}\right\}_0^2\right) \tag{56}$$

where n is the number of molecules per cm^3, c is the velocity of light, μ_x μ_y and μ_z are the components of the dipole moment and Q_n is the normal co-ordinate associated with the fundamental mode.

If the "bond dipole moment" approach is used, then it is assumed that the dipole is directed along the bond and hence so is the change in dipole, and that these bond dipoles are additive. Then by use of equation (48)

$$\frac{\partial \mu}{\partial Q_n} = \sum_i \left(\frac{\partial \mu}{\partial R_i}\right)\left(\frac{\partial R_i}{\partial Q_n}\right) = \sum_i \left(\frac{\partial \mu}{\partial R_i}\right) L_{iN} \qquad (57)$$

Thus equation (56) becomes

$$A_N = \frac{n\pi}{3c}\left(\left(\sum_i \frac{\partial \mu_x}{\partial R_i} L_{iN}\right)_0^2 + \left(\sum_i \frac{\partial \mu_y}{\partial R_i} L_{iN}\right)_0^2 + \left(\sum_i \frac{\partial \mu_z}{\partial R_i} L_{iN}\right)_0^2\right) \qquad (58)$$

$$= \frac{n\pi}{3c} \sum_i \left(\left(\frac{\partial \mu_x}{\partial R_i}\right)_0^2 + \left(\frac{\partial \mu_y}{\partial R_i}\right)_0^2 + \left(\frac{\partial \mu_z}{\partial R_i}\right)_0^2\right) (L_{iN})^2 \qquad (59)$$

This equation thus shows that infrared intensities are dependent upon both $\frac{\partial \mu}{\partial R}$ and $\underline{L}$ matrix element values.

The $\underline{L}$ matrix elements are calculated by the SOTONVIBP program and contained in the $\underline{L}_R$ matrix, which gives the change in internal co-ordinate (bond) during the vibration. In order to quantify the intensities a relative dipole value is assigned to each bond, this value is then combined with the relevant $\underline{L}_R$ matrix elements which enables the components of the dipole change along the cartesian directions to be calculated(11).

The $\underline{L}_R$ values are obtained from the $\underline{L}_x$ matrix thus

$$\underline{L}_R = \underline{B}\,\underline{L}_x \qquad (60)$$

and the $\underline{L}_x$ matrix is defined as the matrix that expresses the relative displacements of the atoms in terms of rectangular co-ordinates (X) for a given normal co-ordinate (Q) thus

$$\underline{X} = \underline{L}_x \, \underline{Q} \tag{61}$$

and the values are normally calculated from

$$\underline{L}_x = \underline{M}^{-1} \, \underline{\tilde{B}} \, \underline{G}^{-1} \, \underline{L} \tag{62}$$

As can be imagined the bond dipole model is very satisfactory if one is just dealing with stretching modes, if however bending modes are to be included then the results are not satisfactory as the dipole change is now no longer directed along the bonds.

In equation (60) the $\underline{L}_x$ matrix was used to calculate the $\underline{L}_R$ matrix and it was noted that the $\underline{L}_x$ matrix expresses the relative displacements of the atoms. If each atom is assigned an effective charge and it is assumed that in any given vibration this effective charge moves with the atom, then the product of the charge and appropriate $\underline{L}_x$ matrix elements can be used to obtain a measure of the dipole change during the vibration. If these products are summed they give a measure of the total dipole change which can be related to an intensity value. This approach is known as the "point charge model"([11]).

For the band intensities calculated using SOTONVIBP the point charge model was used as this allows the inclusion of non-stretching modes.

If the frequencies have been obtained using the $\underline{G}$ matrix elements calculated on a microcomputer then it is possible to generate the $\underline{L}_x$ and $\underline{L}_R$ matrices but in practice this is rarely done. Usually one makes use of isotope intensity rules thus:

If the integrated intensity of a fundamental infrared band is proportional to the expression(4).

$$I_k = \left\{\frac{\partial \mu_x}{\partial Q_k}\right\}_0^2 + \left\{\frac{\partial \mu_y}{\partial Q_k}\right\}_0^2 + \left\{\frac{\partial \mu_z}{\partial Q_k}\right\}_0^2 = \left\{\frac{\partial \underline{\mu}}{\partial Q_k}\right\}_0 \cdot \left\{\frac{\partial \underline{\mu}}{\partial Q_k}\right\}_0 \qquad (63)$$

Then by using the internal symmetry co-ordinates, the intensities can be expressed(4) as

$$\sum_k I_k = \sum_{k'k''} \frac{\partial \underline{\mu}}{\partial S_{k'}} \cdot \frac{\partial \underline{\mu}}{\partial S_{k''}} G_{k'k''} \qquad (64)$$

and

$$\text{and} \sum_k \frac{I_k}{\lambda_k} = \sum \frac{\partial \underline{\mu}}{\partial S_{k'}} \cdot \frac{\partial \underline{\mu}}{\partial S_{k''}} F^{-1}{}_{k'k''} \qquad (65)$$

If the molecule under consideration has no dipole moment and/or its symmetry species of the vibrations over which the summation of the intensities is carried out are not the same as any rotation of the molecule which moves the permanent dipole moment, these expressions will give rise to simple relations between the isotopic molecules because the $(\frac{\partial \underline{\mu}}{\partial S})$ terms are the same for both species. It can also be seen that they can only be solved directly if there are two frequencies under consideration that have an intensity greater than zero.

These considerations have been used for the intensities of the stretching modes of small molecules such as $CsAsO_2$, $NaPO_2$ and $KSbO_2$ on $^{16}O/\ ^{18}O$ substitution(12), and they have been used in the intensity calculations for boric acid.

9. Conclusions

In this Chapter the theoretical background and the various procedures used for determing molecular shapes from symmetry principles and then confirming this assignment by use of Wilson's GF form of normal co-ordinate analysis have been described in some detail. It has also been seen that isotopic substitution is an extremely important factor in carrying out these assignments.

Appendix B contains a worked example of the construction of $\underline{F}$ and $\underline{G}$ matrices for the bent XY_2 molecule.

10. References

1. Herzberg G.
"Molecular Spectra and Structure" Vol I "Spectra of Diatomic Molecules" Van Nostrand Princeton N. J. 1950. Vol II "Infrared and Raman Spectra of Polyatomic Molecules" Van Nostrand Princeton N. J. 1945.

2. Nakamoto K.
"Infrared and Raman Spectra of Inorganic and Co-ordination Compounds" 3 ed., Wiley, 1977.

3. Woodward L.A.
"Introduction to the Theory of Molecular Vibrations and Vibrational Spectroscopy". Oxford University Press, 1972.

4. Wilson E.B., Decius J.C. and Cross P.C.
"Molecular Vibrations" McCraw Hill 1955, Dover 1980

5. Cotton F.A.
"Chemical Applications of Group Theory" 2 ed, Wiley, 1971.

6. p105 of Ref 4.

7. Arthers S.A., Beattie I.R., Gomme R.A., Jones P.J. and Ogden J.S.
J. Chem. Soc. Dalton Trans., 1983, 1461.

8. Gans P.
"Vibrating Molecules", Chapman and Hall, 1971.

9. Gardner M.
PhD Thesis, University of Southampton, 1972.

10. Beattie I.R., Cheetham N., Gardner M. and Rogers D.E.
J. Chem. Soc. (A), 1971, 2240.

11. Gomme R.A.
PhD Thesis, University of Southampton, 1984.

12. Ogden J.S. and Williams S.J.
J. Chem. Soc. Dalton Trans., 1982, 825.

CHAPTER FOUR

MATRIX ISOLATION AND MASS SPECTROMETRIC STUDIES OF A TERNARY SULPHIDE WHICH IS STABLE IN THE VAPOUR PHASE

1. Introduction

The main thrust of this thesis is concerned with the identification and characterisation of vapour phase species that are postulated to be released during a severe reactor accident. This chapter however, deals with the identification of the first ternary metal sulphide to be stable in the vapour phase, and thus shows how the combination of mass spectrometry and matrix isolation can be used with great effect for any unknown high temperature system.

The study of volatile sulphides is an area which is of great importance both fundamentally and also from an applied point of view. This is of particular relevance to fossil fuel electricity generating plants, where the corrosion of steels in sulphur rich combustion conditions and the release of sulphur oxides to the atmosphere is a cause for concern.

Many metal sulphides can undergo vapour transport in the presence of species such as halogens(1) or elemental sulphur(2). However most binary metal sulphides decompose on heating in vacuo. If the metal is in its maximum formal oxidation state then the observed vapour species are usually elemental sulphur (S_n), the metal and the diatomic sulphide or its (small) oligomers(3). The recent synthesis(4) of sodium thioferrate (Na_5FeS_4) at approximately 700°C with discrete FeS_4 units suggests that some thiometallates may have an appreciable thermal stability.

The alkali metal oxyanions are well known stable vapour phase species and have been studied extensively (5-9) by Beattie and Ogden et al at Southampton over the last decade. Therefore vapour transport of the alkali metal salts of some thiometallates appeared a possibility as there is no reported data on stable vapour phase ternary sulphides.

In order that the central transition element is co-ordinatively saturated and will not form complexes (such as $M(N_2)_n$ or $M(O_2)_n$) with the matrix gases or impurities it needs to be in its highest formal oxidation state. The stability of the higher oxidation states of the transition elements generally increases from the 3d to the 4d to the 5d species. If it is assumed that a minimum of four sulphur ligands are required to "coat" the central metal atom and that the thiometallate anion has a net overall charge of not greater than 2^-, this then leads to WS_4^{2-} and ReS_4^- as the most likely candidates.

Previous studies([9], [10]) on the vapour transport of compounds containing alkali metal cations indicated that the caesium salts would be the most volatile and also less susceptible to thermal decomposition.

Data in the literature suggested that the alkali metal thioperrhenates were unstable([11]). In contrast the alkali metal thiotungstates have been known for over a hundred years([12]). It was therefore considered that the most likely ternary sulphide to be stable in the vapour would be Cs_2WS_4.

2. Experimental

The Cs_2WS_4 was prepared by Willson and Jones (of this Department) using the following procedure, which is a modification of the method used by Gattow and Franke([13]) (The Raman spectra were recorded by Dr T R Gilson). WO_3 (5g 21.6 mmole) was added to aqueous ammonia (50 cm^3 ca 25% w/w) and water (10 cm^3). The suspension was stirred for 18 hours and the residue removed by filtration. The solution was saturated with H_2S until an orange solution was obtained (30-45 minutes) accompanied by the precipitation of a variable quantity of a citron yellow solid. (This solid was removed by filtration and its Raman spectrum corresponded to that of $(NH_4)_2 WO_2S_2$)). An equal volume of ethanol was added to the filtrate to precipitate the $(NH_4)_2WS_4$. This was removed by filtration, washed with ethanol, dried and dissolved in the minimum quantity of water. In order to precipitate the required Cs_2WS_4 from this solution, concentrated aqueous CsCl was added. The yellow precipitate was filtered, washed with ethanol and dried in vacuo. In a few cases this yellow product was heated to 650-700°C in a stream of argon saturated with CS_2 to remove any oxide contaminent. The resultant solid had a dark green coloration. When either of the samples were sublimed in vacuo they gave a golden yellow condensate with an identical Raman spectrum to that given in the literature for Cs_2WS_4(15,16). Silica apparatus was used for the sublimations. There was a small amount of very dark coloured residue left after the sublimation process.

The isotopic labelling of Cs_2WS_4 with ^{34}S was carried out by heating Cs_2WS_4 at 600°C with enriched elemental sulphur (90% ^{34}S) in a sealed evacuated silica tube, having a cooler portion at 400°C.

The vapour above Cs_2WS_4 heated to 800-900°C was examined in this case by matrix isolation and quadrupole mass spectrometry. The mass spectrometry experiments were carried out at AEE Winfrith using a VG SXP600 instrument which has a higher mass range (0 to ≈ 700) than that available in this laboratory.

In the matrix experiments the sample was vaporised using the apparatus for induction heating shown in Figure 1(b) of Chapter 2, except that silica rather than alumina was used as the sample holder. In the mass spectrometric experiments the sample was vaporised from a 'conventional' silica sample holder, as in Figure 1(a) of Chapter 2.

Induction heating was chosen for the matrix ir work because of the observed problem of maintaining a constant flux from the resistively heated samples.

3. **Results and Discussion**

3.1 Mass Spectrometric Studies

When the Cs_2WS_4 was heated in the silica holders degassing was observed (on the pressure gauges) at 300-400°C. This was accompanied by an increase in the intensity of the following ions; H_2O^+, H_2S^+, $CO_2{}^+$, $CS_2{}^+$, $S_{2-6}{}^+$ and $S_8{}^+$. At 680°C Cs^+ was detected and by 850°C $Cs_2WS_4{}^+$ was the principal species observed above m/e = 350. A typical spectrum can be seen in Figure 1. The region between 570 and 590 amu is shown under higher resolution in Figure 2(a). Figure 2(b) shows the theoretical spectra calculated for Cs_2WS_4 from the known isotopic abundancies (^{133}Cs 100%, ^{180}W 0.1%, ^{182}W 26.3%, ^{183}W 14.3%, ^{184}W 30.7%, ^{186}W 28.6%, ^{32}S 95.0%, ^{33}S 0.76% and ^{34}S 4.22%). From these two spectra it can therefore be concluded that the cluster of peaks around 580 amu is indeed due to the $Cs_2WS_4{}^+$ parent ion. Very low intensity peaks were occasionally observed that could be assigned to $Cs_2WOS_3{}^+$ and $Cs_2WO_2S_2{}^+$ but were not reproducible. The maximum value of m/e available with this spectrometer is approximately 700 amu and therefore the occurrence of polymers cannot be ruled out except that no fragments (such as $Cs_2WS_5{}^+$ etc) which could be directly attributed to polymers were observed. The energy of the ionising electrons was varied from 10eV to 30eV and this only affected the intensity of the parent ion. No accurate appearance potential data was obtained because it proved very difficult to obtain a steady flux even for a single scan let alone 20 measurements for an ionisation efficiency curve. However it is possible to say that the appearance potential is less than 10 volts.

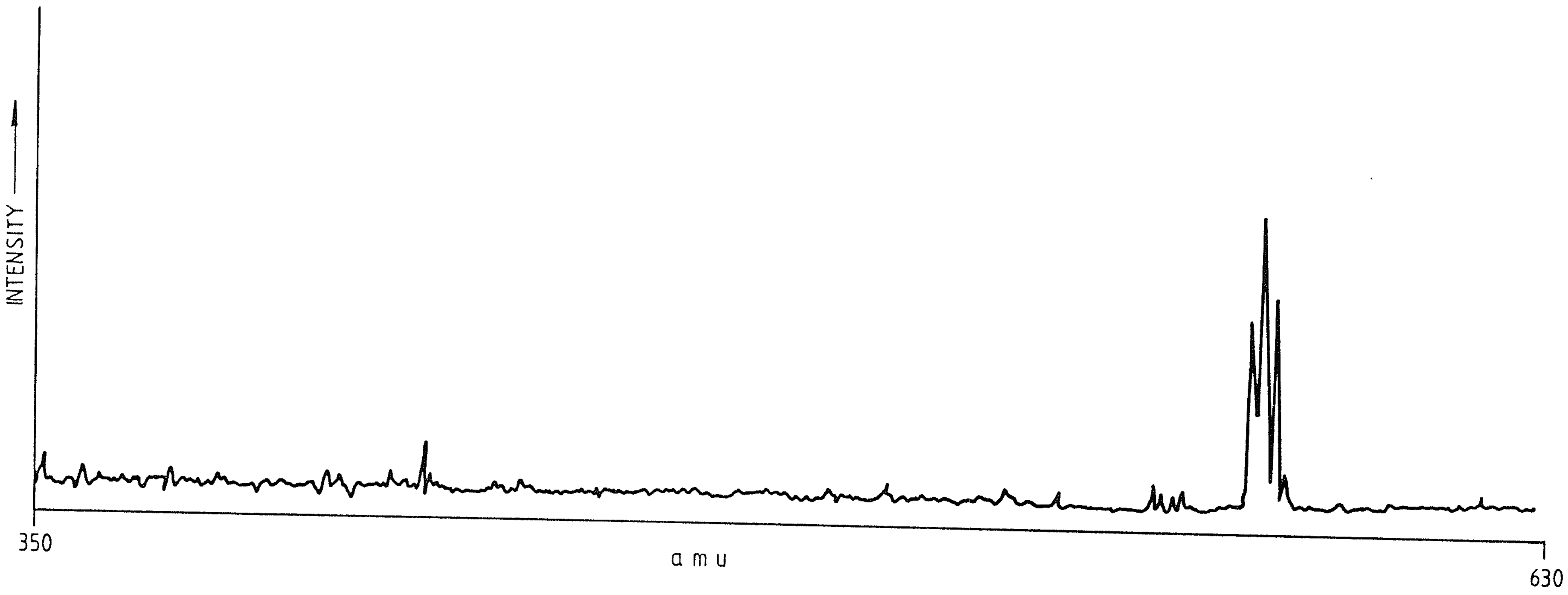

FIG. 1 MASS SPECTRUM OF THE VAPOUR ABOVE HEATED Cs_2WS_4

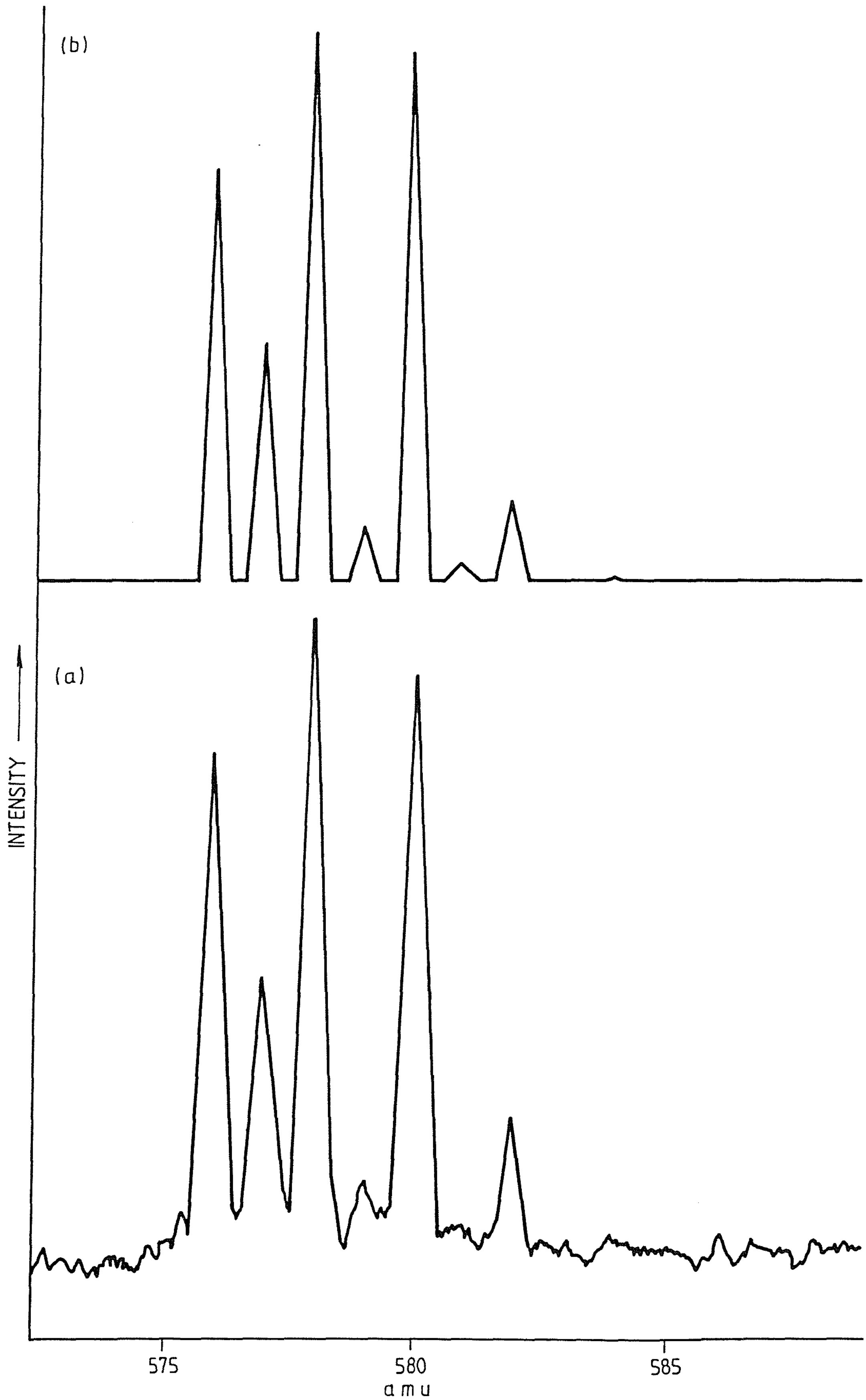

FIG. 2 MASS SPECTRUM OF Cs_2WS_4 IN THE PARENT ION REGION : (a) OBSERVED (b) CALCULATED

Having established that the vapour above heated Cs_2WS_4 is predominantly Cs_2WS_4 and probably monomeric (with some elemental sulphur), matrix isolation ir spectroscopy was then used to try to determine the structure.

3.2 Matrix Isolation Infrared Studies

The survey spectra of the vapour above Cs_2WS_4 heated to 800-900°C isolated in nitrogen and argon matrices are shown in Figures 3(a) and 3(b) respectively. From these spectra it can be observed that the most intense bands are those in the region 500-400 cm^{-1}. The other features at ≃ 1000 and 800 cm^{-1} are of variable intensity as can be noted by comparision of Figures 3(a) and 3(b). These bands probably arise from traces of tungsten oxide impurity which have very intense absorptions in these spectral regions.

In the solid, the two stretching frequencies (ν_1 and ν_3) of the tetrahedral WS_4^{2-} ion are at 480 and 460 cm^{-1} respectively.(15,16) Therefore it is possible to assign the features in the region 500-400 cm^{-1} as arising from tungsten - sulphur stretches. The isolated WS_4^{2-} ion is likely to have T_d symmetry(17) and $\Gamma_{w-s\ str} = A_1 + T_2$ of which only the triply degenerate T_2 mode will be ir active. (Although planar WS_4 groups have been reported(18), for instance in the $(W_3S_8)^{2-}$ ion it is unlikely that this geometry will be present in Cs_2WS_4).

As the two caesium cations are brought close to the T_d ion, its symmetry will be lowered and hence the degenerate T_2 mode will be split. The exact nature of this splitting depends on how the caesium atoms are co-ordinated to the central WS_4^{2-} ion.

Alkali metal salts of oxyanions frequently show bidentate interactions between the oxyanion and the alkali metal cation in $MClO_4$(8) or $MReO_4$(7) or between the oxyanion and

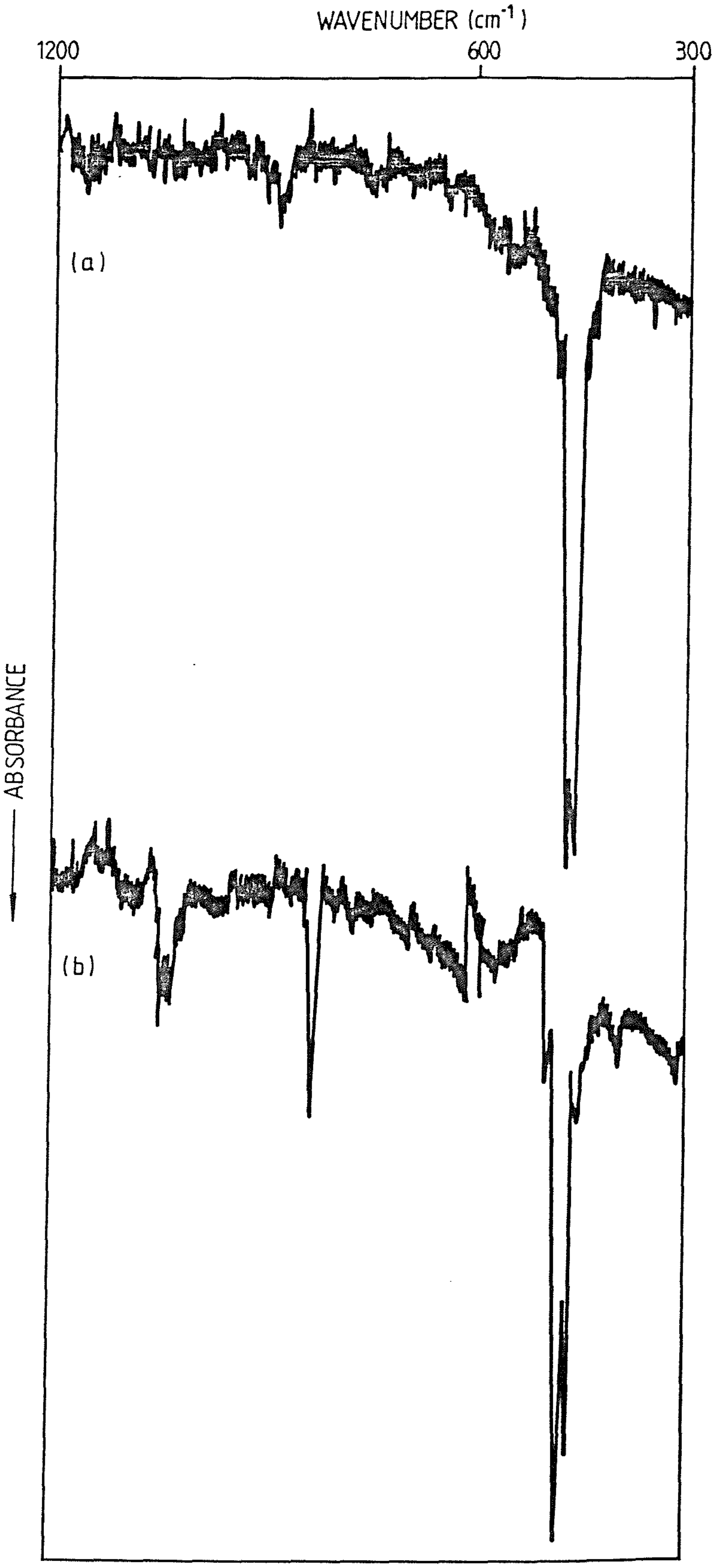

FIG. 3 SURVEY MATRIX IR SPECTRA OF Cs_2WS_4
(a) ISOLATED IN NITROGEN (b) ISOLATED IN ARGON

the pair of cations in M_2XO_4(5) (X = S, Cr, Mo, W). A tridentate interaction occurs only rarely, eg $MClO_3$(6).

By analogy with K_2WO_4(5), and to minimise the $Cs^+ \ldots\ldots Cs^+$ repulsions in a bidentate co-ordination, the anticipated shape of the molecule would be D_{2d} as below:

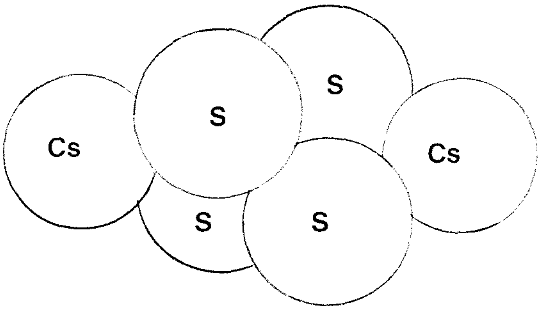

$\Gamma_{\text{W-S str}}$ for this is A_1+B_2+E of which B_2 and E are ir active. Therefore 2 bands are expected in the W-S stretching region with an intensity ratio of 1:2 if the S-W-S bond angles are all tetrahedral.

The high resolution spectra of the intense bands in the 460 cm^{-1} region in Figure 3 are shown in Figure 4(a) for a nitrogen matrix and Figure 4(b) for an argon matrix. From these spectra it can be observed that the pattern obtained from both argon and nitrogen matrix spectra is very similar but shifted by about 3.3 cm^{-1}. The frequency positions are given in Table 1. It can also be seen that a three band pattern is observed rather than a two band pattern expected for the D_{2d} structure. This then implies that either one of these bands is due to an impurity or that the symmetry is less than D_{2d}. The impurity argument fails because this three band pattern has been observed consistently over a period of a year or so with many different samples. Also the pattern seems to remain constant even when the W-O bands are of variable intensity, thus ruling out the hypothesis that the absorptions in the 460 cm^{-1} region

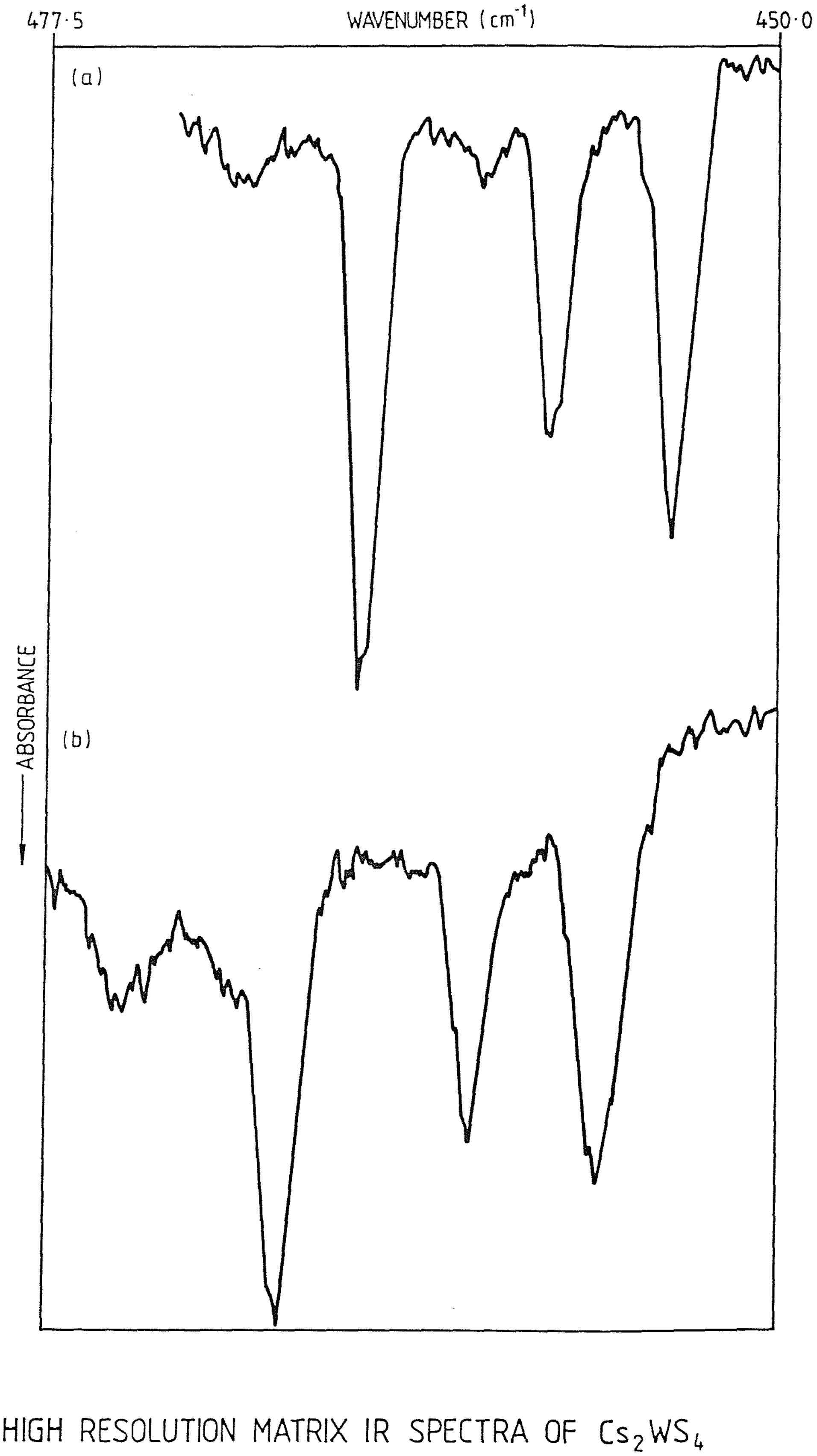

FIG. 4 HIGH RESOLUTION MATRIX IR SPECTRA OF Cs_2WS_4
(a) ISOLATED IN NITROGEN (b) ISOLATED IN ARGON

TABLE 1

Principal ir Bands of Cs_2WS_4 Observed in Nitrogen and Argon Matrices

Matrix Gas	Frequency (cm^{-1})		
Nitrogen	466.0	459.1	454.4
Argon	469.2	462.4	457.9

could be due to, for example Cs_2WOS_3 overlapping with Cs_2WS_4 absorptions.

Therefore in nitrogen and argon matrices it appears that the Cs_2WS_4 must have low enough symmetry so that the triply degenerate T_2 mode is completely resolved.

In the previous study(5) of the oxyanions M_2CrO_4, M_2MoO_4 and M_2WO_4 it was found that the E mode was split by a few wave numbers. Because the total separation between the three bands in Cs_2WS_4 is only 12 cm^{-1} it can be assumed that there are no terminal bound sulphur atoms by comparision with the $CsReO_4$ case(7). In this molecule there is a bidentate interaction between the caesium and two of the oxygen atoms, whilst the other two oxygen atoms can be regarded as terminal and

$$\Gamma_{\text{Re-O str}} = 2A_1+B_1+B_2$$

$$\text{ir active} = 2A_1+B_1+B_2$$

The matrix ir spectrum revealed 3 intense bands and one weak band. The three intense bands were assigned as the resolved T_2 mode and their total splitting was 60 cm^{-1} in argon whilst only 48 cm^{-1} in nitrogen. If the case for the hypothetical $CsReS_4$ molecule is considered, then by using the crude formula below it should be able to estimate the splitting for bridging and terminal sulphur atoms:-

$$\Delta\nu_{\text{calc}}\ CsReS_4 = \frac{\nu[ReS_4]^- \times \Delta\nu_{\text{obs}}\ CsReO_4}{\nu_m CsReO_4}$$

$\nu[ReS_4]^-$ is taken(11) as 486 cm^{-1}, ν_m $CsReO_4$ is the baricentre of the ν_3 vibrations and $\Delta\nu_{\text{obs}}$ is the total observed splitting of the ν_3 mode.

For argon matrices this gives an estimated splitting for $CsReS_4$ of 32.2 cm^{-1}, whilst for nitrogen 25.3 cm^{-1}. In the case of Cs_2WS_4 the observed separations between the highest and lowest components of the triplet is 11.3 cm^{-1} for argon and 11.6 cm^{-1} for nitrogen. Therefore it is unlikely that there are any terminal sulphur atoms in Cs_2WS_4. This also implies that the sulphur atoms are all in similar, but not necessarily identical environments.

The remaining probable shapes are either C_{3v} or C_{2v} where the caesium is co-ordinated in a tridentate fashion. The C_{3v} case is shown below

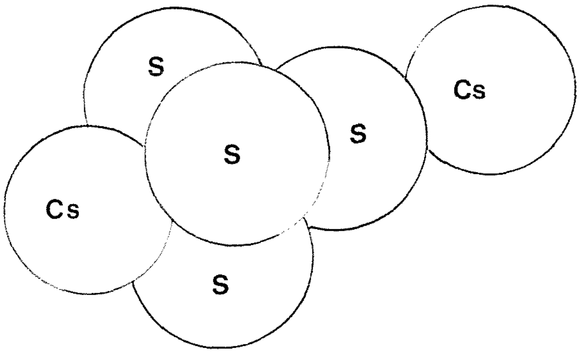

where the caesium is bound in both a monodentate and tridentate fashion, $\Gamma_{W-S\ str} = 2A_1 + E$ and all three are ir active. Hence this structure appears to account for the observed three line pattern, but it must be remembered that one of the A_1 modes is derived from the ir-inactive A_1 mode in T_d symmetry and will hence have very low intensity. In $CsReO_4$ the residual A_1 has an intensity of approximately an $^1/_8$th of that of the weakest component of the split T_2 mode. Thus this geometry does not account for the observed spectra either.

The final shape has the caesium cations in the faces of the three sulphurs and hence has at the most C_{2v} symmetry, ie:

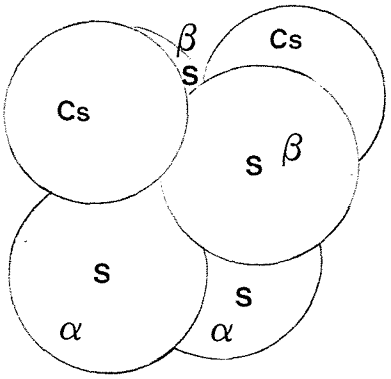

thus both caesium atoms are bound in a tridentate manner.

$\Gamma_{\text{w-s str}}$ for this is $2A_1 + B_1 + B_2$, all of which will be ir active, although three ($A_1 + B_1 + B_2$) will have a much greater intensity than one (A_1).

Therefore on band counting a structure that accounts for the observed spectrum of three intense bands seems to have been arrived at.

Although the weak A_1 component has been searched for in the range 500-400 cm^{-1} no significant feature was observed above the noise level under varying degrees of resolution. The ν_1 band in the solid has been found at 485 cm^{-1}(15, 16) using Raman spectroscopy.

However, the observed intensity pattern is not that for a C_{2v} species where the sulphur atoms are arranged tetrahedrally around the central tungsten atom and the caesium cations are exactly in the faces. If the bond angle between the α sulphur atoms is reduced to 100-105° and that for the β sulphur atoms increased to 115-120° then an approximate intensity pattern can be calculated. The intensity pattern could also be due to the cations lowering the symmetry below C_{2v} by not sitting exactly in the faces. The computer modelling of this is not straight forward, especially if the caesium cations do not sit exactly in the faces, and results in the problem of having many more force constants than frequencies.

The other C_{2v} possibility is where both the caesium atoms are co-ordinated in a bidentate fashion and the bond angles are distorted as above. It is felt however that the bond angle distortion is chemically more acceptable in the former rather than the latter case.

It is therefore concluded that in argon and nitrogen matrices the caesium thiotungstate species adopts the unusual C_{2v} structure, where the caesiums are both tridentatly bound in the sulphur faces and that the bond angles are probably not tetrahedral.

It is usually assumed in M_2XY_4 species that in order to reduce the $M^+ \ldots M^+$ interactions the cations need to be as far apart as possible, hence the bidentate D_{2d} structure. In order to compare this effect, the W-Cs non bonded distances in a variety of compounds need to be estimated. To do this the known, W-S(19,20) or W-O(21) bond lengths of 2.165A and 1.784A respectively and the ionic radii of S^{2-}(1.84Å), O^{2-}(1.32Å), Cs^+(1.67Å) and K^+(1.33Å)(22) were used to determine the Y^{2-} - M^+ bond length and hence the non-bonded distance X-M. The bond angles were assumed to be tetrahedral.

For D_{2d} Cs_2WS_4 it was calculated that W - Cs = 4.28Å
and Cs - Cs = 8.56Å

D_{2d} Cs_2WO_4 it was calculated that W - Cs = 3.64Å
Cs - Cs = 7.28Å

For D_{2d} K_2WO_4 it was calculated that W - K = 3.24Å
K - K = 6.48Å

For C_{2v} Cs_2WS_4 it was calculated that W - Cs = 3.61Å
(tridentate) Cs - Cs = 5.89Å

The analogous tungstate(5) case was only studied under high resolution with potassium as the cation and in this case the cation - cation distance was 6.48Å . For Cs_2WS_4 the Cs - Cs distance is now 8.56Å . Because this is as far as we are aware the first ternary sulphide to be studied in a matrix it is not clear whether it is safe to assume that the bonding will be the same, because the sulphur is both larger and "softer" than the oxygen in the oxyanion species. It is also feasible that the low lying vacant 3d orbitals may be involved in the bonding. It should be noted that the S - S distance with a W - S bond length of 2.165Å and a tetrahedral bond angle is 3.54Å, whereas the sum of the ionic radii is 3.68Å .

The short Cs - Cs distance (5.87Å) in the C_{2v} case leading to higher Cs - Cs interaction may be offset by the change in the nature of the bonding in the WS_4^{2-} ion.

The ionic radii for Cs^+ (1.67Å), S^{2-} (1.84Å) and the atomic radius of the argon(23) (1.875Å) are all very similar. For a genuine comparison the van der Waals radii should be used, however these are not readily available except for the rare gases. Therefore it could be imagined that this unusual structure is due to the matrix forcing the guest Cs_2WS_4 molecule to adopt a structure that is best accommodated within the crystal lattice. Although nitrogen is an oblate molecule (4.52 x 3.42Å(24)) the electron cloud is nearly spherical and of a comparable size to that in argon. It can also be calculated that the approximate size of the D_{2d} Cs_2WS_4 molecule is 10.23Å x 7.08Å x 7.08Å whilst that for the C_{2v} will be 7.54Å x 7.08Å x 7.08Å which means that the C_{2v} molecule is nearly spherical.

It should be noted that because of the small shift between argon and nitrogen (3.3 cm^{-1}) the interaction between the matrix and the Cs_2WS_4 is similar in both cases and hence the spectral patterns cannot arise from interaction of the Cs_2WS_4 with the nitrogen matrix.

In the majority of cases isotopic data can be used to confirm the spectral assignments and characterisation of the species of interest. In the present case there is no central atom isotope data which could be used to estimate bond angles(5) because of the heavy central atom. In the oxyanion systems studied previously, oxygen-18 labelling was used extensively to confirm the mode of co-ordination because the isotopic splitting was greater than the separation of the bands in the initial spectrum. In the case of ^{34}S labelling, the estimated frequency shift is 13-14 cm^{-1}. Therefore the band separation and isotopic splitting is of the same order and will result in extensive overlap and obscuring of bands.

In the hope that these problems could be mitigated by the use of slow careful deposition and extended averaging of the spectra, matrix ir spectra of ^{34}S isotopically enriched Cs_2WS_4 were carried out. The calculated incorporation was 50% and by observing the S_2^+ peak in the mass spectra the actual enrichment was estimated to be $\approx$ 45%. The high resolution spectra of the vapour above this sample isolated in a nitrogen matrix is shown in Figure 5(b). Figure 5(a) is a spectrum of normal abundance Cs_2WS_4 recorded the following day for comparison. The band positions are tabulated in Table 2.

The most striking feature of Figure 5(b) is the relative simplicity of the pattern. For example in K_2WO_4(5) 9 distinct bands were observed on isotopic labelling, whilst in the $CsReO_4$ case a total of in excess of 20 bands were observed. Therefore as anticipated the isotopic labelling has not been able to either confirm or deny the band counting assignment from the normal Cs_2WS_4 spectrum.

4. Conclusions

These studies have shown for the first time that a ternary sulphide is stable in the vapour phase. The mass spectrometric results indicate that it is probably in the form of monomeric Cs_2WS_4. The matrix ir experiments result in a complex pattern that is not assignable using a D_{2d}

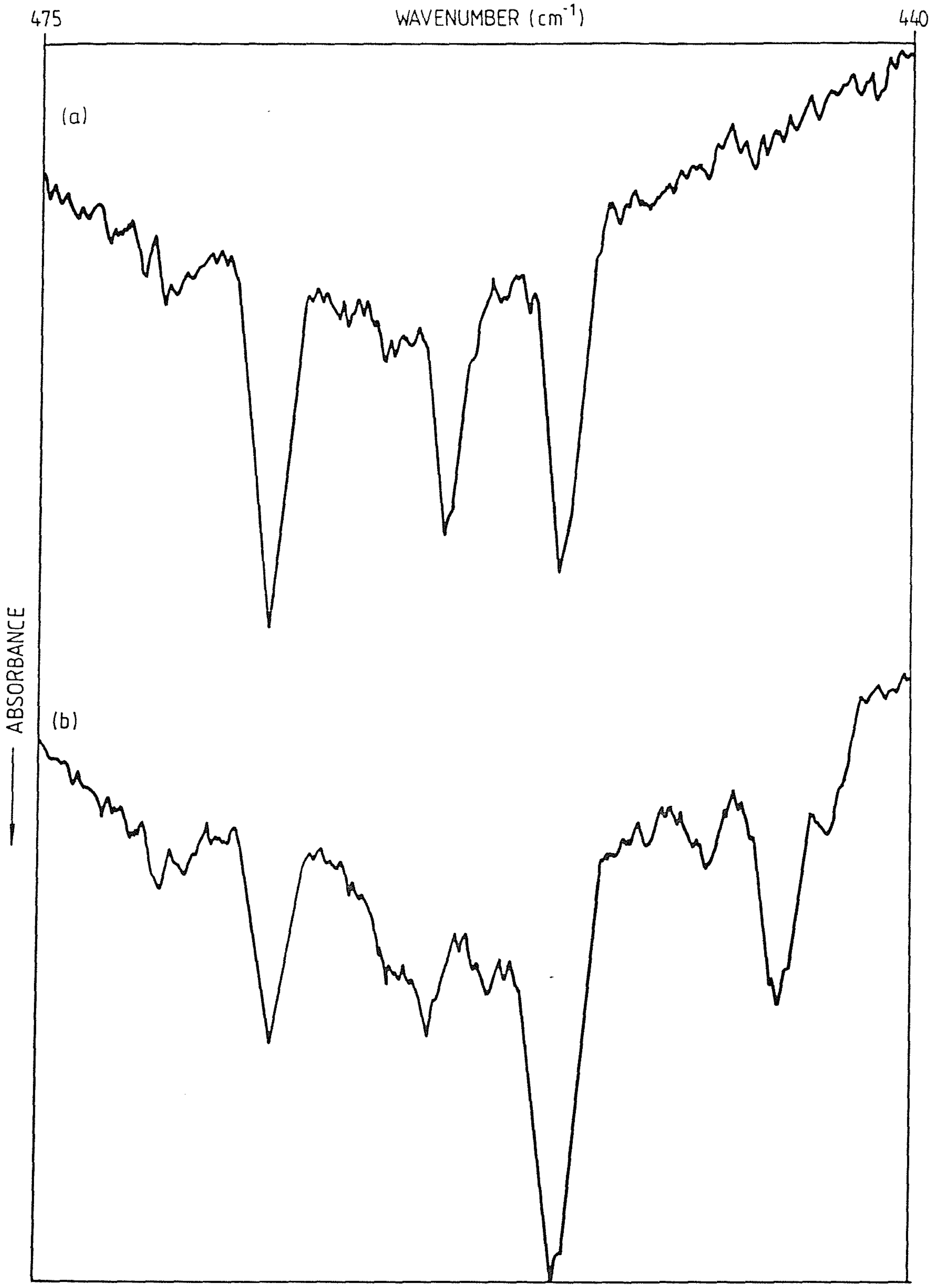

FIG. 5 HIGH RESOLUTION NITROGEN MATRIX IR SPECTRA OF Cs_2WS_4
(a) NORMAL ISOTOPIC SAMPLE (b) $\simeq 45\%$ ^{34}S ENRICHED SAMPLE

TABLE 2

Ir Bands Observed for Normal and ^{34}S Enriched Cs_2WS_4 Isolated in Nitrogen Matrices

Normal isotopic abundance frequency/cm^{-1}	45% ^{34}S enriched frequency/cm^{-1}
	470.4 (w)
	469.4 (w)
466.0	465.9 (s)
	461.0 (vw)
	459.8 (m)
459.1	
	457.2 (w)
454.4	454.5 (s)
	450.9 (w)
	448.5 (w)
	445.7 (s)
	443.8 (w)

model and indicate that the highest possible symmetry Cs_2WS_4 can have in argon or nitrogen matrices is C_{2v} with some angular distortions.

In order to confirm these observations further work is needed. In the ir matrix experiments, different matrix gases need to be employed to see if the proposed structure is a result of lattice considerations. Matrix EXAFS([20], [25]) of both the Cs L(III) and W L(III) edges should be able to confirm the mode of cation co-ordination, both by determining the Cs - W non bonded distance and by observing whether the Cs is bonded to 2 or 3 sulphur atoms.

5. References

1. See for example
Otero - Diaz L.C., Hiraga K., Sellar J.R. and Hyde B.G.
Acta. Cryst., B40, 355, 1984.
and
Negishi H., Sasaki M., Yasenga T. and Inove M.
J. Phys. Chem., 88, 1455, 1984.

2. Schafer H.
Z. Anorg. Allg. Chem., 486, 33, 1982.

3. For a recent survey see:
Wild D.J.
MPhil Thesis, University of Southampton 1986.

4. Klepp K.O. and Bronger W.
Z. Anorg. Allg. Chem., 532, 23, 1986.

5. Beattie I.R., Ogden J.S. and Price D.D.
J. Chem. Soc. Dalton Trans., 1982, 505.
Price D.D.
Phd. Thesis, University of Southampton, 1980.

6. Beattie I.R. and Parkinson J.E.
J. Chem. Soc. Dalton Trans., 1983, 1185.

7. Arthers S.A, Beattie I.R., Gomme R.A., Jones P.J. and Ogden J.S.
J. Chem. Soc. Dalton Trans., 1983, 1461.

8. Beattie I.R. and Parkinson J.E.
J. Chem. Soc. Dalton Trans., 1984, 1363.

9. Ogden J.S.
Ber. Bunsen. Phys. Chem., 86, 832, 1982.

10. Hastie J.W.
"High Temp. Vapours", Academic Press, N. Y., 1975.

11. See for example
Stewart B. and Peacock R.D.
Chem. Phys. Lett., 120, 307, 1985.
and
Muller A., Diemann E. and Krishna Rao V.V.
Chem. Ber., 103, 2961, 1970.

12. Corleis E.
Liebigs. Ann. Chem., 232, 244, 1886.

13. Gattow G. and Franke A.
Z. Anorg. Allg. Chem., 352, 11, 1967.

14. Muller A., Krebs B., Vebabcioglu R., Stockburger M. and Glemser O.
Spectro-Chim. Acta., 24A, 1831, 1968.

15. Muller A., Weinstock N. and Schulze H.
Spectro-Chim. Acta., 28A, 1075, 1972.

16. Muller A., Krebs B., Rittner W. and Stockburger M.
Ber. Bunsen. Phys. Chem., 71, 182, 1967.

17. Leroy M.J.F. and Kaufmann G.
Bull. Soc. Chim., 1966, 3090.

18. Bhaduri S. and Ibers J.A.
Inorg. Chem., 25, 3, 1986.

19. Sasvari, K.
Acta. Cryst., 16, 719, 1963.

20. Antonio M.R., Teo B.K. and Averill B.A.
J. Am. Chem. Soc., 107, 3583, 1985.

21. Ugarov V.V., Ezhov Yu.S. and Rambidi N.G.
Zh. Struckt. Khim., 14, 359, 1973.

22. CRC "Handbook of Chemistry and Physics", 62nd, 1981.

23. See for example
Moskovits M. and Ozin G.A.S.
"CryoChemistry", Wiley, 1976.

24. See for example
Hallam H.E.
"Vibrational Spectroscopy of Trapped Species", Wiley,
1973.

25. Beattie I.R., Ogden J.S. and Young N.A.
University of Southampton.
Unpublished Observations 1988.

CHAPTER 5

SOME ASPECTS OF TELLURIUM REACTOR CHEMISTRY

1. Introduction

It is generally accepted that tellurium is an important fission product in severe reactor accidents because a substantial quantity of this radiobiologically hazardous element is present as a relatively volatile form in irradiated fuel. The precise chemical forms of tellurium evolved from an overheating core are not known with any degree of accuracy and are hence the subject of considerable debate.

The predominant tellurium containing species in the uranium oxide fuel is predicted by Potter(1) from thermodynamic considerations to be caesium telluride (Cs_2Te). This however has never been substantiated experimentally apart from the observation(2) of $CsTe^+$ in the mass spectrum of a heated simulant fission product urania mix. A review of out-of-pile studies(3) suggests that tellurium can form mixed oxide phases such as barium-strontium and barium-caesium oxytellurides within the matrix of the fuel. The major species released from the fuel is believed(9) to be elemental tellurium (Te, Te_2). Subsequent transport of the tellurium away from the fuel depends critically on the oxygen potential of the system.

Under reducing steam conditions the major species are believed(1,3) to be H_2Te, Te and Te_2 whilst an increase in the oxygen potential (higher H_2O/H_2 ratio) is likely to result in an increase in the concentrations of oxide and hydroxide species such as TeOH, $Te(OH)_2$, TeO and TeO_2. This complex situation is further aggravated by the interaction of any released elemental tellurium with structural materials. For example the reaction of tellurium vapour with Zircaloy, Inconel 600 and 304 stainless steel was found to result in zirconium, nickel, chromium and iron tellurides(5). The Zircaloy cladding is particularly important in assessing the attenuation of any tellurium release because of its close proximity to the fuel.

It has been found(6) that this interaction is only effective if the cladding remains unoxidised and the tellurium can react with the metal components (98% Zr, 1.6% Sn) to form zirconium or stannous telluride. The tellurium can then be re-released under steam-oxidising conditions due to the reaction of steam with the zirconium telluride. Recent experiments at AEE Winfrith(7) indicate that the tellurium can also be re-released as stannous telluride (SnTe) from zircaloy coupons reacted with tellurium.

The aim of the work in this chapter was to react water vapour and/or steam with various metal tellurides (eg Cs_2Te, ZrTe, SnTe, SrTe) in order to evaluate the extent of hydrogen telluride evolution. Hydrogen telluride has not previously been studied by matrix isolation ir spectroscopy and therefore this molecule had to be fingerprinted first. Also the two stretching modes have never been resolved in the gas phase and hence it and its deuterated analogues have been characterised.

There is considerable interest in the vapour phase chemistry of caesium and tellurium in steam oxidising conditions. Many of the matrix ir spectra are very complex (8,9) and it was hoped to be able to assign some of the features unambigiously by studying the co-deposition of alkali metal atoms and tellurium dioxide.

2. The Characterisation of Hydrogen Telluride

2.1 Introduction

Hydrogen telluride is a very unstable gaseous molecule at room temperatures and in the presence of moist air will decompose to give a tellurium mirror within minutes. It can only be formed from the elements at high temperatures(11) and the more usual synthetic routes are either the electrolysis of sulphuric acid with a tellurium cathode(14) or the hydrolysis of aluminium telluride(14). Figure 1 gives the various reactions and properties of hydrogen telluride.

Despite its instability, hydrogen telluride has been studied by a number of spectroscopic techniques and these include gas phase ir(15-25), nmr(26), mass spectrometry (27,28), microwave(29), uv-vis(30-33), PES(34) and by Mossbauer spectroscopy in argon matrices(35,36). Even though numerous reports have been devoted to the gas phase ir study of hydrogen telluride, the two stretching fundamentals (ν_1 and ν_3) have never been resolved from each other satisfactorily to enable their assignment.

The early infrared work using cooled cells identified (15,16) the position of the bending mode near 869 cm^{-1} and the stretching fundamentals were believed to be overlapping in the 1800-2200 cm^{-1} region. Rossmann subsequently carried out higher resolution (0.1 cm^{-1}) studies and assigned the ν_2 bending mode of hydrogen telluride to be 860.765 ($\pm$0.022) cm-1(17) or 860.79 ($\pm$0.01) cm^{-1}(19). The values for the assignments for the stretches at 2060(ν_1) and 2073 (ν_3) were not published except in his thesis(17). Many of the subsequent papers use these values to calculate moments of inertia(21,22) dissolution effects in various solvents(18) or the calculation of force constants(20).

Note added in proof. A very recent report(58) claims that all the hydrogen chalcogenides are linear because the vibrational spectra show mutual exclusion of Raman and ir. This is probably due to the combined problems of the weakness of the Raman effect and the overlapping of the stretching modes, and therefore does not conflict with the earlier observations that all these molecules are severely bent.

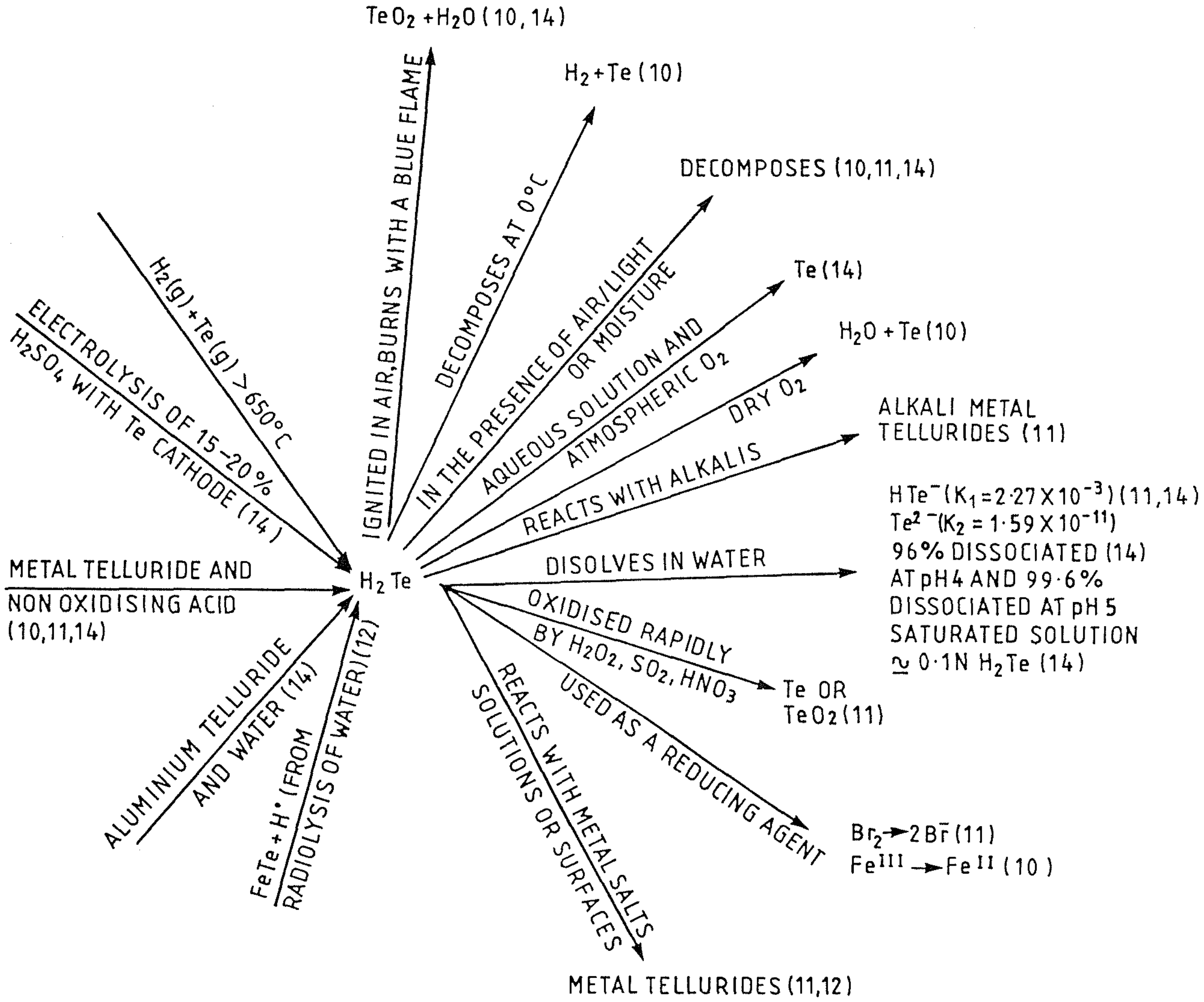

FIG.1 METHODS OF PREPARATION AND REACTIONS OF HYDROGEN TELLURIDE

Edwards and his group at Michigan have more recently studied the combination ([23],[24]) and overtone ([24],[25]) bands of H_2Te and HDTe.

It was therefore hoped that with the characteristic narrow band widths, matrix isolation ir spectroscopy would allow the assignment of all the fundamentals of hydrogen telluride.

2.2 Experimental

From Figure 1 one can see that hydrogen telluride cannot be synthesised easily from the elements but is more conveniently generated either by electrolysis of a sulphuric acid solution with a tellurium cathode, or the action of water or mineral acids on metal tellurides, usually aluminium telluride. This latter approach was the one chosen because of the ease of deuteration. Water was added drop wise to powdered aluminium telluride (Ventron) under a nitrogen atmosphere. The resultant hydrogen telluride was carried out of the reaction vessel by a nitrogen flow through a trap maintained at -23°C to remove any residual water and was collected in a trap held at -196°C by liquid nitrogen. When the reaction had ceased the nitrogen flow was stopped and the hydrogen telluride pumped on at -196°C. It was then purified by vacuum distillation into the sample holder (see Figure 2) for the matrix ir studies.

The sample holder was transferred to the matrix rig and the white hydrogen telluride solid was maintained at -196°C. During deposition the finger of the sample holder was immersed in a methylcyclohexane slush at -126°C. Deposition times were typically 30-60 minutes and the 'V' shaped window was used to monitor the deposition rate to avoid the build up of polymer bands.

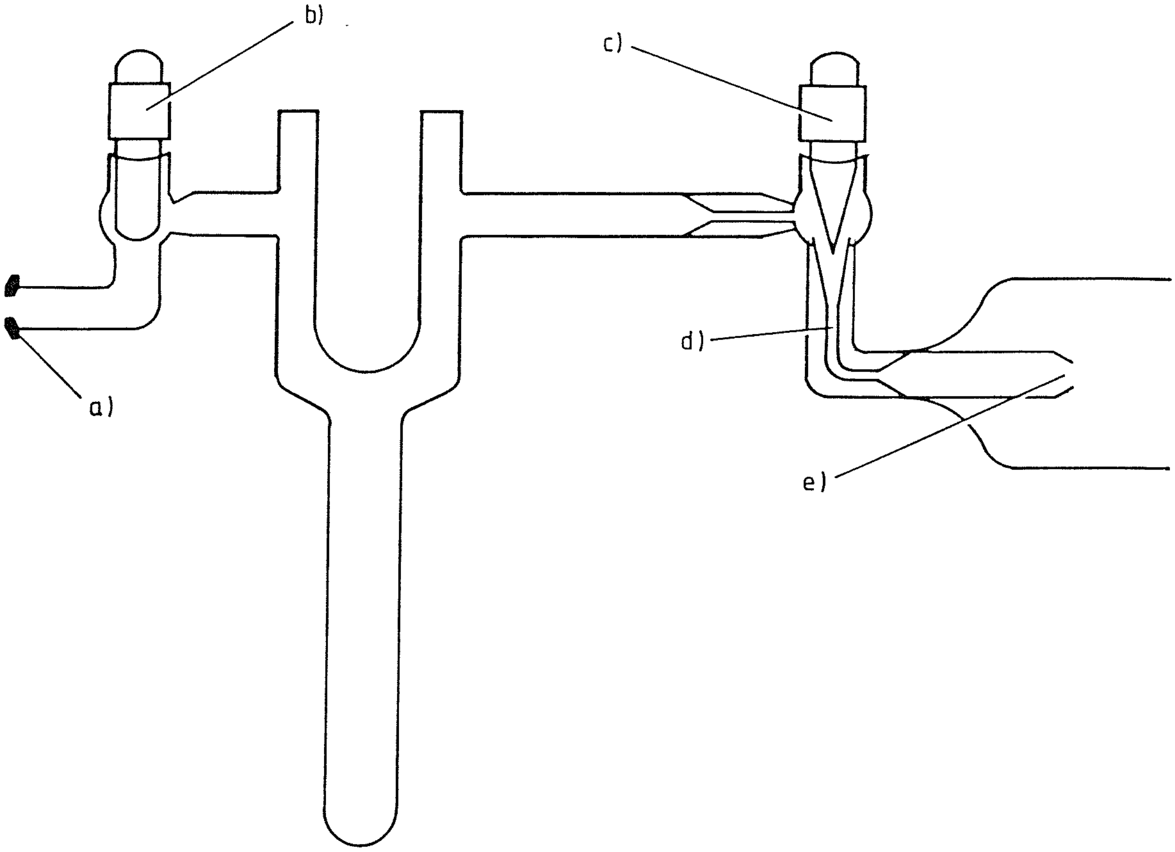

a) S13 BALL JOINT
b) YOUNG'S TAP
c) YOUNG'S NEEDLE VALVE
d) 1mm CAPILLARY TUBING
e) B10 CONE JOINT

FIG. 2 SAMPLE PREPARATION AND VAPORISATION APPARATUS FOR HYDROGEN TELLURIDE

When the preparative apparatus and the sample holder were dismantled a tellurium mirror formed within minutes, thus indicating the instability of H_2Te in the presence of moisture and oxygen. When a Nichrome furnace was wound round the apparatus and heated to 100-150°C during the deposition, a tellurium mirror was formed. If a "tesla" coil was discharged near the glass then a tellurium mirror was also formed.

2.3 Results and Vibrational Assignments

The matrix ir spectra of H_2Te in nitrogen matrices gave sharp reproducible bands. However, the spectra from argon and krypton matrices gave non-reproducible and poorly defined bands. Therefore in this section the results from the nitrogen matrix spectra only will be considered.

Hydrogen telluride is known from the previous ir studies to be a bent XY_2 molecule with C_{2v} symmetry and with a bond angle very close to 90°. It was shown in Chapter 3 that a bent triatomic is expected to have 3 ir active vibrational fundamentals ($2A_1 + B_1$), and that the two stretches, A_1 + B_1 will have almost the same intensity if the bond angle is 90°. The monodeuterated species, HDTe, will have C_s symmetry and will also have 3 ir active fundamentals. Therefore one anticipates observing 3 relatively intense bands for each of the species H_2Te, HDTe and D_2Te.

In the case of the H_2Te and D_2Te (C_{2v} point group) the two A_1 representations correspond to totally symmetric vibrational modes, and these are one stretching (ν_1) and one bending (ν_2) mode. The B_1 representation corresponds to the anti-symmetric stretching mode, (ν_3).

eg

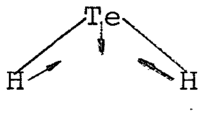

ν_1

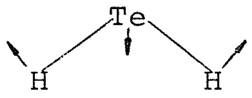

ν_2

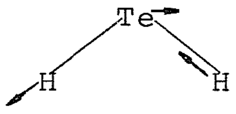

ν_3

For the HDTe case (C_s point group) all the vibrational modes have the same representation (A'). As before the ν_2 mode is the bending mode. In the case of ν_1 and ν_3 these may be taken to be, to a first approximation, the Te-D and Te-H stretches respectively, because tellurium is a heavy central atom.

eg

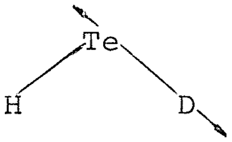

ν_1

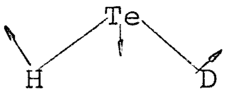

ν_2

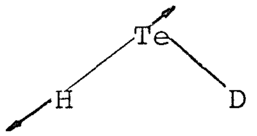

ν_3

In both sets of diagrams the arrows indicating the displacement of the tellurium atom during the vibrations is very exaggerated.

Figure 3 is a survey spectrum of hydrogen telluride isolated in a nitrogen matrix and several of the prominent bands can readily be assigned to matrix isolated CO_2 and H_2O as marked. The three remaining intense bands are therefore assigned to hydrogen telluride. Figure 4 is a higher resolution spectrum of the region 2100-2025 cm^{-1} and this reveals that the apparent doublet is in fact due to two sharp bands and one broad feature. Diffusion experiments (Figure 5) showed that the relative intensity of the two sharp bands remained constant during diffusion, but that the broader feature centred at 2065 cm^{-1} gained intensity relative to the doublet during matrix warm up.

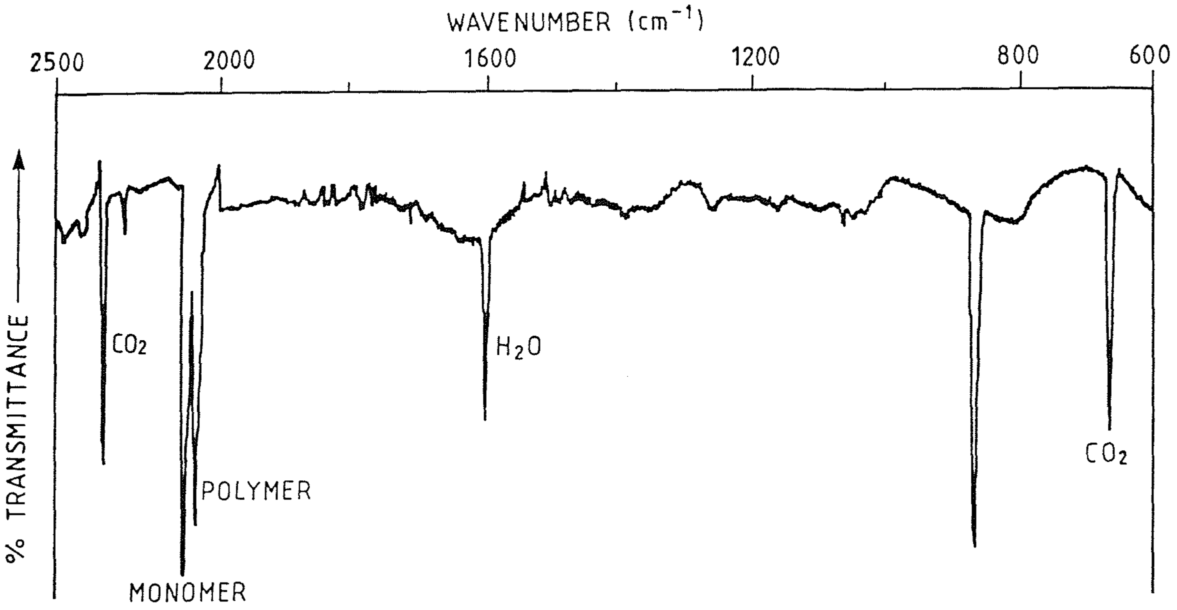

FIG. 3 IR SURVEY SPECTRUM OF H_2Te VAPORISED AT −126°C ISOLATED IN A NITROGEN MATRIX

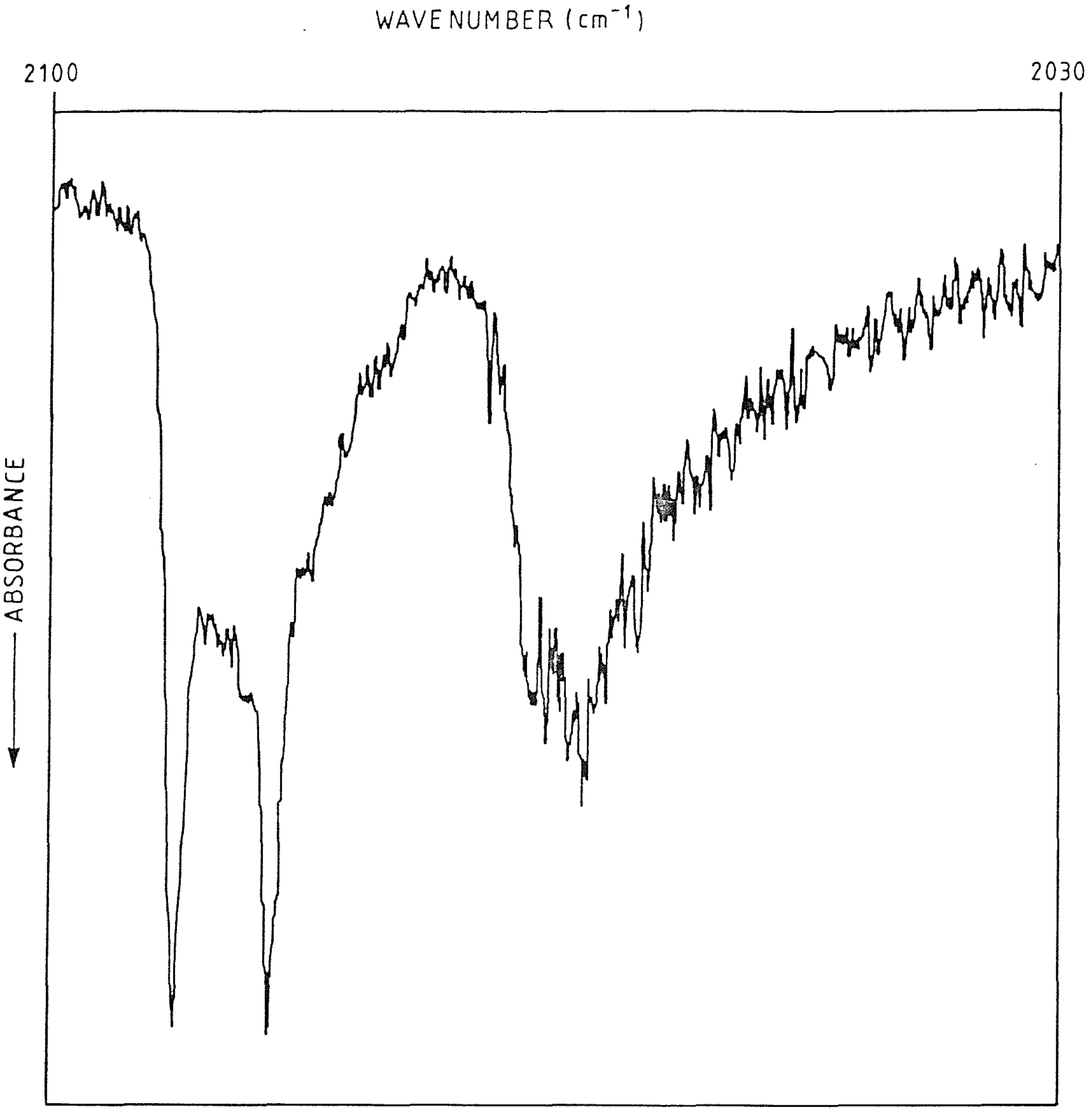

FIG. 4 HIGH RESOLUTION NITROGEN MATRIX IR SPECTRUM OF H_2Te IN THE STRETCHING REGION

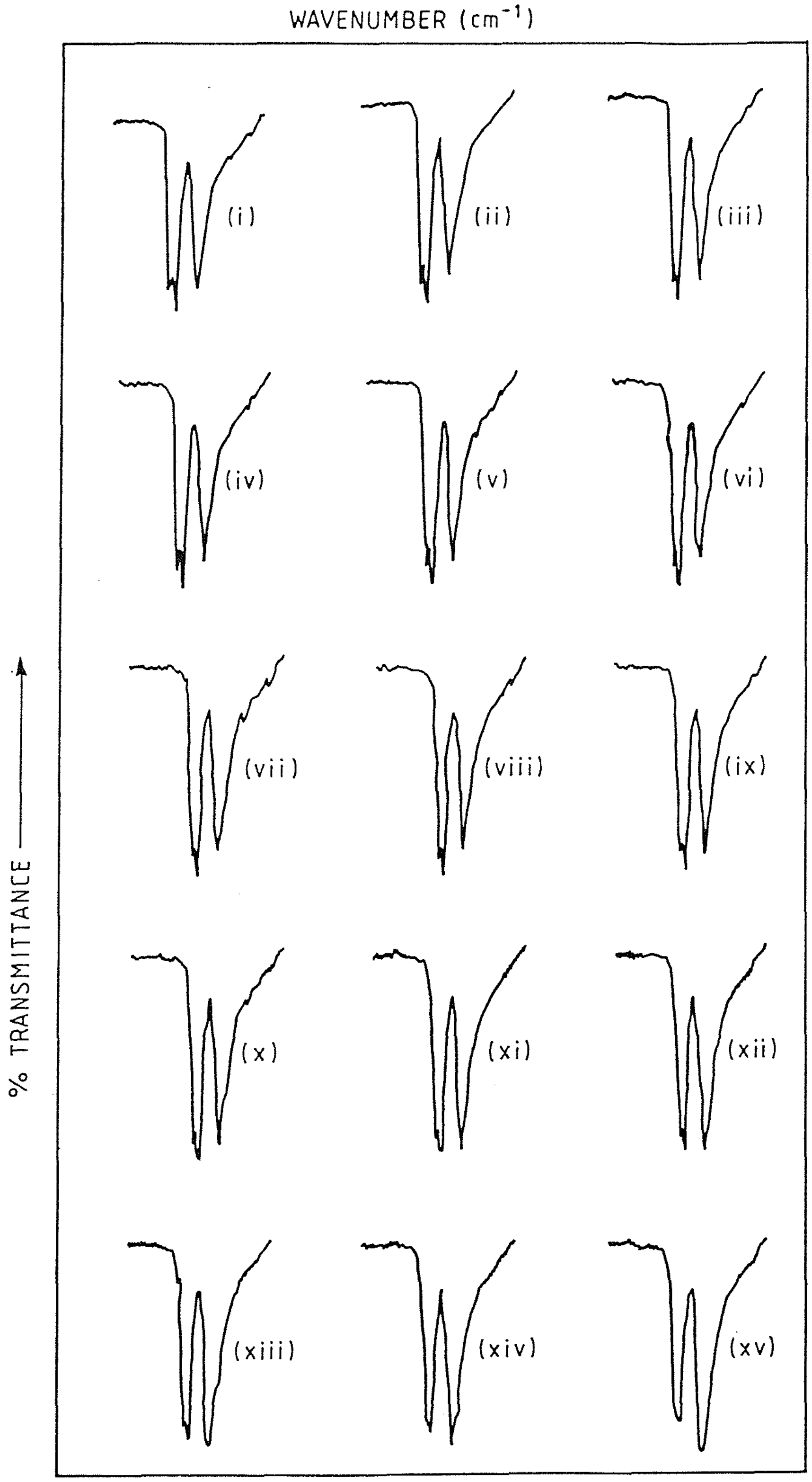

FIG.**5** SUCCESSIVE IR SPECTRA IN THE RANGE 2150-2000 cm^{-1} RECORDED DURING THE WARM UP OF THE MATRIX, SHOWING THE EFFECT OF DIFFUSION ON H_2Te IN NITROGEN MATRICES

Therefore the two sharp bands at 2091.7 and 2085.1 cm^{-1} are assigned to monomeric hydrogen telluride, and the broad feature to polymeric or aggregate species. Figure 6 is also a higher resolution spectrum but of the 870-860 cm^{-1} area. From this it can be seen that there is only one sharp band in this spectral region.

The assignment of the A_1 bending mode (ν_2) to the band at 864.75 cm^{-1} is straight forward. It is the assignment of the two stretching modes that is more problematical. In most bent triatomics it is possible to assign ν_1 and ν_3 from their relative intensities. Indeed in many cases one can estimate the bond angle (α) by use of the relative intensity of ν_3 and ν_1 from the equation below

$$\frac{I_{B_1}}{I_{A_1}} = \tan^2(\alpha/2) \frac{\mu_y + \mu_x (1-\cos \alpha)}{\mu_y + \mu_x (1+\cos \alpha)} \qquad (1)$$

(α = full angle)

assuming that the uncoupled oscillator approximation is valid and that the central atom, x, is "heavy" compared to the terminal atoms y.

If, however, the bond angle is close to 90° this equation predicts that the intensities will be very similar and hence no assignment can be made using this method. Therefore the assignment must rely on comparison with the other hydrogen chalcogenides.

Table 1 lists the observed frequencies of water, H_2S and H_2Se for gas phase and matrix isolated species.

If the bond angle of H_2Te (90.25°)(24, 25) is compared to that of the other hydrogen chalcogenides it can be seen that it is very similar to H_2S and H_2Se. In these two molecules ν_3 is higher in frequency than ν_1 and the value

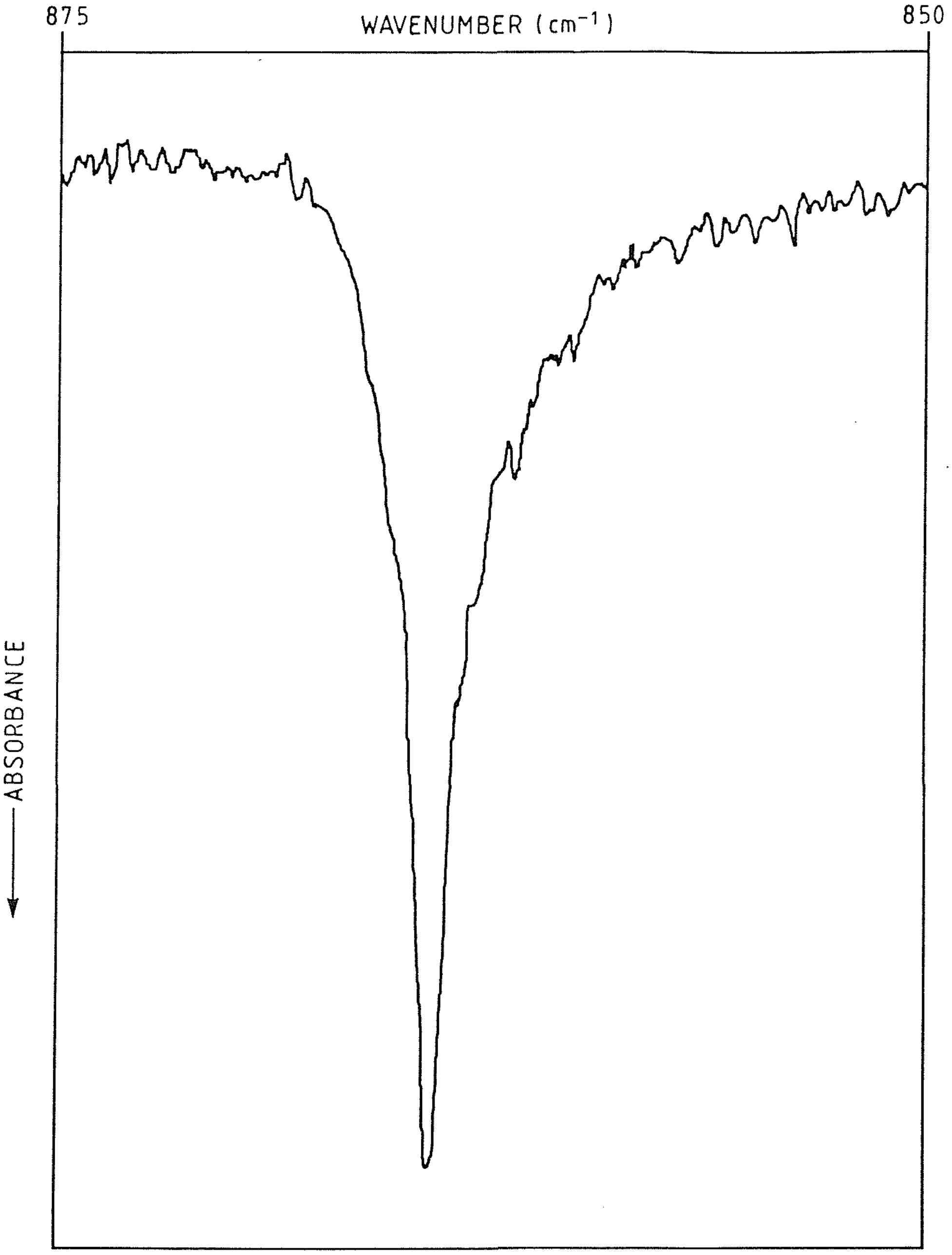

FIG. **6** HIGH RESOLUTION NITROGEN MATRIX IR SPECTRUM OF H_2Te IN THE BENDING REGION

TABLE 1

Comparison of Gas Phase and Matrix Frequency Data for the Hydrogen Chalcogenides

	ν_3 /cm^{-1}	ν_1/cm^{-1}		$\Delta\nu$/cm^{-1}
		(a) gas phase		
H_2O	3755	3650	(37)	105
α = 104.523°	3755.79	3656.65	(38)	99.14
H_2S (40)	2628.440	2614.409	(41)	14.031
α = 92.07°				
H_2Se	2350	2260	(44)	90
α = 91.0°	2357.66	2344.362	(45)	13.302
		(b) N_2 matrix		
H_2O	3725.7	3632.5	(39)	93.2
α = 104.523°				
H_2S (40)	2632.6	2619.5	(42)	13.1
α = 92.07	2633	2620	(43)	13
H_2Se		no data available		

of $\Delta\nu$ changes by less than 1 cm^{-1} on going from H_2S to H_2Se. Therefore by analogy, ν_3 in hydrogen telluride should be above ν_1 by about 10 cm^{-1}. The observed separation is 6.6 cm^{-1} and this indicates that ν_3 is at 2091.7 cm^{-1} and ν_1 at 2085.1 cm^{-1}. This assignment is in agreement with the overtone and combination studies of hydrogen telluride as given in Table 2 which also indicate that ν_3 is at a higher frequency than ν_1.

Caution should be exercised however as Edwards et al([23], [25]) do not state how they arrived at their assignments and may have used the arguments outlined above. Table 3 contains the frequencies of the observed transitions and their assignments.

2.4 Isotope Enrichment Studies

On deuteration one anticipates observing new bands in the ir spectrum and the survey spectra in Figure 7 show the effect of increasing the extent of deuterium in the sample. Figure 7(a) is of a non-deuterated sample (Figure 3) and is included for purposes of comparison. Figure 7(b) is a spectrum of a sample containing ~ 30% D whilst Figure 7(c) has an deuterium enrichment level of approximately 75%. From these spectra it can be deduced that the Te-D stretching modes are located near 1500 cm^{-1} and that the new bending modes lie between 800 and 600 cm^{-1}. The high resolution spectra of the Te-H and Te-D stretching modes and the bending modes are shown in Figures 8, 9 and 10 respectively. The extent of deuteration has been estimated from the relative intensities of the stretching modes using the point charge model within SOTONVIBP.

In Figure 8, four bands are observed in the Te-H stretching region. The two outer components are ν_3 and ν_1 of H_2Te as observed in Figure 4 and therefore the two central

TABLE 2

Overtone and Combination Bands observed for Hydrogen Telluride

$2\nu_1$	4062.8890 cm^{-1}	(25)
$\nu_1 + \nu_3$	4063.3774 cm^{-1}	(25)
$\nu_1 + \nu_2$	2911.415 cm^{-1}	(23)
$\nu_2 + \nu_3$	2915.97 cm^{-1}	(23)

TABLE 3

Observed Frequencies and Assignments for H_2Te isolated in a Nitrogen Matrix

Frequency/cm^{-1}	Assignment
2085.1	ν_1 Te-H symmetric stretch A_1
864.75	ν_2 H-Te-H bend A_1
2091.7	ν_3 Te-H asymmetric stretch B_1

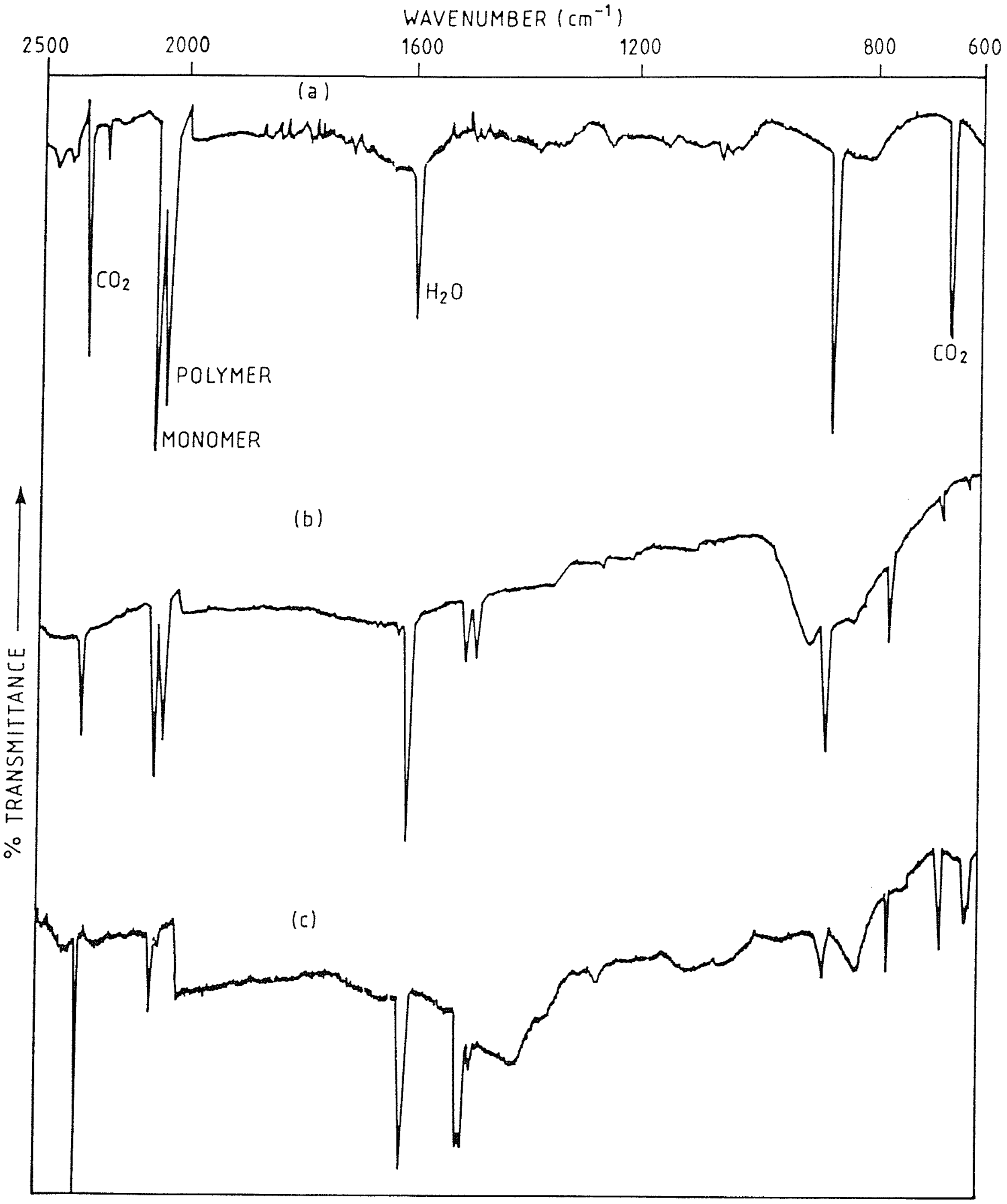

(a) NO ENRICHMENT
(b) ≃ 30% ^{2}D ENRICHMENT
(c) ≃ 75% ^{2}D ENRICHMENT

FIG. 7 SURVEY NITROGEN MATRIX IR SPECTRA FOR DIFFERENT LEVELS OF DEUTERIUM ENRICHMENT IN HYDROGEN TELLURIDE components must arise from a deuterated molecule. A similar pattern is also observed in the Te-D stretching region, (Figure 9) and the outer components at 1501.6 and $1496.1cm^{-1}$ are assigned to ν_3 and ν_1 respectively in monomeric D_2Te. This assignment is based on their increase in intensity relative to the two central components on increasing deuteration. From these two sets of spectra it appears that the two central components in each of the patterns are due to partially deuterated species.

The spectra in the bending region, (Figure 10) also show a four line pattern. The band at 864.75 cm^{-1} has previously been assigned to H_2Te and if this is multiplied by$(1/\sqrt{2})$ (assuming no tellurium atom motion) it gives an expected value of ~610 cm^{-1}. Therefore the sharp band at 618.2 cm^{-1} is assigned to the D-Te-D bending mode in D_2Te. The doublet at 753 cm^{-1} must hence arise from a partially deuterated molecule.

From these spectra it has been possible to assign the fundamental transitions of both H_2Te and D_2Te. However for the partially substituted species 6 bands have been observed whilst only 3 are expected for HDTe.

The fact that the bands assigned to H_2Te and D_2Te are readily understood, and have the appropriate isotope shifts, implies that monomeric hydrogen telluride is being isolated in the matrix. Therefore it seems unlikely that the peculiar behaviour of the partially deuterated species can be explained in terms of dimer (or trimer) formation exclusively for the HDTe molecule. The behaviour has to be explained in terms of a phenomena that affects H_2Te, D_2Te and HDTe, but only becomes apparent in HDTe. Nitrogen matrices often lift the degeneracy of doubly and triply degenerate modes because of the presence of asymmetric sites. In the case of hydrogen telluride there is no degeneracy that could give rise to this splitting but it is possible that the HDTe molecule could be located in the

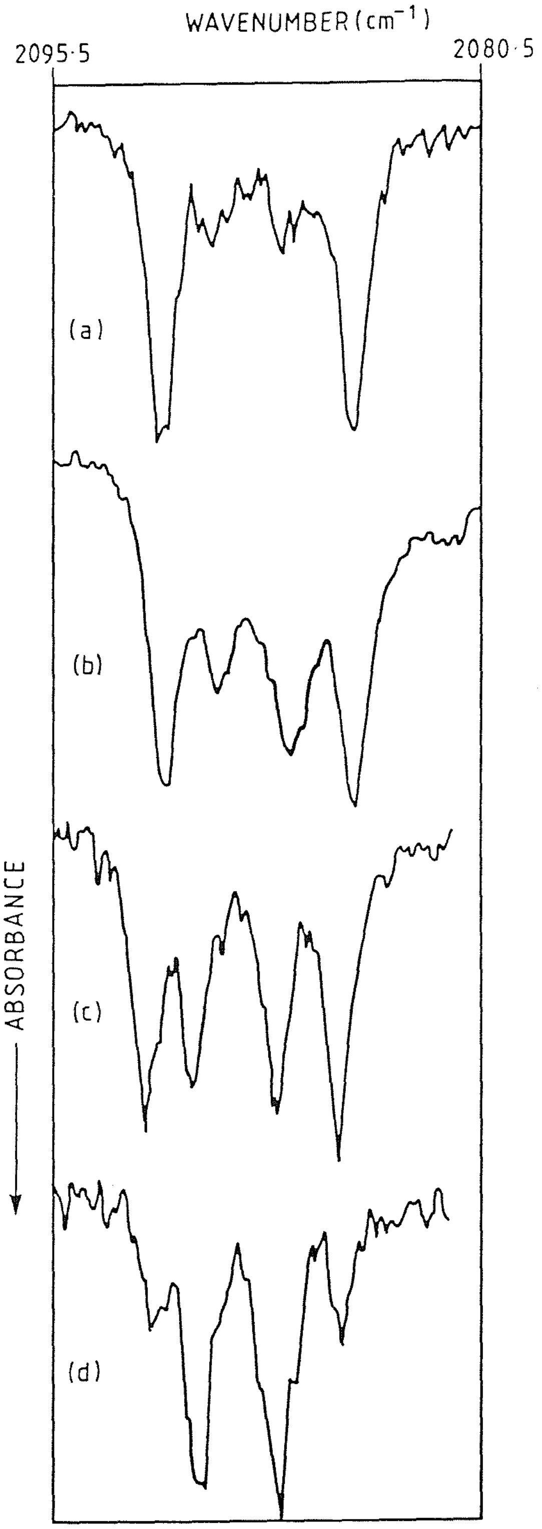

a) FOR ≃ 15% ^{2}D ENRICHMENT
b) FOR ≃ 30% ^{2}D ENRICHMENT
c) FOR ≃ 40% ^{2}D ENRICHMENT
d) FOR ≃ 75% ^{2}D ENRICHMENT

FIG. 8 HIGH RESOLUTION NITROGEN MATRIX IR SPECTRA IN THE Te-H STRETCHING REGION

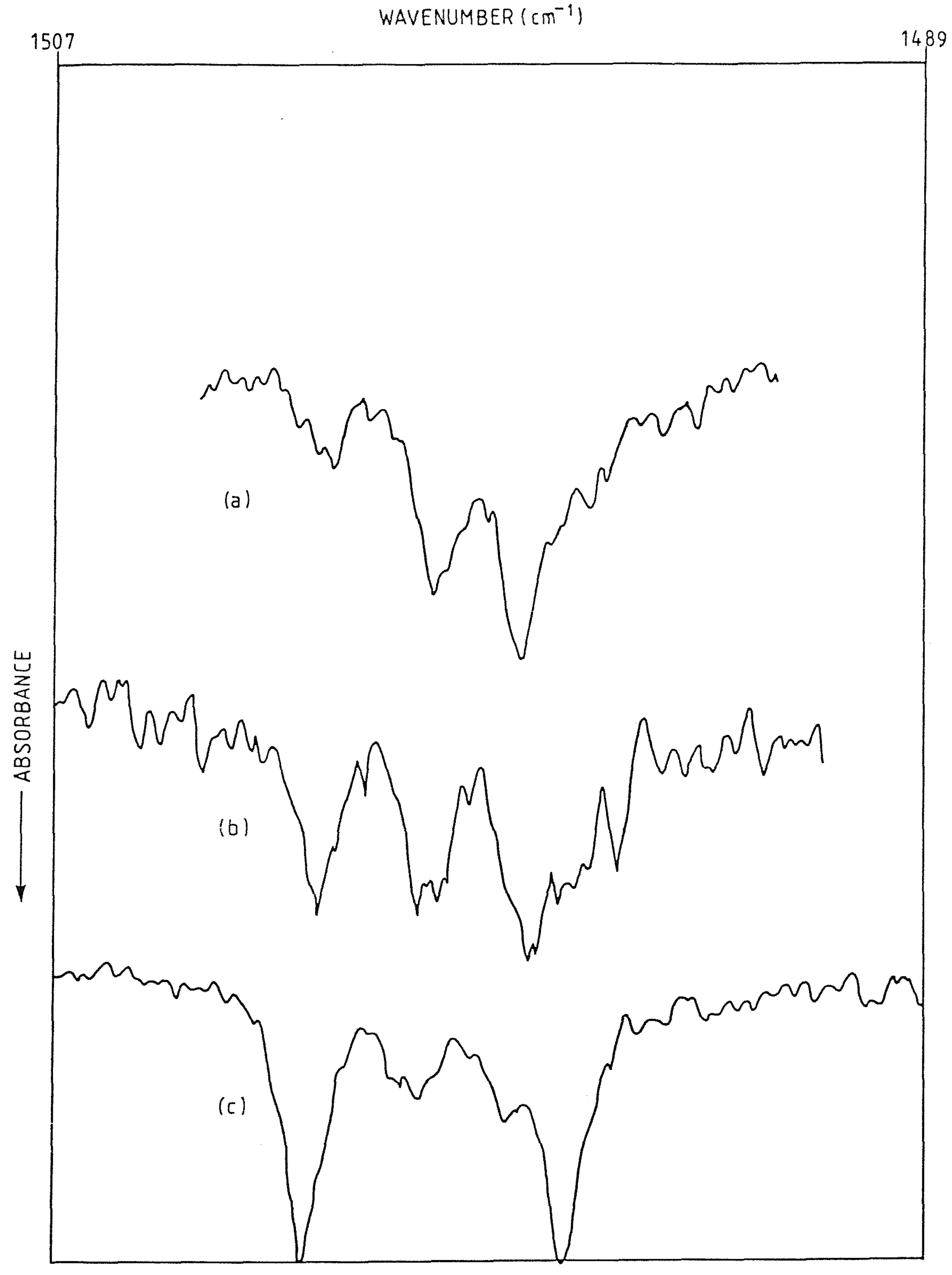

(a) FOR ≃ 30% ENRICHMENT
(b) FOR ≃ 40% ENRICHMENT
(c) FOR ≃ 75% ENRICHMENT

FIG. 9 HIGH RESOLUTION NITROGEN MATRIX IR SPECTRA IN THE Te – D STRETCHING REGION

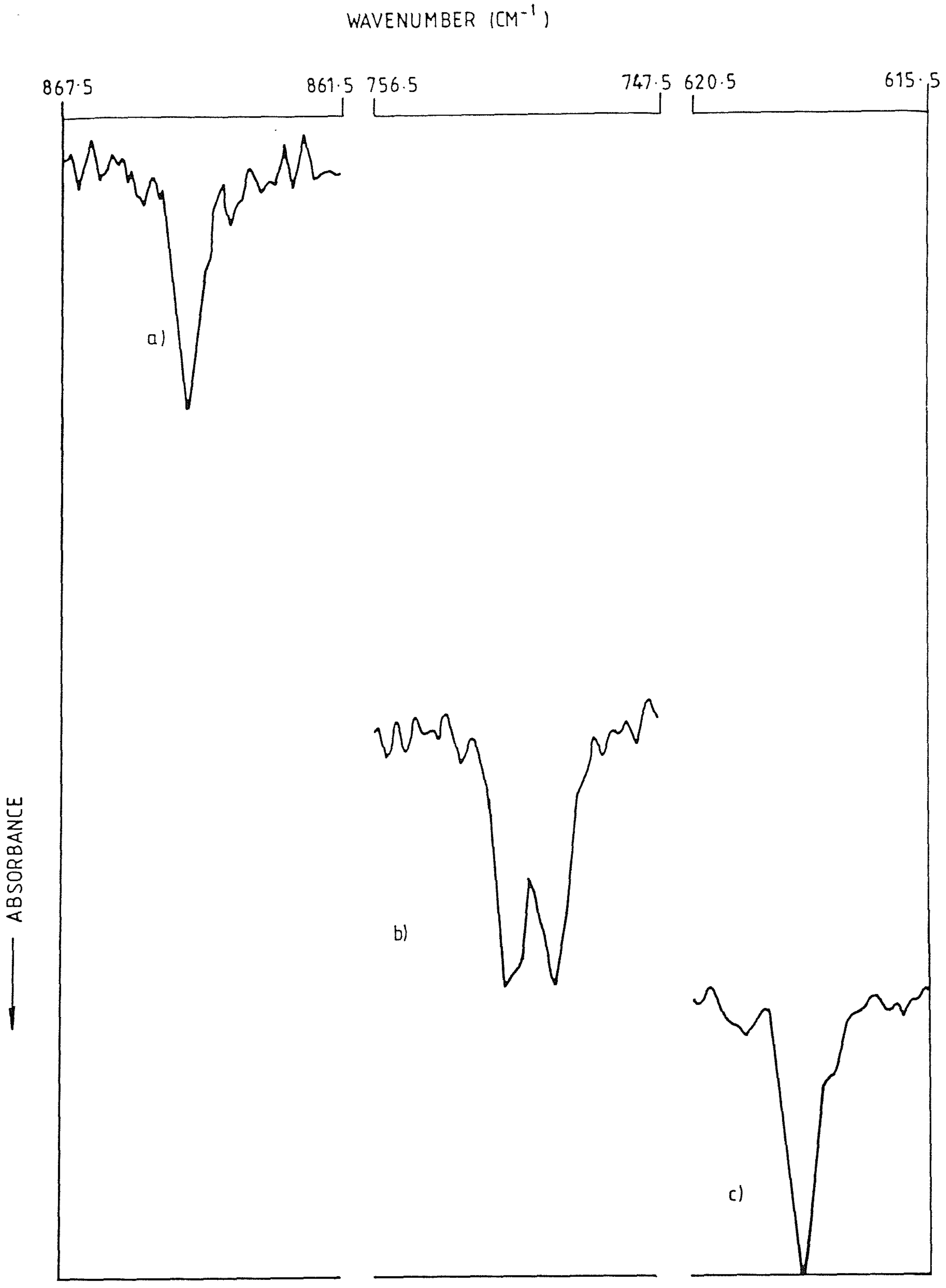

a) FOR ≃ 15 % ^{2}D ENRICHMENT
b) FOR ≃ 40 % ^{2}D ENRICHMENT
c) FOR ≃ 75 % ^{2}D ENRICHMENT

FIG.10 HIGH RESOLUTION NITROGEN MATRIX IR SPECTRA IN THE BENDING REGION asymmetric sites in a number of different orientations with respect to the site axes.

In HDTe the two stretching modes are well separated (~600 cm^{-1}) and it is usually assumed that one mode consists of almost 100% change in the TeH bond (ν_3) whilst the other mode is almost 100% change in the Te-D bond (ν_1). Therefore if the molecule can be accommodated in the site in more than one orientation and the potential surface of the site is asymmetric it can be imagined that each orientation will give rise to a slightly different frequency. This explanation also accounts for the fact that no splitting is observed in the H_2Te and D_2Te stretching frequencies, because both hydrogen and deuterium atoms will be moving in phase with each other and the asymmetric potential surface may result in a frequency shift but not a splitting.

Splitting of the bending mode is also probably due to this, because the hydrogen and deuterium in HDTe will move to a different extent during the vibration, whereas in H_2Te and D_2Te both halves of the molecule are undergoing the same motion and in phase with each other.

Therefore it can be concluded that the 6 observed lines for a partially deuterated species can be interpreted in terms of a matrix isolated HDTe molecule which is located in an asymmetric site.

The frequencies and assignments for all three species are given in Table 4.

2.5 Vibrational Analysis and the Calculation of Harmonic Frequencies

In order to set up a force field, 4 force constants need to be defined, these are the two principal force constants f_r and f_α and the two interaction force constants f_{rr} and $f_{r\alpha}$.

TABLE 4

Observed Spectral Features and Assignments for Deuterated Hydrogen Telluride Isolated in Nitrogen Matrices

	ν_1/cm^{-1}	ν_2/cm^{-1}	ν_3/cm^{-1}
H_2Te	2085.1	864.75	2091.7
D_2Te	1496.1	618.2	1501.6
HDTe	1497.3	752.7	2087.0
	1499.1	753.6	2089.7

The molecular geometry is fairly well established from the ir rotation-vibration studies with r = 1.658Å and $\alpha = 90.25°$(24,25) and these values were used throughout in the SOTONVIBP program(46).

When the frequencies for H_2Te were used the following force constants were obtained:

f_r = 2.568114 mdyne/Å
f_{rr} = -0.007963 mdyne/Å
f_α = 0.605265 mdyneÅ/rad²
$f_{r\alpha}$ = 0.010436 mdyne/rad

if these were then used to calculate the frequencies for HDTe and D_2Te the following resulted.

	ν_1/cm^{-1}		ν_2/cm^{-1}		ν_3/cm^{-1}	
	obs	calc	obs	calc	obs	calc
H_2Te	2085.1	2085.1	864.75	864.75	2091.7	2091.7
HDTe*	1498.2	1483.0	753.15	750.0	2088.35	2088.4
D_2Te	1496.1	1480.7	618.2	614.1	1501.6	1485.4

[*The observed values for HDTe have been taken as the average of the two bands in each case.]

From these data it can be seen that the fit for the modes involving hydrogen motion is very good, but for the deuterium modes a poor fit is obtained. When the D_2Te frequencies were used the reverse was observed. When the HDTe frequencies were used the program failed unless one specified a principal stretching force constant to the Te-H bond, f_{rH}, and a different principal stretching force constant, f_{rD}, to the Te-D bond. (It was also necessary to define $f_{r\alpha H}$ and $f_{r\alpha D}$).

The fact that if one uses hydrogen frequencies to predict deuterium frequencies and finds that they are too low, and that on using deuterium frequencies to calculate hydrogen frequencies that they are too high implies that the poor correlation between observed and calculated is due to anharmonicity. It was therefore decided to calculate the harmonic frequencies of hydrogen telluride and deuterium telluride in order to see whether a reasonable fit could then be obtained.

The method chosen for the evaluation of the anharmonic correction terms and hence the harmonic frequencies was based on the work of Gamo(47) who compared the accuracy of various approaches using the available data for H_2O, H_2S and H_2Se. He found that for water one needed to use an elaborate method as the amount of data would allow, whereas for heavier central atoms less sophisticated and more approximate methods gave reasonable solutions. Of the available methods, the one chosen, utilised the product rule and Dennison's rule(48).

The anharmonic corrections x_i are defined as:

$$\omega_i = \nu_i \ (1 + x_i)$$

where ν_i is the observed frequency of the ith mode,

ω_i is the harmonic frequency of the ith mode,

and x_i is the anharmonic correction for the ith mode.

In Chapter 3 it was seen that the product rule could be expressed as

$$\frac{\lambda_1 \ \lambda_2 \ \lambda_3}{\lambda'_1 \ \lambda'_2 \ \lambda'_3} = \frac{|\underline{G}|}{|\underline{G}'|}$$

The remaining equation that needs to be defined is the Dennison rule.

$$\frac{\omega_i}{\omega_i'} = \frac{x_i}{x_i'}$$

where the prime indicates the deuterated species. The Dennison rule is only strictly true for diatomics and becomes the Darling - Dennison approximation when applied to polyatomics.

The anharmonic corrections are then calculated thus:

$$\frac{x_i}{x_i'} = \frac{\omega_i}{\omega_i'} = \sqrt{\frac{|\underline{G}_i|}{|\underline{G}_i'|}} = \frac{\nu_i\,(1 + x_i)}{\nu_i'\,(1 + x_i')}$$

$$G = \sqrt{\frac{|\underline{G}_i|}{|\underline{G}_i'|}}\ ; \qquad A = \frac{\nu_i}{\nu_i'}$$

$$\therefore\ x_i = x_i'G$$

$$\therefore \frac{G}{A} = \frac{1 + x_i'G}{1 + x_i'}$$

$$\therefore \frac{G}{A} + x_i'\frac{G}{A} = 1 + x_i'G$$

$$x_i' = \frac{(G/A) - 1}{G\ (1 - 1/A)}$$

The only mode for which these calculations are valid without further approximations is the ν_3, B_1, asymmetric stretch, because in this case $|\underline{G}| = G$. This arises out of the fact that it is the only mode having the representation B_1. For the two A_1 modes, (ν_1 and ν_2) the determinant, $|\underline{G}|$, is expressed as a quadratic and hence the problem is not easily soluble. However, if the uncoupled oscillator approximation is invoked, the interaction force constant terms $f_{r\alpha}$ are set to zero. This is a valid approximation because the two modes are separated by ~1000 cm^{-1} and one expects little interaction. This however leaves the $\underset{\sim}{G}$ matrix interaction terms in the equations. These are very small because they are proportional to the reduced mass of the central atom. This is no doubt why Gamo found that this approach was satisfactory for H_2S and H_2Se but not for H_2O. The ν_1 and ν_2 frequencies can now be treated in exactly the same manner as the ν_3 frequency.

The results of these calculations are given in Table 5.

Whilst carrying out the anharmonic correction calculations the assignment of the stretching modes was varied, and it was found that reasonable values could only be obtained if ν_3 was greater than ν_1 for both H_2Te and D_2Te or vice versa. This indicates that the ordering of ν_1 and ν_3 must be the same in both H_2Te and D_2Te but does not shed any more light on the actual ordering.

Using this approach it is not possible to calculate exactly the harmonic frequencies for HDTe. One possible way of estimating them is to average the harmonic frequencies as Nibler and Pimentel(49) have done for H_2S and H_2Se. Thus the average of the anharmonic corrections for ν_1 and ν_3 of H_2Te gives a reasonable estimate of an anharmonic correction for the Te-H stretch in HDTe. This can also be

TABLE 5

Harmonic Frequencies and Anharmonic Corrections for H_2Te and D_2Te

	Observed Frequency	Harmonic Frequency	Anharmonic Correction
	ν/cm^{-1}	ω/cm^{-1}	x
H_2Te	2085.1 864.75 2091.7	2161.9 885.0 2172.4	0.03684 0.02339 0.03859
D_2Te	1496.1 618.2 1501.6	1535.2 628.5 1542.8	0.02616 0.01661 0.02741

carried out for ν_1 and ν_3 of D_2Te. In order to obtain a value of the anharmonic correction for the bending mode one needs to use:

$$\omega^2 = \tfrac{1}{2} (\omega^2_{H_2Te} + \omega^2_{D_2Te})$$

The results of these calculations are given in Table 6, the observed frequency given, is the average of the two in Table 4.

The harmonic frequencies for H_2Te were used to generate the force field below:-

f_r = 2.7655 mdyne/Å

f_{rr} = -0.0133 mdyne/Å

f_α = 0.6339 mdyneÅ/rad^2

$f_{r\alpha}$ = 0.0092 mdyne/rad

This was then used to calculate the harmonic frequencies for HDTe and D_2Te and the agreement between observed and calculated was within 0.1 cm^{-1} for all the isotopomeric frequencies. In order to confirm the veracity of the harmonic frequencies the sum rule was used where

$$\sigma = \sum_{\kappa} \lambda_\kappa = 4\pi^2 \sum \nu^2_\kappa$$

and $2\sigma(HTeD) = \sigma(HTeH) + \sigma(DTeD)$

The discrepancy for the harmonic frequencies was 309.15 cm^{-2} which is equivalent to 0.002% compared to 3146.5 cm^{-2} for the observed frequencies which is equivalent to 0.021%. Therefore the harmonic frequencies are better by an order of magnitude.

TABLE 6

Calculated Harmonic Frequencies and Anharmonic Corrections for HDTe

ν/cm^{-1}	ω/cm^{-1}	x
1498.2	1539.0	0.02723
753.15	767.5	0.01991
2088.35	2167.1	0.03772

The previous literature values for the force constants were either estimated from first principles or by use of the limited gas phase data(20). Gordy(50) in 1946 calculated the value of the bond stretching force constant to be 2.68 mdyne/Å with an anticipated frequency of 2300 cm^{-1}. The more recent value of 2.54 mdyne/Å obtained by Smithers and Krouse(20) appears to be based on "the two observed symmetric frequencies were 2047 cm^{-1} and 2133 cm^{-1} and the anti-symmetric frequency observed was 860.79 cm^{-1}". Therefore this value and the other force constants they quote should probably be regarded with some scepticism.

2.6 Conclusions

This work has identified the two stretching modes in hydrogen telluride for the first time. The assignment of ν_3 to 2091.7 cm^{-1} and ν_1 to 2085.1 cm^{-1} is based on analogy with the other hydrogen chalcogenides. On deuteration 9 new bands are observed and these are assigned to deuterium telluride and hydrogen deuterium telluride. The unexpected splitting of the HDTe frequencies is explained in terms of an asymmetrical site in the nitrogen matrix, in which the HDTe senses a different potential depending on its orientation within that site.

In order to obtain a force field which could reproduce the observed isotopomeric frequencies, the harmonic frequencies were calculated and the resultant fit between harmonic and calculated frequencies was better than 0.1 cm^{-1} for all the isotopomers.

3. The Interaction of Water Vapour with Metal Tellurides

The interaction of steam with metal tellurides is believed(9) to be a potential source of hydrogen telluride in a severe reactor accident. Having finger printed H_2Te, a series of matrix isolation ir experiments was embarked upon to try to determine the extent of the reaction of water vapour with a range of metal tellurides.

However, no bands that could be assigned to H_2Te were observed for either SrTe or Cs_2Te in a variety of experimental configurations. This is probably due to the problem of maximising the reaction cross section of the telluride with the water, whilst avoiding an excessive build up of ice on the cryogenically cooled deposition window. One possible alternative is to react the water vapour and metal telluride off the matrix rig and then spray the resultant volatile reaction products onto the window. This was not pursued because of the lack of time.

4. The Interaction of Tellurium Dioxide with Alkali Metals

4.1 Introduction

Earlier work by Gomme and Ogden(8, 9, 51, 52, 53) on the vapour phase chemistry of caesium and tellurium in oxidising conditions gave rise to very complex matrix ir spectra. In particular they studied Cs_2UO_4/Te, Cs_2CO_3/TeO_2, CsOH/Te, $CsOH/TeO_2$ and $CsOH/TeO_3$ mixtures, as well as a number of experiments involving potassium and rubidium salts. A number of the bands in the complex spectra were assigned to TeO_2 and its polymeric species by comparison with the previously published work (54, 55). The remainder were left largely unassigned except for two bands at 749 and 737 cm^{-1} which were tentatively assigned to Cs_2TeO_3. More recent work by Brisdon, Gomme and Ogden(56) on the analogous alkali metal selenites and selenates has identified M_2SeO_4 and M_2SeO_3 as vapour phase species above the heated solids. In addition to these, a new $MSeO_2$ species was identified and its assignment confirmed using the co-deposition of alkali metal atoms with selenium dioxide in nitrogen matrices.

It was therefore decided to carry out similar experiments using potassium and tellurium dioxide to confirm whether any of the bands in Gomme's earlier studies could be assigned to $MTeO_2$ species.

4.2 Experimental

For the supporting experiments of TeO_2 in nitrogen matrices, the TeO_2 (BDH) was heated in a platinum boat within a conventional induction furnace. For the co-deposition experiments the TeO_2 was heated in a silica tube to ≈ 650°C whilst the potassium (BDH) was heated in a pyrex tube to ≈ 200°C. The apparatus is shown in Fig 11. The apparatus could not be entirely of silica because of the problems of reaction between silica and potassium. The matrix gas used was nitrogen and typical deposition times were 10-30 minutes. The studies of the vaporisation of the remaining systems were all carried out by Gomme ([9], [51], [52], [53]).

4.3 Results and Discussions

The 1000-600 cm^{-1} survey spectrum of tellurium dioxide isolated in a nitrogen matrix is given in Fig 12(a). Higher resolution spectra were obtained but are not presented here as they add little to the already published data ([52], [54], [55]). The band positions and assignments are given in Table 7. Fig 12(b) is a survey spectrum from the co-deposition of potassium and tellurium dioxide in a nitrogen matrix. From this spectrum it can be seen that there is a small amount of monomeric TeO_2 at 849 cm^{-1} and some polymeric species at 619 cm^{-1}. The most prominent features at 749.2 cm^{-1} and 740.4 cm^{-1} are not observed in the TeO_2 spectrum and must therefore be due to a K/Te/O species. The position of these bands indicates that they are due to Te-O bond stretching modes. The spectrum was scanned to lower frequency (200 cm^{-1}) but there was no

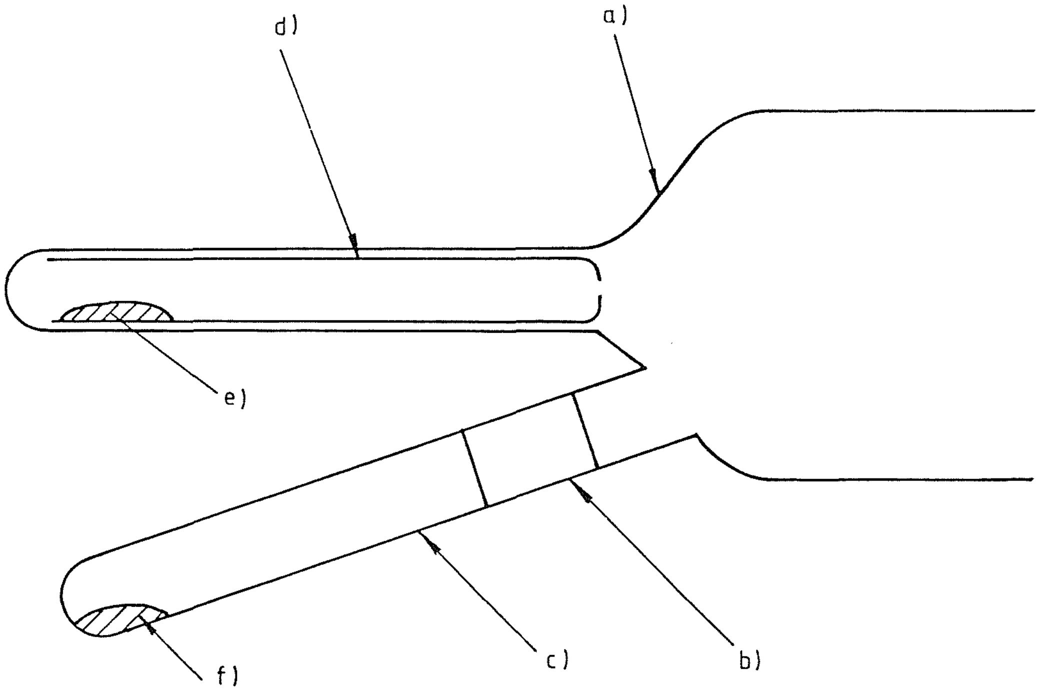

a) SILICA
b) SILICA/PYREX GRADED SEAL
c) PYREX
d) SILICA INSERT
e) TELLURIUM DIOXIDE
f) POTASSIUM

FIG.11 APPARATUS USED FOR THE CO-DEPOSITION OF TELLURIUM DIOXIDE AND POTASSIUM (FURNACES AND THERMOCOUPLES NOT SHOWN.)

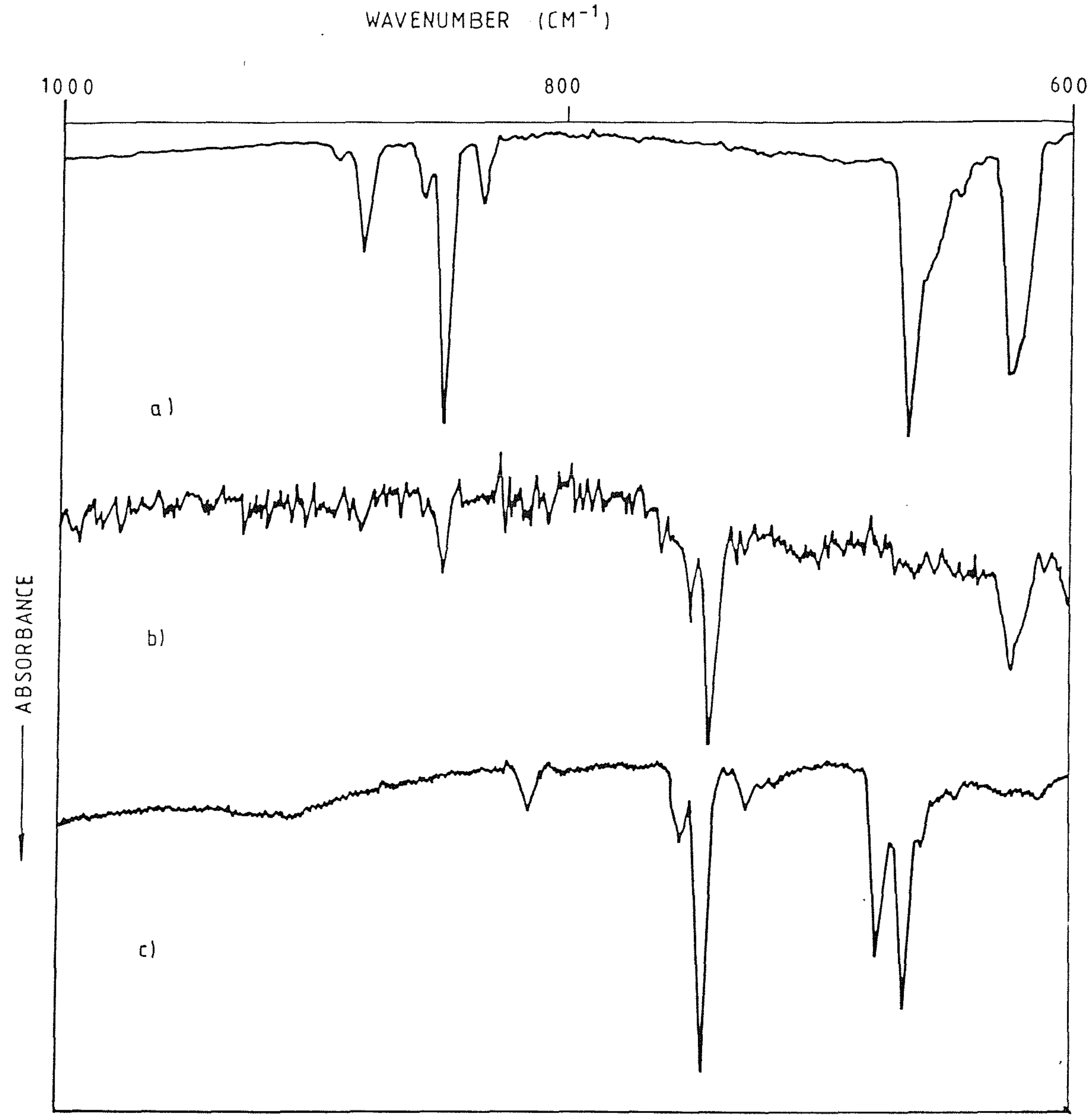

a) FROM THE VAPORISATION OF TELLURIUM DIOXIDE

b) FROM THE CO-DEPOSITION OF TELLURIUM DIOXIDE AND POTASSIUM.

c) FROM THE VAPORISATION OF POTASSIUM TELLURITE (K_2TeO_3)

FIG.12 SURVEY NITROGEN MATRIX IR SPECTRA OBSERVED FROM DIFFERENT TELLURIUM-OXYGEN SYSTEMS

TABLE 7

Observed Frequencies and Assignments for Matrix Isolated TeO_2 and $KTeO_2$

TeO_2		$KTeO_2$	
obsd freq/cm^{-1}	assignment[45]	obsd freq/cm^{-1}	assignment
891.8			
882.1	$(TeO)_n$	749.2	ν_1 $KTeO_2$
856.9	$(TeO)_n$		
848.6	ν_3 TeO_2	740.4	ν_3 $KTeO_2$
833.9	ν_1 TeO_2		
655.0			
619.4	Te_2O_2		

evidence above the noise level for the position of a bending mode.

When the matrix was warmed up slowly to enable diffusion to take place, the intensity of these bands rapidly decreased.

In the analogous oxyselenium studies by Brisdon(56) et al, the selenate (SeO_4^{2-}) and selenite (SeO_3^{2-}) frequencies have been assigned unambiguously by use of the central atom isotope effect. In addition to these species, they also observed a pair of low intensity bands at 815 and 805 cm^{-1} which they assigned to $M^+SeO_2^-$. This assignment was confirmed using alkali metal and selenium dioxide co-deposition experiments and they also observed that this pair of bands rapidly lost intensity on diffusion.

Therefore the bands at 749.2 and 740.4 cm^{-1} are assigned as the ν_1 and ν_3 stretching modes of $K^+TeO_2^-$. The assignment of ν_1 to 749.2 cm^{-1} and ν_3 to 740.4 cm^{-1} is based upon their relative intensities. By use of equation (1) the bond angle can be estimated to be ≃ 117° compared with 115° for TeO_2(53). The fact that the bands lose intensity on matrix warm-up implies that the $K^+TeO_2^-$ moeity is unstable and it is probably wise to consider that it is only formed when potassium atoms and tellurium dioxide molecules are close or adjacent to each other in the matrix.

If these results are compared with those of Gomme, then it can be seen from Fig 12(c) that the most prominent bands in his spectrum of K_2TeO_3 (BDH) are the same as those observed for the potassium tellurium co-deposition experiments. The higher resolution spectra of K^+TeO_2 and K_2TeO_3 in the 760-720 cm^{-1} region are shown in Fig 13(a) and 13(b) respectively. He also reported (52,53), that the heating of KOH and Te and KOH and TeO_2 mixtures gave rise to two bands at 750.5 and 741.3 cm^{-1} and that when CsOH was used they shifted to 747.1 and 738.9 cm^{-1}. The slight frequency

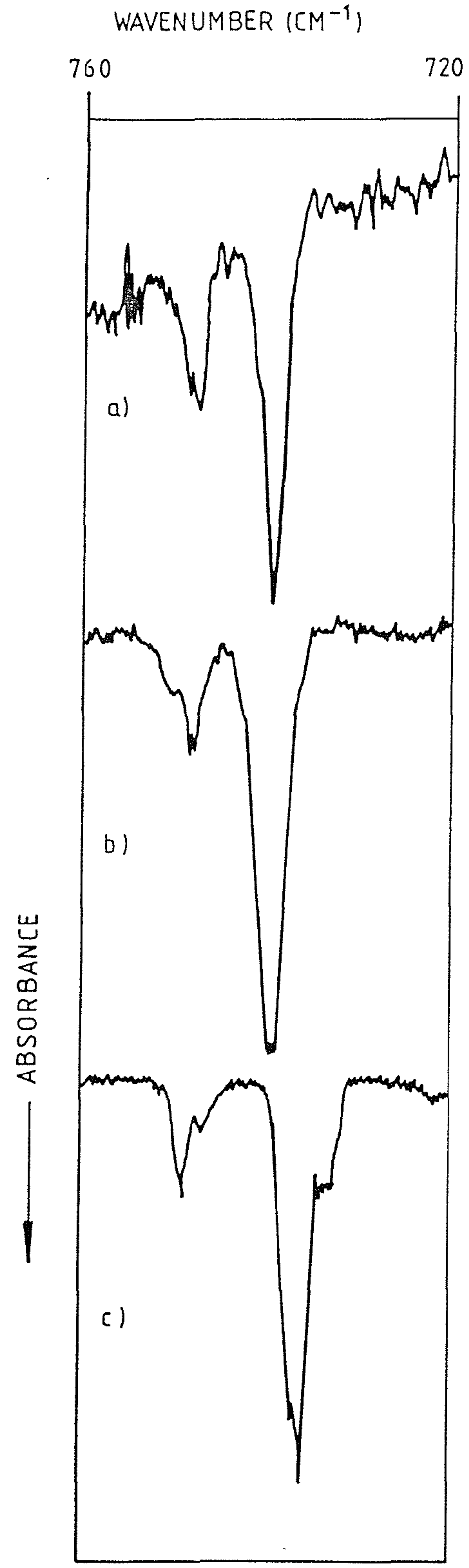

a) FROM THE CO-DEPOSITION OF TELLURIUM DIOXIDE AND POTASSIUM.

b) FROM THE VAPORISATION OF POTASSIUM TELLURITE (K_2TeO_3)

c) FROM THE VAPORISATION OF A MIXTURE OF CAESIUM HYDROXIDE AND TELLURIUM TRIOXIDE.

FIG.13 MEDIUM RESOLUTION NITROGEN MATRIX IR SPECTRA OBSERVED FROM TELLURIUM-OXYGEN SYSTEMS shift is within experimental error as the KOH and tellurium spectra were recorded on different instruments to the K and TeO_2 co-deposition experiments. Fig 13(c) is a medium resolution spectrum obtained from a heated mixture of caesium hydroxide and tellurium trioxide, and from this one can see a small cation effect, which indicates that the trapped species contains at least one alkali metal. Gomme also observed that no bands in the Te-O bridging region (650-600 cm^{-1}) could be found that correlated with this pair even when they were very intense. He thus concluded that they must arise from a monomeric species.

When Gomme studied the vaporisation of Cs_2TeO_3 he was hampered by problems of non-reproducibility of the complex spectra. This was probably due in part to the uncertainties in the chosen preparative method of heating Cs_2CO_3 and TeO_2. However, he did find that by increasing the Cs:Te ratio from 1 to 2 the spectrum was considerably simplified. In the latter case he only observed bands at 747 and 739 cm^{-1}, other than CO_2, and assigned tham to the A' and E modes respectively of a pyramidal C_{3v} TeO_3^{2-} unit in caesium tellurite (Cs_2TeO_3).

This assignment was made because of the simplification of a Cs:Te 2:1 ratio which he assumed implied that the vaporising species was Cs_2TeO_3. He was however, unable to determine the mode of co-ordination of the caesium cations within this model despite oxygen-18 studies. The work on the selenite species has shown that the SeO_3^{2-} unit has a distorted pyramidal shape and that the symmetry of the M_2SeO_3 unit is C_s. This implies that one cation is bound monodentatly whilst the other is bound in a bidentate fashion. In addition to the matrix ir studies, Gomme also carried out a number of mass spectrometric experiments on the vaporisation of K_2TeO_3 and Rb_2TeO_3, Cs_2TeO_3 was not studied because of the limited mass range (0-400 amu) of the instrument used. In both of these cases he saw clusters of peaks which could be assigned to $K_2TeO_3^+$ and $Rb_2TeO_3^+$, thus implying that tellurite is stable in the vapour above heated tellurite. He also observed decomposition products such as Te_2^+ in the spectra.

4.4 Conclusions

From the comparison of Gomme's earlier work with the present study two main possibilities exist.

(a) That the bands in the ir spectra from heated K_2TeO_3 belong to the same species formed on the co-deposition of potassium atoms and TeO_2. This species may be either K_2TeO_3, $KTeO_2$ or some other potassium oxytellurium compound.

(b) That the bands at similar frequencies belong to different species, most likely K_2TeO_3 and $KTeO_2$. As a result of a heavy central atom, it is expected that the modes of the M_2TeO_3 unit having C_s symmetry involving the bidentate co-ordination would be very similar in frequency to those of the $KTeO_2$ unit. In the selenium case the bands assigned to $MSeO_2$ were only several wavenumbers higher than the M_2SeO_3 absorptions. There is some evidence for this in Figs 13(b) and 13(c). Fig 13(b) is a medium resolution spectra obtained from K_2TeO_3, whilst Fig 13(c) is from a heated mixture of CsOH and TeO_3. In this latter spectrum there appears to be four bands which could be due to two species or to site effects.

It is not possible from these limited studies to say which of these two cases is the most probable. However the most likely co-deposition product is $KTeO_2$ and it may be that in Gomme's spectra this is present, but also that the vibrational modes of K_2TeO_3 and $KTeO_2$ will have very similar frequencies.

Therefore from this work it appears that some of Gomme's work needs to be repeated and perhaps revaluated to check the presence of more than one species; and that the co-deposition of caesium and tellurium dioxide should be studied in order to confirm or deny the presence of $CsTeO_2$ in his spectra of Cs_2TeO_3. The most convenient method for generating caesium atoms is to heat lithium metal with caesium chloride(57).

5. References

1. Potter P.E., Rand M.H. and Alcock C.B.
J. Nucl. Mat., 130, 139, 1985.

2. Johnson I., Steidl D.V. and Johnson C.E.
Proc. ANS Topical Meeting on Fission Product Behaviour and Source Term Research, Snowbird, Utah.
NP-4113-SR, p40, 1984.

3. Kleykamp H.
J. Nucl. Mat., 131, 221, 1985.

4. Garisto F.
AECL-7782, 1982.

5. Sallach R.A., Greenholt G.J. and Taig A.R.
NUREG/CR-2921, 1984.

6. Bowsher B.R. and Jenkins R.A.
AEEW R-1915, 1985.

7. Dickinson S.
AEE Winfrith
Unpublished Observations 1986.

8. Ogden J.S.
AEEW R-1700, 1984.

9. Bowsher B.R., Dickinson S., Nichols A.L., Gomme R.A., Ogden J.S. and Young N.A.
ACS Symposium on Chemical Phenomena Associated with Radioactivity Releases During Severe Nuclear Plant Accidents.
Anaheim, Calif. 9-12 Sept 1986. NUREG/CP-0078, 3-93, 1987.

10. Hurd H.T.
'Chemistry of the Hydrides'
J. Wiley and Sons, 1952.

11. Bagnell K.W.
'The Chemistry of Selenium, Tellurium and Plonium'
Elsevier, 1966.

12. Walton G.N.
AERE Harwell
Personal Communication via Bowsher B.R.
AEE Winfrith 1986.

13. Deane A.M.
AERE R-10444, Sect 3, 1986.

14. Chizhikov D.M. and Schastlivya V.A.
'Tellurium and Tellurides', Colletts, 1970.

15. Jarrel H. and Straley J.W.
Phys. Rev., 76, 199, 1949.

16. Rossmann K. and Straley J.W.
J. Chem. Phys., 24, 1276, 1956.

17. Rossmann K.
PhD Thesis Ohio State University 1958.
Dist. Abst., 19, 341, 1958.
cited as personal communication by H.H. Nielsen in ref 18.

18. Lascombe J., Huong P.V., Morisson H., Devaure J. and Josien M.L.
J. Chim. Phys., 61, 1414, 1964.

19. Hill R.A., Edwards T.H., Rossman K., Rao K.N. and Nielsen H.H.
J. Mol. Spect., 14, 221, 1964.

20. Smithers R.M. and Krouse H.R.
Can. J. Chem., 46, 583 1968.

21. Moncur N.K. and Edwards T.H.
J. Opt. Soc., 56, 1422, 1966.

22. Moncur N.K. and Edwards T.H.
J. Chem. Phys., 51, 2638, 1969.

23. Moncur N.K., Willson P.D. and Edwards T.H.
J. Mol. Spect., 52, 181, 1974.

24. Willson P.D., Moncur N.K. and Edwards T.H.
J. Mol. Spect., 52, 196, 1974.

25. Moncur N.K., Willson P.D. and Edwards T.H.
J. Mol. Spect., 52, 380, 1974.

26. Schmidbaur H. and Siebert W.
Z. Naturforsch., 20B, 596, 1965.

27. Balkis T., Gaines A.F., Oezgen G., Oezgen I.T. and Flowers M.C.
J. Chem. Soc. Farad. Trans. II, 72, 524, 1976.

28. Churbanov M.F., Gaivoronskii P.E., Larin N.V. and Nikolaev I.F.
Russ. J. Inorg. Chem., 22, 617, 1977.

29. Burenin A.V., Krupnov A.F., Mart'yanov S.V., Mel'nikov A.A. and Nikolayev L.I.
J. Mol. Spect., 75, 333, 1979.

30. Goodeve C.F., and Stein N.O.
Trans. Farad. Soc., 27, 393, 1931.

31. Price W. C.
J. Chem. Phys., 16, 551, 1948.

32. Price W.C., Teegan J.P. and Walsh A.D.
Proc. Royal Soc., A201, 600, 1950.

33. Mayhew C.A., Connerade J.P. and Baig M.A.
J. Phys., B19, 4149, 1986.

34. Potts A.W. and Price W.C.
Proc. Royal Soc., A326, 181, 1972.

35. Barrett P.H., Montano P.A. and Mann J.B.
Phys. Rev., B14, 4755, 1976.

36. Montano P.A., Nagarathna H.M., Newlin D. and
Stewart G.W.
J. Chem. Phys., 74, 5558, 1981.

37. Darling B.T. and Dennison D.M.
Phys. Rev., 57, 128, 1940.

38. Benedict W.S., Gailar N. and Plyler E.K.
J. Chem. Phys., 24, 1139, 1956.

39. Tursi A.J. and Nixon E.R.
J. Chem. Phys., 52, 1521, 1970.

40. Edwards T.H., Moncur N.K. and Snyder L.E.
J. Chem. Phys., 46, 2139, 1967.

41. Gillis J.R. and Edwards T.H.
J. Mol. Spect., 85, 55, 1981.

42. Tursi A.J. and Nixon E.R.
J. Chem. Phys., 53, 518, 1970.

43. Barnes A.J. and Howells J.D.R.
J. Chem. Soc. Farad. Trans. II, 68, 729, 1972.

44. Cameron D.M., Sears W.C. and Nielsen H.H.
J. Chem. Phys., 7, 994, 1939.

45. Gillis J.R. and Edwards T.H.
J. Mol. Spect., 85, 74, 1981.

46. Refs 9 and 10 in Chapter 3

47. Gamo I.
J. Mol. Spect., 30, 216, 1969.

48. Dennison D.M.
Rev. Mod. Phys., 12, 175, 1940.

49. Nibler J.W. and Pimentel G.C.
J. Mol. Spect., 26, 294, 1968.

50. Gordy W.
J. Chem. Phys., 14, 305, 1946.

51. Bowsher B.R., Nichols A.L., Gomme R.A., Ogden J.S. and Young N.A.
'Speciation of Fission and Activation Products in the Environment' p27
Eds. Bulman R.A. and Cooper J.R.
Elsevier. 1986.

52. Gomme R.A.
PhD Thesis, Southampton University, 1984.

53. Gomme R.A., Ogden J.S. and Bowsher B.R.
AEEW - R 2204, 1986.

54. Hinchcliffe A.J.
D. Phil. Thesis, Oxford University, 1972.

55. Meunow D.W., Hastie J.W., Hauge R., Bautista R. and Margrave J.L.
Trans. Farad. Soc., 65, 3210, 1969.

56. Brisdon A.K., Gomme R.A. and Ogden J.S.
J. Chem. Soc. Dalton Trans., submitted for publication.

57. Tevault D.E., Chi F.K. and Andrews L.
J. Mol. Spect., 51, 450, 1974.

58. Keinosuke, H.
Spectrosc. Lett., 20, 537, 1987.

CHAPTER SIX

THE CHARACTERISATION OF MOLECULAR ORTHOBORIC ACID

1. Introduction

Light water reactors (eg PWR) contain significant quantities of boron in various forms to act as neutron absorbers or poisons. The primary coolant water contains between 50 and 1200 ppm of boron as boric acid, the precise level depending on the status of the reactor. Even higher quantities are available from the emergency core cooling systems (ECCS) and some reactors use boron carbide in control rods and borosilicate glass as burnable poisons. On average, approximately 700 kg of boric acid is present in the primary coolant ([1]), whilst almost 40 tonnes could enter the damaged core as part of the emergency core cooling systems. In a severe reactor accident it is postulated that the boric acid may be released as vapour or aerosol by the following mechanisms:

i) flashing of the reactor coolant in the early stages of a reactor accident, with the formation of boric acid aerosols;

ii) extensive overheating of the core causing evaporation of the primary system coolant, volatilisation of boric acid and crystallisation of boron oxide in the dried-out regions of the core;

iii) injection of the borated emergency core cooling system onto the degrading core, resulting in flash boiling and the formation of boric acid aerosols;

iv) vaporisation of boric acid by flashing of water when the core slumps into the lower plenum.

v) reaction of steam with boron carbide control rods to generate boric acid ([2]).

Boric acid in the primary coolant is an important potential source of aerosol, and significant deposits of boric acid crystals have been observed in the damaged core of the reactor at Three Mile Island 2 (TMI-2)(3) and in the LOFT FP-1 tests(4). Furthermore, airborne boric acid debris would provide suitable nucleation centres for the condensation of volatile fission products, with the potential for some form of chemical reaction(5-8).

Orthoboric acid, $B(OH)_3$ or H_3BO_3, has been known as a white crystalline solid for many years and numerous papers have been devoted to its structure, based on hydrogen-bonded planar $B(OH)_3$ units (9). When heated to above 100°C at atmospheric pressure, orthoboric acid is converted into metaboric acid, HBO_2 (10). The initial product has a flaky crystalline appearance (form III) when the conversion occurs below 130°C, which can then be converted to a coarser structure (form II) by heating to above 130°C. Additional changes in the crystalline structure occur above 150°C (HBO_2 I form) with the loss of further water. The evolution of water continues at higher temperatures, but heating to 1000°C will not produce anhydrous boron oxide because the water vapour above HBO_2/B_2O_3 is in equilibrium with the melt (9).

Despite the fact that boric acid is often cited as a 'classic' example of a molecule possessing C_{3h} symmetry, experimental evidence for its existence as a vapour phase species is remarkably sparse. The volatility of boric acid was first investigated (12) by Tchjevski in 1884, who found that on evaporating a dilute solution to dryness, up to 75% of the boric acid was lost.

The subsequent work appears to fall into three distinct sections. The first group of about a dozen papers (13-25), published between 1910 and 1937, were primarily concerned with whether boric acid vaporises from its solutions, or if the weight loss observed on distillation was attributable to mechanical transfer. Although the debate gives the impression of being bitter and acrimonious, as evidenced by polemical articles ([17,21]) about the previous work ([16,20]), the consensus of opinion was that boric acid is volatile and "distils in the gas phase because of its vapour pressure and not because of the formation of a volatile hydride" ([22]). In the presence of steam the rate of vaporisation was found to be greater. It should be noted that von Stackelberg ([23,24]) observed the sublimation of orthoboric acid in a steam atmosphere at 110°C to 180°C. None of these papers describe how they ascertained that the sublimate or distillate was indeed orthoboric acid and not one of many of its partially dehydrated relatives.

The assumption that the boric acids are volatile has long been held by analytical chemists because of the problem of loss of boron on boiling of boron solutions ([26]) and also by geologists because of the deposits of H_3BO_3 found around fumarates and hot springs ([27]).

It has been found more recently ([28]) that the loss of boric acid in acidic solutions (HNO_3, H_2SO_4, $HClO_4$) is less than 3% until 90-95% of the solution has evaporated. It has also been noted ([29]) that boric acid in sea water has a vapour pressure at ordinary sea temperatures, indeed it has even been suggested ([30]) that the major source of boron in the atmosphere is as a result of boric acid evaporation from the sea.

Interest in vapour phase boric acid and other related boron-oxygen-hydrogen compounds was re-awakened in the fifties and sixties when the US Pentagon proposed the use of boranes and boron esters as jet propellants ([31], [32], [33]) in place of the more conventional hydrocarbons. The thrust of this work was to calculate thermodynamic parameters so that better calculations of the processes occurring during combustion could be made. It appears that the Pentagon were not aware that unlike hydrocarbon combustion, the products from borane combustion include B_2O_3, which is a hard glassy solid at room temperature. As a result, within a couple of years papers were appearing describing how to remove the boron oxide deposits from the turbines and other innards of the jet type engines using HF/BF_3 mixtures(31) or high pressure super saturated steam (32, 33). Because of the high combustion temperatures only a few experiments were carried out at lower (150-200°C) temperatures and as a result the data in the literature of this period on vapour phase boric acid are fairly limited.

In 1956, Margrave presented a paper (37) at a Geochemical Conference, reporting work on the B_2O_3/H_2O system in the temperature range 280-900°C. He concluded from constructing weight loss of B_2O_3 versus partial pressure of water (P_{H_2O}) plots, that the vaporising species was probably HBO_2. Infrared and uv-vis spectroscopy was attempted using heated cells but no characteristic spectra were found. He also claimed that the work of von Stackelberg et al (24) indicates the existence of both vapour phase H_3BO_3 and HBO_2, and that at lower temperatures, H_3BO_3 is the preferred form.

In a subsequent report(38) on the passage of a variety of gases (H_2, N_2 and Ar) over B_2O_3 Margrave reported that the vaporisation of B_2O_3 was greatly enhanced by the addition of water to the flow gas. At high temperatures (~500°C) it was found that $H_2B_2O_4$ was formed, with the possibility of some HBO_2, whilst at lower temperatures orthoboric acid solid, vaporised as orthoboric acid vapour. However, in a second paper(39), with the same title, he claimed that at 500°C the reaction products were H_3BO_3 and possibly HBO_2 vapours.

In a review article (40), on the characterisation of gaseous oxides and hydroxides, Margrave described the problems of identification and characterisation of these systems, and suggested that spectroscopic methods should be applied to them. This of course included the boron oxides and acids. He however added the caveat: "The complete characterisation of such gaseous molecules, which exist only in high temperature systems, is a formidable task, even with all the modern tools of chemistry and physics" ([40]).

Within several months spectroscopic evidence had been presented indicating the presence of HBO_2 over B_2O_3 at low water partial pressures. The first of these by White et al ([41]) was an emission ir spectrum whilst the second was a mass spectrometric study ([42]). In this latter study the reaction of water vapour and B_2O_3 at ≃ 1000°C was found to result in mainly HBO_2^+ with very small amounts of $H_3BO_3^+$ and $(HBO_2)_3^+$.

In order to establish which boric acid was volatile at high water pressure, Margrave ([43]) embarked upon a gas phase ir study of the $B_2O_3/B(OH)_3/H_2O$ system in the temperature range 100-200°C and a transpiration study in the range 700-1000°C. The transpiration experiments showed, by partial pressure measurements, that at temperatures around 800°C, H_3BO_3 is the predominant vapour phase product if the water vapour pressure is above several torr. If the temperature is increased to 1000°C and the water vapour pressure kept below 150 torr then HBO_2 vapour becomes predominant over H_3BO_3. The problem with observing these systems using ir spectroscopy is the huge absorptions that one would expect from several hundred torr pressure of water vapour. In order to try and overcome this problem Margrave used much lower temperatures, 100-200°C, and obtained some spectral features from a closed heated cell system. These are given later in Table 1 with the more recent gas phase studies of Gilson (44). With hindsight, some of these bands were correctly assigned to boric acid but it is worth pointing out that although the transpiration studies were subsequently published in the open literature (45), no trace of the ir work can be found in Chemical Abstracts. A similar situation exists regarding the only previous matrix isolation study of orthoboric acid by Mack and Wilmot (33) which was presented at a Rocket Propellant Conference but of which there is no trace in the open, available literature.

During this time, Soviet scientists were also investigating the B_2O_3/H_2O system (46-52), and found that in general the volatilisation of boron increased in the presence of water. In particular (51,52) they estimated that the vapour pressure of orthoboric acid in the range 383-415K is (51):

$$\log P_{H_3BO_3} = -(3940/T) + 10.17$$

in the range 415-488K is (52):

$$\log P_{H_3BO_3} = -(1910/T) + 5.42$$

and in the range 488-673K is (52):

$$\log P_{H_3BO_3} = -(1120/T) + 3.72$$

The discontinuities are because of the presence of other substances in the vapour.

During a single crystal X-ray study (53, 54) Zachariasen noted that after a period of time the crystal had vaporised away.

Therefore from this survey it appears that orthoboric acid is volatile, (one author (55) however states that gas phase boric acid does not exist) but that hardly anything is known about it in the gas phase.

The present renaissance of interest in boric acid is due to the concerns mentioned earlier about its extensive use in PWRs and the need to obtain accurate thermodynamic data for all chemical species that could conceivably be involved in a severe reactor accident. Unfortunately, the available thermodynamic data ([56,57]) for the molecular species, H_3BO_3, is still based on the vibrational data of the solid orthoboric acid assuming either free rotation of the hydrogen atoms ([56]) or a planar species ([57]). Therefore if there is any large discrepancy between the frequencies for the solid and gas phase molecules then the veracity of the thermodynamic calculations has to be questioned.

As a result of the interest in the reactions between boric acid and alkali metal halides, bands had been observed in the spectra that indicated the presence of a boron containing species in the vapour. This study of the vaporisation of boric acid was therefore embarked upon in the hope that the volatile boron species would be identified and characterised and some relevant thermodynamic parameters determined.

2. Experimental

Samples of boric acid with "normal" isotope composition (~ 80%^{11}B, 20%^{10}B) were obtained from Aldrich (Gold Label ≥ 99% pure) and used without further purification. This material was used to prepare the ^{18}O and ^{2}D enriched samples by dissolving the parent solid in isotopically labelled water ($H_2{}^{18}O$ ~ 70 atom % (Amersham) or D_2O 99.9 atom % (Aldrich Gold Label)) and allowing equilibration to take place over several days at room temperature in Pyrex ampoules sealed with Young's Taps, (see Fig 1).

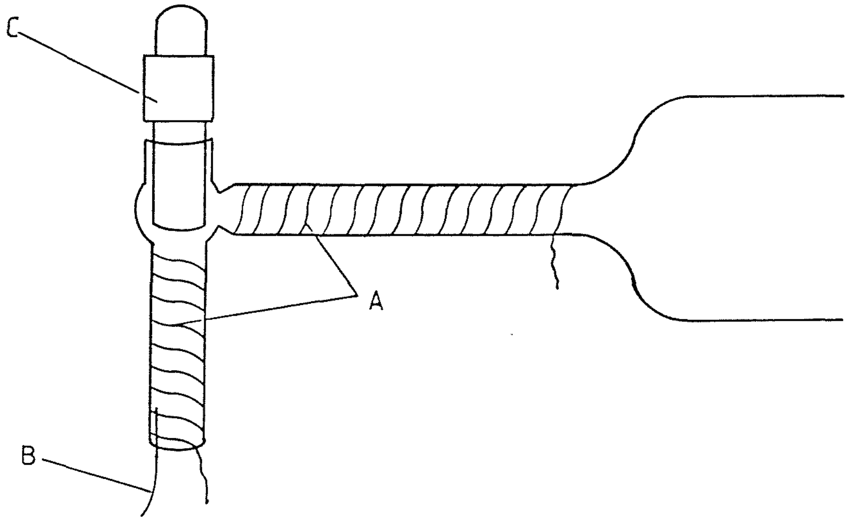

A NICHROME FURNACE

B CHROMEL-ALUMEL THERMOCOUPLE

C 'YOUNGS' TAP

FIG.1 PYREX SAMPLE HOLDER USED FOR THE PREPARATION AND VAPORISATION OF BORIC ACID

At the end of this period, the solution was evaporated to dryness under vacuum at ambient temperatures. ^{10}B enriched samples of boric acid were obtained by dissolving B_2O_3 (90 atom % ^{10}B, kindly donated by AEE Winfrith) in either $H_2{}^{16}O$, $H_2{}^{18}O$ or D_2O and similarly evaporating to dryness. The deuterium exchange is anticipated to be facile and it is reported (58) that the exchange of heavy oxygen between water and boric acid is rapid at 100°C.

The sealed ampoules were then mounted on either the mass spectrometer or matrix rig and pumped under high vacuum (10^{-6} torr) for 1-2 hours at room temperature in order to remove absorbed water. In the case of the matrix experiments the tap was shut whilst the cryostat cooled down in order to avoid solid subliming onto the window. The samples were heated externally by a nichrome wire furnace and the temperatures were monitored by a chromel-alumel thermocouple and digital thermometer.

3. Mass Spectrometric Studies

During the course of the investigation into the caesium iodide-boric acid system (Chapter 7), it became apparent from the mass spectral studies that molecular orthoboric acid could be observed in the vapour when these mixtures were heated to 400-500°C. Therefore the first experiments performed were carried out in this temperature range; however, the matrix ir spectra were very badly affected by ice bands. To overcome these problems it was decided to follow the effect of heating boric acid by mass spectrometry, and once having found the appropriate conditions to study the vapour using matrix isolation ir spectroscopy.

Fig 2(a) shows a typical spectrum obtained from "normal" boric acid heated to only 40-50°C. The prominent ions at 44/45 and 61/62 amu may readily be identified as $B(OH)_2^+$ and $B(OH)_3^+$ respectively.

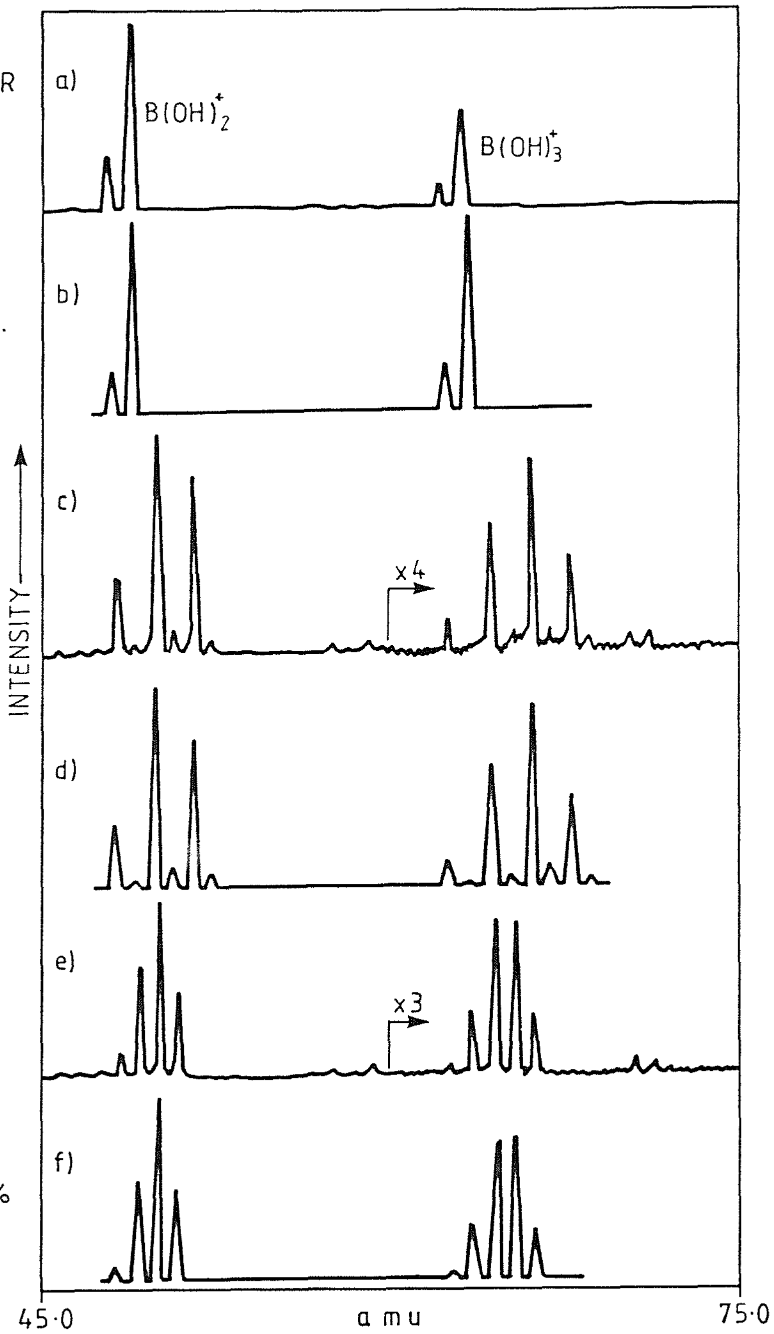

a) OBSERVED SPECTRUM FOR NORMAL BORIC ACID.

b) CALCULATED SPECTRUM ASSUMING ^{10}B:^{11}B OF 1:4.

c) OBSERVED SPECTRUM FROM A ^{10}B, ^{18}O ENRICHED SAMPLE.

d) CALCULATED SPECTRUM WITH 90% ^{10}B AND 60% ^{18}O.

e) OBSERVED SPECTRUM FROM A ^{2}D ENRICHED SAMPLE.

f) CALCULATED SPECTRUM WITH 20% ^{10}B AND 55% ^{2}D.

FIG.2 MASS SPECTRA OF THE VAPOUR ABOVE BORIC ACID HEATED TO 40°C

Fig 2(b) is a calculated spectrum using the natural isotope abundance of boron. The ionisation efficiency curves for these two ions are shown in Figs 3(a) and 3(b) and from these there is no indication of any unusual behaviour. The appearance potentials for $B(OH)_3^+$ and $B(OH)_2^+$ have been calculated from these plots and found to be 10.8 ± 0.5 volts and 13.8 ± 0.5 volts respectively. These values are typical for a parent-daughter relationship and indicate that the $B(OH)_2^+$ ion is a fragment of the $B(OH)_3^+$ parent ion. The appearance potential for HBO_2 has been estimated previously (^{42}) to be 12.6 ± 0.2 volts.

The only other boron containing species detected in these studies was a very small amount of $(HBO_2)_3^+$, and this was only observed using the very sensitive departmental MS30 mass spectrometer.

Fig 2(c) shows the mass spectrum obtained under similar conditions from a sample of $^{10}B/^{18}O$ enriched boric acid. Initially mass spectrometry of these isotopically enriched species was used to confirm the presence of a B-O-H species in the vapour and identify that species as $B(OH)_3$. Subsequently it was used to calculate the extent of ^{18}O (or ^{2}D) enrichment in a sample. Therefore the spectrum in Fig 2(c) corresponds closely to an isotopically scrambled sample containing ≈ 90% ^{10}B and ≈ 60% ^{18}O, and the calculated spectrum is shown in Fig 2(d). Similar studies were carried out on deuterated samples and these are shown in Figs 2(e) and 2(f) with a normal boron isotope distribution and 55% ^{2}D enrichment.

These mass spectral studies have therefore shown that the vapour above boric acid heated to 40°C is composed primarily of <u>molecular</u> H_3BO_3.

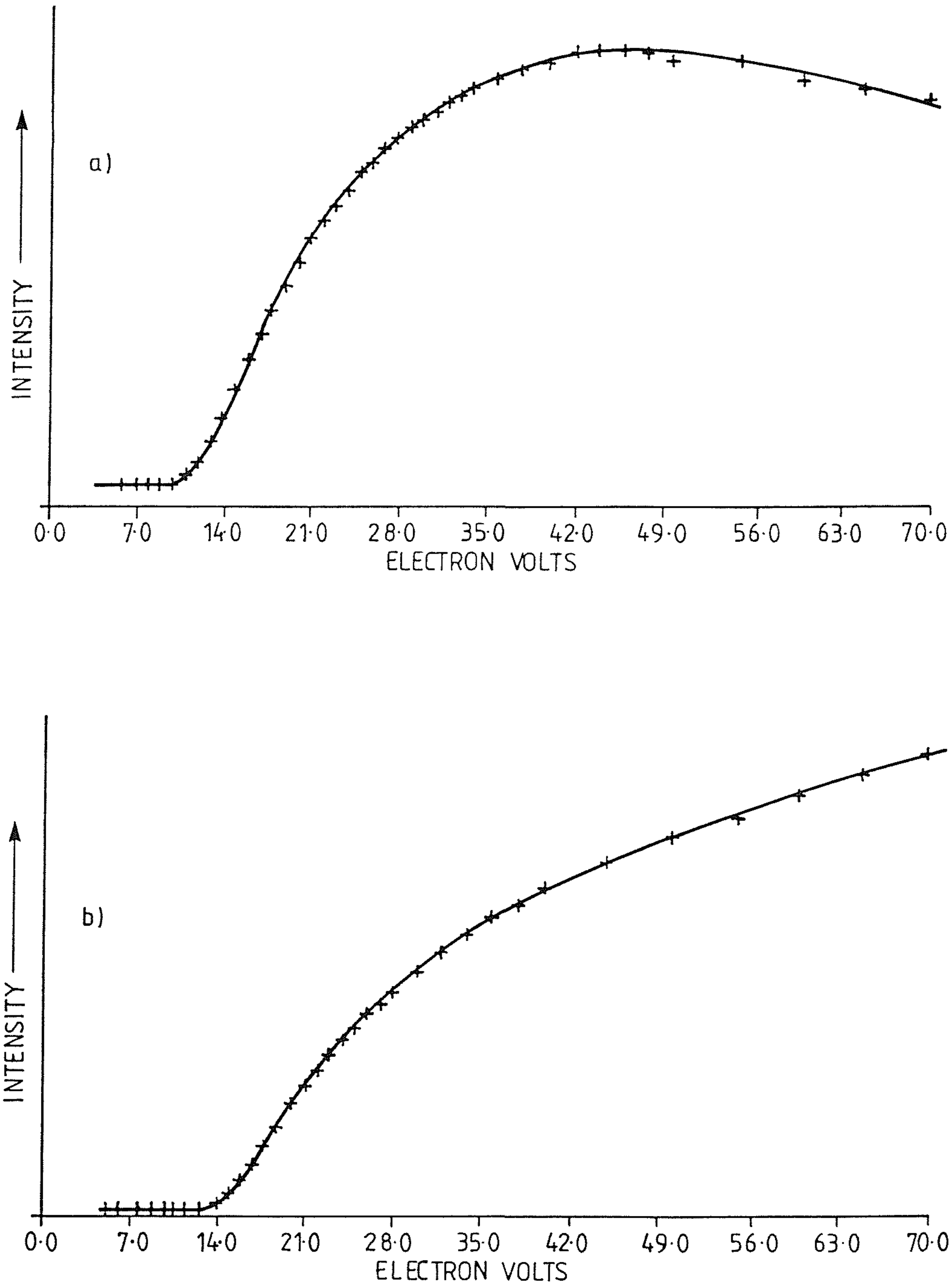

a) $H_3BO_3^+$ AT 62 amu

b) $H_2BO_2^+$ AT 45 amu

FIG.3 IONISATION EFFICIENCY CURVES OBSERVED FOR BORIC ACID

4. Matrix Isolation Studies

4.1 Preliminary Results

Fig 4(a) shows a typical ir survey spectrum obtained after co-condensing "normal" boric acid vapour generated at 35°C with a large excess of nitrogen onto the cryogenically cooled caesium iodide window for 2-3 hours. Prominent peaks can be observed at 3726, 3668.5, 1597, 1478.0, 1426.2, 1009.9, 675.0 and 513.8 cm^{-1} with weaker features at 3633, 1460, 1080, 700.9 and 448.9 cm^{-1}. Three of these absorptions (marked *) may be identified as arising from matrix isolated monomeric water(59), but the remaining features have not previously been observed. The effect of exchanging the ^{11}B for ^{10}B is shown in Fig 4(b). All the features present in Fig 4(a) can also be observed in this spectrum, but the relative intensities of certain pairs of bands have altered significantly. In particular the features at 1478.0 and 1426.2 cm^{-1} have an approximate intensity ratio of 1:2 in Fig 4(a) whilst in Fig 4(b) this ratio has changed to 10:1. A similar effect can also be seen on the bands at 700.9 and 675.0 cm^{-1}. These effects are a direct result of changing the $^{10}B/^{11}B$ isotopic abundance and therefore indicates which modes involve significant boron atom motion.

The effect of introducing ^{18}O or ^{2}D into the molecule can be seen in Figs 4(c) and 4(d). Whilst they show which modes involve oxygen or hydrogen motion, the spectra are not sufficiently well resolved to be able to make any general comments at this stage. The weak peaks at ≃ 1460 and 1080 cm^{-1} remained broad under higher resolution and did not appear to correlate with any of the more intense features and hence remain unassigned.

Several experiments were also carried out in argon matrices and a similar pattern of new bands was produced. These however were significantly broader than those observed in

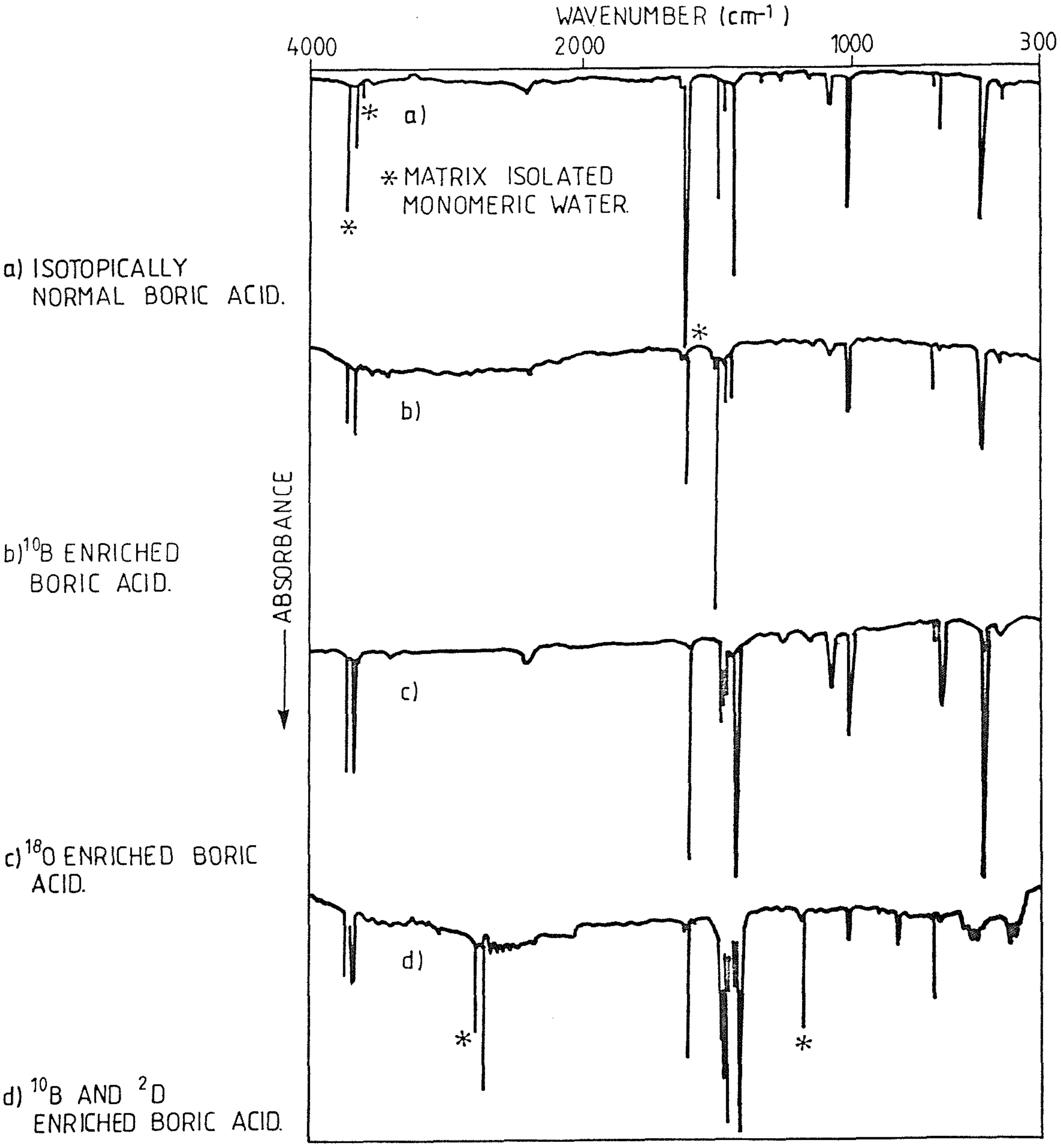

FIG.4 INFRARED SURVEY SPECTRA OF THE VAPOUR ABOVE BORIC ACID HEATED TO 35° C, ISOLATED IN NITROGEN MATRICES

nitrogen, and as a result of this the subsequent isotope enrichment experiments were all carried out using nitrogen matrices.

On the basis of the mass spectrometric results these ir bands are provisionally assigned to molecular boric acid.

4.2 Ir Spectral Assignments

The assignments proposed for the various matrix frequencies listed in Table 1 are based on a group frequency approach, and at this level of description may be compared with previous data for crystalline boric acid ([9]). The structure of this material has been investigated by single crystal x-ray ([53,54]), neutron ([60]) and electron ([61]) diffraction techniques and found to consist of discrete $B(OH)_3$ units linked together by hydrogen bonds to form infinite layers of nearly hexagonal symmetry. These layers are randomly displaced with respect to each other, indicating that only van der Waals forces bind the layers together. As a result, one might anticipate substantial differences in frequency and intensity between the isolated molecule and the solid as regards modes involving hydrogen atom motion, but might hope for a closer correspondence in the case of the central BO_3 unit.

Unfortunately, there is considerable variation in the literature concerning the vibrational frequencies and assignments for H_3BO_3 in the solid and this is summarised in Table 2. Not included in this table are the data of Sen ([76]) and Duval and Lecomte ([77]) because they bear no resemblance to the other cited frequency values. It will be noticed that there is a general consensus about the frequencies of the in-plane (ν and δ) modes but the assignment of the out of plane (γ and τ) modes is switched between the various reports. The values that have gained general acceptance ([9,55]) are those of Bethell and

TABLE 1

IR Spectral Features Observed for Boric Acid in Different Phases

Solid(65,68) (cm^{-1})		Vapour(43,44) (cm^{-1})		N_2 Matrix (cm^{-1})	Assignment
3200	3150	3750(?)	3710	3668.5	O-H stretch
1450	1428	1430	1425	1426.2	^{11}B-O stretch
1197	1183	1015(?)	1015	1009.9	H-O-^{11}B bend
540	544			448.9	$^{11}BO_2$ bend
648	800			675.0	$^{11}BO_3$ out of plane bend
824	639	303		513.8	OBOH torsion

TABLE 2

COMPARISON OF SOLID STATE IR DATA

Assignment			Matossi & Bluschke (62)	Miller & Wilkins (63)	Mortimer (64)	Bethell & Sheppard (65)	Sidorov & Sobolev (66)	Hornig & Plumb (67)	Servoss & Clark (68)	Goubeau & Hummel (69)	Krishnan (70)	Durig et al (71)	Vizi (72)	Broadhead & Newman (73)	Now-djavan (74)*	Janda & Heller (75)
ν_{O-H} (stretch)	H_3BO_3	^{11}B	3060	3270	3194	3200		3120	3150		3251	3220	3217	3210	3160	
	10 D_3BO_3					2400			2380			2440		2400	2390	
	H_3BO_3	^{10}B							3150							
	D_3BO_3															
ν_{B-O} (stretch)	H_3BO_3	^{11}B	1470	1450	1457	1450	1448	1490	1428	1460	1460	1440	1455	1450	1440	1189
	D_3BO_3								1428	1420		1415		1425	1420	
	H_3BO_3	^{10}B					1464		1490						1470	1200
	D_3BO_3														1450	
δ_{B-O-H} (bend)	H_3BO_3	^{11}B	1203	1195	1188	1197	1198		1183	1067	1195	1185	1195	1190		
	D_3BO_3					929			914			910		910		
	H_3BO_3	^{10}B					1199		1195							
	D_3BO_3															

*Measured at -180°C.

TABLE 2 (continued)

COMPARISON OF SOLID STATE IR DATA

Assignment			Matossi & Bluschke (62)	Miller & Wilkins (63)	Mortimer (64)	Bethell & Sheppard (65)	Sidorov & Sobolev (66)	Hornig & Plumb (67)	Servoss & Clark (68)	Goubeau & Hummel (69)	Krishnan (70)	Durig et al (71)	Vizi (72)	Broadhead & Newman (73)	Now-djavan (74)*	Janda & Heller (75)
δ_{O-B-O} (bend)	H_3BO_3	^{11}B	532			540		552	544	547	547	538	546	542	555	549
	D_3BO_3					485**			522			510		510	550	
	H_3BO_3	^{10}B							545							545
	D_3BO_3															
γ_{BO_3} (out of plane bend)	H_3BO_3	^{11}B	633	807		824	637	632	639	647	798	625	810	635	640	650
	D_3BO_3					709			654			665		642	640	
	H_3BO_3	^{10}B					621	666	668	674					675	620
	D_3BO_3														670	
$\tau_{O-B-O-H}$ (torsion)	H_3BO_3	^{11}B	769	(640)	799	648			800	715	647	808	639	720	590	
	D_3BO_3					545**						566		550	530	
	H_3BO_3	^{10}B							800							
	D_3BO_3															

*Measured at -180°C.

**Derived from product rule calculations.

Sheppard (^{65}) and Servoss and Clark (^{68}) although Durig's (^{71}) paper should not be overlooked. These values are included in Table 1 for the purposes of comparison. The case for the Raman data is equally confused and made worse by the possibility of erroneous assignment of arc lines to fundamentals in the early studies, which used a mercury lamp as the exciting source.

Table 1 also includes values for the fundamentals of boric acid in the gas phase. The first column is that of Margrave's (^{43}) from 1959 whilst Gilson's (^{44}) values were obtained after the work described presently. The former values are presented without any spectra in the paper and were obtained in a heated cell at 100°C with silver chloride windows. There is therefore the distinct possibility that the values do not relate to vapour phase boric acid at all.

Comparison of the matrix, gas phase and solid phase data supports the expectation that the frequencies assigned to B-O motion show a reasonable correspondence whilst significant differences occur in modes involving hydrogen atom motion, notably the O-H stretch, B-O-H bend and O-H torsion. In attempting to understand the spectra of molecular boric acid, it was decided to base the analysis entirely on the matrix data and to rely on the isotope patterns generated by ^{18}O and ^{2}D enrichment for both qualitative and quantitative support. Before discussing these results in detail however, it is helpful to consider the ir spectrum predicted for molecular $B(OH)_3$.

There are relatively few molecular species with $X(YZ)_3$ stoichiometry and the generally accepted shape for $B(OH)_3$ of C_{3h} point group is based entirely on the solid phase, as there is no vapour phase structural determination reported. Nevertheless this must also be considered the most likely vapour phase structure by comparison with $B(OMe)_3$ which from gas phase electron diffraction(78) has been shown to have a C_{3h} framework. Departures from the C_{3h} structure to C_3 or lower point groups are conceivable by loss of overall planarity. A D_{3h} structure is also a possibility where either the B-O-H groups are linear or the protons could be symmetrically placed between the oxygen atoms. The various possible structures are shown in Fig 5.

The approach chosen was to assign the boric acid spectra initially on the basis of C_{3h} symmetry and then to consider if any of the spectral features indicated a departure from this model.

4.3 Vibrational Analysis - Results of Isotopic Substitution

Despite the paucity of experimental data pertaining to the isolated molecule, the vibrational analysis of the C_{3h} $X(YZ)_3$ framework has attracted considerable attention (55, 79-82).

The first study by Pistorius (55) used the G matrix elements as tabulated by Wilson and Decius(83, 84) to determine the force constants. His results were challenged by Cyvin et al (79-82) who started from first principles and used complex notation to derive the G matrix elements. It is believed that Pistorius's error for the out of plane modes is due to a typographical error in equation (22) on page 61 in Ref 83(a) which has subsequently been corrected in Ref 83(b). In both of these cases the authors only dealt with the C_{3h} cases and not the partially substituted C_s species, therefore the G matrix elements had to be derived in order to simulate the partially isotopically substituted (C_s) species.

The determination of the irreducible representation Γ_{vib} for the C_{3h} structure is not straightforward because of the

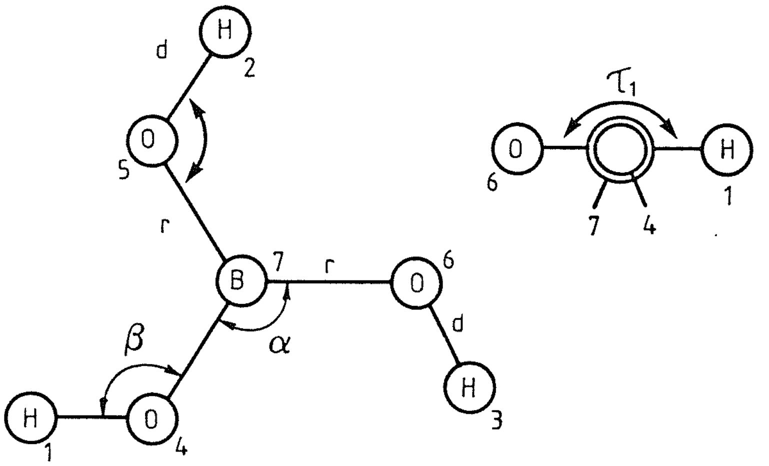

(a) C_{3h} SYMMETRY (WITH DEFINITIONS OF INTERNAL CO-ORDINATES)

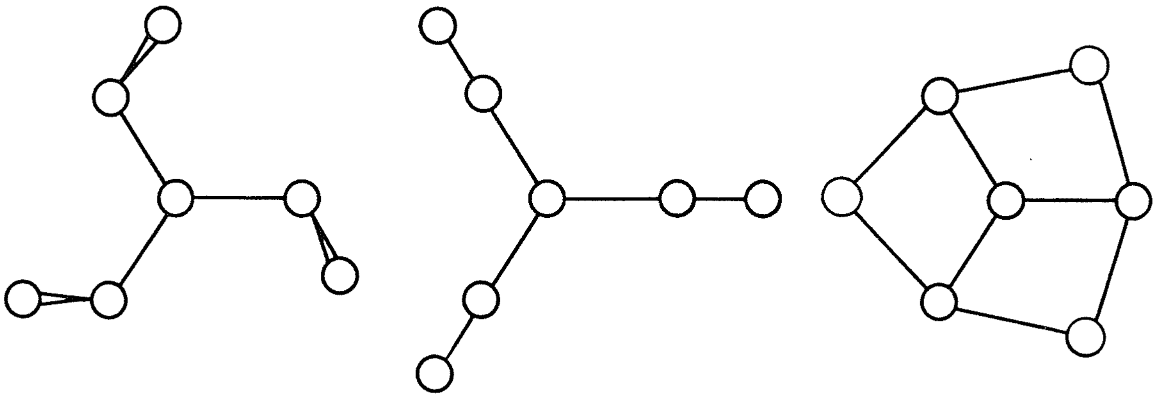

(b) C_3 SYMMETRY

(c) D_{3h} SYMMETRY

(d) D_{3h} SYMMETRY

FIG. 5 POSSIBLE STRUCTURES FOR MOLECULAR BORIC ACID presence of complex numbers in the character table. The method employed was to determine Γ_{vib} for a D_{3h} structure and then by use of correlation tables ([83]), Γ_{vib} for C_{3h} can be obtained thus:

$$\Gamma_{vib}\, D_{3h} = 2A'_1 + A'_2 + 2A''_2 + 4E' + E''$$

$$\Gamma_{vib}\, C_{3h} = 3A' + 2A'' + 4E' + E''$$

By consultation with character tables ([11]) the ir active modes are 2A" + 4E'. The character tables also inform us that the A" representations are the out of plane modes whilst the E' representations are the in plane modes. The out of plane modes can be considered to be a BO_3 out of plane bend and an OH torsion. The in plane modes are made up of an O-H stretch and a B-O stretch, a B-O-H bend and an O-B-O bend. These qualitative descriptions also serve as an indication of the likely effect of isotope substitution. Thus all modes nominally involving hydrogen atom motion should show a large frequency shift (≃ 30%) on deuteration. The partially substituted species should permit a distinction to be made between degenerate and non-degenerate modes because the patterns arising from non-degenerate modes are only dependent on the statistical distribution of the isotopes, whereas the degenerate modes are usually more complicated.

The interpretation of the large number of spectra recorded is most conveniently discussed in the context of the five ir spectral regions associated with the various $B(OH)_3$ absorptions.

4.4 Spectral Region 650-750 cm^{-1}

The nitrogen matrix ir spectra of "normal" boric acid (20% ^{10}B, 80% ^{11}B) in this region show sharp features at 700.9

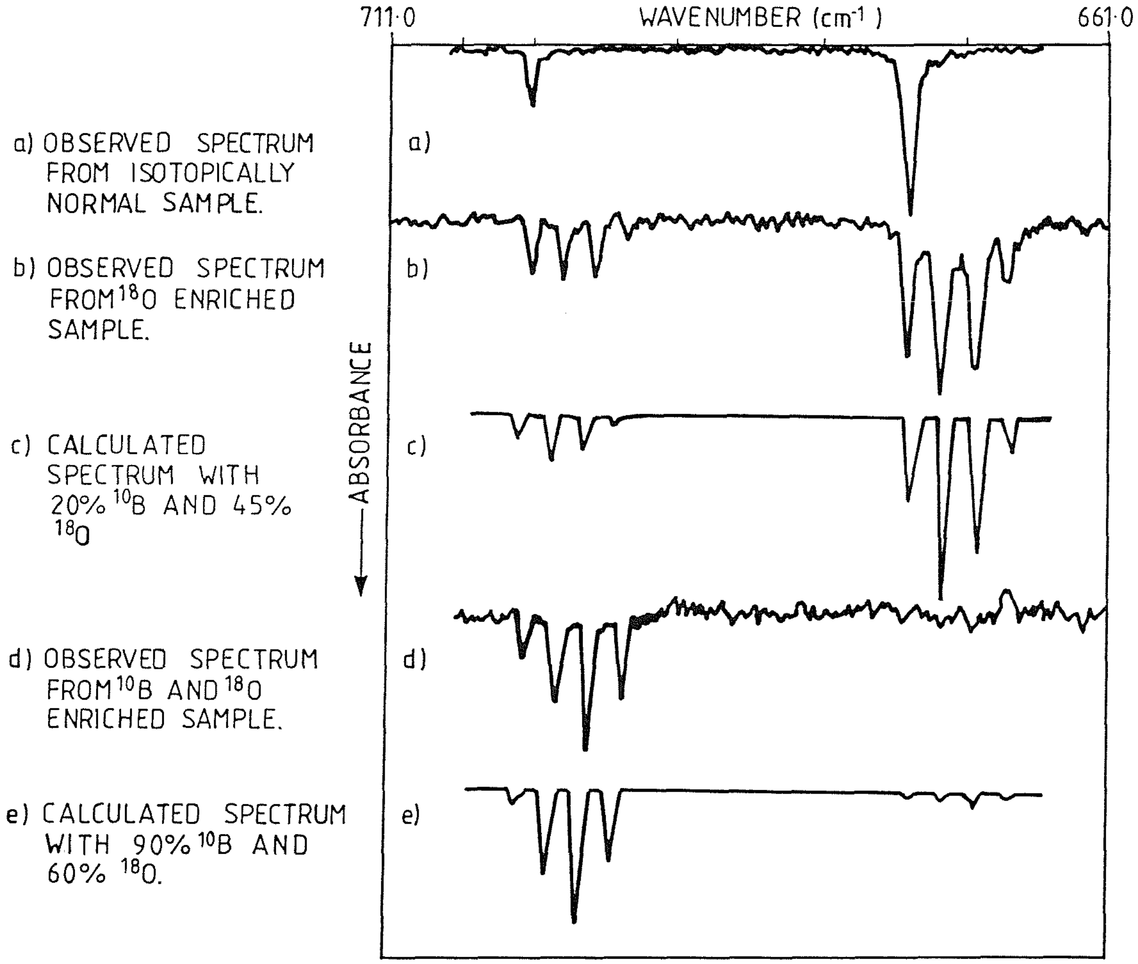

FIG. 6 HIGH RESOLUTION NITROGEN MATRIX I R SPECTRA OF BORIC ACID IN THE OUT OF PLANE BO_3 BENDING REGION

and 675.0 cm^{-1} with an intensity ratio of ≃ 1:4 and a typical spectrum is shown in Fig 6(a). An almost identical spectrum is obtained for all levels of deuterium enrichment and the frequencies are shifted by less than a wavenumber. This spectral region is too low for O-H or B-O stretching modes and absorptions here must either arise from torsion modes or more conventional bending modes. The boron isotope effect is quite large (25.9 cm^{-1}) and because of the negligible deuteration effect this mode must correspond to either the in plane (E') or out of plane (A") bending mode of the BO_3 unit.

Fig 6(b) shows a spectrum obtained from a sample of boric acid containing ≃ 20% ^{10}B and ≃ 45% ^{18}O. Two quartets can be observed, one at around 697 cm^{-1} and the other centred at 671 cm^{-1}. If the boron isotopic composition is changed (Fig 6(d)) to 90% ^{10}B then only one prominent quartet is observed at 697 cm^{-1} thus indicating that the higher frequency pattern arises from ^{10}B whilst the lower frequency pattern arises from ^{11}B. The quartets arise from the $H_3B^{16}O_2{}^{18}O$, $H_3B^{16}O^{18}O_2$ and $H_3B^{18}O_3$ components. The individual components of these quartets show an intensity variation which corresponds to the binomial distribution expected for three equivalent oxygen atoms participating in a non-degenerate vibration. These features must therefore be associated with the A" BO_3 out of plane bending mode.

Figs 6(c) and 6(e) show the results of spectral simulation in this region. Although a knowledge of the position of the other A" (torsion) mode in $B(OH)_3$ is necessary to calculate the isotope patterns exactly, it has been assumed that because there is little or no deuterium isotope effect on this mode there is no interaction between the two modes and that they are therefore effectively decoupled. The simulated spectra have as a result been calculated by considering the BO_3 unit in isolation.

TABLE 3

Observed and Calculated Frequencies for the Out of Plane BO_3 Bend

Observed (cm^{-1})	Calculated (cm^{-1})	Assignment
675.0	674.4	$^{11}B\ ^{16}O_3$
672.6	672.1	$^{11}B\ ^{16}O_2\ ^{18}O$
670.2	669.7	$^{11}B\ ^{16}O\ ^{18}O_2$
668.1	667.4	$^{11}B\ ^{18}O_3$
700.9	701.3	$^{10}B\ ^{16}O_3$
698.6	699.0	$^{10}B\ ^{16}O_2\ ^{18}O$
696.4	696.8	$^{10}B\ ^{16}O\ ^{18}O_2$
694.1	694.5	$^{10}B\ ^{18}O_3$

The relevant secular equation has been derived previously (85) and is given as (86):

$$\lambda = K \left\{ \frac{9}{M_B} + \frac{1}{M_{O_1}} + \frac{1}{M_{O_2}} + \frac{1}{M_{O_3}} \right\} = \left\{ \frac{\nu}{1302.83} \right\}^2$$

where M_B, M_{O_1}, M_{O_2} and M_{O_3} are the masses of the boron and oxygen atoms and K is a constant. Hence the frequencies of all the isotopic species can be predicted once K has been determined from one (correct) isotopic component.

It was found that if the isotopic component used to generate K was the $H_3{}^{11}BO^{16}{}_3$ band then the ^{11}B pattern was predicted exactly but the ^{10}B values were ≈ 1 cm^{-1} out. Therefore it was decided to use an average value of K of those derived from the $H_3{}^{10}B^{18}O_3$ and $H_3{}^{11}B^{16}O_3$ components. This was 0.2665 mdyne/Å and the observed and calculated frequencies are tabulated below, together with the assignments.

The relative intensities of the various components were determined by the appropriate statistical weightings and it can be seen that there is very good correspondence between the observed and calculated spectra for both frequency position and intensity.

4.5 Spectral Regions 3600-3700 cm^{-1} and 2650-2750 cm^{-1}

These are the spectral regions associated with O-H and O-D stretching modes in non-hydrogen bonded systems. Fig 7(a) shows a typical nitrogen matrix ir spectrum obtained from normal $B(OH)_3$. The bands at 3726 and 3633 cm^{-1} are due to matrix isolated water monomer (59). The central feature at

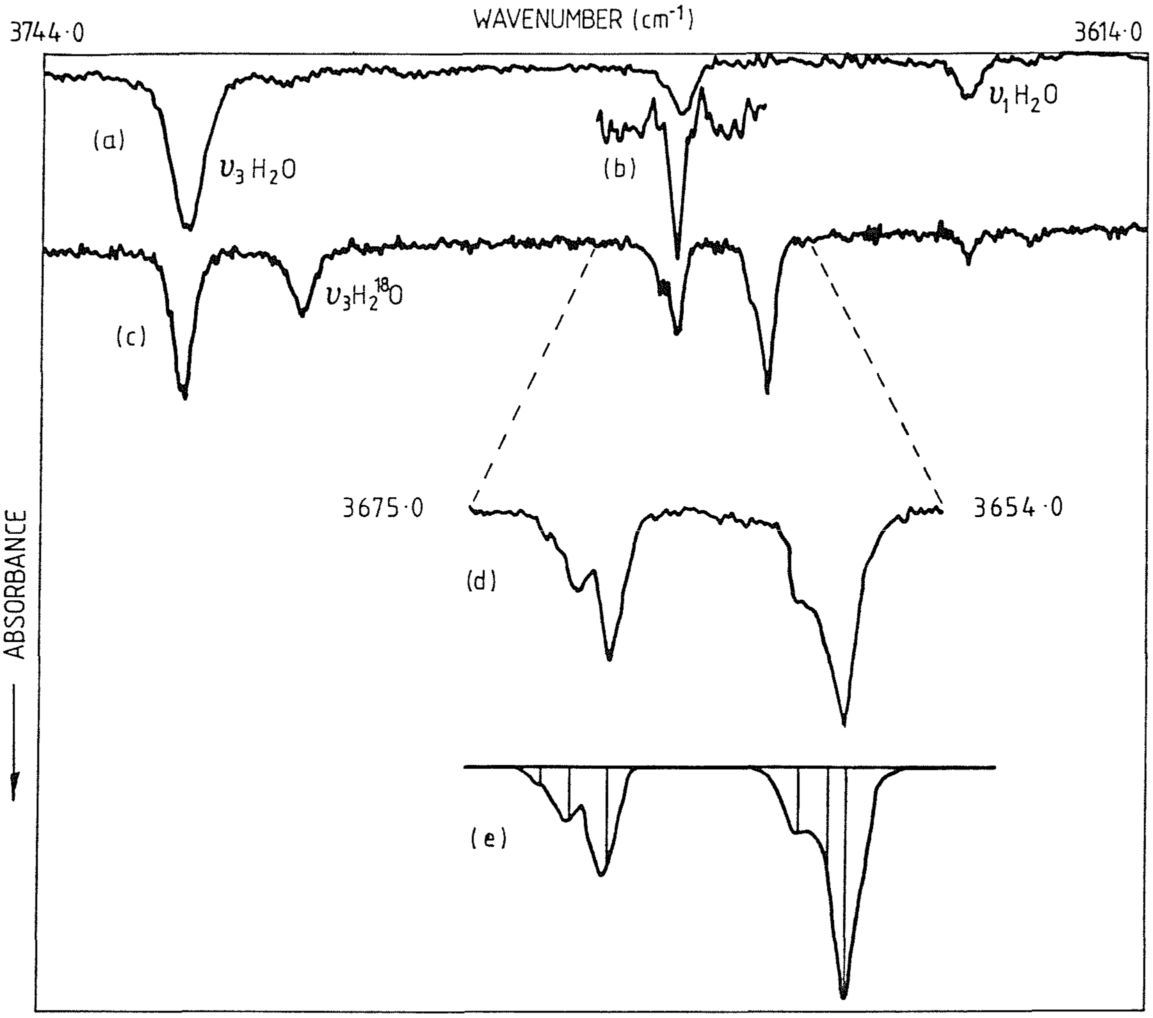

(a) MEDIUM RESOLUTION SPECTRUM FROM NORMAL BORIC ACID
(b) AS ABOVE BUT UNDER HIGHER RESOLUTION
(c) MEDIUM RESOLUTION SPECTRUM OF ^{18}O ENRICHED SAMPLE
(d) AS ABOVE BUT UNDER HIGHER RESOLUTION
(e) CALCULATED SPECTRUM WITH 60 % ^{18}O AND A BANDWITH OF 1·1 cm^{-1}

FIG. 7 NITROGEN MATRIX IR SPECTRA OF BORIC ACID IN THE O-H STRETCHING REGION

3668.5 cm^{-1} is assigned to $B(OH)_3$ and is shown under higher resolution in the inset Fig 7(b). This band proved to be insensitive to changes in the ^{10}B : ^{11}B ratio.

Enrichment with ^{18}O however, (Fig 7(c)) produced two shoulders at 3671.8 and 3670.2 cm^{-1} on the high frequency side of the 3668.5 cm^{-1} band and another relatively intense, asymmetric absorption at ~ 3658 cm^{-1}. In contrast to the ^{18}O isotope pattern for the A" BO_3 mode this pattern is highly asymmetric and the relative intensities bear little or no resemblance to binomial statistics.

Spectra of partially deuterated samples, (Fig 8), also revealed shoulders on the high frequency side of the initial band at 3668.5 cm^{-1} and a new set of bands just above 2700 cm^{-1}. These latter bands also display a similar pattern although there is some interference from matrix isolated HOD (at 2705.5 cm^{-1}) but this is not a problem in the O-H region as the HOD absorption is higher (at 3680.2 cm^{-1}). From the position of the new bands midway between the ν_1 and ν_3 absorptions of matrix isolated water and the very near coincidence with matrix isolated HOD it can immediately be stated that the boric acid must be isolated monomerically, (in HOD the two stretches are to a first approximation an O-H stretch and an O-D stretch) and is therefore not involved in either inter-or intra-molecular hydrogen bonding.

These patterns are characteristic of partial isotope substitution in doubly degenerate modes involving three weakly coupled oscillators. They were first encountered in connection with the analysis of the terminal CO stretching modes in D_{3h} transition metal tricarbonyls(87) and were observed experimentally shortly afterwards in Ozin's study of $Pd(N_2)_3$ (88). In these studies, the high frequency separation approximation was assumed and the only coupling between the CO or N_2 groups was through off diagonal

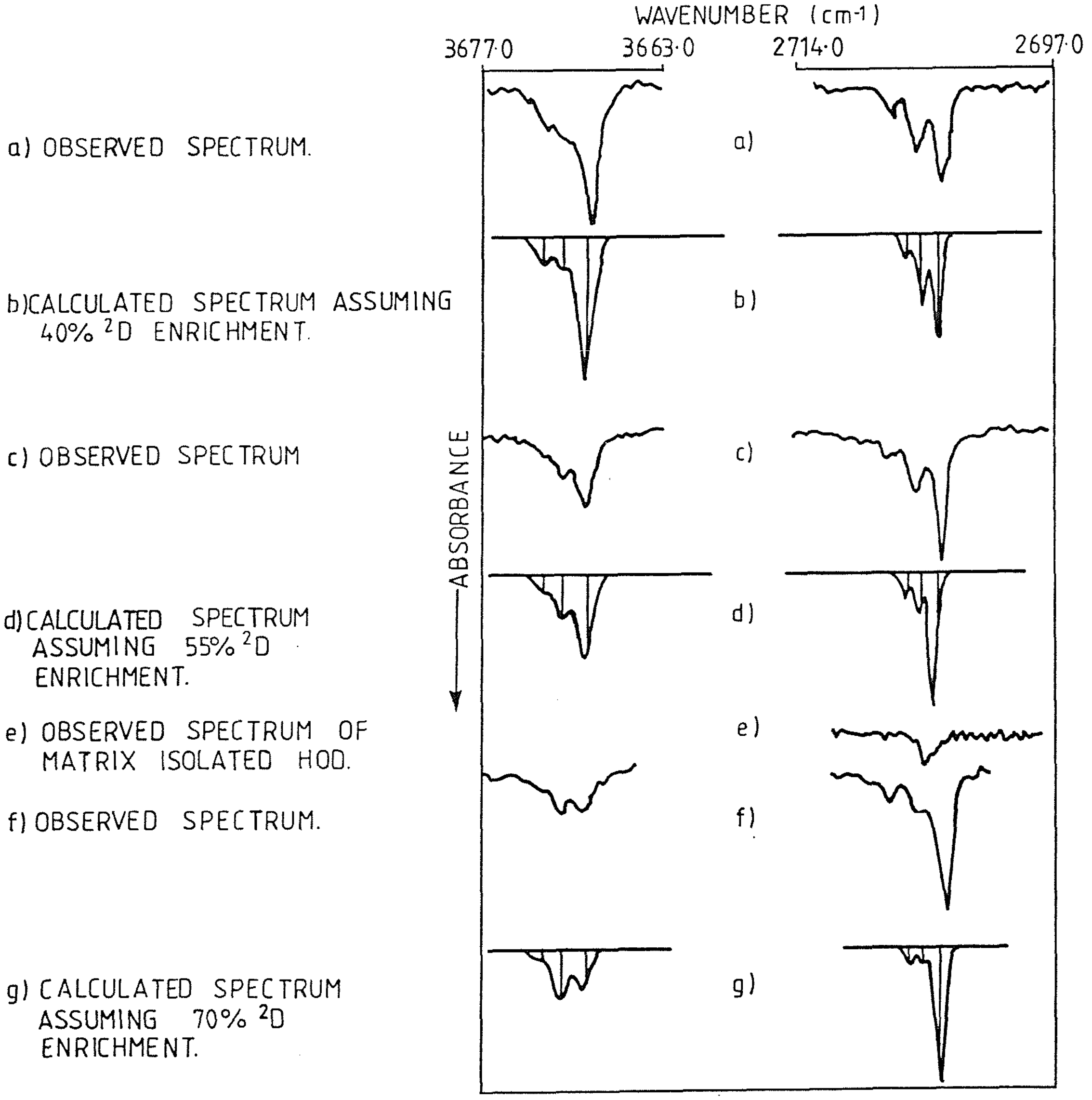

FIG.8 HIGH RESOLUTION NITROGEN MATRIX I R SPECTRA OF THE O-H AND O-D STRETCHES IN DEUTERATED BORIC ACID

F matrix terms. In $B(OH)_3$ an analogous situation arises regarding the OH stretching modes.

Even though the symmetry here is C_{3h}, it turns out that the secular equations are identical to those derived for D_{3h} (89). This can be rationalised because if the O-H units are taken in isolation then they can be imagined to have a "hidden" symmetry of D_{3h}.

Therefore it should be possible to simulate the observed isotope patterns using a simple two parameter force field, $F_{11} = F_{22} = F_{33} = F_d$ and a single interaction constant F_{dd} for all the off diagonal terms. The G-matrix elements are:

$$G_{11} = \mu_{H_1} + \mu_{O_4}; \quad G_{22} = \mu_{H_2} + \mu_{O_5}; \quad G_{33} = \mu_{H_3} + \mu_{O_6}$$

These were then used to solve $\left| FG - E\lambda \right| = 0$, by the method of Appendix D.

The results of these calculations are tabulated as CALC(A) in Tables 4(a) and 4(b). From these it can be seen that the agreement for the ^{18}O substituted species is quite satisfactory. This adds further credence to the presence of a three fold axis in $B(OH)_3$ and the analysis predicts a value of 3672.6 cm^{-1} for the totally symmetric A' ^{16}O-H stretch. In C_{3h} symmetry this mode is inactive but if the boric acid has lower symmetry then it should be observable in the spectrum.

It will be observed from this Table that the correlation between calculated and observed frequencies for the deuterated samples is good in the O-H region but very poor in the O-D region. This discrepancy could be due to a breakdown of the high frequency separation approximation but is more likely to be due to anharmonicity. Modes

TABLE 4a

Observed and Calculated Frequencies (cm^{-1}) for the In Plane O-H Stretch in Boric Acid Isotopically Labelled with Oxygen-18

Observed	Calc A (a)	Calc B (b)	Assignment
-	3672.6	3672.6	A' $H_3\ B^{16}O_3$
3668.5	3668.5	3668.5	E' $H_3\ B^{16}O_3$
3668.5	3668.5	3668.5	A' $H_3\ B^{16}O_2{}^{18}O$
3658.2	3657.6	3658.1	
3671.8	3671.5	3671.5	
3670.2	3670.2	3670.2	A' $H_3\ B^{16}O^{18}O_2$
3659.2	3658.9	3659.4	
3657.6	3656.5	3657.1	
-	3660.6	3661.2	A' $H_3\ B^{18}O_3$
3657.6	3656.5	3657.1	E' $H_3\ B^{18}O_3$

a Assuming harmonic motion with F_d = 7.468 mdyne/Å and F_{dd} = 0.0056 mdyne/Å.

b Assuming $\omega_e x_e$ = 90 cm^{-1}, with F_d = 8.219 mydne/Å and F_{dd} = 0.0064 mdyne/Å.

TABLE 4b

Observed and Calculated Frequencies (cm^{-1}) for the In Plane O-H Stretch in Boric Acid Isotopically labelled with Deuterium

Observed	Calc A (a)	Calc B (b)	Assignment
-	3672.6	3672.6	A' H_3BO_3
3668.5	3668.5	3668.5	E' H_3BO_3
3668.5	3668.5	3668.5	A' H_2DBO_3
3671.1	3671.2	3671.2	
2705.8	2670.2	2705.9	
3669.7	3669.9	3669.9	A' HD_2BO_3
2707.7	2671.2	2706.9	
2704.6	2669.2	2704.9	
-	2672.4	2707.7	A' D_3BO_3
2704.6	2669.2	2704.9	E' D_3BO_3

a Assuming harmonic motion with F_d = 7.468 mdyne/Å and F_{dd} = 0.0056 mdyne/Å.

b Assuming $\omega_e x_e$ = 90 cm^{-1}, with F_d = 8.219 mydne/Å and F_{dd} = 0.0064 mdyne/Å.

involving light atoms such as hydrogen are known to be very anharmonic. Therefore several calculations were carried out in order to estimate the harmonic frequencies to see if a better correlation between observed and calculated frequencies could be achieved.

The ω_e and $\omega_e x_e$ value for the ^{16}O-H diatomic molecule are given[90] as 3735.2 and 82.81 cm^{-1} respectively. ($\omega_e = 2\omega_e x_e + \nu_{obs}$). Therefore if this value of $\omega_e x_e$ is used for $B(OH)_3$, ω_e can be estimated to be 3834.1 cm^{-1}. If this value is then used in the calculations a set of harmonic frequencies will be generated. In order to retrieve the transition frequencies from the calculated harmonic frequencies the Darling-Dennison Relationship is required.

This states that for a diatomic $\frac{x_e}{\omega_e} = \frac{x_e'}{\omega_e'}$ (where the prime

indicates the isotopically substituted species). The assumption is then made (Darling-Dennison approximation) that this also holds for polyatomics. Having used this method it was found that the correspondence between observed and calculated frequencies was good (within 1.5 cm^{-1}) over the range 3700-2700 cm^{-1}.

If a value of $\omega_e x_e$ = 90 cm^{-1} is adopted then the fit is within 0.5 cm^{-1} over the entire range. It should be noted that ν_1 of gas phase[91] H_2O is 3656.7 cm^{-1} and $\omega_e x_e$ = 87.8 cm^{-1} thus indicating the efficacy of this approach. The results of these calculations are given as CALC(B) in Tables 4(a) and 4(b). The spectral simulation of this data is shown in Figure 7(e) and Figure 8. In the O-H region a bandwidth of 1.1 cm^{-1} was used whilst 0.6 cm^{-1} was used for the O-D region. This variation in bandwidth reflects the change in resolving power of the spectrometer over these two regions.

The simulation for the oxygen spectra is very good whilst that for the deuterated spectra in the O-H region is equally good but the correspondence is slightly lower in the O-D region. This is largely because the separation between the bands is larger in the O-D region and is probably indicative of a slight breakdown in the high frequency oscillator approximation.

The other problem is the presence of the O-D stretching mode(ν_1) of matrix isolated HOD at 2705.5 cm^{-1} overlapping with other bands in the spectrum. Figure 8(e) shows a spectrum of matrix isolated HOD and the position of ν_1 with respect to the other bands. If it is assumed that the relative intensity of the ν_{O-H} and ν_{O-D} bands in HOD is always constant then it is possible to calculate the proportion of the central band's intensity derived from ν_1 of HOD. Fortunately the ν_3 (O-H) of HOD (at 3680.2 cm^{-1}) is sufficiently far away from the other bands to allow its integrated intensity to be measured. As a result of these calculations it can be assumed that approximately 15% of the 2705.8 cm^{-1} band intensity in the 40% deuterated sample is due to HOD whilst approximately 27% is due to HOD in the 55% and 70% deuterated samples. It can then be imagined that the intensity fit is much better.

Therefore from these two spectral regions it can be inferred that in monomeric $B(OH)_3$ the three O-H units are co-planar and have a three fold rotation axis.

4.6 Spectral Region 800-1200 cm^{-1}

The survey spectra (Fig 4) reveal that there are two bands in this region arising from "normal" boric acid. One of these (1009.9 cm^{-1}) is reasonably sharp whilst the other at ~ 1080 cm^{-1} is broad and ill-defined. When ^{10}B boric acid is used it can be seen that there is negligible effect on either of these bands, whilst the use of oxygen-18 enriched samples results in some structure being observed on the 1009.9 cm^{-1} band. The largest isotopic effect is observed when the sample is deuterated. In this case a large new band at ≈ 830 cm^{-1} and two small bands at 887.5 cm^{-1} and 894.5 cm^{-1} are found to be due to the isotopic enrichment.

In this region of the spectrum one might expect to see the frequencies arising from the B-O stretch or the B-O-H bend. The band at 1009.9 cm^{-1} can be assigned to the B-^{16}O-H,E' bending mode, because both the boron and oxygen isotope effects are small, whilst the hydrogen isotope effect is relatively large.

The effect of deuteration will be considered first and in Fig 9 the effect of increasing the extent of deuteration in the sample can be seen. At first sight it appears that there is the necessary 6 line pattern for a degenerate E' mode. However, under higher resolution (Fig 10) it is observed that the apparent doublet at ~ 1012 cm^{-1} is in fact probably a closely spaced triplet. Higher resolution studies of the doublet at 832 cm^{-1} were not able to positively identify this as a triplet. This then puts us into a quandary over the assignment. However, in the previous section the symmetric A' O-H stretch was very close to the E' O-H stretch with the result that the isotope patterns were very complicated, but interpretable.

If it is imagined that the A' symmetric B-O-H bend is very close and higher in frequency than the E' bend, this will then result in patterns very similar to those for the analogous stretching modes. It will be noticed that the intensity patterns are not the same, but the fact that there are three closely spaced bands is a good indication that this is indeed the case. Preliminary calculations using SOTONVIBP indicated that the frequencies can be modelled if the A' value was set to ~ 1016 cm^{-1}. Further calculations were not carried out however, because the

(a) OBSERVED SPECTRUM FROM SAMPLE OF ≃ 40% DEUTERATED BORIC ACID SAMPLE

(b) OBSERVED SPECTRUM FROM ≃ 55% DEUTERATED ^{10}B BORIC ACID SAMPLE

(c) OBSERVED SPECTRUM FROM ≃ 65 % DEUTERATED BORIC ACID SAMPLE

(d) OBSERVED SPECTRUM FROM ≃ 80% DEUTERATED BORIC ACID SAMPLE

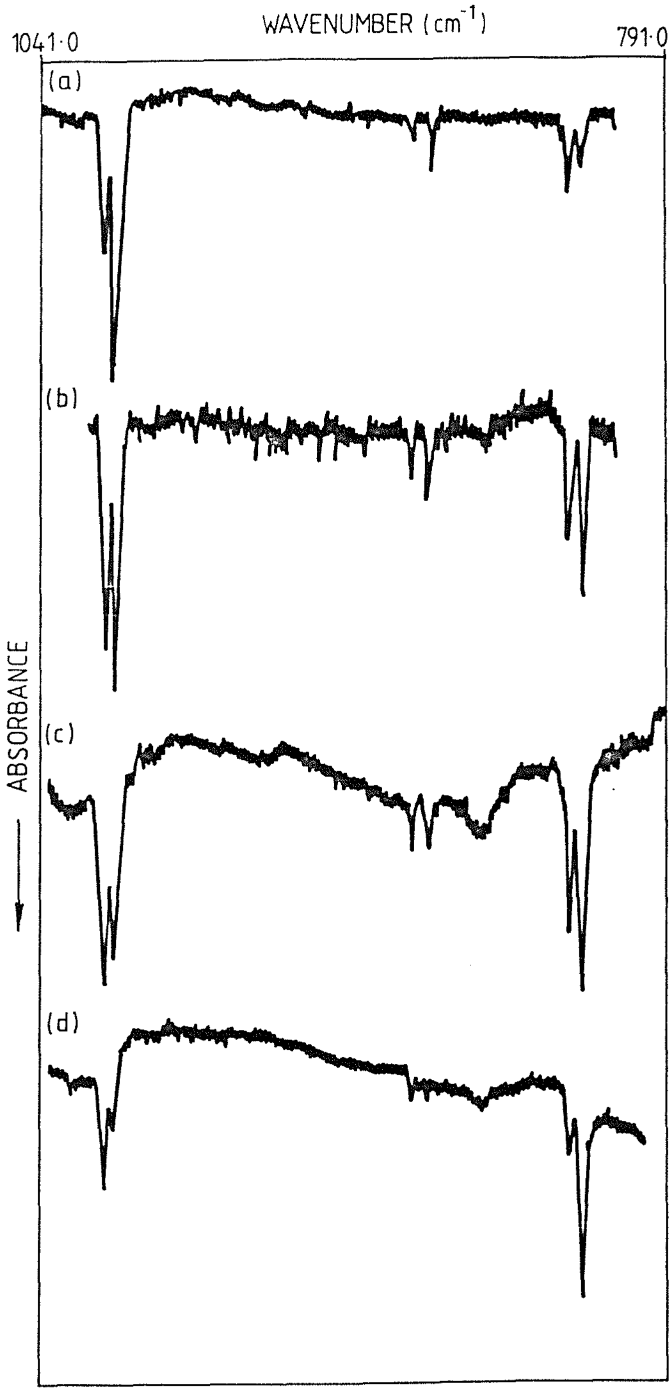

FIG. 9 MEDIUM RESOLUTION NITROGEN MATRIX I R SPECTRA IN THE H-O-B BENDING REGION

(a) OBSERVED SPECTRUM FROM NORMAL BORIC ACID

(b) OBSERVED SPECTRUM FOR ≃ 40% ^{2}D ENRICHMENT

(c) OBSERVED SPECTRUM FOR ≃ 65% ^{2}D ENRICHMENT

(d) OBSERVED SPECTRUM FOR ≃ 80% ^{2}D ENRICHMENT

FIG. 10 HIGH RESOLUTION NITROGEN MATRIX I R SPECTRA IN THE H-O-B BENDING REGION OF BORIC ACID

B-O-H bond angle is not known to any accuracy for the gas phase or matrix isolated species. (In principle it should be able to determine this angle by microwave spectroscopy of H_2DBO_3, if this could be separated from the other isotopomers). In addition there is the problem of anharmonicity. It is not possible to determine its extent because the vibrational modes will also be interacting with other modes and this may result in an increase or decrease of the observed frequency. Accurate frequencies ($\pm$ 0.7 cm^{-1}) and tentative assignments are given in Table 5.

From the above arguments the triplet centred at 1013 cm^{-1} can be assigned to the hydrogen components of the B-O-H bend. The doublet at 828 cm^{-1} is obviously the deuterium components of this mode because of the almost complete disappearance of the bands at 887.5 and 894.5 cm^{-1} on 80% deuteration. The fact that only two bands in the B-O-D bending region are observed is slightly worrying but can be explained by comparison with the O-D stretches. In this case the weakest component was the centre band of the triplet. The individual modes will also be subject to a different amount of interaction to those in the B-O-H region and this may result in two of the components being pushed together under one band envelope. It is possible however say that the A' B-O-D bend will be 5-15 cm^{-1} above the E' mode and is hence in the range 830-840 cm^{-1}.

Having assigned the principal features in this spectral region to the B-O-H bending modes, the source of the two bands at 894.5 and 887.5 cm^{-1} needs to be considered. They appear from Fig 9 to be at their most intense when the deuteration level is about 50%. The band at 887.5 cm^{-1} seems to correlate with lower deuteration levels whilst that at 894.5 cm^{-1} with higher deuteration levels. It should be noted that the symmetric A' B-O stretch in both the solid and gas phase spectra (Tables 1 and 2) is in this

TABLE 5

Observed and Estimated Frequencies (cm^{-1}) from Boric Acid in the Range 1200-800 cm^{-1}

Observed Frequency	Assignment
1009.9	E' B-O-H bend H_3BO_3
1011.4	A' B-O-H bend H_2DBO_3
1014.9	A' B-O-H bend HD_2BO_3
831.5	A' B-O-H bend H_2DBO_3/HD_2BO_3
825.5	E' B-O-H bend D_3BO_3
1009.9	E' B-O-H bend H_3BO_3
1007.6	A' B-O-H bend $H_3{}^{16}BO_2{}^{18}O/H_3B{}^{16}O{}^{18}O_2$
1002.3	
999.6	
997.5	E' B-O-H bend $H_3B^{18}O_3$
894.5	A' B-O stretch HD_2BO_3
887.5	A' B-O stretch H_2DBO_3
Estimated Frequency	
~ 1016	E' B-O-H bend H_3BO_3
~ 1003	A' B-O-H bend $H_3B^{18}O_3$
830-840	A' B-O-H bend D_3BO_3
880.5	A' B-O stretch H_3BO_3
901.5	A' B-O stretch D_3BO_3

region. The fact that only two bands are observed is indicative of an ir inactive non-degenerate mode becoming active on lowering of symmetry ($C_{3h} \rightarrow C_s$) as a result of isotopic substitution. Therefore the band at 887.5 cm^{-1} is assigned to the H_2DBO_3 component of the A' B-O symmetric stretch and the band at 894.5 cm^{-1} is assigned to the HD_2BO_3 component of the A' H_3BO_3 B-O symmetric stretch. If one assumes that the isotopic splitting between these two is the same as that between all the components of this mode, this predicts the H_3BO_3 A' frequency to be 880.5 cm^{-1} and the D_3BO_3 A' frequency to be 901.5 cm^{-1}.

The fact that the all deuterated frequency is 21 cm^{-1} above the all hydrogen frequency is most unusual and can only really be understood if this mode interacts very strongly with the other modes in this region. Cyvin ([82]) noted that the interaction between the two in plane bends was the most important one. Gilson ([44]) has also observed the deuterated component to be 21 cm^{-1} above the hydrogen component for this mode in Raman vapour phase studies (887 and 866 cm^{-1} respectively).

For H_3BO_3 the A' bend is estimated to be at 1016 cm^{-1} and the A' stretch at 880 cm^{-1} whilst on complete deuteration the A' bend is thought to be at 835 cm^{-1}. In general one would expect the A' stretch in D_3BO_3 to be at a lower frequency, however this will interact strongly with the A' bend at ~ 835 cm^{-1} and the net result is that both will be pushed apart so that the A' stretch for D_3BO_3 is now higher than it is for H_3BO_3. The interaction between the two A' modes in H_3BO_3 will be less, because they are further apart, but will have the effect of pushing the A' stretch to a lower frequency.

The effect of varying the extent of oxygen-18 in the sample is shown in Fig 11. The top spectrum is of "normal" boric acid whilst those below it are enriched with ~45% ^{18}O and

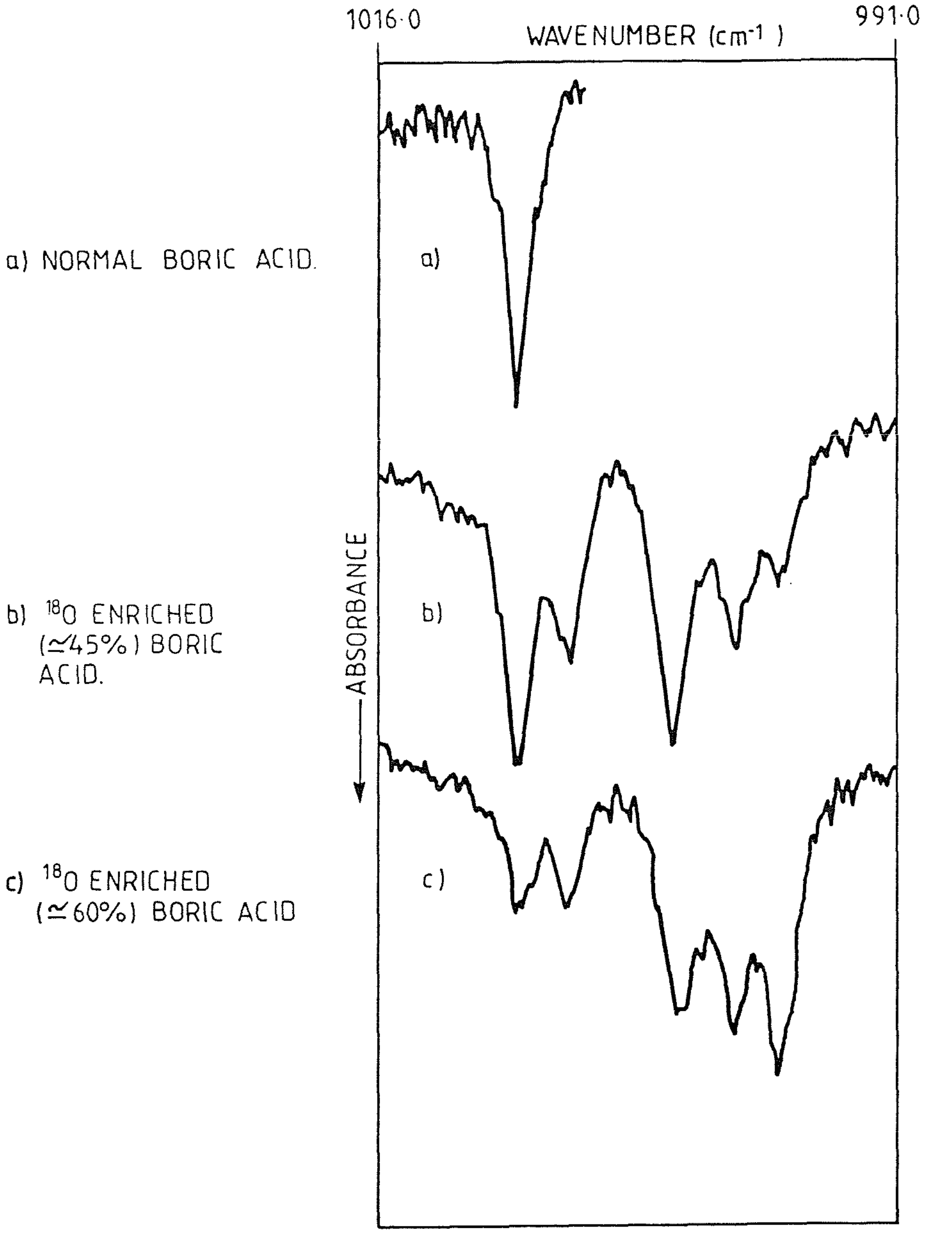

FIG.11 HIGH RESOLUTION NITROGEN MATRIX IR SPECTRA OF BORIC ACID IN THE H-O-B BENDING REGION

~60% ^{18}O respectively. One would expect to observe 6 bands from the degenerate bending mode, however as has been seen previously the A' mode is very close, (≃ 6 cm^{-1}) and therefore it might be anticipated that the spectra will be very complex. From the spectra in Fig 11(b) and Fig 11(c) it can be seen that a five line pattern is observed but that all the structure is on the low frequency side of the 1009.9 cm^{-1}. This is because the other E' mode ($H_3B^{18}O_3$) is sufficiently close so that the isotope patterns will be derived from this and not the A' modes.

If it is assumed that the A'-E' separation is the same for the all oxygen-16 and all oxygen-18 species and that the lowest frequency component observed (997.5 cm^{-1}) is the all oxygen-18 E' mode, then the $H_3BO^{18}{}_3$ A' mode is predicted to be at ≃ 1003.4 cm^{-1}. This value is where the gap in the pattern is observed. The presence of this A' mode in the midst of the bands makes the analysis and assignments very complicated. The frequency positions and tentative assignments are given in Table 5.

A normal co-ordinate analysis of these oxygen-18 patterns using the methods of the previous section was attempted by assuming that this was a non-interacting mode as in the case of the O-H stretches. This was unsuccessful because it was not possible to select a bond angle that allowed the following equation to be satisfied. (The prime indicates the isotopic species).

$$\left| \frac{\underline{FG}}{\underline{FG'}} \right| = \frac{\lambda}{\lambda'}$$

(The relevant $\underline{G}$ matrix elements for the C_{3h} species are listed in Ref 80).

This gives further confirmation that this mode is in fact interacting with the other modes.

No bands were observed in the region 910-870 cm^{-1} that could be assigned to the B-O symmetric stretch, although two bands should be active as in the deuterated case. This non-observance is because the symmetry selection rules only predict the number of ir active modes and not their relative intensities. Hence in the deuterated case there is a sufficient change in the dipole moment for the vibrational modes of the partially substituted species to be observed, whilst oxygen-18 incorporation does not result in a significant enough dipole change to result in the observation above the noise level. Therefore the oxygen-18 gives rise to a small perturbation whilst deuteration leads to a much greater perturbation.

The observed shift (184.4 cm^{-1}) on deuteration of the B-O-H bend E' mode is considerably less than that expected (295.8 cm^{-1}) by use of the conventional relationship. This discrepancy is unlikely to be due to anharmonicity because in the case of the hydrogen telluride the error in applying $\left(\nu_H/\sqrt{2}\right)$ to get ν_D was only 7 cm^{-1}. Therefore the discrepancy is probably due to the large amount of interaction between the three in plane modes between 1500 and 400 cm^{-1} or that there is substantial oxygen motion involved. The frequency shift on ^{18}O incorporation (12.4 cm^{-1}) is also lower than that expected (57.8 cm^{-1}). Therefore it appears that the E' mode involves considerable hydrogen motion and some oxygen motion but that it is also severely affected by the interaction with the B-O stretch and especially O-B-O bend. This interaction is highly complex because of the large shift in the E' bending frequency on deuteration and the much more modest isotope shifts for the other modes.

4.7 Spectral Region 1350-1500 cm^{-1}

From the survey spectra (Fig 4) it can be seen that on either deuteration or oxygen-18 exchange this region becomes very complex. Fig 12(a) shows a typical nitrogen matrix spectrum obtained from a sample of "normal" boric acid. From this two sharp bands can be observed at 1478.0 and 1426.2 cm^{-1} with an intensity ratio of 1:4. The assignment of these to the ^{10}B and ^{11}B components of the E' B-O stretch is confirmed in Fig 12(b) which is a spectrum with a ^{10}B : ^{11}B ratio of approximately 1:1. From this spectrum one can also see that the absorption at 1478.0 cm^{-1} is considerably broader than that at 1426.2 cm^{-1}. The cause of this is not immediately apparent and does not appear to be due to inverse water bands. The effect however is to broaden all the resonances of the ^{10}B components (see for eg. Fig 12(d)) which results in the spectra being less well resolved.

The effect of incorporating ^{18}O into the molecule is shown in Fig 12(c) and Fig 12(d). Fig 12(c) has a normal boron isotope distribution whereas Fig 12(d) has 90% ^{10}B. From these it can be seen that a doublet of sextets is observed, one for ^{10}B and one for ^{11}B. The ^{11}B components are much sharper than those of the ^{10}B isotopic species. A similar effect is also observed if the sample is enriched with deuterium (Fig 12(d) and Fig 12(f)). The assignments in Table 6 are based on the change in relative intensity of the bands on different enrichments.

For a non-interacting, stretching 'E' mode the isotope splitting should be(92) for example:

for 50% enrichment

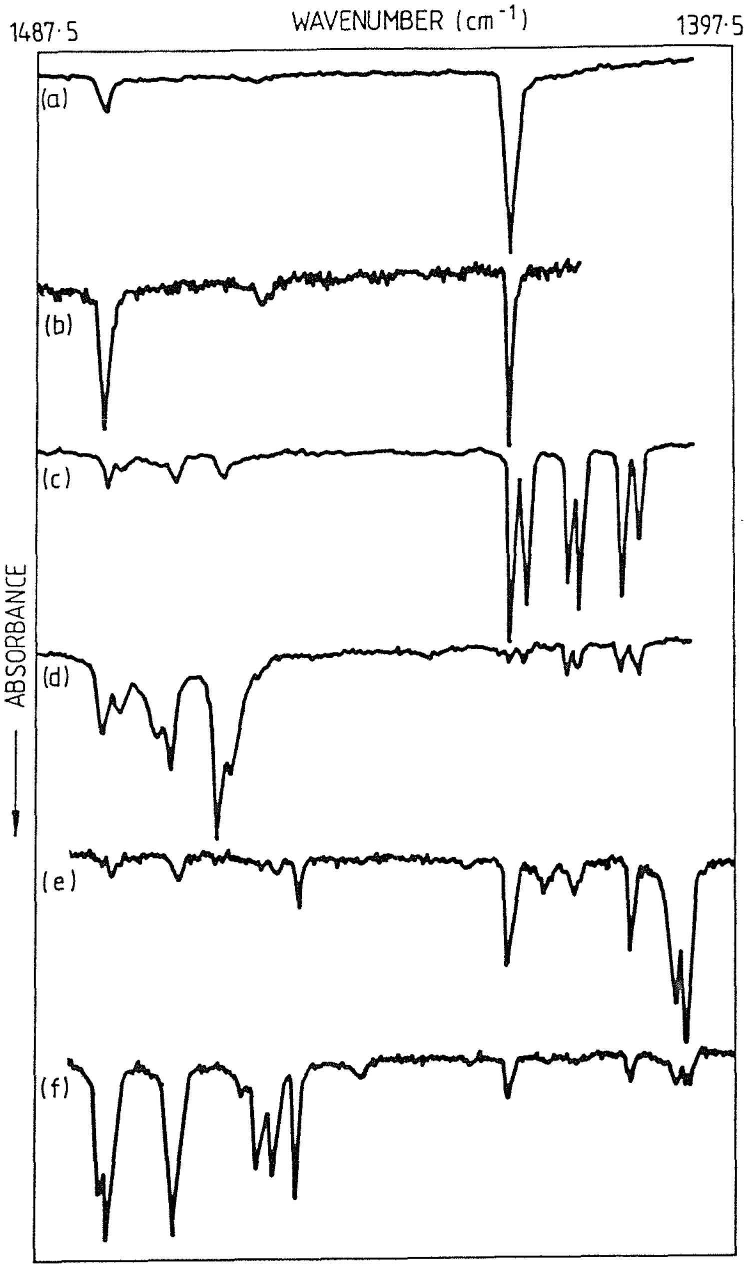

(a) OBSERVED SPECTRUM FROM NORMAL BORIC ACID

(b) OBSERVED SPECTRUM WITH A $^{10}B : ^{11}B$ RATIO OF 4 : 6

(c) OBSERVED SPECTRUM OF ^{18}O ENRICHED (≃45%) BORIC ACID

(d) OBSERVED SPECTRUM OF ^{18}O ENRICHED (≃60%) ^{10}B BORIC ACID

(e) OBSERVED SPECTRUM OF ^{2}D ENRICHED (≃55%) BORIC ACID

(f) OBSERVED SPECTRUM OF ^{2}D ENRICHED (≃40%) ^{10}B BORIC ACID

FIG. 12 HIGH RESOLUTION NITROGEN MATRIX IR SPECTRA OF BORIC ACID IN THE B-O ASYMMETRIC STRETCHING REGION

TABLE 6

Observed Frequencies (cm^{-1}) for the Asymmetric B-O Stretch in Isotopically Labelled Boric Acid

Observed frequency		Assignment
^{10}B	^{11}B	
1478.0	1426.2	E' B-O stretch H_3BO_3
1475.7	1424.5	A' B-O stretch $H_3B^{16}O_2{}^{18}O$
1469.0	1417.5	
1471.0	1419.0	A' B-O stretch $H_3B^{16}O^{18}O_2$
1463.0	1411.9	
1461.2	1409.7	E' B-O stretch $H_3B^{18}O_3$
1478.0	1426.2	E' B-O stretch H_3BO_3
1476.8	1421.6	A' B-O stretch H_2DBO_3
1457.5	1410.7	
1468.3	1417.7	A' B-O stretch HD_2BO_3
1455.6		
	1403.2	
1452.7		E' B-O stretch D_3BO_3

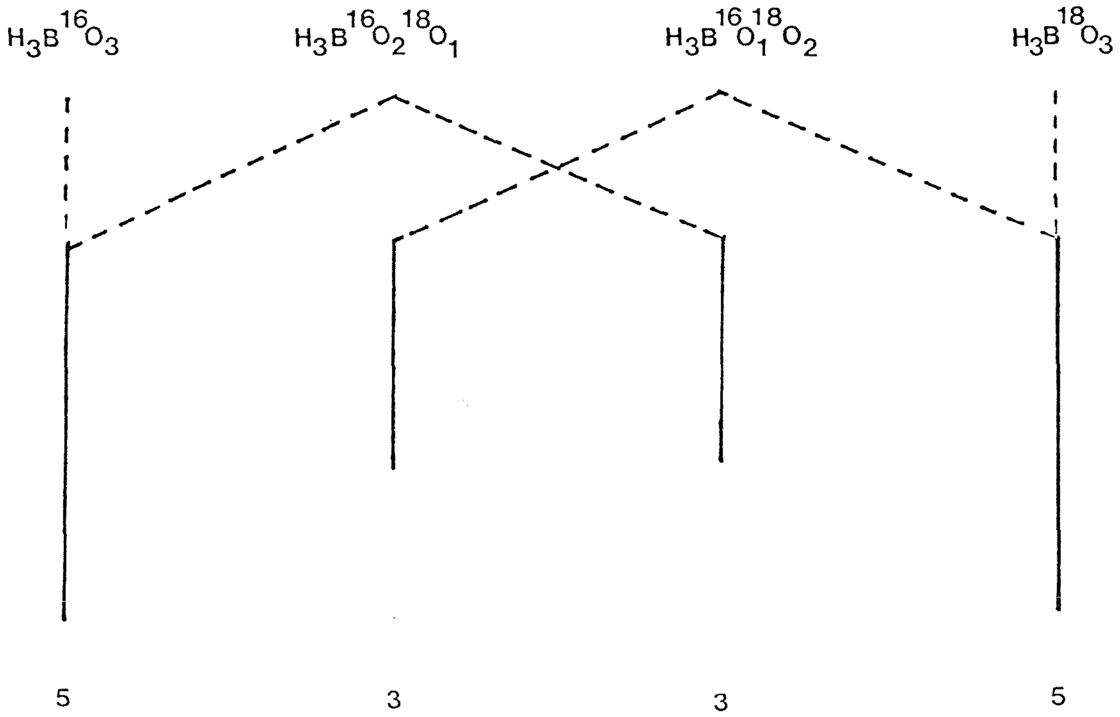

because one form of the doubly degenerate stretches is the same for $H_3B^{16}O_3$ and $H_3B^{16}O_2{}^{18}O$ if the ^{18}O is at position α. And similarly for the $H_3B^{16}O^{18}O_2$ and $H_3B^{18}O_3$ cases. This is shown schematically below.

The presence of six bands in the ^{18}O enriched samples is thus indicative of an interacting degenerate mode, and no deuterium isotope effect is allowed unless interaction force constants such as $f_{r\alpha}$ or $f_{r\beta}$ are introduced into the problem.

In the oxygen-18 case all the components can be resolved easily on the ^{11}B component but due to the problem of the broadness of the ^{10}B bands these are not so well resolved, but all of them can be identified. From Fig 12(d) it can also be seen that the intensity ratios of the various components are different for the two boron isotopic components. At first sight this appears to be due to the broadness of the bands around 1470 cm^{-1}, indicative of too fast a spraying on, but the bands around 1415 cm^{-1} from the ^{11}B species are resolved back to the baseline. This intensity discrepancy is still not really understood but is probably due to the same phenomenon as the general broadening of the bands. This does not appear to be due to another mode interacting differentially because the O-H stretches are over 2000 cm^{-1} higher and will therefore have the same negligible effect on both the ^{10}B and ^{11}B components. Indeed the high frequency oscillator approximation has been used in a preceding section to factor off the O-H stretches and this was found to simulate the observed spectra very satisfactorily. The lower frequency modes of the B-O-H bends, the O-B-O bend and the symmetric B-O stretch are probably also too far away to have this substantial differential effect.

The case for the deuterium enriched samples is anticipated to be more complex because this is not a small perturbation and the isotope splitting patterns are a result of the interaction of the B-O stretch and one or more of the other modes. At first sight it appears that there is a sextet on both the ^{10}B and ^{11}B components. This however is not that straightforward because of the problem of the ν_2 mode of matrix isolated HOD at 1405.2 cm^{-1} interfering with the six line pattern observed for the ^{11}B species. The six components of the ^{10}B species have been assigned by their change in relative intensity at different levels of enrichment but it is only feasible to assign unambiguously four of the bands in the ^{11}B pattern. It has not been possible, despite very slow depositions and high resolution studies (0.2-0.3 cm^{-1}) to identify whether the two remaining bands both lie under the peak centred at 1403.2 cm^{-1} or whether one of them lies under the ν_2 of HOD at 1405.2 cm^{-1}.

Detailed calculations have been attempted using SOTONVIBP, but were largely unsuccessful because the program is not configured to calculate force constants from two or more isotopomers. Cyvin's (80) $\underline{G}$ matrix elements for the C_{3h} species could have been used but some of the interaction $\underline{G}$ matrix elements contain complex variables and the determination of the solution thus becomes harder. Indeed Pistorius (55) has set these interaction $\underline{G}$ matrix elements to zero, but Cyvin (80) claims that this is wrong and the error is a result of not using the complex character table properly.

This problem could be overcome by deriving the $\underline{F}$ and $\underline{G}$ matrix elements for the C_s species but because of the problem of interaction, all the in plane modes would have to be considered simultaneously. Whilst the $\underline{F}$ and $\underline{G}$ matrices have been constructed it was not thought worthwhile to proceed because the B-O-H bond angle is not known with any accuracy. In addition there is the problem of anharmonicity which arises because all the atoms involved are light atoms. For example the $\omega_e x_e$ for the B-O diatomic (90) is 12 cm^{-1}. In order to define all the interactions of the in plane modes, 25 force constants are required (82), 11 of these can be excluded if the high frequency oscillator approximation is employed to factor off the O-H stretches. This then leaves 14 force constants. (The number of independent force constants in each case is, 16, 5 and 9 respectively).

Therefore if a fit could be generated, there is no guarantee that it is meaningful or genuine because of the large number of unknown variables in the analysis.

4.8 Spectral Region 300-600 cm^{-1}

The survey spectra of this region of $B(OH)_3$ show a strong band at 513.8 cm^{-1} and a (very) weak feature at 448.9 cm^{-1}. Higher resolution studies on these bands showed that whereas $^{10}B/^{11}B$, $^{16}O/^{18}O$ and H/D isotope shifts could all be resolved for the 448.9 cm^{-1} band from suitably enriched samples, only deuterium enrichment produced a significant and thus observable frequency shift for the 513.8 cm-1 feature. As a result of these isotopic shifts the 513.8 cm^{-1} band is assigned to the A' HOBO torsion whilst the 448.9 cm^{-1} absorption is assigned to the E' in plane BO_2 bend. This latter mode will be dealt with first.

4.8.1 E' In Plane BO_2 Bend

Fig 13(a) is a spectrum under high resolution of the 448.9 cm^{-1} band in a sample of "normal" boric acid. The shoulder on the high frequency side at 450.5 cm^{-1} is assigned to the ^{10}B component. Fig 13(b) shows a spectrum of a sample containing ≈ 90% ^{10}B and this confirms the assignment.

On 45% oxygen-18 enrichment of a ^{11}B sample the spectrum in Fig 13(c) is observed whilst 60% enrichment of a ^{10}B sample results in the spectrum in Fig 13(d). In each case a six line pattern is observed and these bands are therefore assigned to the O-B-O bending E' mode. From the change in relative intensity it can be seen that in this case the mixed isotope species $H_3B^{16}O_2{}^{18}O$ and $H_3B^{16}O^{18}O_2$ are adjacent to each other rather than overlapping as in the B-O stretching case.

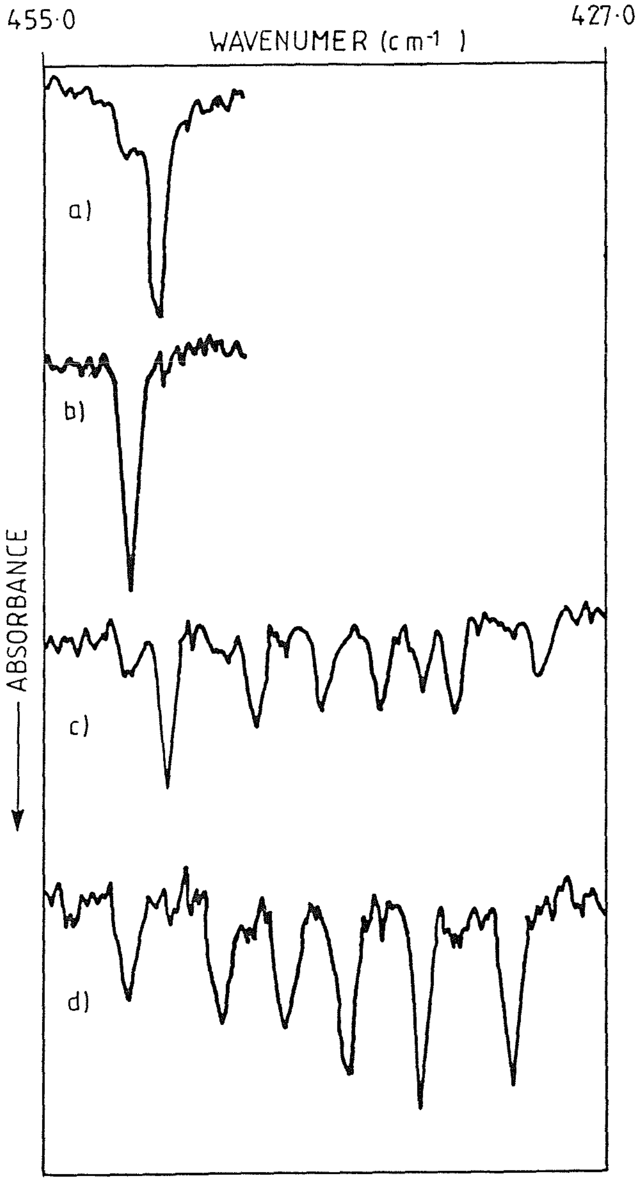

a) OBSERVED SPECTRUM FROM NORMAL BORIC ACID.

b) OBSERVED SPECTRUM FROM ^{10}B (90 %) BORIC ACID.

c) OBSERVED SPECTRUM FROM ^{18}O ENRICHED (~45%) BORIC ACID

d) OBSERVED SPECTRUM FROM ^{18}O ENRICHED (≃60%) ^{10}B (90%) BORIC ACID

FIG.13 HIGH RESOLUTION NITROGEN MATRIX IR SPECTRA OF BORIC ACID IN THE O-B-O BENDING REGION

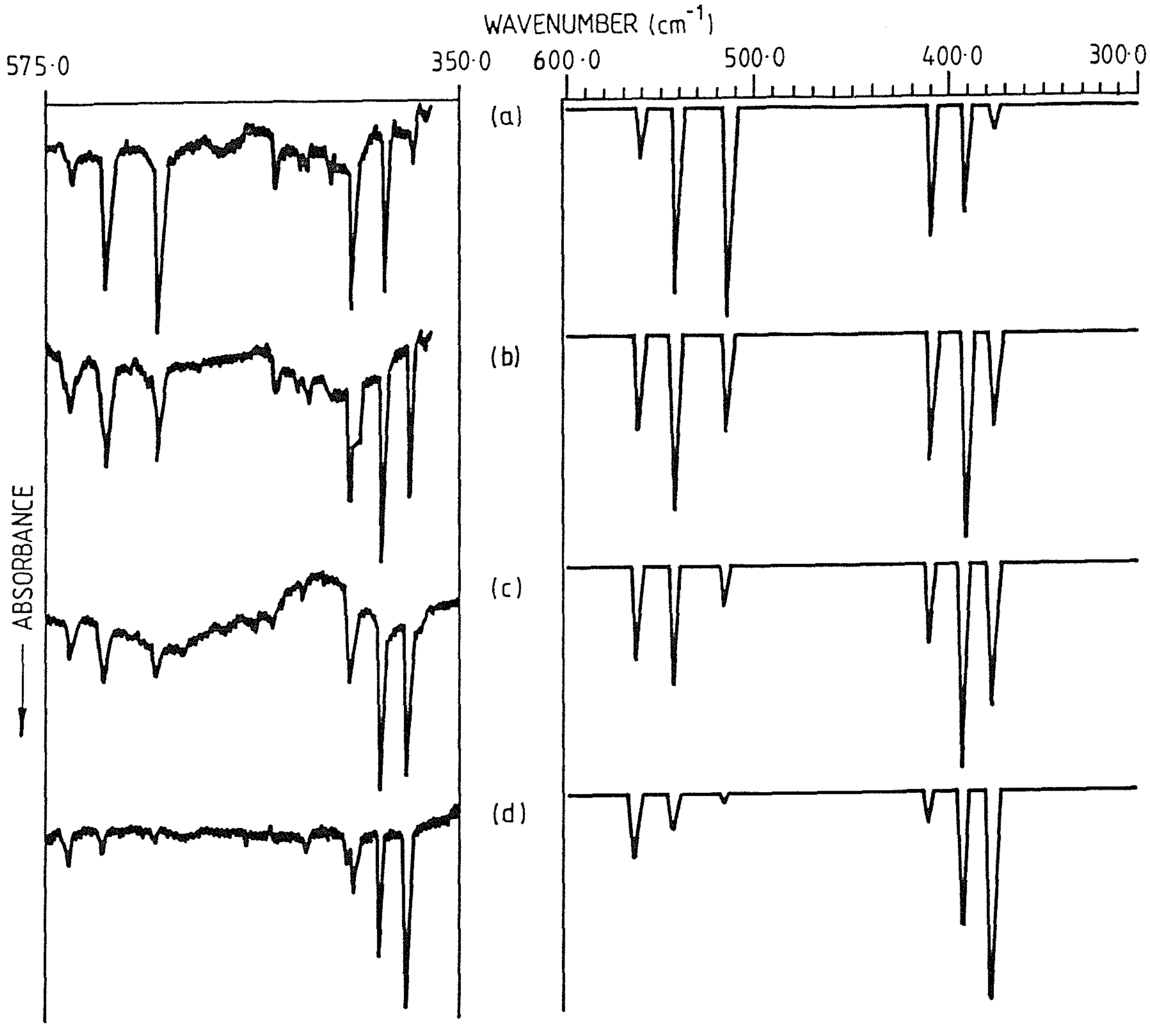

(a) OBSERVED AND CALCULATED SPECTRA (TORSION MODE ONLY) FOR $\simeq$ 40% ^{2}D ENRICHMENT
(b) OBSERVED AND CALCULATED SPECTRA FOR $\simeq$ 55% ^{2}D ENRICHMENT
(c) OBSERVED AND CALCULATED SPECTRA FOR $\simeq$ 65% ^{2}D ENRICHMENT
(d) OBSERVED AND CALCULATED SPECTRA FOR $\simeq$ 80% ^{2}D ENRICHMENT

FIG. 14 MODERATE RESOLUTION NITROGEN MATRIX I R SPECTRA OF BORIC ACID IN THE OH TORSION AND O-B-O BENDING REGIONS

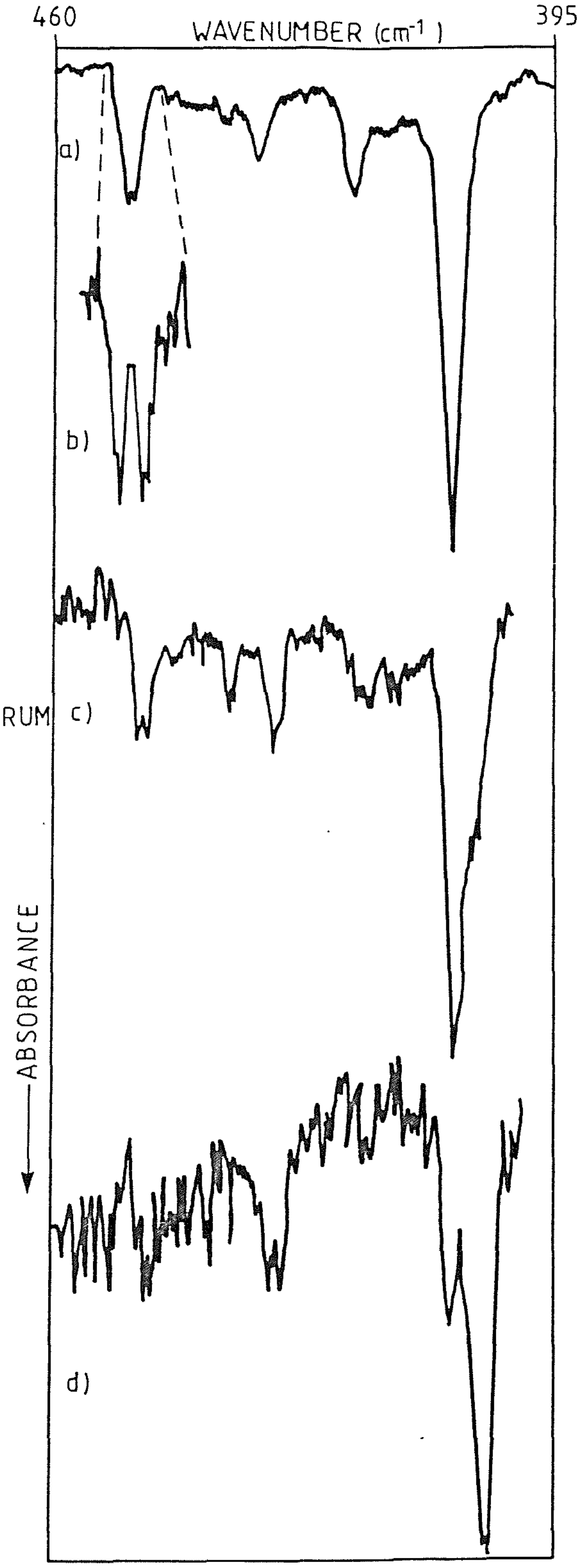

a) MEDIUM RESOLUTION SPECTRUM FROM ≃40% DEUTERATED SAMPLE.

b) AS ABOVE, BUT UNDER HIGHER RESOLUTION SPECTRUM.

c) MEDIUM RESOLUTION SPECTRUM FROM ≃ 55 % DEUTERATED SAMPLE

d) MEDIUM RESOLUTION SPECTRUM FROM ≃ 80% DEUTERATED SAMPLE

FIG. 15 NITROGEN MATRIX IR SPECTRA IN THE O-B-O BENDING REGION

TABLE 7

Spectral Features Arising from the In Plane BO_2 Bend In Isotopically Labelled Boric Acid

Observed Frequency (cm^{-1}) ^{10}B	^{11}B	Assignment	
450.5	448.9	E' BO_2 bend	H_3BO_3
445.8	444.5	A' BO_2 bend	$H_3BO^{16}O_2{}^{18}O$
442.9	441.2		
440.0	438.6	A' BO_2 bend	$H_3B^{16}O^{18}O_2$
436.4	434.8		
431.9	430.7	E' BO_2 bend	$H_3B^{18}O_3$
450.5	448.9	E' BO_2 bend	H_3BO_3
449.2	447.8	A' BO_2 bend	H_2DBO_3/HD_2BO_3
436.9	436.6		
432.6	431.0		
420.7	419.3		
405.2	404.7	E' BO_2 bend	D_3BO_3

When the sample is deuterated the spectrum in the region 350 to 575 cm^{-1} becomes very complex. In Fig 14 there appears to be six prominent bands and a number of weaker features. These weaker features are shown under higher resolution and amplification in Fig 15.

Fig 15 indicates that six bands are also observed in this region on deuterium enrichment. In this case however the pattern is dominated by a relatively intense feature at 408.4 cm^{-1}, this however has been shown not to belong to the BO_2 bending modes, but to the torsion mode. The band at 405 cm^{-1} does belong to the BO_2 bending modes and is assigned to the D_3BO_3 species. From these spectra, it is not possible to assign each band to a particular species but the band positions are given in Table 7.

Having assigned all the in plane modes it is now possible to confirm this assignment using the Teller Redlich product rule (83). Indeed if it is assumed that all the frequencies are harmonic then it is possible to check that the $^{10}B/^{11}B$ isotope shift for the E' B-O-H bending mode is negligible. This has been done and the calculated shift is 0.3 cm^{-1}, which is not observable on our instruments. Therefore the assignment of the in plane modes seems very satisfactory.

4.8.2 <u>The A" Torsion Mode</u>

The more intense bands in this region show a large deuterium isotope effect. On ^{10}B and ^{18}O enrichment the band at 513.8 cm^{-1} was merely broadened or displaced by less than a wavenumber. If the Teller Redlich product rule (83) is used for the two A" modes, ie the BO_3 out of plane bend (ω_1) and the O-H torsion (ω_2) and it is assumed that these frequencies are harmonic, it is then found that

$$\frac{\omega_1'\omega_2'}{\omega_1\omega_2} = \left(\frac{11}{10} \times \frac{61}{62}\right)^{\frac{1}{2}} = 1.04032$$

on going from ^{11}B to ^{10}B. Because these frequencies are well separated and resolved they can be used to get an indication of the boron isotope shift on the torsion mode, ie

$$\omega_2' = \frac{1.04032 \times 675.0 \times 513.8}{700.9} = 514.76$$

This therefore implies that there should be a splitting of approximately 1 cm^{-1} which is right at the limit of the resolving power of our instrument. This mode was also found to be fairly broad (~ 1.5 fwhm) and so this will also add to its non-observance.

The effect of full ^{18}O enrichment using the values for ^{11}B is to generate a shift of 1.2 cm^{-1} to 512.6 cm^{-1}. This will never be detected because the enrichment of ^{18}O water used was 70% and this would result in 3 (or 4) bands within a wavenumber. The limitations of assuming the frequencies are harmonic is illustrated when the product rule is used to calculate the deuterium isotope shift on the A" BO_3 bend. This gives a calculated value of 667.8 cm^{-1} compared to the non-observance of any effect. This however does not invalidate the arguments about the ^{10}B and ^{18}O effect on the torsional mode because the BO_3 out of plane bend will be less susceptible to anharmonicity than the torsion mode which involves extensive hydrogen atom motion.

Fig 14(a) through Fig 14(d) are spectra with an increasing deuterium content. From these, the lowest frequency component at 376.0 cm^{-1} is assigned as the A" mode in $B(OD)_3$. The surprising feature of these spectra is the occurrence of two absorptions at higher frequency than the

$B(OH)_3$ parent band and its fully deuterated analogue. Their origin is not immediately obvious because the representation of the ir active torsion mode is A" and is non-degenerate. The resultant isotope pattern on deuteration should contain at most four components (H_3, H_2D, HD_2 and D_3). However, if one refers back to the Γ_{vib} it can be seen that this is 3A' + 2A" + 4E' + E" and that from the character tables the E" mode is an out of plane mode and Raman active. When the symmetry falls to C_s during partial substitution, Γ_{vib} becomes 11A' + 4A" and therefore all the out of plane modes can mix and interact with each other. One would then expect three bands for each of the partially deuterated species leading to an eight line pattern in total, this however is not observed.

The reason for this discrepancy can be seen from the diagram below which contains the two descriptions for the normal vibrations of the E" (9,55) mode.

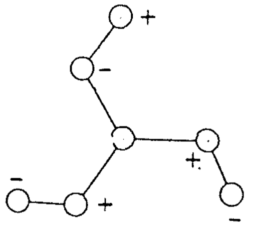

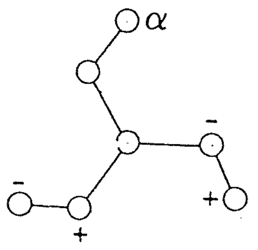

This mode is ir active if the molecular symmetry is C_s but it can be seen that if the unique proton or deuteron in HD_2BO_3 and DH_2BO_3 is at position α then it is not involved in the vibration and that the vibration is the same as in the C_{3h} parent species. This is inactive and therefore in

C_s symmetry, although it is ir active, it has zero intensity. If the two modes that have intensity can be calculated then the position of the band with zero intensity will also be calculated and hence give an indication of the frequency position of the E" mode in the C_{3h} species.

Although two analyses of the torsional mode have been carried out ($^{55,79-82}$) for C_{3h} symmetry there is no literature analysis of the C_s torsional modes. The SOTONVIBP program was used but it was found impossible to define the torsion mode satisfactorily and yet calculations carried out on H_2O_2 gave satisfactory results. It is hence assumed that the problem is due to the two ends of the torsion mode being different in boric acid. Therefore the $\underline{G}$ matrix and $\underline{F}$ matrix elements were derived from first principles and used in a BBC Basic program to generate the frequencies and intensities. This derivation is given in Appendix C and the $\underline{G}$ matrix elements for the C_s species are given below.

$$G_{11} = \mu_{H_1}A + \mu_{O_4}B + \mu_B C + \mu_{O_6}D$$

$$G_{22} = \mu_{H_2}A + \mu_{O_5}B + \mu_B C + \mu_{O_4}D$$

$$G_{33} = \mu_{H_3}A + \mu_{O_6}B + \mu_B C + \mu_{O_5}D$$

$$G_{12} = G_{21} = \mu_B C + \mu_{O_4}E$$

$$G_{13} = G_{31} = \mu_B C + \mu_{O_6}E$$

$$G_{23} = G_{32} = \mu_B C + \mu_{O_5}E$$

μ is the reciprocal mass of the appropriate atom, as defined in Fig 5a.

$$A = \frac{r}{d}\,\mathrm{cosec}^2\beta$$

$$B = \frac{r}{d}\,\mathrm{cosec}^2\beta - 2\,\mathrm{cosec}\beta\left\{\cot\beta + \frac{1}{\sqrt{3}}\right\} + \frac{d}{r}\left\{\cot\beta + \frac{1}{\sqrt{3}}\right\}^2$$

$$C = \frac{d}{r}\left\{\cot\beta + \sqrt{3}\right\}^2$$

$$D = \frac{4}{3}\,\frac{d}{r}$$

$$E = \frac{2}{\sqrt{3}}\left(\left\{\cot\beta + \frac{1}{\sqrt{3}}\right\} \times \left\{\frac{d}{r}\right\} - \mathrm{cosec}\beta\right)$$

$$F_{11} = F_{22} = F_{33} = F_{\tau}$$

$$F_{12} = F_{21} = F_{23} = F_{32} = F_{13} = F_{31} = F_{\tau\tau}$$

The $\underline{G}$ matrix elements for the C_{3h} species are:

$$G_{11} = \frac{\mu_H}{d\sin^2\beta} + \frac{\mu_O}{\sin^2\beta}\left(\frac{r}{d} + \frac{d}{r} + \frac{2d}{r}\sin\beta\left\{\sqrt{3}\cos\beta + \sin\beta\right\} - 2\left\{\cos\beta + \sqrt{3}\sin\beta\right\}\right) + \frac{3\mu_B d}{r}\left\{\sqrt{3} + \cot\beta\right\}^2$$

$$G_{22} = G_{33} = \frac{r\,\mu_H}{d \sin^2\beta} + \mu_O \left\{ \frac{d}{r} + \frac{r}{d} - 2\cos\beta \right\}$$

$$G_{12} = G_{21} = G_{13} = G_{31} = G_{23} = G_{32} = 0$$

$$F_{11} = F_\tau + 2F_{\tau\tau}$$

$$F_{22} = F_{33} = F_\tau - F_{\tau\tau}$$

$$F_{12} = F_{21} = F_{13} = F_{31} = F_{23} = F_{32} = 0$$

From the derived $\underline{G}$ matrix elements it can be seen that there are three variables for which values are required before the calculations can proceed. These are the B-O and O-H bond lengths and the B-O-H bond angle. The bond lengths were chosen to be 1.362 Å and 0.95 Å by comparison with the orthoboric acid crystal structure(54) for the former and water for the latter. The crystal structure value of the bond angle is 114°, if this value is used in a product rule type calculation for H_3BO_3 and D_3BO_3 then the fit between observed and calculated values for the $\nu_{A''}$O-H torsion in D_3BO_3 was found to be very unsatisfactory. In principle this could give an indication of the harmonic frequencies but they will not be reliable because the B-O-H bond angle in the solid and in molecular boric acid is likely to be different. The approach used was to estimate the B-O-H angle by using the product rule in conjunction with the assumptions that the observed transition frequencies were harmonic and that the BO_3 and O-H out of plane modes were uncoupled.

ie $FG_{O-H} = 4\pi^2 c^2 \nu^2_{O-H}$

and $FG_{O-D} = 4\pi^2 c^2 \nu^2_{O-D}$

$$\therefore \quad \frac{G_{O-H}}{G_{O-D}} = \left\{\frac{\nu_{O-H}}{\nu_{O-D}}\right\}^{2} \quad \text{for the "right" value of } \beta$$

G_{O-H} and G_{O-D} are the symmetrised, C_{3h}, $\underline{G}$ matrix elements derived earlier and if this calculation is done then the values of β for which the above holds are 130.9° and 153.4°. The fact that there are two solutions is a trifle puzzling but by determining the relative motions of the hydrogen, boron and oxygen atoms it was found that for the 130.9° case it is H down, O up and B up whilst for the 153.4° case it is H down, O up and B down, ie

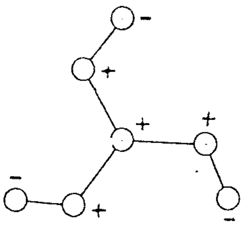

for 130.9°

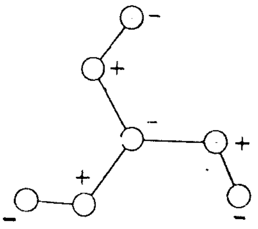

for 153.4°

It was decided to use a bond angle of 131° as this seems chemically more appropriate. No particular significance should be attached to this value because the B-O-H bond angle has essentially been used as a "sink" for any anharmonicity and also for any errors introduced by the use of the uncoupled oscillator approximation.

It is instructive however to compare this value of H-O-B angle of ~ 130° with the predictions of <u>ab initio</u> calculations on H_3BO_3 and with experimentally determined angles in related molecules. In particular, Gundersen has carried out a series of calculations on $B(OH)_3$ (93) and related hydroxy boron species (94). These calculations indicate that the HOB angles are expected to be in the range 110-115°, and for some of these species there is supporting experimental evidence (95) (eg $HB(OH)_2$ and H_2BOH). In electron diffraction experiments on $B(OMe)_3$ (78) and other methoxy boranes (96) the corresponding COB angles were found to be significantly wider and lay in the range 120-125°. (Electron diffraction experiments in collaboration with Dr D A Rice at Reading University have been attempted, but these were unfruitful because of the twin problems of getting enough boric acid in the vapour in the vicinity of the electron beam whilst keeping the water concentration low enough to permit the detection of only boric acid.)

Having achieved a value for the B-O-H angle it was then possible to use this to calculate a set of frequencies and force constants. The methodology and flow diagram for the program used is presented in Appendix D. An internal check is whether the C_s, $\underline{G}$ matrix elements calculate the same frequency as the C_{3h}, $\underline{G}$ matrix elements for H_3BO_3 and D_3BO_3. It was found that they did and therefore the C_s, $\underline{F}$ and $\underline{G}$ matrices had been derived correctly. The result of these calculations is in Table 8. From this it can be seen that there is a good correlation between observed and calculated frequencies and as anticipated earlier one of the components of H_2DBO_3 has the same frequency as that calculated for the E" mode of H_3BO_3. A similar case is also present for HD_2BO_3 and D_3BO_3. Therefore it is possible to estimate the E" value for H_3BO_3 as 577 cm^{-1}.

In order to confirm that this assignment is correct, the relative intensities of the bands is required. To do this the following equations (83) need to be evaluated.

$$\sum_{k} I_k = \sum_{k'k''} \frac{\partial \underline{\mu}}{\partial S_{k'}} \cdot \frac{\partial \underline{\mu}}{\partial S_{k''}} \quad G_{k'k''}$$

TABLE 8

Spectral Features Arising from the Torsion Mode in Deuterated Boric Acid

Observed (cm^{-1})	Calculated[(a)] (cm^{-1})	Assignment
-	577.7	E" O-H torsion H_3BO_3
513.8	513.8	A" O-H torsion H_3BO_3
408.4 541.8 -	408.3) 541.7) 577.7)	A" O-H torsion H_2DBO_3
561.2 390.5 -	561.4) 390.3) 434.3)	A" O-H torsion HD_2BO_3
-	434.3	E" D_3BO_3
376.0	375.7	A" D_3BO_3

(a) Assuming F_τ = 0.0644 mdyne/Å

$F_{\tau\tau}$ = - 0.0035 mdyne/Å and B-O-H bond angle of 131°.

$$\sum_{k} \frac{I_k}{\lambda_k} = \sum_{k'k''} \frac{\partial \underline{\mu}}{\partial S_{k'}} \cdot \frac{\partial \underline{\mu}}{\partial S_{k''}} F^{-1}_{k'k''}$$

The $\partial\underline{\mu}/\partial S$ terms are the same for all isotopic species because H_3BO_3 has no permanent dipole moment(83).

If it is assumed that the A" mode in H_3BO_3 has an intensity of 3, ie

$$I_{A''H_3BO_3} = 3$$

then it can be shown by using the second equation that

$$I_{A''D_3BO_3} = \frac{3\lambda_{A''D_3BO_3}}{\lambda_{A''H_3BO_3}}$$

For the partially substituted species (H_2DBO_3 and HD_2BO_3), each of these will produce three roots λ_1, λ_2 and λ_3 with intensity I_1, I_2 and I_3.

It would therefore appear that the intensity problem is insoluble because there are three roots but only two equations. It will be remembered however that one of these roots has zero intensity and therefore the intensities of the remaining two bands can be defined thus:

$$\frac{I_1}{\lambda_1} + \frac{I_2}{\lambda_2} = \frac{3}{\lambda_{A''H_3BO_3}}$$

$$I_1 + I_2 = \frac{G_{11} + G_{22} + G_{33} + 6G_{12}}{G_{A''_{H_3BO_3}}}$$

The last equation only holds if

$$3G_{A''} = G_{11} + G_{22} + G_{33} + 2(G_{12} + G_{13} + G_{23})$$

and this has been shown to be true.

G_{ij} are the C_s matrix elements and for

H_2DBO_3 $G_{11} = G_{22} \neq G_{33}$ and

HD_2BO_3 $G_{11} \neq G_{22} = G_{33}$

all the cross terms G_{ij}, (where $i \neq j$) are identical. Once these intrinsic intensities had been calculated they were multiplied by the relevant statistical weighting.

The results of these spectral simulations are shown in Fig 15 and it can be seen from these that the correlation is very good and therefore confirm that these bands are indeed due to the torsional mode in H_3BO_3.

The sum rule can also be used to confirm these assignments and the error is 0.13%.

5. Further Isotopic Studies

In the preceding sections extensive use was made of singly and doubly labelled isotopic species to characterise boric acid. In this section the effect of triply labelling, (ie $^{10}B/^{11}B$, $^{16}O/^{18}O$ and H/D) boric acid will be considered. Although these spectra shed no further light on the characterisation they can be used to confirm the assignments made and also to make the study complete. As above the various spectroscopic regions in turn will be considered.

5.1 2000-4000 cm^{-1}: O-H and O-D Stretches

The high resolution spectra of the O-H and O-D stretches are shown in Fig 16. Fig 16(a) are those observed for the triply labelled species, Fig 16(b) is that observed for ≃ 60% ^{18}O enrichment whilst Fig 16(c) is that of ~ 55% ^{2}D enrichment. As anticipated the patterns are very similar although the changes in relative intensity of the bands from the ^{16}O/^{18}O and H/D spectra should be noted. This change comes about because the band envelopes are made up of contributions from ^{16}OH, ^{16}OD, ^{18}OH and ^{18}OD species and hence the intensity of the "mixed" species is greater in these spectra than in the corresponding doubly labelled spectra. The new feature centred at 2688 cm^{-1} is obviously due to $D_nB^{18}O_m$ species, although the intense feature could be due to matrix isolated $H^{18}OD$. Table 9 gives the observed frequencies of these bands.

5.2 1300-1500 cm^{-1}: Asymmetric B-O Stretching Region

For the triply labelled species a total of 56 bands is expected in this region. Some of these transitions may have the same energy whilst one can also assume a high degree of accidental overlap, due to the finite (~ 0.5-1.0 cm^{-1}) resolution of the instrument. Therefore one anticipates observing less than 56 bands, but that the spectrum will be very complex. This is confirmed in Fig 17(a). Fig 17(b) is that from a deuterated sample, whilst Fig 17(c) is of a ^{10}B/^{18}O enriched sample. By comparison with these latter two spectra it can be seen that several of the bands in Fig 17(a) are due to $H_xD_{3-x}B^{16}O_3$ species (marked x) whilst others are from $H_3B^{16}O_y\,^{18}O_{3-y}$ species (marked ‡). The observed

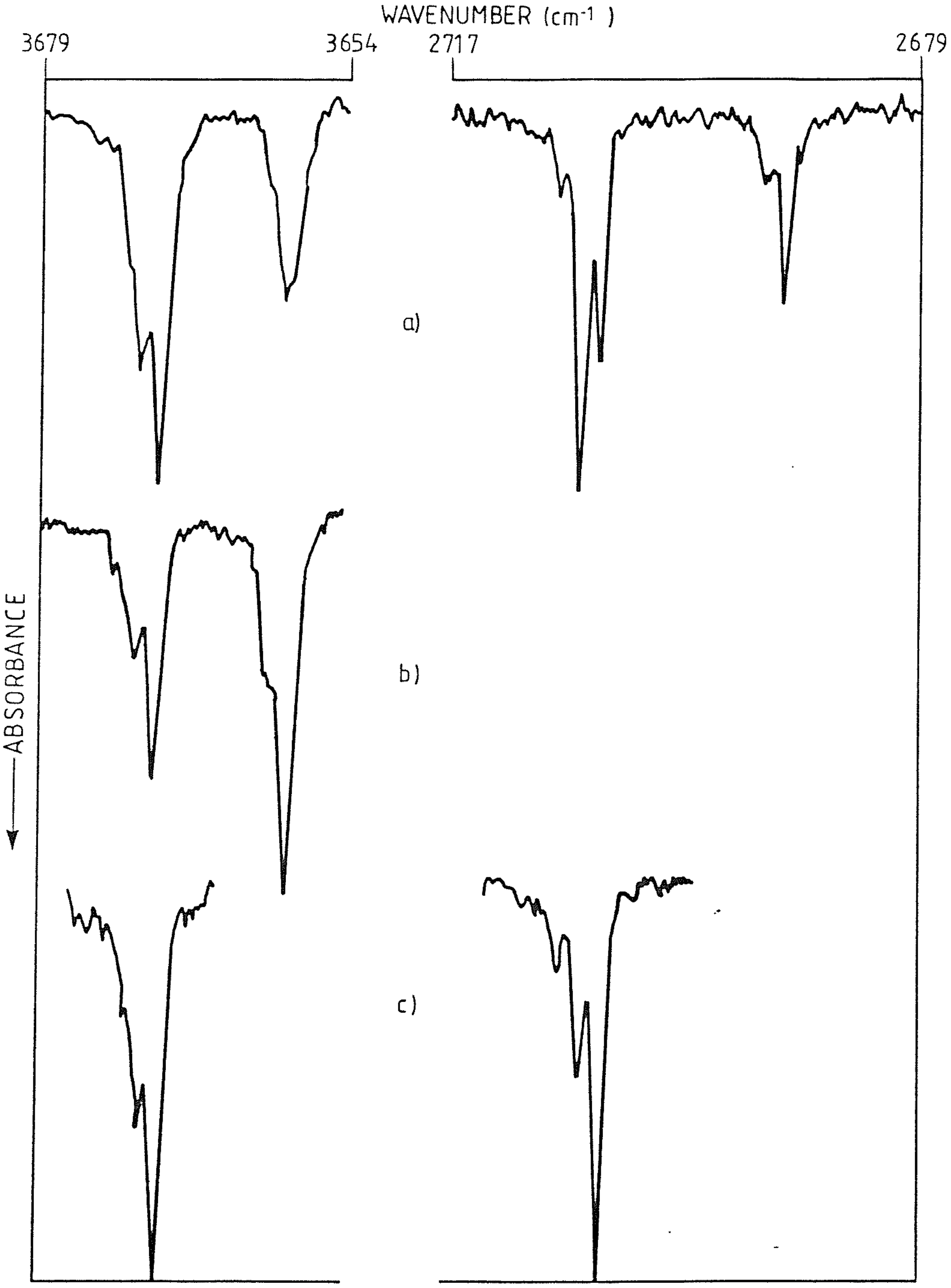

a) OBSERVED SPECTRUM FROM A TRIPLY LABELLED SAMPLE. ($^{10}B/^{11}B$, $^{16}O/^{18}O$ AND $^{1}H/^{2}D$).
b) OBSERVED SPECTRUM FROM AN ^{18}O ($\simeq$60%) ^{10}B(90%) SAMPLE.
c) OBSERVED SPECTRUM FROM A ^{2}D ($\simeq$55%) SAMPLE.

FIG.16 HIGH RESOLUTION NITROGEN MATRIX IR SPECTRA OF BORIC ACID IN THE O-H AND O-D STRETCHING REGIONS

TABLE 9

Observed Frequencies and Partial Assignment for the O-H and O-D Stretches in Triply Labelled Boric Acid

Frequency/cm^{-1}	Assignment
3671.2	$H_3B^{16}O_3$
3670.2	
3668.5	
3658.5	
3657.8	
2707.9	$D_3B^{16}O_3$
2706.2	
2704.6	
2691.2	
2689.6	
2688.5	

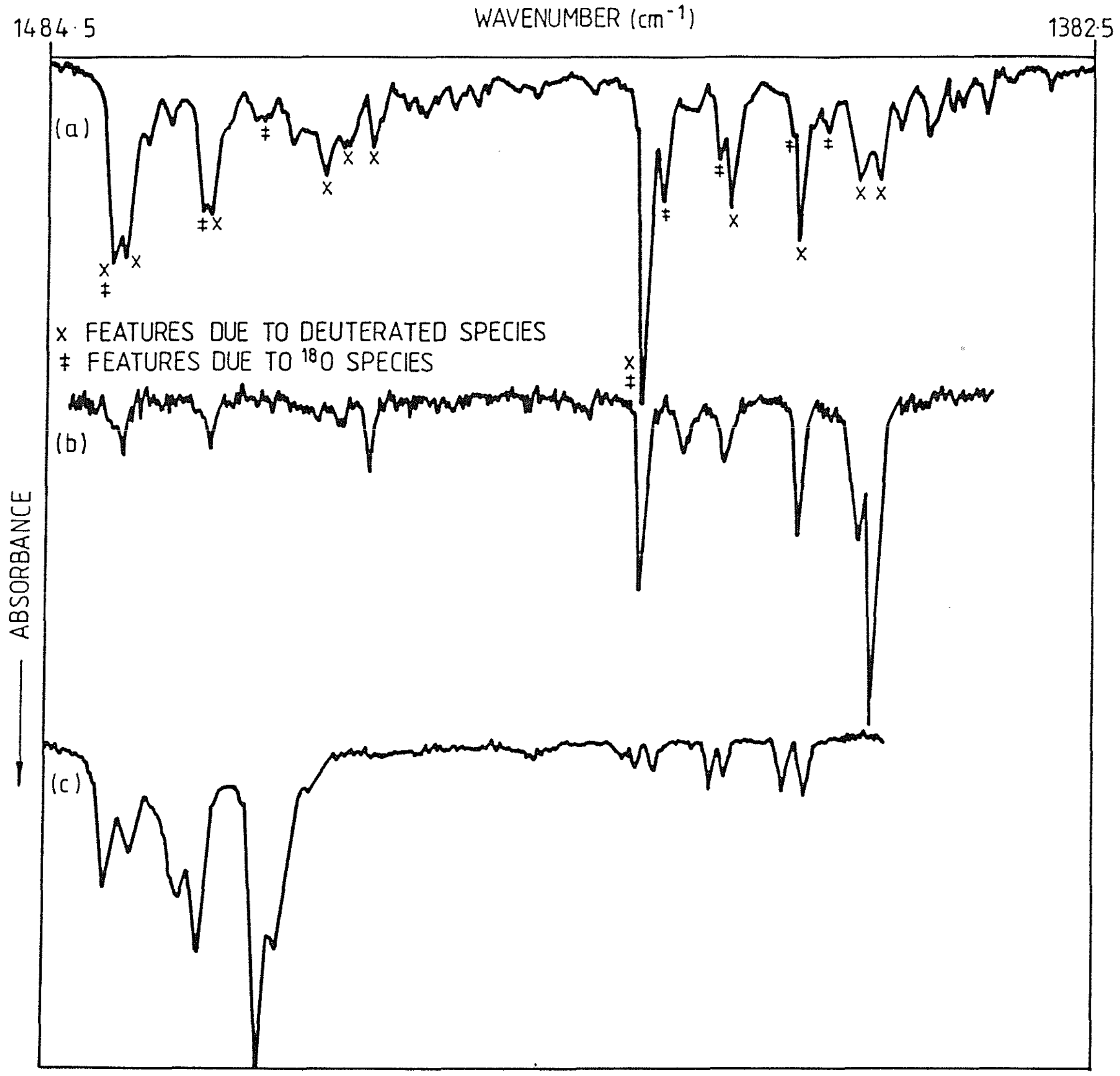

(a) SPECTRUM OBSERVED FROM A TRIPLY LABELLED SAMPLE
(b) SPECTRUM OBSERVED FROM A DEUTERATED (≃55%) SAMPLE
(c) SPECTRUM OBSERVED FROM A ^{10}B (90%) AND ^{18}O (≃65%) SAMPLE

FIG. 17 HIGH RESOLUTION NITROGEN MATRIX I R SPECTRA OF BORIC ACID IN THE B-O ASYMMETRIC STRETCHING REGION

TABLE 10

Features Observed in the ^{11}B-O Asymmetric Stretching Region of Triply Labelled Boric Acid

Frequency/ cm^{-1}	Assignment
1426.2	$H_3B^{16}O_3$
1424.5	$H_3B^{16}O_2{}^{18}O$
1421.3	
1419.0	$H_3B^{16}O^{18}O_2$
1417.7	$HD_2B^{16}O_3$
1417.5	$H_3B^{16}O^{18}O_2$
1411.9	$H_3B^{16}O^{18}O$
1410.7	$H_2DB^{16}O^{18}O_2$
1409.7	$H_3B^{18}O_3$
1408.2	
1405.0	$H^{16}OD$, $HD_2B^{16}O_3$, $D_3B^{16}O_3$
1403.1	
1401.1	
1398.4	
1398.0	
1398.6	
1396.1	
1395.2	
1393.1	
1390.6	
1386.9	
1385.5	

TABLE 11

Features Observed in the ^{10}B-O Asymmetric Stretching Region of Triply Labellec Boric Acid

Frequency/ (cm^{-1})	Assignment
1478.0	$H_3B^{16}O_3$
1476.8	$H_2DB^{16}O_3$
1474.6	
1472.4	
1469.0	$H_3B^{16}O_2{}^{18}O$
1468.3	$HD_2B^{16}O_3$
1466.8	
1464.0	
1463.0	$H_3B^{16}O^{18}O_2$
1462.7	
1460.4	
1457.5	$H_2DB^{16}O_3$
1455.6	$HD_2B^{16}O_3$
1452.7	$D_3B^{16}O_3$
1451.9	
1449.4	
1448.2	
1447.5	
1446.5	
1444.7	
1444.4	
1443.7	
1442.5	
1441.5	
1438.8	
1436.8	
1435.7	
1431.3	

frequencies and partial assignments are given in Tables 10 and 11. Further assignments cannot really be made without detailed calculations being carried out. As mentioned earlier this is not feasible because of the various parameters whose values are not known with any degree of accuracy, and also because of the limited use that SOTONVIBP can put isotopic data to.

5.3 800-1100 cm^{-1}: B-O-H Bending and B-O Symmetric Stretching Regions

The spectra in this region for the deuterium and oxygen-18 enriched samples were very complex and not completely assignable. In the case of the triply labelled species, large band overlaps were found with the result that broad features were observed. The sharper features on these envelopes are listed in Table 12 with possible assignments.

The significant feature is that in the 900-850 cm^{-1} region only two bands were observed and in the same place as for the H/D species. The relative intensities were also in the same relationship.

5.4 650-750 cm^{-1}: BO_3 Out of Plane Bending Region

This spectral region in a preceding section showed only boron and oxygen isotope effects. Therefore for the triply labelled species a very similar isotope pattern is expected to that observed previously. Indeed, it should be possible to estimate both the ^{10}B and ^{18}O enrichment from these spectra. The observed spectra as shown in Fig 18(a), Fig 18(b) and Fig 18(c) are from 45%, ^{18}O enriched and 60%, ^{18}O/90%, ^{10}B enriched samples respectively and are included for comparison. Fig 18(a) is as anticipated, and consists

TABLE 12

Spectral Fetaures Observed in the 1100-500 cm^{-1} Region for Triply Labelled Species

Frequency/ cm^{-1}	Assignment	
1015.8		
1009.9 1002.2	B-O-H bend	H_3BO_3
894.4	B-O stretch	HD_2BO_3
887.6	" " "	H_2DBO_3
831.0 825.5	B-O-H bend	D_3BO_3
781.9 773.9 (768.4 ?)		

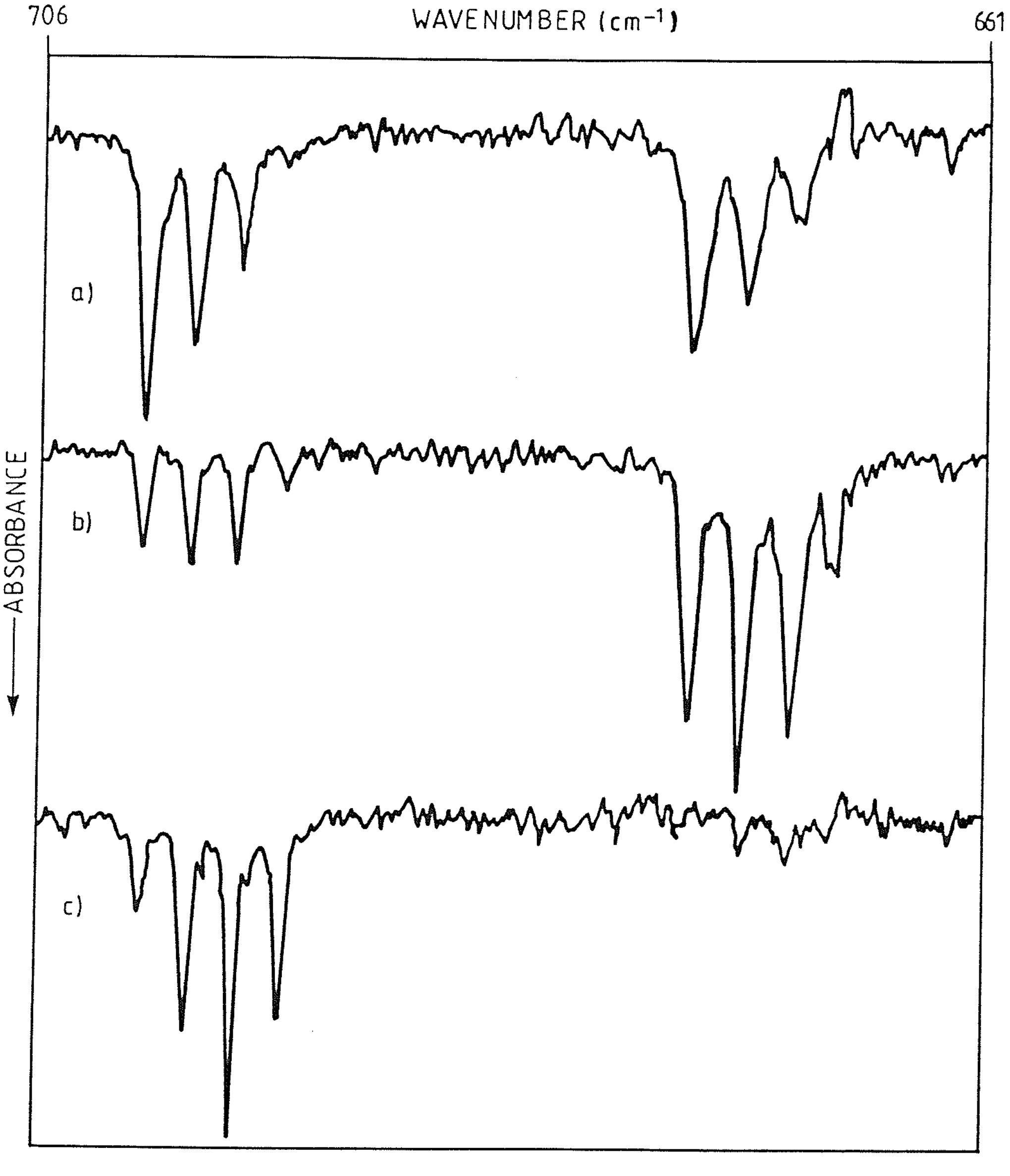

a) SPECTRUM OBSERVED FROM TRIPLY LABELLED SPECIES.
b) SPECTRUM OBSERVED FROM ^{18}O ($\simeq$45%) SAMPLE.
c) SPECTRUM OBSERVED FROM ^{18}O ($\simeq$60%), ^{10}B (90%) SAMPLE.

FIG.18 HIGH RESOLUTION NITROGEN MATRIX I R SPECTRA OF BORIC ACID IN THE BO_3 OUT PLANE BEND REGION

TABLE 13

Spectral Features and Assignments for the BO_3 Out of Plane Bend in Triply Labelled Boric Acid

Frequency/ cm^{-1}	Assignment	
700.7	$H_3B^{16}O_3$	^{10}B
698.4	$H_3B^{16}O_2{}^{18}O$	
696.2	$H_3B^{16}O^{18}O_2$	
694.2	$H_3B^{18}O_3$	
674.7	$H_3B^{16}O_3$	^{11}B
672.3	$H_3B^{16}O_2{}^{18}O$	
669.9	$H_3B^{16}O^{18}O_2$	

of a doublet of quartets, it should be noted that each quartet is displaced very slightly (0.2-0.3 cm^{-1}) as a result of deuteration. The band centres for these absorptions are given in Table 13 together with their assignments.

5.5 300-600 cm^{-1}: BO_2 Bend and O-H Torsion Regions

For the O-B-O bending mode in the triply labelled species 56 bands are anticipated as in the B-O stretching case. However because of the inherent weakness of these bands the effect will be to smear out the intensity throughout the 400-450 cm^{-1} range between these 56 bands. Fig 19(a) is a spectrum observed from the triply labelled system whereas Fig 19(b) is that of a 40% deuterium enriched sample. These two spectra indicate that the above postulate is probably true. Under higher resolution conditions several bands could be identified and these are given in Table 14.

The remaining features in this spectral region can be assigned to the O-H torsion mode by comparison with the 40% deuterated sample spectra in Fig 19(b). As observed previously there is very little boron or oxygen isotope effect on these bands and this is confirmed in Fig 19(a), where the band positions for the triply labelled spectrum have the same almost energy as those of the deuterated species.

From these two spectra it can also be concluded that the extent of deuterium enrichment is 35-40%. Table 15 lists the observed frequencies and their assignments for the torsional mode.

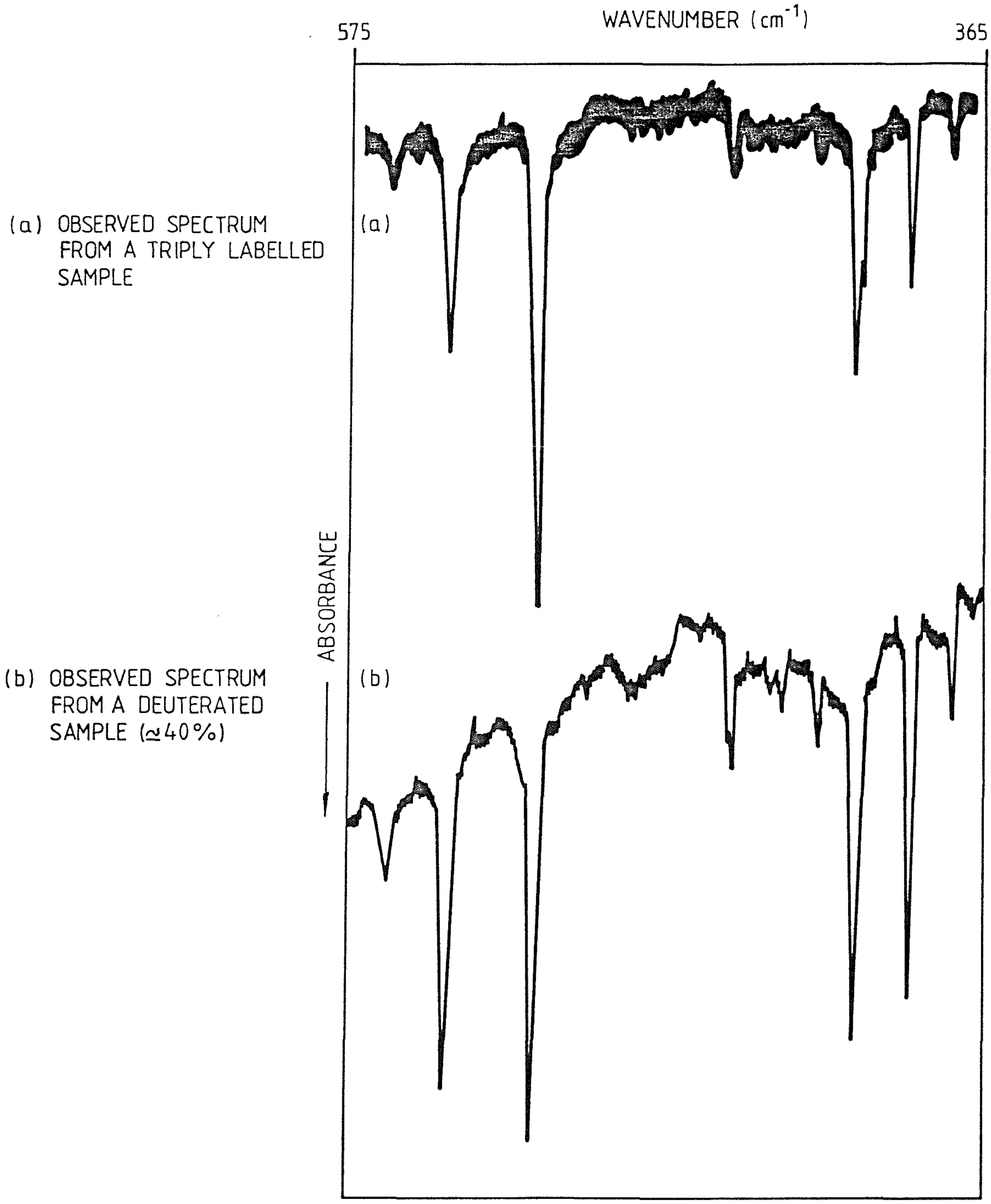

FIG. 19 MEDIUM RESOLUTION NITROGEN MATRIX I R SPECTRA IN THE O-H TORSION REGION

TABLE 14

Spectral Features Observed in the BO_2 Bending Region for Triply Labelled Boric Acid

Frequency/ cm^{-1}	Assignment
450.8	$H_3{}^{10}B^{16}O_3$
449.1	$H_3{}^{11}B^{16}O_3$
447.6	
436.5	
420.6	
419.0	
405.9	

TABLE 15

Spectral Features Observed in the Torsion Region for Triply Labelled Boric Acid

Frequency/ cm^{-1}	Assignment
513.4	H_3BO_3
408.2	H_2DBO_3
541.4	H_2DBO_3
560.8	HD_2BO_3
390.0	HD_2BO_3
375.9	D_3BO_3

5.6 Summary

Although the spectra presented in this last section have not been used extensively to characterise boric acid, they have however shown that the assignments made in the preceding sections are also valid for triply labelled samples.

6. Alternative Structures for H_3BO_3

The matrix ir spectra for monomeric $B(OH)_3$ have been satisfactorily assigned on the assumption of C_{3h} symmetry. However as was suggested earlier it is worth considering whether any alternative shapes will also account for the observed spectra. The evidence for the presence of a C_3 axis is compelling not only because of the $^{16}O/^{18}O$ patterns of the out of plane BO_3 mode but also because of the clear demonstration of degenerate modes. The co-planarity of the OH groups is indicated by the observation of only one OH stretch and the presence of a C_3 axis relating the three O-H groups is implied by the patterns derived from both $^{16}O/^{18}O$ and H/D isotope substitution. The central BO_3 unit similarly appears to be planar because of a lack of evidence for the symmetric B-O stretch in the parent H_3BO_3 molecule. The results thus provide no reason to suspect a symmetry lower than C_{3h}. The only higher symmetry allowed is D_{3h} where the O-H groups could either be linear or the protons could be symmetrically placed between the oxygen atoms. The latter can be ruled out because of the frequency value of the O-H stretches indicating that they are not forming hydrogen bonds.

The observed spectra may in principle be assigned by assuming a D_{3h} model with linear B-O-H groups. For this geometry:

$$\Gamma_{vib} = 2A_1' + A_2' + 2A_2'' + 4E' + E''$$

with the ir active modes being $2A_2'' + 4E'$, and as for C_{3h} six ir bands are expected. For five of these ($A_2'' + 4E'$) it turns out that the qualitative descriptions of the various modes (eg E' B-O stretch) are the same for both point groups. The only difference lies in the description of the ir active out of plane hydrogen atom motion. In D_{3h} this can be regarded as a B-O-H bend (A_2'') whilst in C_{3h} it is the A" torsion. Both of these types of vibration would be expected to occur at low frequency and have large deuterium isotope effects. However, although the basic spectrum of $B(OH)_3$ could be assigned qualitatively assuming either symmetry, the magnitude of the deuterium isotope effect on this low frequency out of plane mode can be used to distinguish between the two structures.

As demonstrated previously the observed frequency shift from 513.8 cm^{-1} (H_3BO_3) to 376.0 cm^{-1} (D_3BO_3) can be reproduced exactly by choosing fairly reasonable values of the geometrical parameters and by making use of the "decoupled oscillator" approximation. This frequency shift is independent of force constant. The vibrational analysis for D_{3h}, $X(YZ)_3$, was carried out by Cyvin et al ([89]) as a prelude to their analysis of the C_{3h} case, when they could find no appropriate example. If a similar decoupling is assumed, the isotope shift from H_3BO_3 to D_3BO_3 for the A_2'' HOB bend will also be independant of force constant. The corresponding $\underline{G}$ matrix terms still include the B-O and O-H bond lengths, but as might be anticipated there is now no flexibility of the choice of the HOB bond angle. If the same bond lengths (r_{B-O} = 1.362Å and d_{O-H} = 0.95Å) are used in the appropriate expressions then the predicted shift on going from H_3BO_3 to D_3BO_3 is 513.8 $\rightarrow \simeq$ 406 cm^{-1}. This is significantly less than the observed shift (513.8 to 376.0 cm^{-1}), and would require an appreciable anharmonic correction in order to fit the experimental data. In view of this, the D_{3h} model should be regarded as less realistic, even on purely spectroscopic grounds.

7. **Conclusions**

The work in this chapter has shown conclusively that at the temperatures employed (25-50°C) boric acid is volatile, and vaporises as monomeric H_3BO_3 units. The matrix ir experiments in conjunction with isotopic substitution and normal co-ordinate analysis indicate that the structure is almost certainly C_{3h}, and this confirms what has always been assumed.

The infrared frequencies of the matrix isolated species have been found to be very similar to those of the solid for the modes of the central BO_3 unit, whereas there is a large discrepancy for those modes that involve substantial hydrogen atom motion. The existing gas phase data for those modes that have been identified is reasonable except for the value of the torsion mode reported by Margrave et al (43). They give a value of 303 cm^{-1} whereas the work described in this thesis assigns the band at 513.8 cm^{-1} to the torsion mode by a partial normal co-ordinate analysis, indeed this analysis predicts the ir inactive torsion mode to be 577.7 cm^{-1}. Cyvin (82) quotes a personal communication from Randall describing a gas phase ir study which appears to give the same values as ref 43 and he states that '... one should await a final assignment of gas-phase frequencies from the significant work of Margrave and Randall...'. This was not forthcoming and therefore it appears that the work described in this chapter gives for the first time the ir frequencies for molecular orthoboric acid with any degree of certainty. The identification and assignment of the low frequency modes (both ir active and inactive) also allows much more accurate thermodynamic calculations to be carried out.

The planarity of the molecule can be assumed to be due to some π character in the B-O bond. Molecular orbital calculations have shown (97) that the LUMO in H_3BO_3 is the boron 2pπ non-bonding (or weakly anti-bonding) orbital. One could therefore anticipate some donation of electron density from the oxygen lone pairs into this unoccupied orbital. Ab initio calculations(98) on H_2BOH reveal a π bonding interaction between the boron and oxygen which results in a barrier to internal rotation of 16.4 kcal/mol.

The fact that there is a barrier to internal rotation casts doubt on the accuracy of the JANAF(56) thermodynamic data which are based on the assumption of free rotation of the O-H groups which Margrave argued in favour of in his gas phase ir paper (43). The other thermodynamic tabulation (57) employs solid state data. Work is currently under way (99) to derive new thermodynamic parameters for molecular boric acid using the vibrational data in this chapter, and it has been found that the differences become significant above 500K, especially in respect of entropy.

One might anticipate that a (large) planar molecule such as boric acid would orientate itself in the matrix as has been found for $Cu(NO_3)_2$ in epr studies (100). This however is not the case because frequencies have been observed that have the dipole moment change in all three cartesian directions.

One surprising feature not observed was the splitting of any of the degenerate modes by the nitrogen matrix. In a recent study by Ogden and Brisdon (101) of the SeO_3 monomer (D_{3h}) trapped in nitrogen it was found that the selenium isotope pattern could only be interpreted in terms of either two sites, or one low symmetry site. If the latter is true then one could make the tentative conclusion that the site symmetry of nitrogen is C_{3h} or higher. If the former is the case then in matrix isolated boric acid, ir spectroscopy cannot differentiate between the two sites.

8. References

1. Kinnersly S.R., Richards G.G. and O'Mahoney R. AEEW - M 1958, 1983. Based on data from the CEGB Sizewell B PWR Pre-Construction Safety Report. April 1982.

2. Elrick R.M. and Sallach R.A.
Proc. Int. Meeting on LWR Severe Accident Evaluation.
Cambridge, Mass, USA
28 August-1 September, TS-4.6, 1983.

3. TMI Unit 2 Technical Information and Examination Programme, UPDATE, 1984.

4. OECD LOFT Fission Product Experiment.
LP-FP-1, Fission Product Data Report, 1985.

5. Bowsher B.R.
Prog. Nucl. Energy, 20, 199, 1987.

6. Bowsher B.R and Nichols A.L.
AEEW - R 1973, 1985.

7. Bowsher B.R., Dickinson S., Grubb S.R., Ogden J.S. and Young N.A.
Proc. of the ACS Symposium on Chemical Phenomena Associated with Severe Reactor Accidents, Anaheim, California.
NUREG/CP-00-78, 6-45, 1987.

8. See Chapter 7.

9. Sprague R.W. "A Comprehensive Treatise on Inorganic and Theoretical Chemistry". Vol 5, Suppl 1, Part A. Ed J.W. Mellor, Longmans, London 1980.

10. Kracek F.C., Morey G.W. and Merwin H.E.
Am. J. Sci., 35A, 143, 1938.

11. Atkins P.W., Child M.S. and Phillips C.S.G.
"Tables for Group Theory". OUP 1970.

12. Tchijevski, B.K.
Acta Phys. Nat., 3, 12, 1884.

13. Jannasch P. and Harwood H.F.
J. Pr. Chem. 80, 134, 1910.
Chem. Abs., 4, 432, 1910.

14. Nasini R. and Ageno F.
Atti. Accad. Lincei., 21, 125, 1912.
Chem. Abs., 6, 3213, 1912.

15. Nasini R. and Ageno F.
Gazz. Chim. Ital., 43, 249, 1913.
Chem. Abs., 7, 2502, 1913.

16. Anschutz R. and Riepenkroger K.
Ber., 58B, 1734, 1925.
Chem. Abs., 20, 25, 1926.

17. Nasini R.
Atti. Accad. Lincei., 3, 247, 1926.
Chem. Abs., 20, 1965, 1926.

18. Banchi G. and Gianatti M.
Ann. Chim. Applicata., 20, 271, 1930.
20, 285, 1930.
20, 296, 1930.
Chem. Abs., 24, 5596, 1930.

19. Bezzi S.
Ann. Chim. Applicata., 22, 713, 1932.
Chem. Abs., 27, 1587, 1933.

20. Thiel A. and Siebeneck H.
Z. Anorg. Allg. Chem., 220, 236, 1934.
Chem. Abs., 29, 977, 1935.

21. Bezzi S.
Ann. Chim. Applicata., 25, 121, 1935.
Chem. Abs., 29, 7158, 1935.

22. Bezzi S.
Gazz. Chim. Ital., 65, 766, 1935.
Chem. Abs., 30, 2827, 1936.

23. Von Stackelberg M. and Quatrum F.
Z. Electrochem., 42, 551, 1936.
Chem. Abs., 30, 7408, 1936.

24. Von Stackelberg M., Quatrum F. and Dressel J.
Z. Electrochem., 43, 14, 1937.
Chem. Abs., 31, 3368, 1937.

25. Jaulmes P. and Gontard A.
Bull. Soc. Chim., 4, 139, 1937.
4, 149, 1937.
Chem. Abs., 31, 2904, 1937.

26. Deford D., Luchesi C. and Thoburn J.
"Analytical Chemistry of Boron".
North Western University, 1953.

27. Rankama K. and Sahama T.
"Geochemistry".
University of Chicago Press, 1950.

28. Feldman C.
Anal. Chem., 33, 1916, 1961.

29. Gast J.A. and Thomson T.G.
Tellus, 11, 345, 1959.

30. Savenko V.S.
Okeanologiya., 17, 445, 1977.
Chem. Abs., 88, 25950q, 1978.

31. "Thermodynamics and Transport Properties of Gases, Liquids and Solids". Feb 23-26, 1959.
Purdue University, La Fayette, Indiana. McGraw Hill.

32. "Proc. of the Propellant Thermodynamics and Handling Conference". Ohio State University, July 20-21, 1959. Ohio State University Special Report 12. 1960.

33. Mack J.L. and Wilmot G.B. "Proc. Meeting Interagency Chem. Rocket Propulsion Gp. Thermochem".
California. 1, 59-70, 1968.

34. Macatician J. and Hubard S.S.
Chem. Abs., 59, 2573f, 1963.

35. David L.J. and RHODES R.P.
Chem. Abs., 54, 16793i, 1960.

36. Loprest L. and Tunkel S.J.
Chem. Abs., 55, 19714h, 1960.

37. Margrave J.L.
J. Chem. Phys., 60, 715, 1956.

38. Margrave J.L., Soulen J.R., Leroi G.F., Greene F.T. and Randall S.P.
Congr. Int. Chim. Pure et Appl, 16th Paris.
Mem. Sect. Chim. Minerale, 521, 1957.
Chem. Abs., 54, 9474, 1960.

39. Margrave J.L., Soulen J.R., Leroi G.E. and Randall S.P.
US Dept. Com. Office, Tech. Serv., PB Rept, 128, 540, 1957.
Chem. Abs., 55, 26584, 1960.

40. Greene F.T., Randall S.P. and Margrave J.L.
"Thermodynamics and Transport Props. of Gases, Liquids and Solids." Purdue University, La Fayette, Indiana, McGraw Hill, Feb 23-26, 1959.

41. White D., Mann D.E., Walsh P.N. and Sommer A.
Proc. Propell. and Thermodyn. Conf. Am. Rocket. Soc, Columbus, Ohio, July 20, 1959.
J. Chem. Phys., 32, 488, 1960.

42. Meschi D.J., Chupka W.A. and Berkowitz J.
135th Meeting Am. Chem. Soc., Boston, Mass, April 1959.
J. Chem. Phys., 33, 530, 1960.

43. Greene F.T., Leroi G.E., Randall S.P., Soulen J.R., Spinar L.H. and Margrave J.L.
Proc. Propell. Thermodyn. and Handling Conf, July 20, 1959.
Ohio State University, University Special Report 12, 23, 1960.

44. Gilson T.R.
University of Southampton.
Unpublished Observations, 1987.

45. Randall S.P. and Margrave J.L.
J. Inorg. Nucl. Chem., 16, 29, 1960.

46. Gropsian Z. and Muranesui P.V.
Chem. Abs., 52, 12519g, 1958.

47. Ashratova Sh.K.
Zavod. Lab., 26, 59, 1960.
Chem. Abs., 54, 9444d, 1960.

48. Konstrikin Yu.M. and Koravin V.A.
Zavod. Lab., 26, 60, 1960.
Chem. Abs., 54, 12733f, 1960.

49. Abrikosov N.Kh., Liang T.U. and Shas'Khov Yu.M.
Chem. Abs., 55, 11005h, 1961.

50. Kostrinkin Yu.M. and Koravin V.A.
Chem. Abs., 58, 2847c, 1963.

51. Petropavlovski I.A. and Torocheshnikov N.S.
Zh. Vses. Khim. Obshchest., 14, 466, 1969.
Chem. Abs., 71, 116797k, 1969.

52. Petropavlovski I.A. and Torocheshnikov N.S.
Tr. Mosk. Chim. Teknol. Inst., 60, 82, 1969.
Chem. Abs., 72 59386v, 1970.

53. Zachariasen W.H.
Z. Krist., 88, 150, 1934.

54. Zachariasen W.H.
Acta. Cryst., 7, 305, 1954.

55. Pistorius C.W.F.T.
J. Chem. Phys., 31, 1454, 1959.

56. Janaf. "Thermochemical Tables"
Vol. 14, Suppl 1.
Nat. Bur. Stand. (US), 1985.

57. Glushko V.P., Gurvich L.V., Bergman G.A., Veits I.V., Medvedev V.A., Khachkuruzov G.A. and Yungman V.S. "Thermodynamic Properties of Individual Substances." Part 1, 3rd Ed. Pergamon. 1988.

58. Winter E.R.S., Carlton M. and Briscoe H.V.A. J. Chem. Soc., 1940, 131.

59. Tursi A.J. and Nixon E.R. J. Chem. Phys., 52, 1521, 1970.

60. Craven B.M. and Sabine T.M. Acta Cryst., 20, 214, 1966.

61. Cowley J.M. Acta Cryst., 6, 522, 1953.

62. Matossi F. and BLUSCHKE H. Z. Physik., 108, 295, 1938.

63. Miller F.A. and Wilkins C.H. Anal. Chem., 24, 1253, 1952.

64. Mortimer H.E. MS Thesis. Rensselaer Polyt. Inst. July 1953. Cited in Ref 9.

65. Bethell D.E. and Sheppard N.N. Trans. Farad. Soc., 51, 9, 1955.

66. Sidorov T.A. and Sobolev N.N. Opt. and Spect., 1, 393, 1956. Chem. Abs., 51, 4820g, 1957.

67. Hornig D.F. and Plumb R.C. J. Chem. Phys., 26, 637, 1957.

68. Servoss R.R. and Clark H.M.
J. Chem. Phys., 26, 1175, 1957.

69. Goubeau J. and Hummel D.
Z. Phys. Chem. (Frank.), 20, 15, 1959.

70. Krishnan K.
Proc. Ind. Acad. Sci., 57A, 103, 1963.

71. Durig J.R., Green W.H. and Marston A.L.
J. Mol. Struct., 2, 19, 1968.

72. Vizi B.
Veszpremi. Vegyip. Egyct. Kozlem., A10, 205, 1966.
Chem. Abs., 69, 71255x, 1968.

73. Broadhead P. and Newman G.A.
J. Mol. Struct., 10, 157, 1971.

74. Now-Djavan I.
Quarterly Bulletin of the Faculty of Science, Tehran University., 7, 123, 1975.

75. Janda R. and Heller G.
Spectro. Chim. Acta , 36A, 997, 1980.

76. Sen M.K.
Ind. J. Phys., 11, 9, 1937.

77. Duval C. and Lecomte J.
Bull. Soc. Chim., 8, 713, 1941.

78. Gundersen G.
J. Mol. Struct., 3, 79, 1976.

79. Mooney R.W., Cyvin S.J., Brunvoll J. and Kristiansen L.A.
J. Chem. Phys., 42, 3741, 1965.

80. Cyvin S.J., Mooney R.W., Brunvoll J. and Kristiansen L.A.
Acta Chem. Scand., 19, 1031, 1965.

81. Kristiansen L.A., Mooney R.W., Cyvin S.J. and Brunvoll J.
Acta Chem. Scand., 19, 1749, 1965.

82. Ottinger R., Cyvin S.J., Mooney R.W., Kristiansen L.A. and Brunvoll J.
Acta Chem. Scand., 20, 1389, 1966.

83. Wilson E.B., Decius J.C. and Cross P.C.
"Molecular Vibrations".
(a) McGraw Hill, New York, 1955.
(b) Dover Publications, New York, 1980.

84. Decius J.C.
J. Chem. Phys., 16, 1025, 1948.

85. Jenny S.N.
PhD Thesis, University of Southampton, 1982.

86. Jenny S.N. and Ogden J.S.
J. Chem. Soc. Dalton Trans., 1979, 1465.

87. Darling J.H. and Ogden J.S.
J. Chem. Soc. Dalton Trans., 1972, 2426.

88. Huber H., Kundig E.P., Moskovits M. and Ozin G.A.S.
J. Am. Chem. Soc., 95, 332, 1973.

89. Mooney R.W., Cyvin S.J. and Brunvoll J.
Acta Chem. Scand., 19, 983, 1965.

90. Herzberg G. "Molecular Spectra and Molecular Structure", Vol I, Spectra of Diatomic Molecules. Van Nostrand, Princeton, N J. 1950.

91. Nibler J.W. and Pimentel G.C. J. Mol. Spect., 26, 294, 1968.

92. Snelson A. High Temp. Sci., 4, 318, 1972.

93. Gundersen G. Acta Chem. Scand., A35, 729, 1981.

94. Fjeldberg T., Gundersen G., Jonvik T., Seip H.M. and Saebo S. Acta Chem. Scand., A34, 547, 1980.

95. Kawashima Y., Takeo H. and Matsumura C. J. Chem. Phys., 74, 5430, 1981.

96. Gundersen G., Jonvik T. and Seip R. Acta Chem. Scand., A35, 325, 1981.

97. Tossell J.A. Am. Mineral., 71, 1170, 1986.

98. Gropen O. and Johansen R. J. Mol. Struct., 25, 161, 1975.

99. Bowsher B.R., Dickinson S., Ogden J.S. and Young N.A. Thermochimica Acta, in press.

100. Kasai P.H., Whipple E.B. and Weltner W. J. Chem. Phys., 44, 2581, 1966.

101. Brisdon A.K. and Ogden J.S. J. Mol. Struct., 157, 141, 1987.

CHAPTER SEVEN

THE INTERACTION OF CAESIUM IODIDE AND BORON OXYGEN COMPOUNDS

1. Introduction

In a previous chapter some of the fission product chemistry of tellurium was considered. In this Chapter some aspects of the chemistry of the remaining two fission products that are thought to be of most importance in severe accident scenarios - namely caesium and iodine, will be considered.

The concern over iodine is because of its high volatility and radiobiological impact - eg the accumulation of ^{131}I in the thyroid. The core inventory of iodine has been calculated (under conditions of zero cooling time and 40 GWd tonne^{-1} burnup) to be 25.6 kg of which ^{131}I would constitute 0.67 kg ([1]). Caesium is a less specific but equally hazardous fission product. It should be noted that even a year after the Chernobyl accident (Soviet Union - April 1986) the levels of ^{137}Cs in sheep in N. Wales, and Cumbria were sufficiently above normal to prevent them being slaughtered for human consumption. The early reactor safety assessments were made using the assumption that the iodine release into the primary circuit would be in the form of elemental iodine ([2]). However, more recent experimental and thermodynamic data suggest that iodine will be predominantly released into the primary circuit as caesium iodide. Cubicciotti and Sanecki([3]) have identified caesium iodide crystals on the Zircaloy cladding of irradiated fuel rods. The observed deposition behaviour ([4]) of caesium and iodine along a thermal gradient during fission product release experiments at Oak Ridge National Laboratory was found to be consistent with the release of caesium iodide.

As a result of the caesium inventory in high burn up fuel being approximately twelve times that of the iodine it has usually been assumed that the iodine would form caesium iodide and the excess caesium (if not combined with other fission products in the form of Cs_2UO_4, Cs_2Te, or Cs_2MoO_4)

would form caesium hydroxide in the reducing steam conditions. The formation of these species has been strongly supported by a number of calculations based on the thermodynamic data of the major radionuclides assumed to be released under degraded core conditions[5, 6, 7].

Caesium iodide is soluble in water and is considerably less volatile than elemental iodine. Therefore significant attenuation of iodine within both the primary circuit and the containment building would be predicted under some accident conditions if the major form of released fission product iodine is caesium iodide rather than elemental iodine. Indeed it has been claimed[8, 9] that the lower than anticipated release of iodine to the environment during the accident at Three Mile Island 2 (Pennsylvania, USA) was because of these considerations. These attentuation effects are based on the assumption that the caesium iodide does not react with any other species within the degrading core or with structural and containment materials to release more volatile iodine species.

One possible reaction is with the boric acid in the primary coolant and emergency core cooling systems (ECCS) of a PWR. The boron-10 in the boric acid has a high neutron absorption coefficient (769 barns)* and is therefore used as the control mechanism in the primary coolant and as a means of stopping the nuclear chain reaction if the ECCS is used. Some reactor systems also use boron carbide control rods and borosilicate glass as a burnable poison. The boric acid inventory is usually about 0.7 tonne in the primary coolant circuit and up to 39 tonnes is potentially available for delivery to the core via the ECCS as emergency cooling ([10]). Elrick and Sallach ([11]) have found that when caesium iodide reacts with boron carbide in the

---

*(1 barn = 10^{-24} cm^2)

presence of steam at 1000°C there is a probable reaction between the caesium iodide and the resultant boron oxide. No iodine was found in the boron oxide, but in parts of the apparatus the iodine concentration was found to be ten times that of the caesium, indicating iodine transport by something other than caesium iodide. They therefore concluded that a reaction had occurred, which had produced a stable caesium-boron compound and released iodine, probably as hydrogen iodide. Several studies have been carried out on the reaction between alkali metal chlorides and boric acid ([12-18]) and one on sodium iodide and boric acid([19]). The majority of these were concerned with how the solubility of the halide was affected by the boric acid. Two of the studies ([12],[13]) report that hydrogen chloride is given off from the mixture of the chloride and boric acid at 100-200°C and that a pentaborate is formed. If the reaction is carried out in a stream of steam then the reaction is accelerated.

Preliminary investigations by Ogden and Gomme ([20]) have shown by using matrix isolation infrared spectroscopy that heated mixtures of caesium iodide and boron oxide yield vapour phase caesium metaborate ($CsBO_2$) at 900°C, although the fate of the iodine was not established.

It was at this stage that the work on the complex system described in this chapter was started. Parallel and subsequent transpiration studies by colleagues at Southampton([21]) and AEE Winfrith([22]) were also undertaken, and where pertinent these results will be discussed.

2. Identification of Reaction Products

Iodine can either be evolved as molecular iodine, or as hydrogen iodide. The former cannot be detected by ir, but can be studied mass spectrometrically. Hydrogen iodide however can be detected both by ir and mass spectrometry.

Therefore it was planned to determine the fate of the iodine using the powerful combination of mass spectrometry and matrix isolation infrared spectroscopy.

The majority of the components in this system are (now) fairly well characterised by ir and mass spectrometry. Boron oxide (B_2O_3) has been studied by ir spectroscopy in the condensed phase(23,24), in the gas phase as an ir emission spectrum(25,26), in matrices by ir (27,28) and Raman(29). It has also been studied mass spectrometrically(30,31) and by electron diffraction(32). Orthoboric acid ($B(OH)_3$) has been studied extensively by ir in the condensed phase(23,24,33). Previous to the work described in this thesis there was no mass spectrometric data in the literature, other than the interaction of water and B_2O_3 (31) at high temperatures (1100°C) where the main product was HBO_2 with only very small quantities of H_3BO_3 and $(HBO_2)_3$.

The only reference to a matrix study was very obscure and unobtainable(34), prior to the work in the previous chapter(35). The other reportedly volatile boric acid, namely metaboric acid, has been studied by ir in the condensed phase(23,24), in the gas phase by ir emission(36) and by matrix isolation ir.(34,37). The ir spectroscopic studies of the condensed phases of the other solid phase boric acids are too numerous to cite and one should see Ref 38 for a pertinent review. The alkali metal metaborates have been extensively studied by ir in the gas phase(39), in argon matrices(40) and in the condensed phase(41). They have also been studied by mass spectrometry(42).

Although molecular caesium iodide is ir active the stretching fundamental is at too low a frequency (109.3 cm^{-1})(43) to be detected by the instruments available and far infrared techniques are required. It has however been studied mass spectrometrically(44). The literature on gas phase ir studies of HI gas is extensive and here is not the place to cite them. It is also a molecule of interest to the matrix isolationist and this is reflected in the large number of reports in the literature dealing with isolated hydrogen iodide(45-62). As a result of the comments in these papers about the difficulty of isolating hydrogen iodide in argon or other noble gases, nitrogen was used almost extensively.

The work in this chapter falls into four sections. The first deals with a number of preliminary, background and supporting experiments on the individual components and anticipated reaction products of the B_2O_3/CsI mixture. The second section is concerned with experiments in which the CsI/B_2O_3 mixtures were heated to temperatures greater than 600°C. The majority of the work carried out is described in the third and fourth sections. In the former the samples are heated to temperatures of less than 600°C whilst in the final section the same conditions were used in a semi-quantitative manner in order to estimate the extent of release of the volatile iodine component.

3. Preliminary Experiments

3.1 Iodine

The purpose of this experiment was to determine the optimum instrument settings for the mass spectrometric detection of molecular iodine. Iodine flakes (BDH) were degassed at -196°C and then sublimed into the spectrometer chamber through a needle valve. Fig 1 shows how the peak intensity is dependant on the ion energy and that the optimum value is 5V. Once this had been set, the electron energy was varied and the resultant ionisation efficiency curves are shown in Fig 2. The presence of peaks at 254 amu and 127 amu can be understood in terms of a parent I_2^+ ion and a

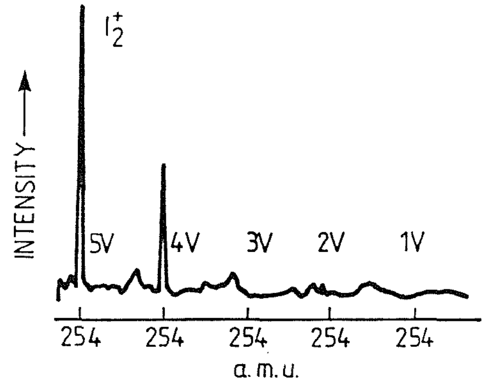

FIG. 1 EFFECT OF ION ENERGY ON INTENSITY OF I_2^+

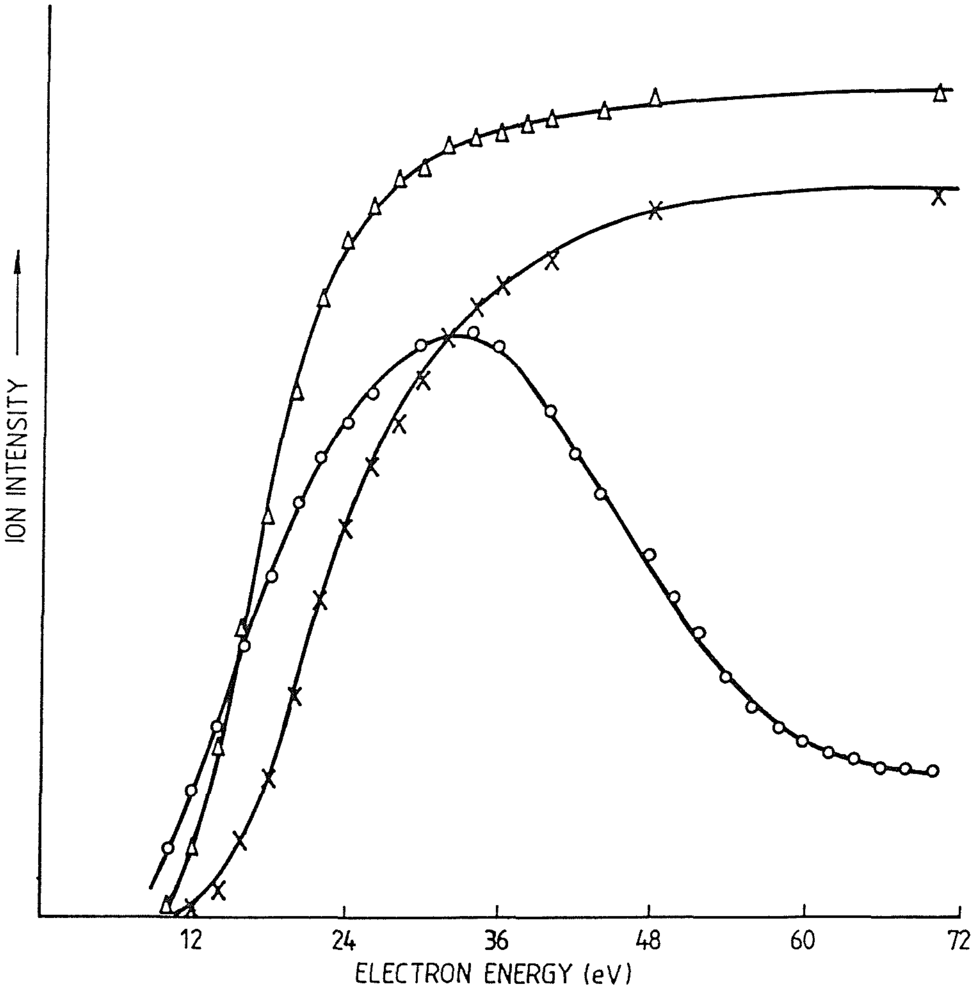

FIG. 2 IONISATION EFFICIENCY CURVES OF I_2^+(○), I^+(x) AND HI^+(Δ) FROM MOLECULAR IODINE

daughter I^+ ion. The origin of the peak at 128 amu, assigned to the HI^+ ion, is less clear but is thought to arise from ion-molecule or ion-ion reactions between the iodine and the many protic sources (water, hydrocarbon greases etc) in the chamber, rather than as a genuine component of vaporising molecular iodine.

The ionisation efficiency curves (Fig 2) indicate that the behaviour of I_2^+ is unusual in that the intensity reaches a threshold and then decays away compared to the more normal behaviour of the I^+ and HI^+ ion intensities which tend towards an asymptotic limit. This behaviour can be understood to arise from the fact that as the electron energy is increased then both the number of molecules ionised and the number of molecules/ions fragmented increases. This is more likely for iodine than hydrogen iodide because of the relatively low bond energy of 152.5 kJ/mol(63) for iodine compared to 298.7 kJ/mol(63) for hydrogen iodide.

The fact that there is substantial decomposition of the molecular iodine means that there will be considerable quantities of iodine atoms or ions to pick up any protons and hence give rise to the peak at 128 amu. From Fig 2 it can be seen that the optimum value of the electron energy to maximise the intensity of the I_2^+ peak at 254 amu is 32 eV. This value was used throughout unless stated to the contrary.

3.2 Caesium Iodide

Supporting experiments were carried out in the mass spectrometer to determine whether molecular iodine is produced on heating caesium iodide. Emons et al(44) have reported the presence of vapour phase iodine above heated sodium iodide but not above caesium iodide.

Caesium iodide (Aldrich) was vaporised by conventional induction heating and the spectra are shown in Figs 3 and 4. Fig 3 shows the effect of increasing sample temperature upon the spectrum. At first sight it appears that both CsI^+ at 260 amu and I_2^+ at 254 amu are genuine peaks, but as the temperature is increased the 254 amu peak reamins constant whilst the 260 amu peak increases rapidly, thus indicating that the CsI^+ is arising from the heated sample whereas the I_2^+ is from the background.

Figs 4(a) and 4(b) show the full spectrum from 2 amu to 270 amu. Fig 4(a) is the background spectrum in the spectrometer showing the extensive hydrocarbon patterns which although they appear to clutter up the low mass end can prove useful calibrants. Fig 4(b) is the spectrum observed when the shutter between sample and spectrometer is open and reveals that in addition to the peak at 260 amu (CsI^+) other peaks due to Cs^+ (133), I^+ (127) and HI^+ (128) are also observed. The Cs^+ and I^+ are daughters from the CsI^+ and the HI^+ is again probably due to collisions or reactions in the chamber.

Therefore the vapour above heated caesium does contain caesium iodide, but not molecular iodine and the reaction

$$2CsI \rightarrow 2Cs + I_2$$

does not occur to any detectable extent under the conditions studied. The actual vapour composition above heated CsI in these experiments with respect to the number of polymers of CsI has not been determined because the mass range is limited to 400 amu.

In order to confirm that the hydrogen iodide detected was not a product of the reaction between caesium iodide and water thus:

$$CsI + H_2O \rightarrow CsOH + HI$$

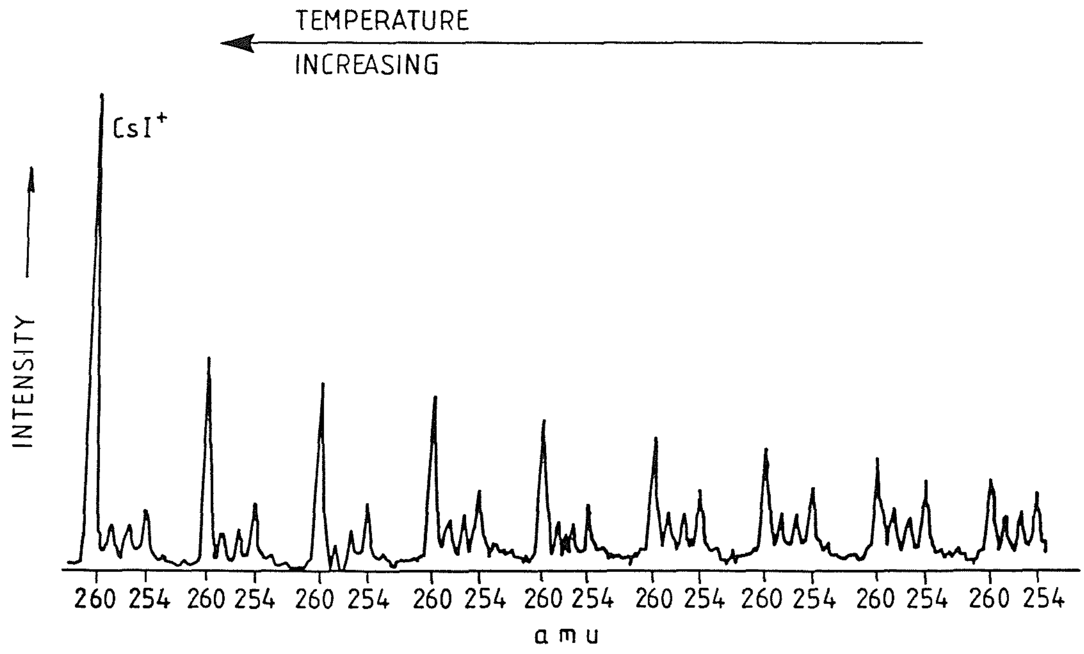

FIG. 3. MULTIPLE SCAN MASS SPECTRA OF CAESIUM IODIDE (252-262 a m u)

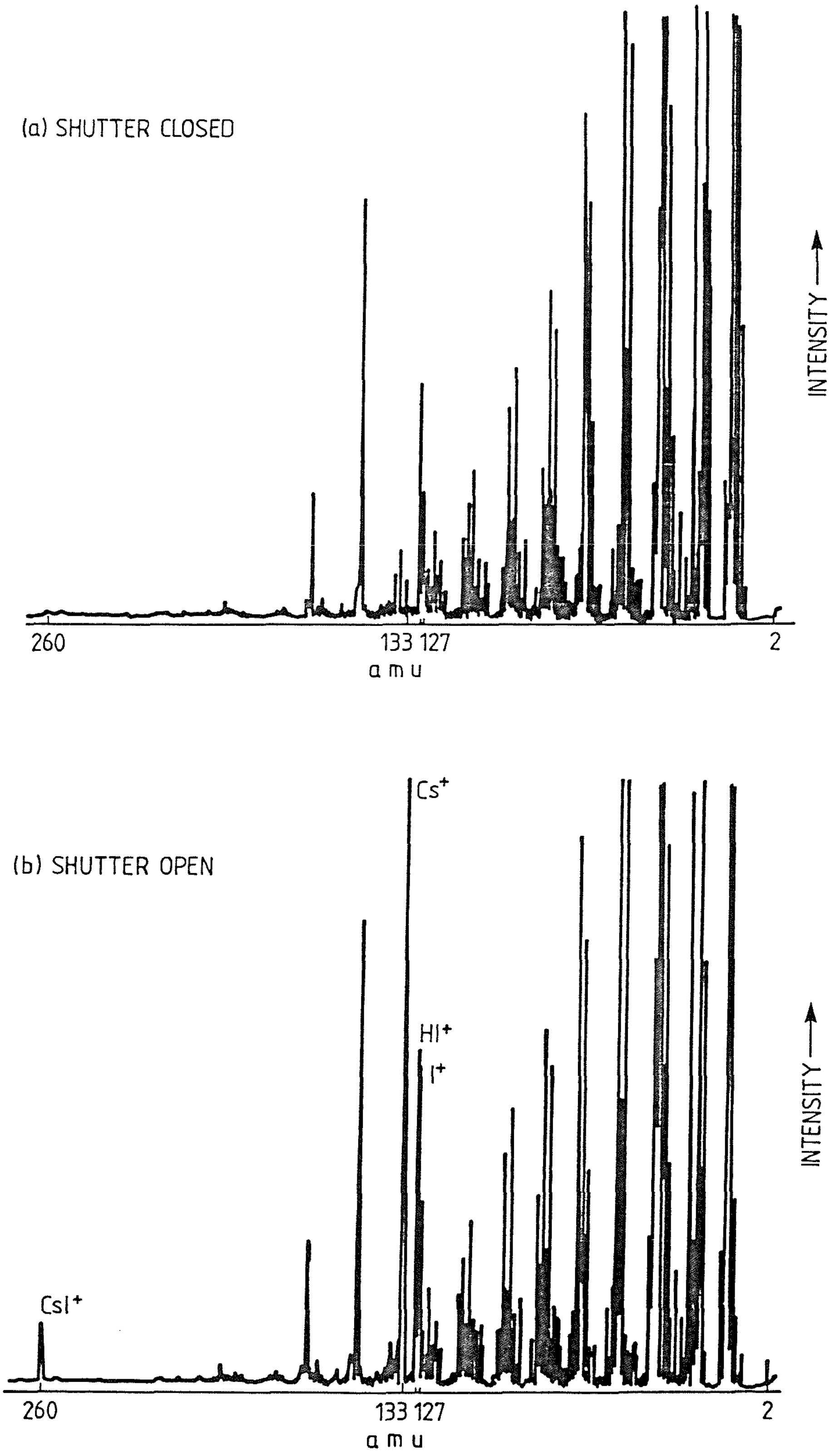

FIG. 4 MASS SPECTRA OF CAESIUM IODIDE 2-270 a m u

a series of matrix ir experiments were carried out in which water vapour was passed over heated CsI. The spectra observed, revealed no bands due to either HI(45-62) or CsOH(64) and therefore one can conclude that the hydrogen iodide is not a product of the CsI and H_2O reaction.

3.3 Heavy Water

It is important to know the source of any hydrogen or deuterium observed in the mass spectra of the CsI/B_2O_3 system. Therefore to investigate whether H_2^+ is a daughter of H_2O, heavy water (D_2O) was studied because of the extensive proton containing background spectrum.

The deuterated water (Aldrich Gold label) was leaked into the spectrometer through a needle valve up to a maximum pressure of 7.6×10^{-6} torr. The observed spectra are shown in Fig 5 and from these it can be seen that in the region 16 to 21 amu there are peaks at 20 (D_2O^+), 19(HOD^+) 18,(DO^+ or H_2O^+) and 17 (OH^+) amu, whilst in the region 1 to 5 amu there are peaks at 4($D_2{}^+$), 3 (HD^+), 2 (D^+ or $H_2{}^+$) and 1 (H^+) amu. The peaks due to normal water are always present but due to the presence of peaks at 4 and 3 amu it is possible to conclude that water does give rise to $H_2{}^+$ and H^+ in the mass spectrometer.

3.4 Hydrogen Iodide

These experiments were used in order to confirm that hydrogen iodide could be detected in our experimental set up and that its fundamental frequency was at that stated in the literature.

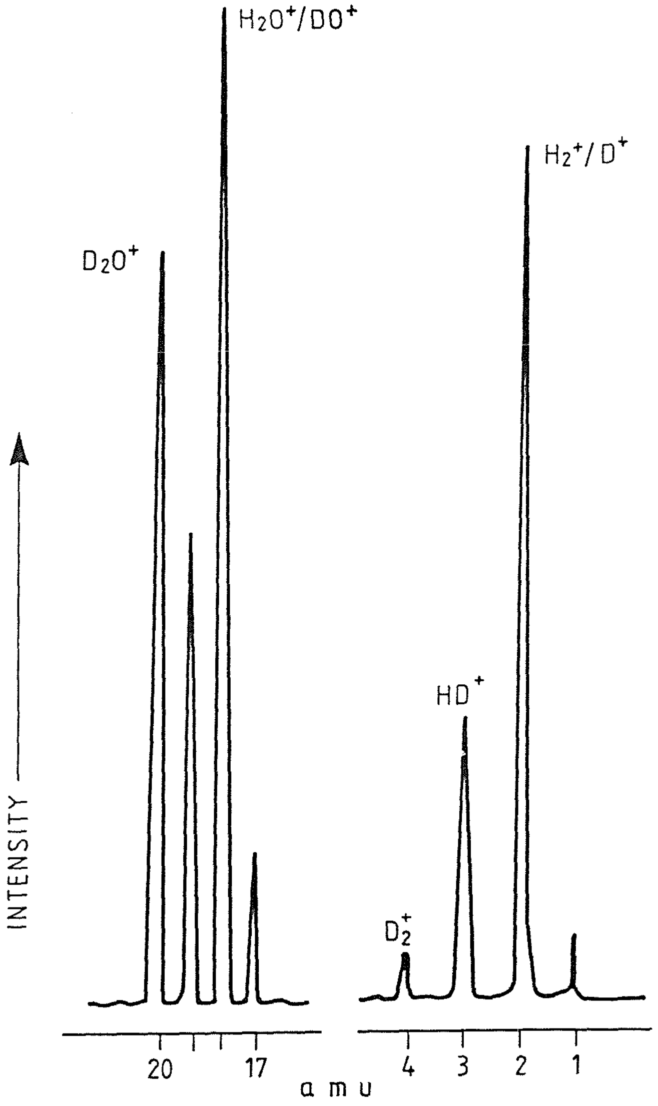

FIG. 5 MASS SPECTRUM OF HEAVY WATER SAMPLE

Anhydrous hydrogen iodide was prepared using Hoffman's method(65) rather than the more conventional use of water, iodine and red phosphorus(66). In Hoffman's method 1,2,3,4 tetrahydronapthalene (tetralin) is dehydrogenated to napthalene by iodine. The resultant iodine species is anhydrous hydrogen iodide.

ie

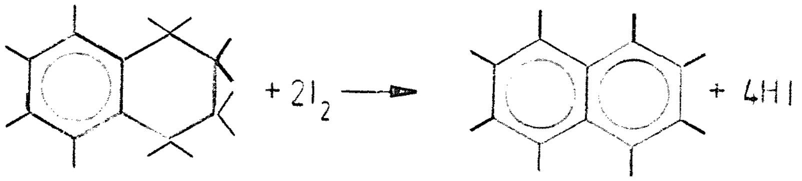

Iodine dissolved in tetralin was added to refluxing tetralin under a nitrogen atmosphere. The anhydrous hydrogen iodide was then carried out of the reaction flask by a nitrogen flow through a series of traps. In the first trap held at -23°C (by a carbon tetrachloride slush bath) the nitrogen/hydrogen iodide gas mixture was passed over silica gel in order to remove any residual water present. (It is reported(67) that silica gel and HI do not react). The HI was then condensed from the gas mixture into the second trap held at -196°C and the nitrogen passed through a mercury bubbler into a fume hood. Once the reaction had finished the nitrogen flow was stopped and the white solid HI was pumped on under vacuum at -196°C.

In order to investigate the effect of changing the concentration of HI in the matrix, various gas mixtures with $HI:N_2$ ratios in the range 1:50 to 1:500 were made up using standard manometric procedures. Darkened apparatus was used to try to limit the extent of decomposition. These gas mixtures were pulsed(68) onto the central CsI window via a Teflon tap, in small amounts in order to encourage monomeric isolation. The ir spectra in the region 2300-2000 cm^{-1} of these mixtures are shown in Fig 6. From these spectra the sharp band at 2237 cm^{-1} can be

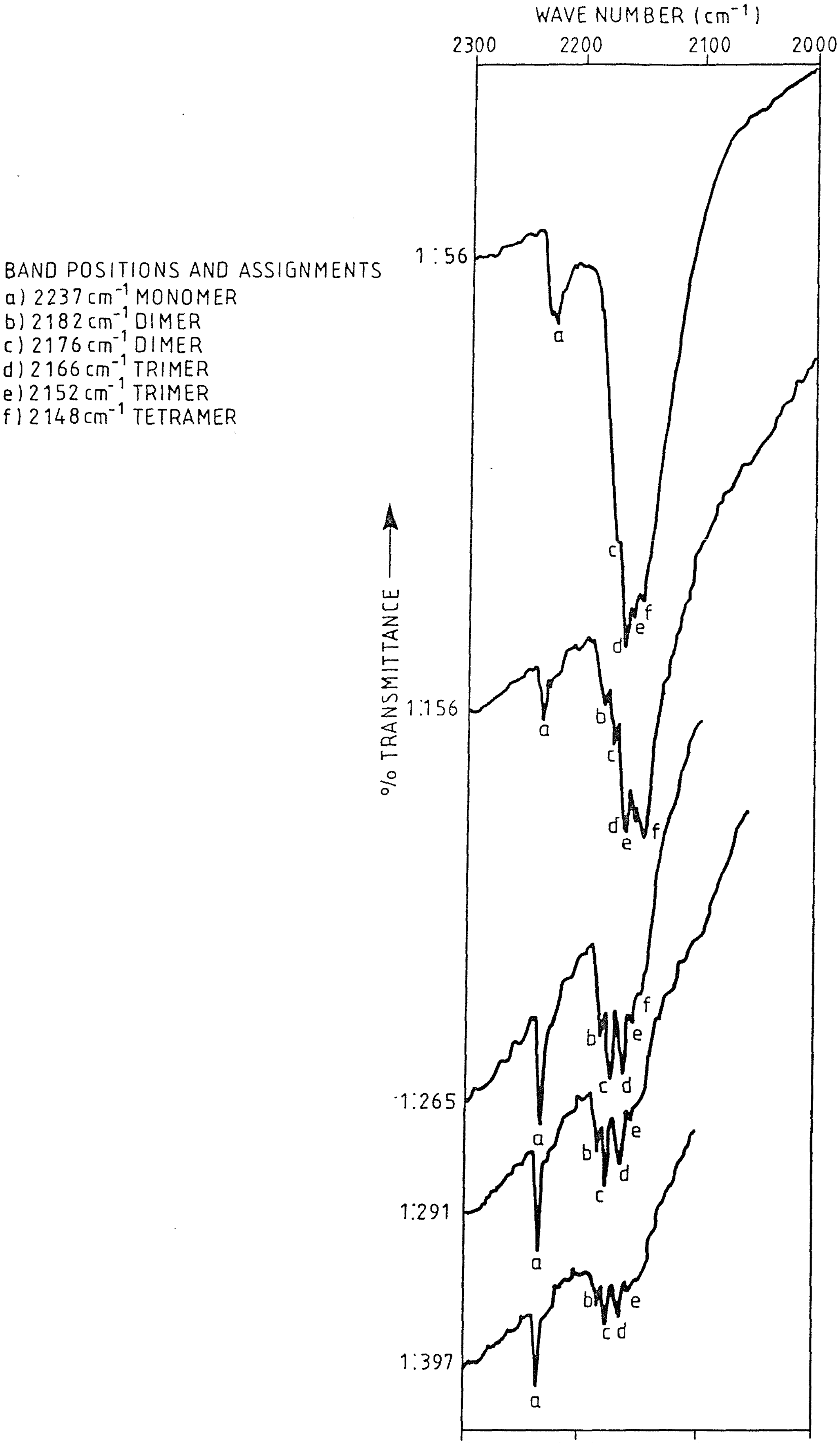

FIG.6 NITROGEN MATRIX INFRARED SPECTRA OBSERVED FOR THE HI/N_2 SYSTEM AT DIFFERENT RATIOS

assigned to monomeric matrix isolated hydrogen iodide because its intensity relative to the other bands increases with dilution. This value compares well with that of Barnes et al(55) (2237 cm^{-1}) and Schriver et al(60) (2237.1cm^{-1}). It should be noted that this value is higher than the gas phase value (2230.1 cm^{-1}) and hence hydrogen iodide is one of the few molecules that has a stretching mode with a blue matrix shift. The remaining bands are due to hydrogen iodide polymers in various conformations. The spectra in Fig 6 are not of high enough resolution to enable the bands to be assigned with any accuracy. However, recent work by Schriver et al(60) on the polymers of hydrogen iodide in nitrogen matrices can be used to assign the bands. The frequencies and assignments are given in Table 1. Barnes et al(55) did not carry out any detailed investigation of the polymers in nitrogen, but did so in argon matrices and these are also listed in Table 1 for comparison. A more recent study by Engdahl and Nelander(61) who have observed both the R_0 and P_1 rotation vibration bands is also given.

The labels (α) and (β) for the dimer and trimer in nitrogen matrices refer to two distinct forms of each. The trimer form (α) is found from isotopic substitution and a force constant analysis to be symmetric whereas the (β) form is found to be asymmetric. The (α) form is the more stable at low temperature (9-10K). The two forms of the dimer (α) and (β) are also temperature dependent. At low temperature (9-10K) the (α) form (2224.7 and 2182.8 cm^{-1}) predominates whilst at temperatures above 14K the (β) form (2231.9 and 2176.1 cm^{-1}) is the major dimeric species. The band at 2229.7 cm^{-1} is thought to arise from a slight modification of the (β) form.

From these considerations and the data in Table 1 the assignments in Table 2 can be arrived at.

TABLE 1

Vibrational Frequencies and Assignments of hydrogen iodide and its polymers isolated in N_2 and Ar matrices

N_2(60)		Ar(55)		Ar(61)	
Freq./cm^{-1}	Assg.	Freq./cm^{-1}	Assg.	Freq./cm^{-1}	Assg.
2237.1	monomer	2255	monomer	2253.4	R_0 monomer
		2246		2244.7	
2231.9 (β)		2178	dimer	2237.1	P_1 monomer
2229.7	dimer	2166		2226.4	
2224.7 (α)					
2186.0	trimer	2155	cyclic trimer	2186.8	
				2204.1	dimer
2182.8 (α)	dimer	2157	open chain	2232.9	
2176.1 (β)		2151	trimer		
		2141		2154.7	trimer
2168.6 (α)			cyclic	2156.6	HI-H_2O adduct
2166.0 (α)	symmetrical	2144	tetramer		
2164.0 (α)	trimer			2157.7	$(HI)_2$-H_2O
				2144.1	adduct
2157.0 (β)	asymmetrical	2151	open chain		
2150.4 (β)	trimer	2141	tetramer		
		2135			
2146.3	tetramer				
				2164.5	HI-I_2 adduct
				2232.9	

TABLE 2

Observed Frequencies and Assignments of hydrogen iodide isolated in nitrogen matrices in this work

Frequency/ cm^{-1}	Assignment
2237	monomer
*	
2182	dimer (α)
2176	dimer (β)
2166	trimer (α)
2152	trimer (β)
2148	tetramer

* The other dimer components at 2225-2232 cm^{-1} are apparent in the spectra but not well enough resolved for a frequency value to be given.

3.5 Ortho and Metaboric Acid

The vibrational frequencies of the naturally abundant orthoboric acid were obtained in the previous chapter and are listed below in Table 3 with their assignments without further comment.

Although metaboric acid (HBO_2) in nitrogen matrices has not yet been studied in detail, Linevsky(37) has carried out a matrix study in argon. Some of his frequencies should be used with care, especially the O-H stretching modes(70). His frequencies and assignments are also given in Table 3.

4. Caesium Iodide/Boron Oxide Mixtures Heated to Temperatures Greater than 600°C

4.1 Introduction

In the earlier work by Gomme(20) et al, the samples of CsI/B_2O_3 were heated inductively to approximately 900°C. The matrix ir spectra revealed that $CsBO_2$ was a volatile product of the reaction between caesium iodide and boron oxide, no iodine species however were detected. These experiments were repeated at lower temperatures (600-700°C) using both matrix ir and mass spectrometry to determine the fate of the iodine.

4.2 Experimental

Caesium iodide (Aldrich) and B_2O_3 (BDH) were mixed in approximately equimolar proportions. These were then loaded into a platinum boat and vaporised using the conventional apparatus for inductive heating. (See Fig 9(a)). No special measures were taken to dry the B_2O_3 extensively prior to use.

TABLE 3

Frequencies observed for boric acid isolated in N_2 matrices and for HBO_2 in Ar matrices

$B(OH)_3/N_2$(35)		HBO_2/Ar(37)	
Freq./cm^{-1}	Assignment	Freq./cm^{-1}	Assignment
3668.5	E' O-H stretch	3191	A' ^{10}B O-H str
		3185	A' ^{11}B O-H str
1478.0	E' ^{10}B-O stretch		
1426.2	E' ^{11}B-O stretch	2106	A' ^{10}O str
		2033	A' ^{11}O str
1009.9	E' B-O-H bend		
		1471	A' ^{10}B=O str
701.0	A" $^{10}BO_3$ out of plane	1454	A' ^{11}B=O str
674.0	A" $^{11}BO_3$ bend		
		928	A' ^{10}B-O-H bend
513.8	A" O-H out of plane torsion	927	A' ^{11}B-O-H bend
		531	A" ^{10}B out of plane bend
480.5	E' ^{10}B BO_2 bend	512	A" ^{11}B
448.9	E' ^{11}B BO_2 bend		
		475	A' O-^{10}B=O bend
		464	A' O-^{11}B=O bend

4.3 Matrix IR Studies

In the nitrogen matrix ir spectra no features assignable to $CsBO_2$ were observed, this however is expected as it is not volatile at the temperatures used. Two new bands in the region 2300-2000 cm^{-1} were observed and these are shown in Fig 7. The sharp band at 2237 cm^{-1} is assigned to matrix isolated hydrogen iodide by comparison with the pure HI spectra. The weaker band at 2283cm^{-1} remains unassigned but is believed to be a contaminant because of its variable intensity and observation in a number of different systems.

In addition to these two bands a number of others were observed, the majority of which could be assigned to boric acid by reference to the preceeding chapter. Indeed when deuteration was attempted the distinctive torsion mode pattern between 600 and 300 cm^{-1} was observed.

Unfortunately the band assigned to HI was not observed in every experiment and as a result the remaining bands were not studied extensively.

A listing of the frequencies is not given because of the problem of non-reproducibility, in as much that the boric acid bands were not always observed in the same spectra as the HI bands.

4.4 Mass Spectrometric Studies

The mass spectra of the inductively heated samples of caesium iodide and boron oxide were observed to have peaks at 127, 128, 133, 254 and 260 amu, in addition to those arising from the background. These can be assigned to I^+, HI^+, Cs^+, I_2^+ and CsI^+ respectively. Fig 8 shows the effect of increasing temperature in the region 250 to 264 amu.

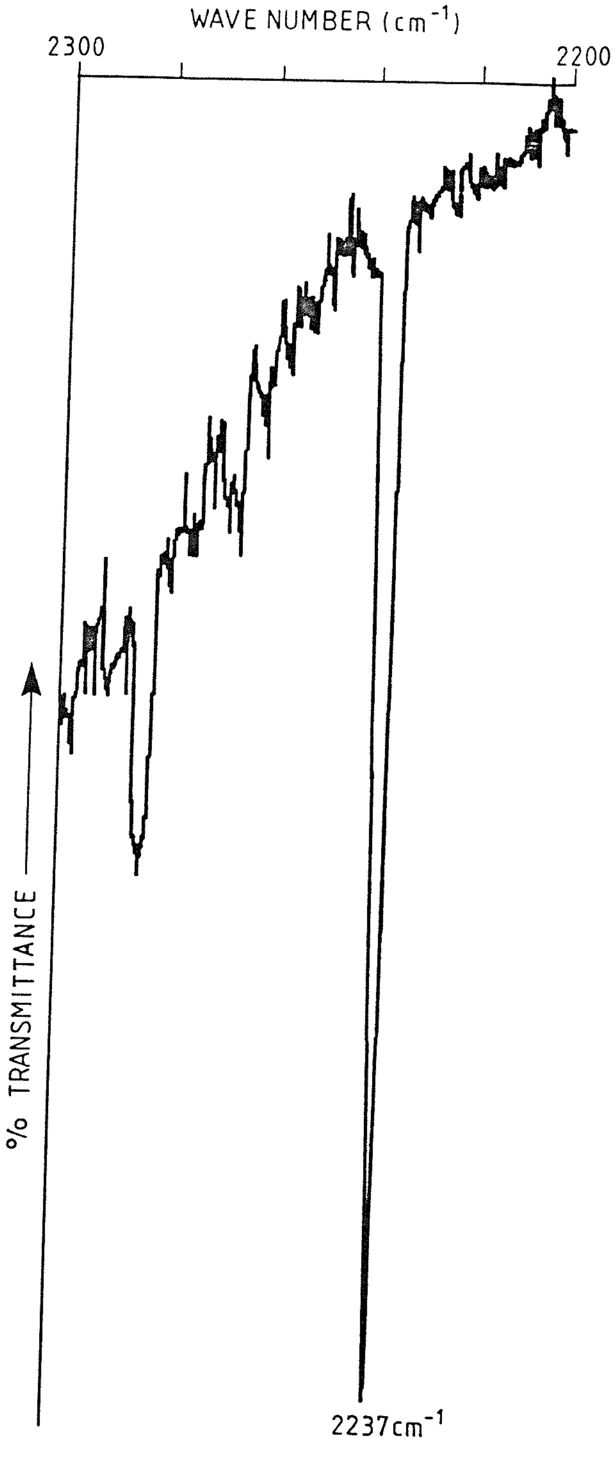

FIG.7 NITROGEN MATRIX INFRARED SPECTRUM OBSERVED FOR THE CsI/B_2O_3 SYSTEM AT TEMPERATURES GREATER THAN 600°C

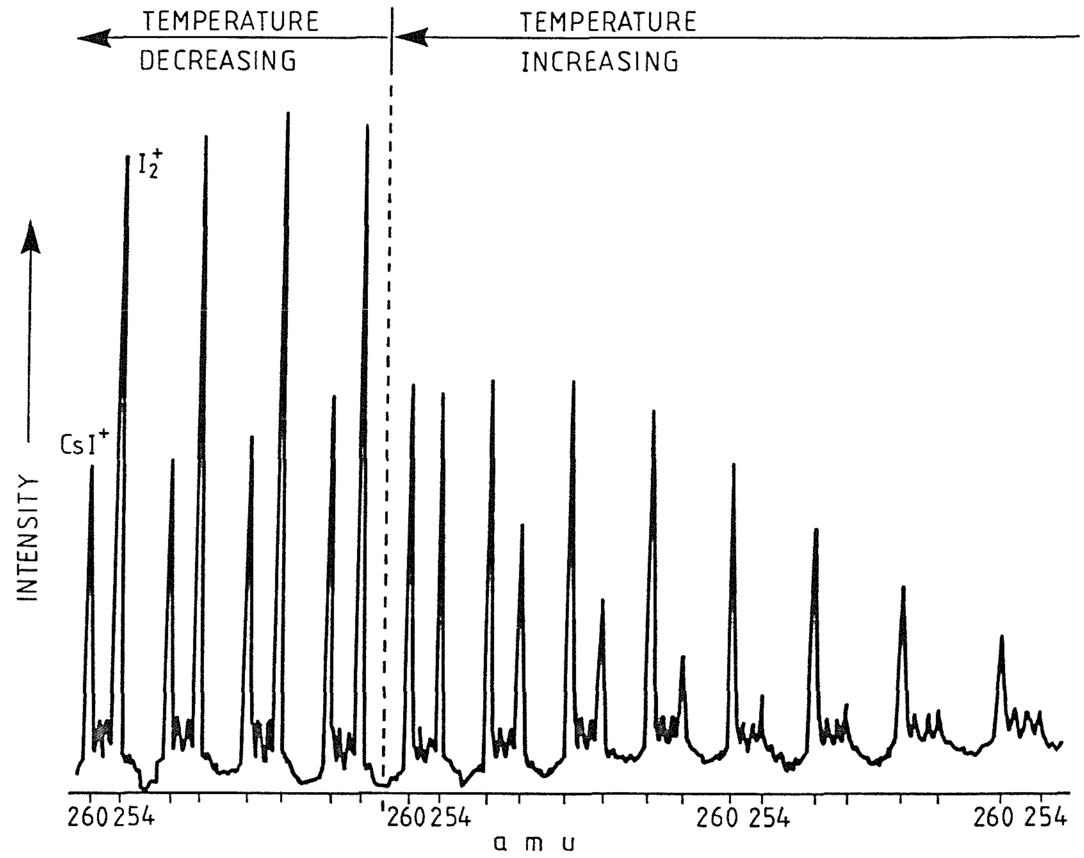

FIG. 8 MULTIPLE SCAN MASS SPECTRA OBSERVED FOR THE CsI/B_2O_3 SYSTEM BETWEEN 250 AND 264 a m u

From this one can see that the production of I_2^+ is only observed once the vaporisation of CsI has become significant. This then leads to the conclusion that the reaction to produce I_2 only occurs once CsI is in the vapour phase. (Later it will be shown that the iodine is not itself a genuine reaction product, but a result of the thermal decomposition of hydrogen iodide).

The peaks due to Cs^+ and I^+ at 133 and 127 amu are the daughter ion peaks of CsI^+ at 260 amu, whilst the peak at 128 amu assigned to HI^+, may either be a parent ion or the result of an ion molecule collision.

4.5 Summary

The lack of hydrogen iodide in Gomme's(20) spectra and the non-reproducibility of it in these experiments was a cause for some concern. It is thought that this was due to the combined problems of degassing of the sample and the sample being in a high vacuum environment for a considerable time prior to heating. Degassing is usually considered to be a necessary part of the experimental procedure of matrix isolation ir in order to avoid the build up of water and/or carbon dioxide in the matrix. The sample is therefore heated to the temperature at which it just sublimes before the cryostat is turned on. In a multi-component system, judging this temperature is difficult and one usually heats the sample to several hundred degrees centigrade to drive off any water. If a reaction occurs during this procedure and if the products are volatile they will be pumped away and not detected. A similar situation also occurs when the sample is exposed to high vacuum if the reaction proceeds at room temperature.

As a result of these considerations it was decided to use a sample vaporisation method that enabled the vacuum chamber to be pumped out, but which also maintained the integrity of the sample. This was done by heating the sample in a silica ampoule sealed off from the vacuum by a Young's Tap. The heating was achieved using an external nichrome wire resistive furnace (see Fig 9(b). For some of the later experiments a trap was inserted and this is shown in Fig 9(c).

5. Caesium Iodide/Boron Oxide or Boric Acid Mixtures Heated to Temperatures Less Than 600°C

5.1 Introduction

From the higher temperature studies it has been seen that volatile iodine products are indeed released upon heating mixtures of caesium iodide and boron oxide. However it has not been possible to say with any great certainty whether this volatile iodine is in the form of molecular iodine or hydrogen iodide. These studies using a different form of apparatus were therefore carried out in order to try and resolve this uncertainty.

5.2 Experimental

Freshly prepared equimolar samples of caesium iodide (Aldrich) and either boric acid (Aldrich Gold Label) or boron oxide (BDH) were heated resistively in silica or pyrex holders (see Fig 9(b)). In order to obtain reproducible spectra, the samples were only degassed for a short time until the air was removed, and then kept either at -196°C or isolated from the system until the vacuum was good enough to allow the experiments to continue. As a result of this procedure the infrared specta showed very prominent broad bands due to ice at 1700 - 1500 cm^{-1} and 900-700 cm^{-1}, thus possibly obscuring features due to reaction products. The effect on the mass spectra was to reduce the sensitivity but not too drastically.

a. ALUMINA TUBE
b. CEMENT
c. ALUMINA ROD
d. TANTALUM SUSCEPTOR
e. VACUUM JACKET
f. INDUCTION COIL
g. YOUNG'S GREASELESS CONE
h. YOUNG'S TAP
i. PYREX OR SILICA HOLDER
j NICHROME WIRE FURNACE
k. THERMOCOUPLE
l. TRAP

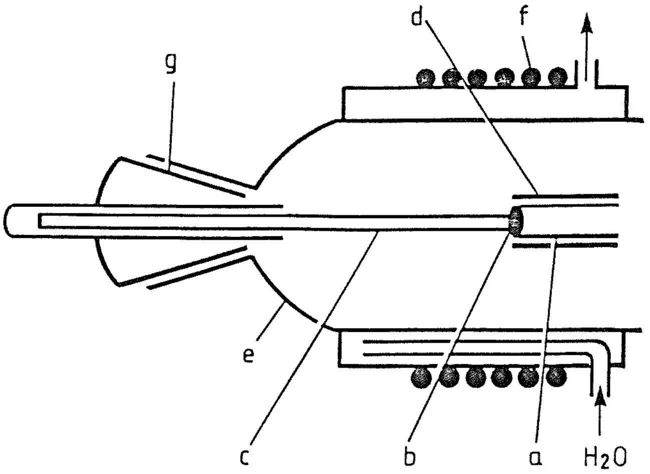

a) INDUCTION HEATING

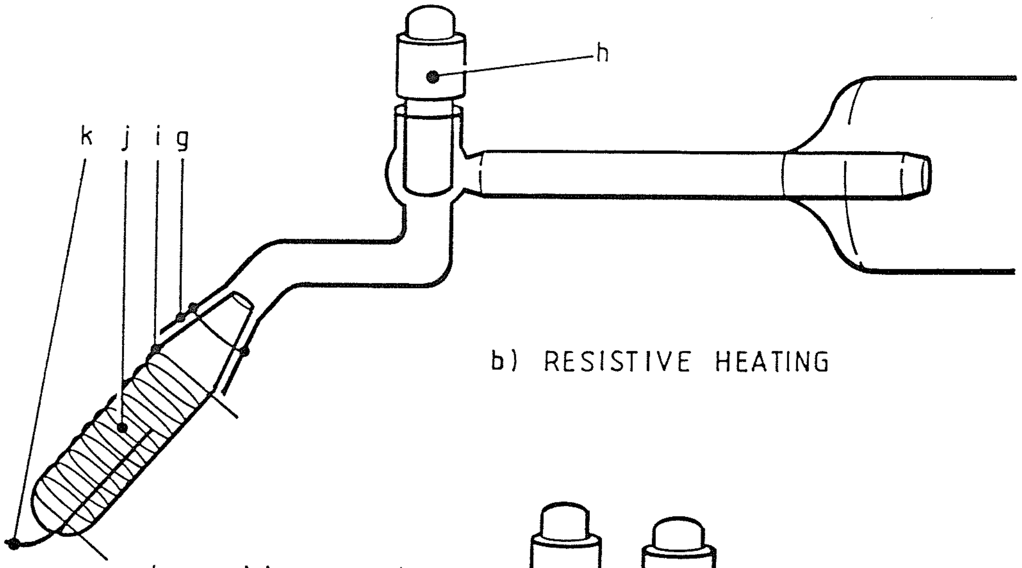

b) RESISTIVE HEATING

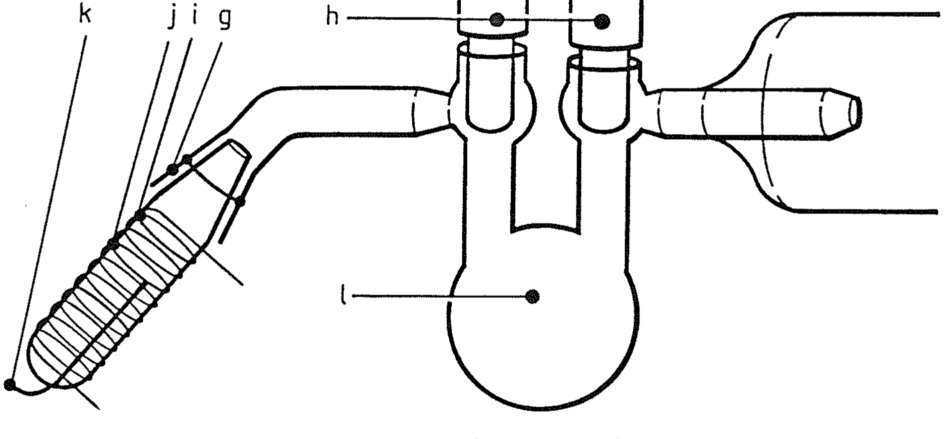

c) RESISTIVE HEATING WITH TRAP

FIG. 9 SAMPLE HOLDERS AND VAPORISATION APPARATUS

To try to overcome these problems a trap was inserted between the sample and spectrometer (see Fig 9(c)) in the hope that by judicious use of solvent slush baths the temperature could be controlled so that the vapour pressure of water was reduced, whilst that of hydrogen iodide remained high. The trap was also used in the infra red studies to try to pulse the products onto the window(68).

Neither of these approaches were successful because hydrogen iodide and water form a constant boiling point mixture (126°C at RTP)(69) and will therefore condense and vaporise together. The pulsing experiments suffered from the well reported(55) difficulty of isolating hydrogen iodide monomerically. The use of the trap did however yield some very pertinent results in the mass spectrometric studies.

Deuteration experiments were only carried out in the case of the mass spectrometry studies because in the infrared the problems of ice and deuterated ice are intolerable. The deuterated ice band obscures the hydrogen iodide peak at 2237 cm^{-1} whilst the normal ice band obscures the deuterium iodide peak at 1604 cm^{-1}(60).

5.3 Matrix Isolation Infrared Spectroscopic Studies

The spectra obtained from the resistively heated samples were much more reproducible than those using induction heating in as much that hydrogen iodide was observed in every experiment.

In the region 2300-2000 cm^{-1} bands from monomeric, and polymeric hydrogen iodide were observed from heated mixtures of caesium iodide and boron oxide in nitrogen and argon matrices and caesium iodide and boric acid in nitrogen matrices. In all of these cases a very small broad band centred at approximately 2200 cm^{-1} was observed at 100° to 150°C, this then did not grow any further. Monomeric hydrogen iodide was not detected until a white sublimate was observed just downstream from the furnace at temperatures of 450 - 500°C. An increase in the temperature caused a cessation of hydrogen iodide production because the components had separated and further reaction could therefore not take place. This sublimate is probably caesium iodide as Emons et al(44) report that caesium iodide vaporised at temperatures as low as 400°C in their mass spectrometric experiments. Analytical tests were attempted for iodide but were inconclusive due to the problem of separating the sublimate from the other components. The remainder of the sample had formed a glassy off-white/brown coloured solid indicating that the B-O-H compounds had melted during the experiments.

The spectra of the volatile products from a heated CsI-B_2O_3 mixture isolated in a nitrogen matrix are shown in Figs 10 and 11. The low resolution spectrum in Figure 10(a) has prominent features due to CO_2 at 2348 cm^{-1} and hydrogen iodide. Figure 10(b) shows a high resolution spectrum of the region 2300-2000 cm^{-1} where the hydrogen iodide absorptions are shown more clearly.

The absorptions at 2236.6, 2176.5 and 2166.5 cm^{-1} correspond closely to those observed earlier for pure HI and those in the literature for monomeric, dimeric and trimeric hydrogen iodide isolated in nitrogen matrices. The other two bands at 2122 and 2097 cm^{-1} were not observed in the pure HI spectrum. As a result of the thermal decomposition and drying of the boron oxide there will be a large amount of water in the matrix and it is therefore believed that these bands are due to HI-H_2O adducts. A subsequent study by Schriver et al(62) on hydrogen bonded HI complexes reports the vibrational frequencies of the HI-H_2O adducts at 2122 and 2096 cm^{-1} thus confirming this assignment.

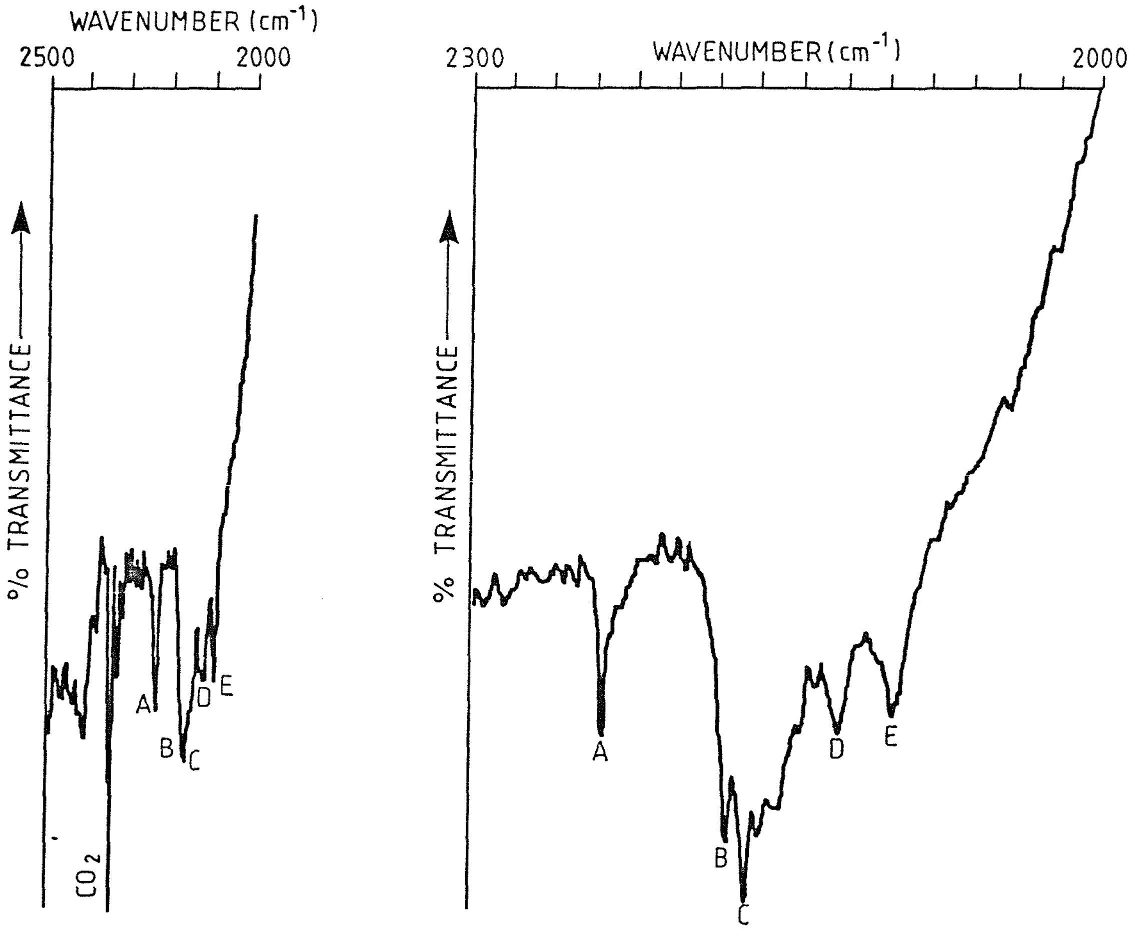

a) LOW RESOLUTION b) HIGH RESOLUTION

BAND POSITIONS AND ASSIGNMENTS

A	2236·6 cm^{-1}	MONOMERIC HI
B	2176·5 cm^{-1}	DIMERIC HI
C	2166·5 cm^{-1}	DIMERIC HI
D	2122 cm^{-1}	HI-H_2O ADDUCT
E	2097 cm^{-1}	HI-H_2O ADDUCT

FIG. 10 NITROGEN MATRIX INFRARED SPECTRUM OBSERVED CsI/B_2O_3 SYSTEM AT 400 - 500°C

The spectral region from 1500 to 400 cm^{-1} is shown in Figure 11(a), the most prominent feature is the broad ice band from 900 to 400 cm^{-1} which may obscure some features. Figure 11(b) is a higher resolution spectrum of the 1490 to 1380 cm^{-1} region. With the exception of the 1405.6 cm^{-1} band the remaining sharp bands at 1477.8, 1425.7, 1009, 701, 675 and 514 cm^{-1} can all be assigned to matrix isolated monomeric boric acid(35). Table 4 contains the observed frequencies and assignments.

In the subsequent experiments the apparatus with the trap between sample and spectrometer was used, and even when the trap was at room temperature there was no detectable signs of boric acid in the spectra, because it had condensed out on the cold glass surfaces. (In the previous chapter, spectra of boric acid recorded at room temperature are reported, but only after 4-5 hrs deposition time, the typical spray on time in these experiments was 30 minutes.)

When argon was used as the matrix gas then the spectra, (Figure 12) in the region 2300-2000 cm^{-1} were very similar to those for nitrogen except that the hydrogen iodide was not as well isolated. The two bands at 2156 and 2144 cm^{-1} can be assigned to hydrogen iodide-water adducts by comparison with the work of Nelander(61) or cyclic trimer and tetramer respectively by reference to Barnes(55).

The effect of using orthoboric acid (H_3BO_3) instead of boron oxide is seen in Figure 13. The spectra indicate that the vapour contains a significant quantity of water due to the thermal dehydration of the boric acid because ice bands obscured the spectra from 1000 to 450 cm^{-1}. The only feature other than ice, observed below 2000 cm^{-1} was a very small sharp band at 1426 cm^{-1}.

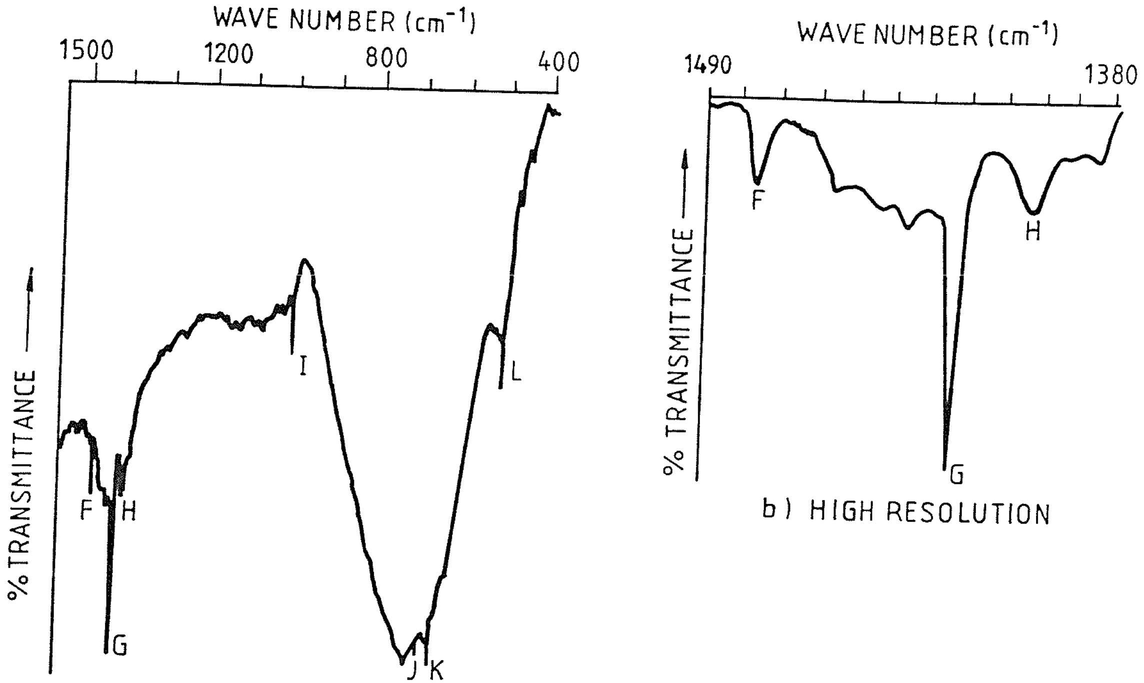

a) LOW RESOLUTION

b) HIGH RESOLUTION

BAND POSITIONS

F	$1477\cdot8\ cm^{-1}$
G	$1425\cdot7\ cm^{-1}$
H	$1405\cdot6\ cm^{-1}$
I	$1009\ cm^{-1}$
J	$701\ cm^{-1}$
K	$675\ cm^{-1}$
L	$514\ cm^{-1}$

FIG. 11 NITROGEN MATRIX INFRARED SPECTRUM OBSERVED FOR THE CsI / B_2O_3 SYSTEM AT 400 - 500°C

TABLE 4

Frequencies Observed in the CsI/B_2O_3 or H_3BO_3 heated to 500°C

Observed Frequency/ cm^{-1}	Assignment
2348	ν_3 CO_2
2236.6	monomeric HI
2176.5	dimeric HI
2166.5	timeric HI
2122	HI - H_2O adduct
2097	HI - H_2O adduct
1477.8	E' ^{10}B-O str. boric acid
1425.7	E' ^{11}B-O str. boric acid
1405.6	?
1009	E' B-O-H bend boric acid
701	A' ^{10}B BO_3 bend boric acid
675	A' ^{11}B BO_3 bend boric acid
514	A'' O-H torsion boric acid

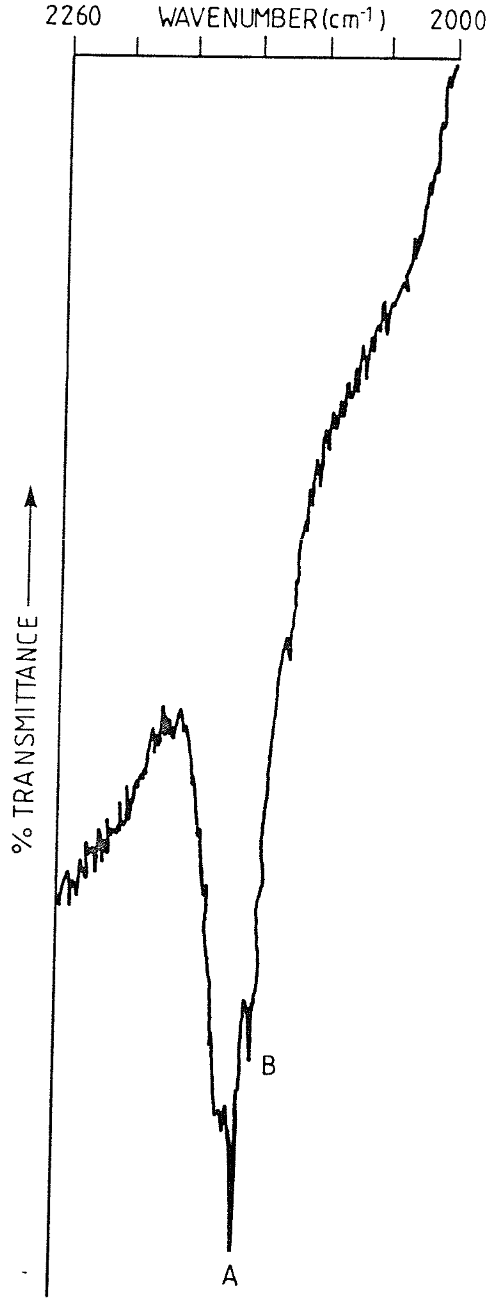

A 2156 cm^{-1} HI-H_2O ADDUCT/TRIMER
B 2144 cm^{-1} HI-H_2O ADDUCT/TETRAMER.

FIG. 12 ARGON MATRIX INFRARED SPECTRUM OBSERVED FOR THE CsI/B_2O_3 SYSTEM AT 400-500°C

Figure 13(a), is a low resolution spectrum of the region 2600 to 2000 cm^{-1}, which shows features due to carbon dioxide at 2348 cm^{-1} and hydrogen iodide. The high resolution spectrum (Figure 13(b)) shows the characteristic set of bands due to monomeric and polymeric hydrogen iodide and hydrogen iodide water adducts. If one compares this spectrum with that obtained from heating CsI and B_2O_3, then the most obvious difference is the increase in the relative intensities of the bands at 2122 and 2096 cm^{-1} with respect to the other bands. This thus indicates that these bands are probably due to hydrogen iodide-water adducts as their intensity increases with the amount of water in the matrix. It can also be seen that the prominent polymer species is now the dimer compared to the trimer in Figure 10(b).

5.4 Mass Spectrometric Studies

The mass spectra were obtained in a similar manner to that outlined above for the ir experiments. Figure 14 shows the change in intensity of the 254 amu (I_2^+), 128 amu (HI^+) and 127 amu (I^+) peaks with temperature. Although it appears that HI^+ and I_2^+ are detected at 100°C these peaks may be due to background peaks. However by 190°C it is obvious that the intensity of these peaks is increasing with temperature.

The signal to noise ratio of the peaks at 450°C and 530°C is very much better than at the lower temperatures, this was also accompanied by a rise in pressure in the mass spectrometer. In the mass spectra between 250 and 265 amu there is a small feature that could possibly be attributed to CsI^+, but the non-observance of this ion is due to the length of the glass tube between the heated sample and the spectrometer chamber on which the CsI could condense.

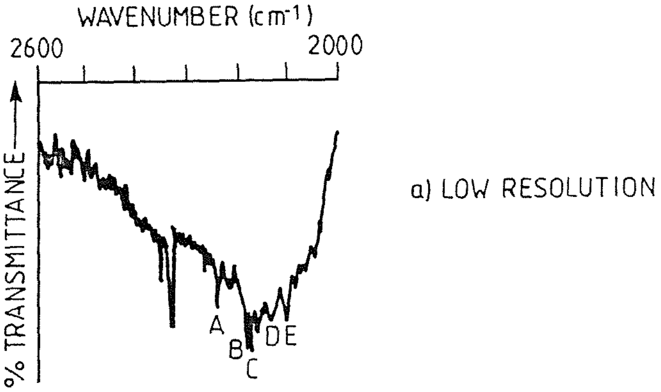

A	2236·6 cm^{-1}
B	2176·5 cm^{-1}
C	2166·5 cm^{-1}
D	2122·0 cm^{-1}
E	2097·0 cm^{-1}

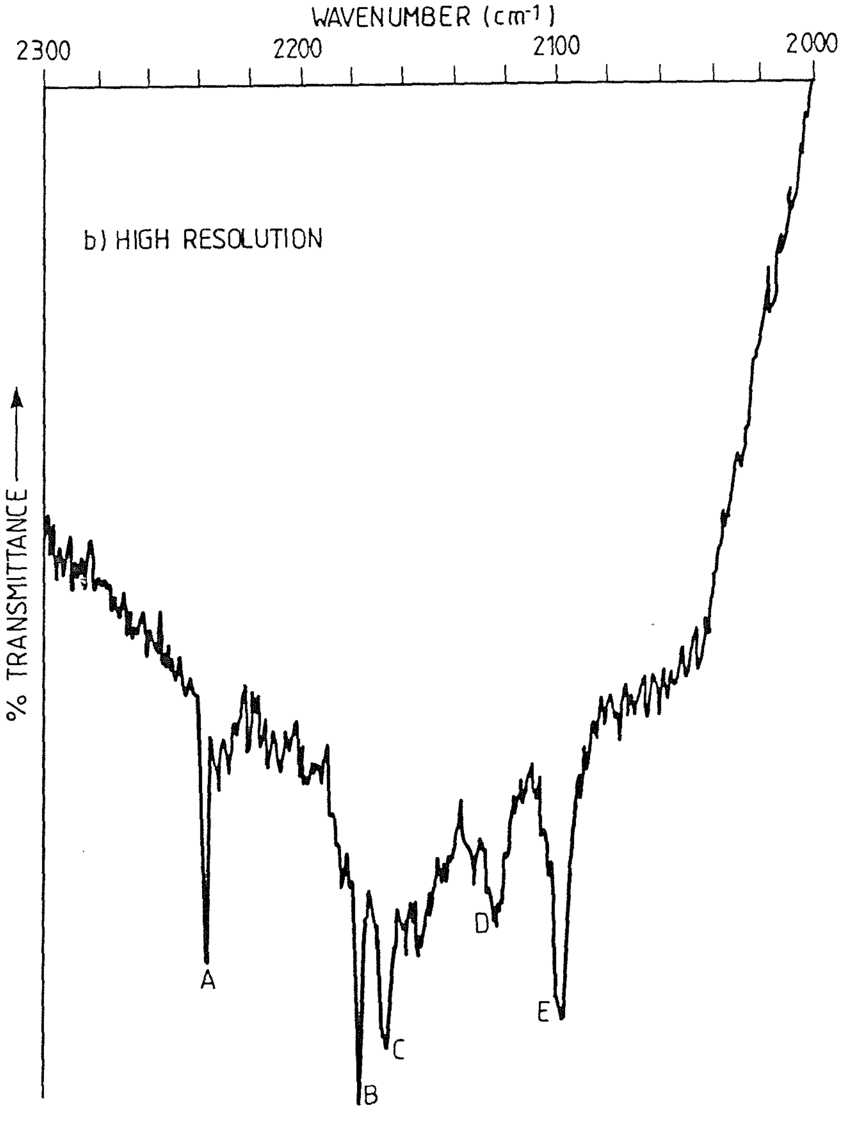

FIG.13 NITROGEN MATRIX INFRARED SPECTRUM OBSERVED FOR THE $CsI/B(OH)_3$ SYSTEM AT 400-500°C

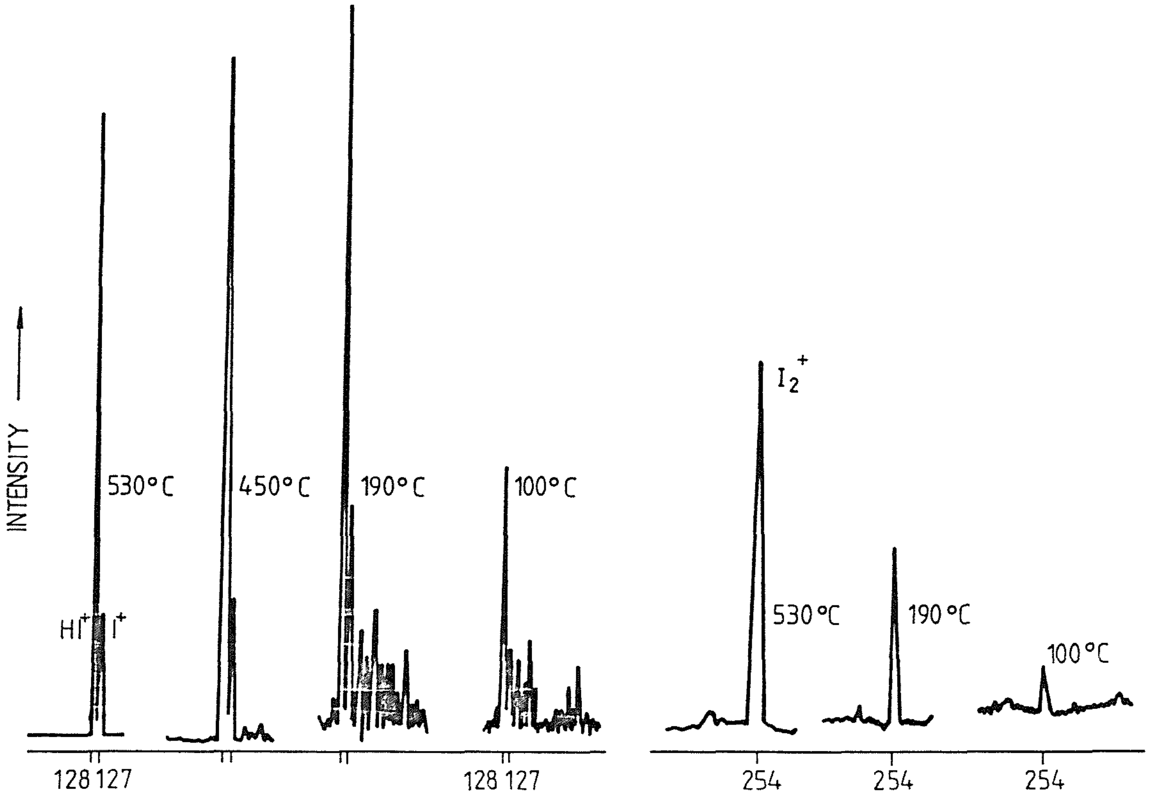

(a) BETWEEN 115 AND 130 a m u

(b) BETWEEN 250 AND 265 a m u

FIG. 14 MASS SPECTRA SHOWING THE EFFECT OF TEMPERATURE ON THE PRODUCTION OF HYDROGEN IODIDE AND IODINE

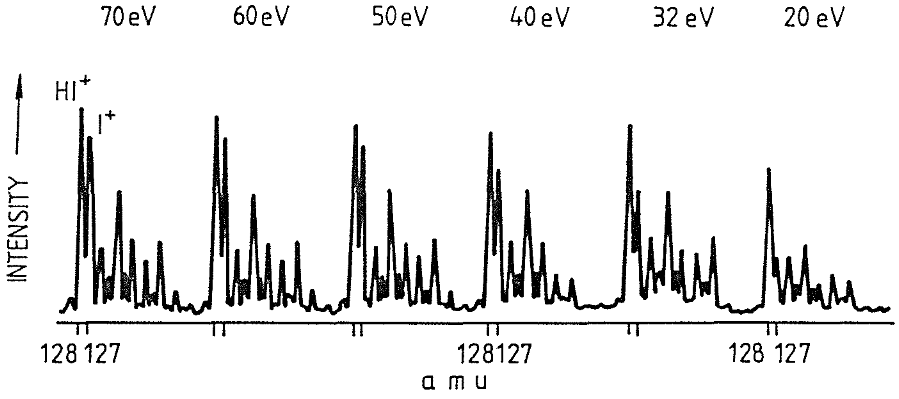

FIG. 15 THE EFFECT OF ELECTRON ENERGY ON THE PEAK HEIGHT OF HI^+ AND I^+ IN THE MASS SPECTRA OF CsI/B_2O_3 HEATED TO 400 - 500 °C

These observations support the results of the ir studies in as much that significant quantities of HI were not observed until approximately 450-500°C, and also the observation in the higher temperature mass spectrometric experiments that molecular iodine was only detected when CsI was subliming.

In the above spectra the electron energy was set at 20eV compared to that of 32eV used previously. The effect of changing this is shown in Figure 15 where it can be concluded that the HI^+ peak at 128 amu is the parent ion and the I^+ ion the daughter. If both were the result of fragmentation of molecular iodine (I_2) then they should grow at approximately the same rate when the electron energy is increased. Whereas if the HI^+ is a parent ion then as the electron energy is reduced, so will fragmentation which will result in the lowering of intensity of the I^+ daughter ion and therefore the HI^+ ion becomes the predominant species.

From these considerations one can conclude that the HI^+ is indeed a parent ion and must either be a reaction product of the heated CsI/B_2O_3 or due to a reaction of iodine with a protic source.

Neither $B_2O_3^+$ or $CsBO_2^+$ at 70 amu and 176 amu respectively were detected at these relatively low temperatures, but a series of peaks in the region 40 to 65 amu were detected (Figure 16) and these are assigned to orthoboric acid, $B(OH)_3^+$, at 61 and 62 amu and its dehydroxylated daughter ion, $B(OH)_2^+$, at 44 and 45 amu. The calculated spectra for normal abundance boron (^{10}B 20%, ^{11}B 80%) are shown below the experimental ones and it is clear that there is a very satisfactory fit for $B(OH)_3^+$. That for $B(OH)_2^+$ is less good, due mainly to background CO_2^+ at 44 amu. This supports the

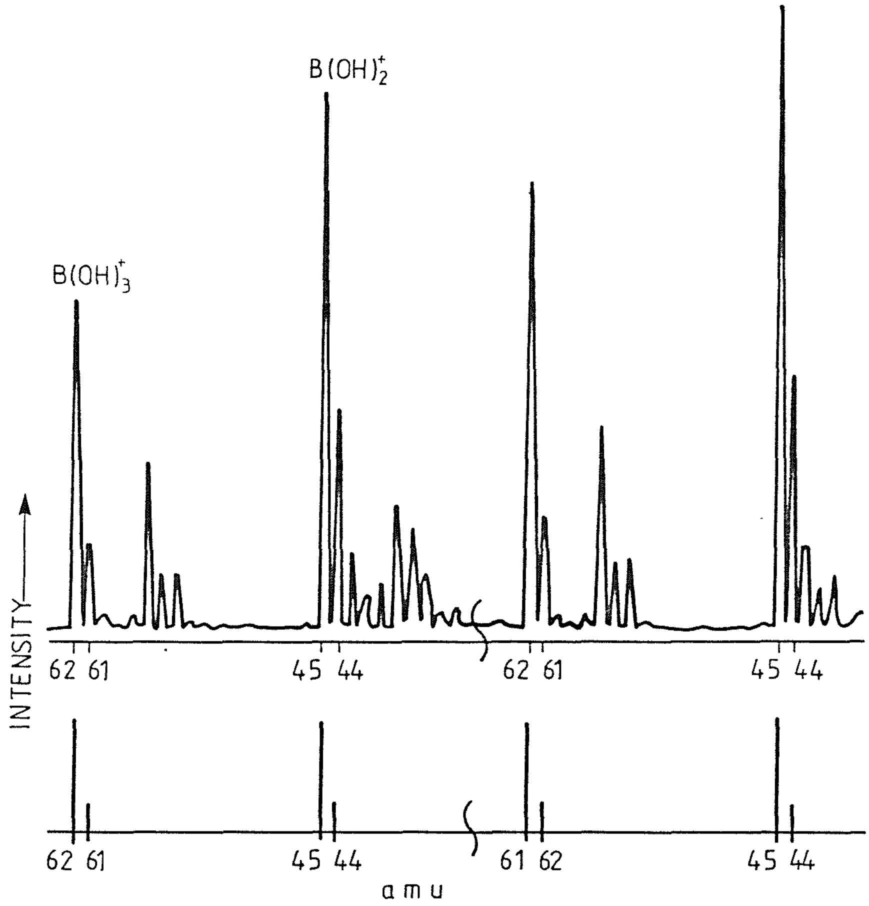

FIG.16 MASS SPECTRUM OBSERVED FOR THE CsI/B_2O_3 SYSTEM BETWEEN 40 AND 65amu THE LOWER SPECTRUM SHOWS THE CALCULATED SPECTRUM

observation from the ir data that orthoboric acid is present in the vapour above the CsI/B_2O_3 mixture at ≈ 500°C. It should be noted that no peaks assignable to HBO_2^+ at 43 and 44 amu could be detected.

The moistening of the samples produced a yellow coloration in the mixture and when this was pumped on by vacuum the yellow colour was replaced by a pale pink colour. The yellow colour is probably due to caesium polyiodides whilst the pink coloration is most likely to be due to small traces of iodine. The mass spectrum of this moistened sample did not differ significantly from those described earlier except that the sensitivity was lower due to the large vapour pressure of water present. (If these moistened samples were left for a period of a couple of years then dark coloured crystals were observed amongst the yellow solid. This is probably due to molecular iodine).

A series of deuteration studies were undertaken to verify the observations and interpretations above. The deuteration of the sample was carried out by two different methods.

i) Addition of deuterated water to the already mixed CsI/B_2O_3 mixture.

or ii) Addition of deuterated water to the boron oxide, followed by careful drying (to avoid the formation of a glass) and then mixing with the caesium iodide.

The first method was used to identify the ions produced, whereas the second was used to determine whether any hydrogen or deuterium was generated on heating the mixture.

Part of the mass spectrum of the vapour above the mixture produced by the first method is shown in Figure 17. From Fig 17(a) it can be seen that the ions detected in the regions 120-130 amu and 250-260 amu were I_2^+ (254 amu), HI^+ (128 amu), DI^+ (129 amu) and I^+ (127 amu).

Figure 17(b) shows the region of the mass spectrum concerned with boric acid. From these spectra and the calculated spectra for 70% ^2D enrichment it is confirmed that these peaks are indeed due to $H_3BO_3^+$ and $H_2BO_2^+$ and the related isotopomers. The fit for the former is as previously, better than that for the latter because of the interference of CO_2^+ at 44 amu. Again there was no evidence for HBO_2^+ at 43 to 45 amu. There is also a very good correlation between these spectra and those observed in the previous chapter for pure orthoboric acid.

The second method of deuteration was used to test whether any hydrogen was produced in the reaction between caesium iodide and boron oxide. Both H^+ and H_2^+ had been observed in many of the previous spectra but the origin of these ions was considered to be either water or hydrocarbons such as the pump oil or vacuum grease. Indeed the supporting experiments had shown that D_2O gives rise to D_2^+.

The vaporisation apparatus fitted with the trap held at -196°C was used in order to isolate all the reaction products and volatile components of the heated mixture except those that still had a significant vapour pressure at -196°C. Table 5 gives the variation of vapour pressure with temperature for the gaseous components of the system. From this it can be seen that at-196°C the only species that have an appreciable vapour pressure are hydrogen and deuterium.

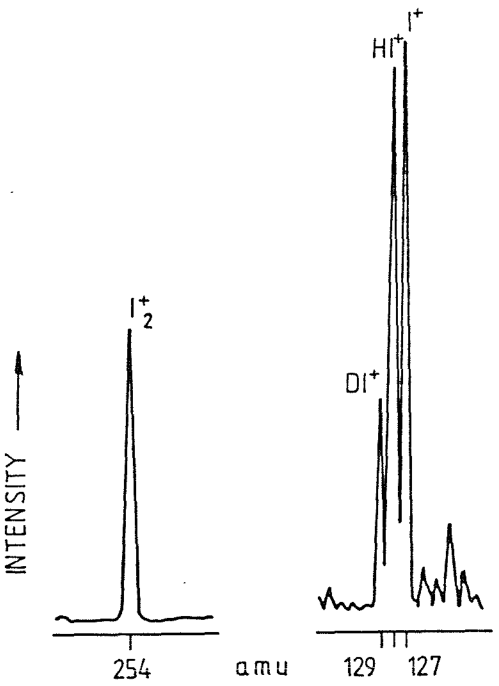

(a) MASS SPECTRUM OBSERVED FOR THE CsI/B_2O_3/D_2O SYSTEM AT 400-500°C

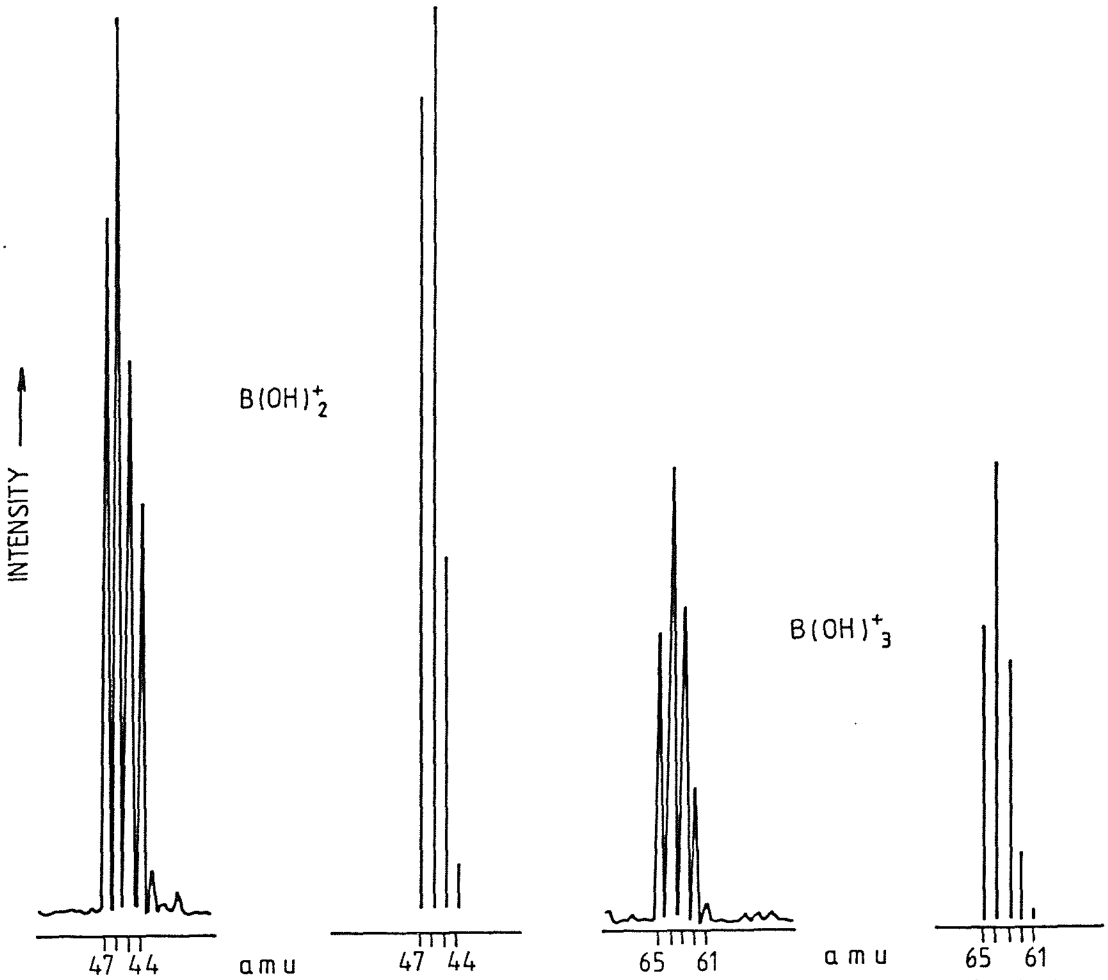

(b) MASS SPECTRA OBSERVED (LEFT) AND CALCULATED FOR 70% DEUTERATION (RIGHT) FOR THE CsI/B_2O_3/D_2O SYSTEM AT 400-500°C

FIG. 17 MASS SPECTRA OBSERVED FROM SAMPLES OF CsI/B_2O_3 TO WHICH D_2O HAS BEEN ADDED

TABLE 5

Vapour Pressure Data for the Various Volatile Components in the CsI/B_2O_3 System(63)

Compound	Temp (°C)					
	1mmHg	10mm	40mm	100mm	400mm	760mm
H_2	-263.3	-261.3	-259.6	-257.9	-254.5	-252.5
HD		-259.8	-258.2	-256.6	-253.0	-251.0
HI	-123.3	-102.3	-85.6	-72.1	-48.3	-35.1
H_2O	-17.3	11.3	34.1	51.6	83.0	100.0
I_2	38.7	73.2	97.5	116.5	159.8	183.0

On heating the sample there was a negligible rise in pressure in the spectrometer chamber, thus indicating that all the volatile species produced (if any) were being trapped. This was also confirmed by the fact that there was no discernable change in the intensity of the HI^+ peak at 128 amu when the sample was isolated (by a tap) from the spectrometer chamber.

After prolonged heating (≈ 20 mins) at approximately 450-500°C, the pressure increased from 7.6×10^{-7} to 4.5×10^{-6} torr indicating that a species had penetrated beyond the trap. A mass spectrum revealed that it was a mixture of H_2^+, HD^+ and D_2^+.

Figure 18(a) confirms that the D_2 originates in the sample holder because the peak at 4 amu from D_2^+ is increasing at a greater rate than the H_2^+ peak at 2 amu. Figure 18(b) also confirms this because the ratio of H_2O^+:D_2O^+ is greater than 200:1 whereas the H_2^+:D_2^+ ratio is approximately 1:2. Figure 18(c) shows the H_2^+:D_2^+ ratio after a further 10 minutes and this indicates that there is a hydrogen background but that the deuterium is a genuine reaction product and its production had either ceased, or at least slowed down, probably due to the separtion of the B_2O_3/CsI components.

When the liquid nitrogen was removed from the trap a yellow solid was observed, which then formed a yellow solution on warming to room temperature. This was then evaporated into the chamber but spectra were not recorded because of the high pressure in the system. The yellow solid/solution was probably a constant boiling mixture of water and hydrogen iodide(69).

From these mass spectrometric experiments it can be concluded that hydrogen iodide is a product of the

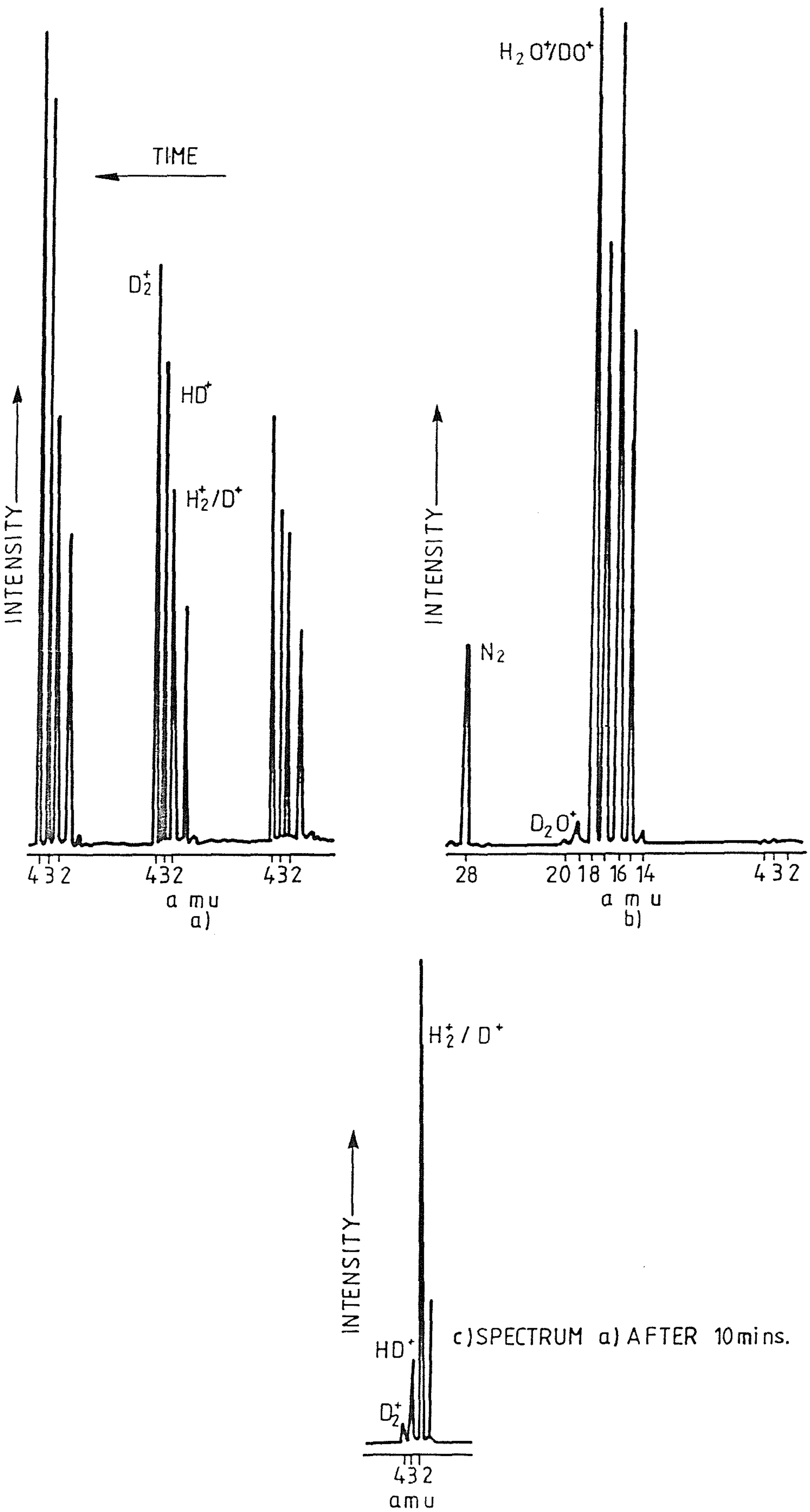

FIG.18 MASS SPECTRA OBSERVED FOR THE $CsI/B_2O_3/D_2O$ SYSTEM AT 400-500°C

interaction of caesium iodide and boron oxide and that this process also liberates hydrogen. The source of the hydrogen is probably the thermal decomposition of hydrogen iodide, this explanation also accounts for the detection of molecular iodine.

6. Quantitative Studies

6.1 Introduction

In the above sections the emphasis had been placed on the determination of the fate of iodine in the reaction of caesium iodide and boron oxide or boric acid. This has been shown to be hydrogen iodide, which in turn liberates molecular iodine. It is also important however to try to quantify the amount of HI that could be produced in order to provide more information for the evaluation of severe reactor accident source terms.

The method chosen was based on the assumption that the absorbance of the infrared active mode of matrix isolated molecular hydrogen iodide at 2236.6 cm^{-1} was proportional to the amount (of hydrogen iodide) deposited on the central window. This assumption then allows the use of the Beer Lambert law ($\log(I_o/I) = \varepsilon cl$) to estimate the amount of hydrogen iodide deposited on the window if the absorption coefficient (ε) and the path length (ℓ) are known. The absorption coefficient for hydrogen iodide is quoted as 0.033 by Bartholomé(71) in 1933 and as 0.37 $cm^2\ atm^{-1}$ by Ameer and Benesch(72) in 1962. There is obviously some uncertainty in its value and, given that the experiments in this work were carried out at ≃ 12K (where one only expects to see the $v = 0 \rightarrow 1$ transistion) it was decided to measure the absorption coefficient for this apparatus. The use of any published values would also have introduced an unacceptable level of error because of the difficulty of establishing the path length.

This series of experiments was divided into two sections. The first was to obtain a plot of absorption versus mole of HI deposited, using a gas mixture prepared in the same manner as those in the supporting experiment section. The second part was to heat known amounts of caesium iodide and boric acid (or boron oxide) and by use of the plot obtained above calculate the amount of HI released from the sample mixtures.

6.2 Preparation of Pure Hydrogen Iodide/Nitrogen Gas Mixtures and Estimation of the Absorption Coefficient

In order to estimate the absorption coefficient the hydrogen iodide/nitrogen gas mixture was deposited on the window in small pulses. After each pulse the absorbance of the monomeric hydrogen iodide band was measured, as was the remaining pressure in the gas bulb. If the concentration of the gas mixture is known then the amount of HI deposited in each pulse is easily calculated. A graph of absorbance versus mole of HI deposited is then plotted and this has a gradient of εl.

The main problem is that not all of the hydrogen iodide will be deposited on the central window. It is however reasonable to assume that the same proportion will "stick" both in the pure HI/N_2 mix and in the heated $CsI/B(OH)_3$ sample. The other major problem is that hydrogen iodide is not easily isolated and therefore one needs the same ratio of monomer:polymer in these experiments as in the heated sample experiments. By comparison of Figures 6, 10 and 13 it can be seen that the best correlation in monomer:polymer ratios is for a mix in the range 1:150 to 1:265. However if these spectra, (Figure 6) are compared to those obtained for use in the quantitative analysis (Figures 20 and 21) it can then be seen that a gas mixture of approximately 1:400 is the best.

Figure 19 shows the plot of the entire deposition of the 1:397, $HI:N_2$ sample mixture. (A similar plot was also obtained from the 1:291 mixture).

The assumption that the Beer Lambert law is valid holds for the first part of the plot, but at higher quantities of HI it fails. This behaviour is typical in matrix experiments and is largely due to the build-up of the matrix where the earlier parts of the deposition are better isolated than the latter ones because the heat released on condensation is not carried away sufficiently quickly and the layer becomes too thick to condense any more onto it. The gradient of the linear part of the graph is 6.3×10^3 $mole^{-1}$, and it is this value that is used to determine the extent of HI production. Although it is feasible to try and calculate the absorption coefficient, ε, from these curves there are so many approximations and assumptions to be made regarding path length, extent of sample deposited on the window etc that the answer would not be meaningful.

6.3 Quantitative Studies with Caesium Iodide and Boric Acid/or Boron Oxide Mixtures

Weighed equimolar mixtures of caesium iodide and boric acid (dried at 95°C) were heated in the same manner as already described. The appearance of a small broad band at low (100°C) temperatures and the characteristic bands observed at 450-500°C are all in good agreement with the previous experiments. The fact that the boric acid was dried at 95°C reduced the intensities of the ice peaks, but probably meant that it was in the form of ortho rhombic metaboric acid([23], [24]) in the solid mixture.

The absorbance of the monomer peak of 2236.6 cm^{-1} was measured at the end of each experiment and by using the graph in Figure 19 the amount of HI in the matrix was determined. A typical spectrum from these experiments is

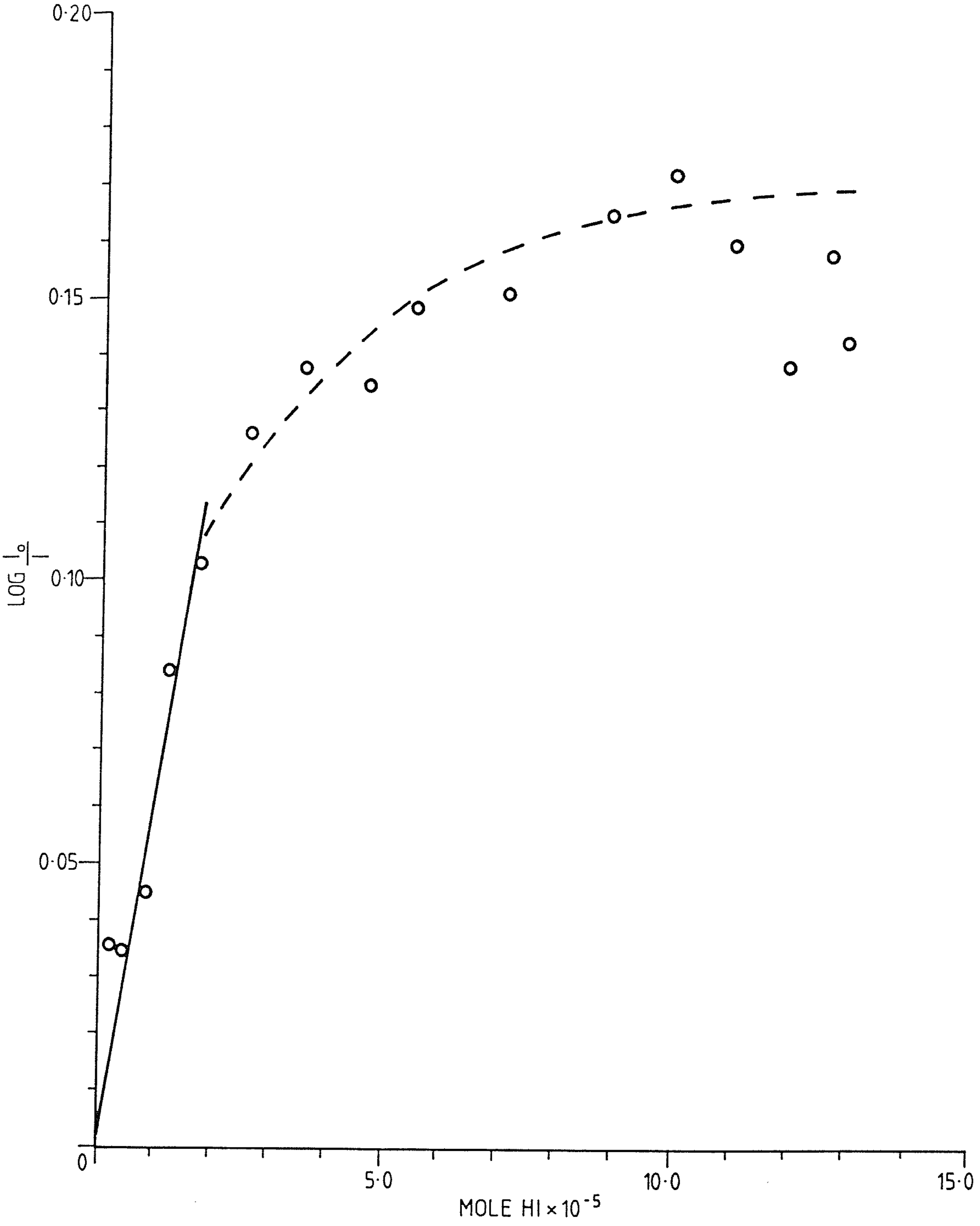

FIG. 19 PLOT OF ABSORBANCE VERSUS MOLE OF HI FOR ENTIRE DEPOSITION OF 1: 397 HI:N_2 MIXTURE

shown in Figure 20. When boron oxide was used instead of boric acid, similar results were obtained and the spectrum is shown in Figure 21. The data for these experiments is presented in Table 6.

From this data one can see that at least 0.5% of the available iodine is transported as HI into the matrix. This value is to be regarded as the absolute lower limit for the following reasons.

i) Not all the HI released from the heated mixtures will co-condense with the N_2 on the cold deposition window. An optimistic value is probably 50%. The geometry for sample collection was less favourable in the heated mixture case than in the pure HI/N_2 experiments.

ii) The hydrogen iodide decomposes to an appreciable extent (22%) at 450-550°C and therefore nearly a quarter of the released iodine will be in the form of molecular iodine in the matrix and will hence not be detected by ir spectroscopy.

iii) The evolution of hydrogen iodide ceased when the components were separated by the sublimation of caesium iodide as evidenced by a two fold variation in percentage iodine transport. If the temperature can be maintained so that the caesium iodide is just vaporising then the yield of hydrogen iodide could probably be made to be nearly quantitative.

Therefore as a result of these considerations it is more realistic to assume, for the purposes of severe accident evaluations, that the proportion of hydrogen iodide release will be of the order of 10% and that the reaction may go to completion under certain conditions. In addition to the

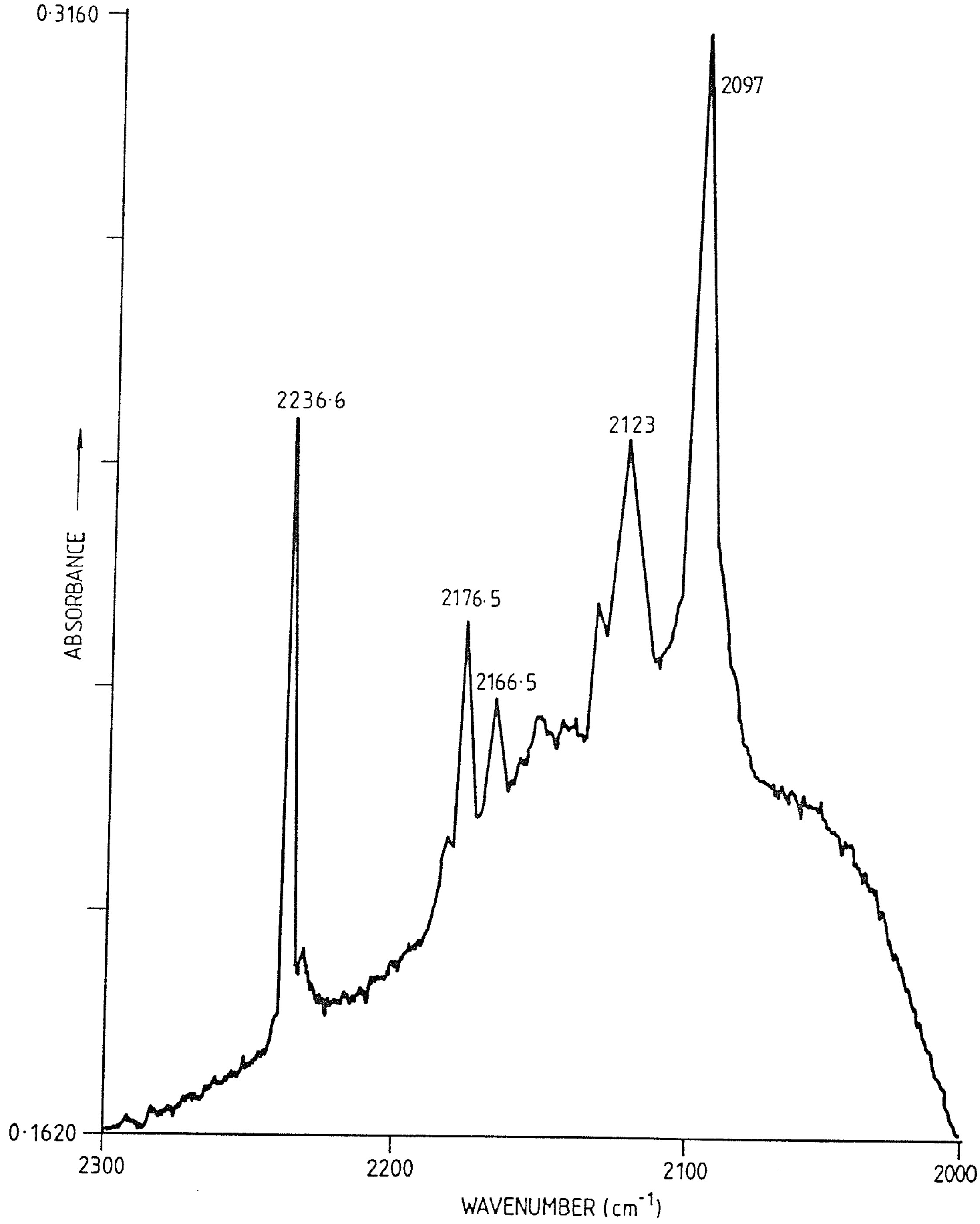

FIG. 20 NITROGEN MATRIX INFRARED SPECTRUM OBSERVED FOR THE CsI / H_3BO_3 SYSTEM HEATED TO 450 - 500°C

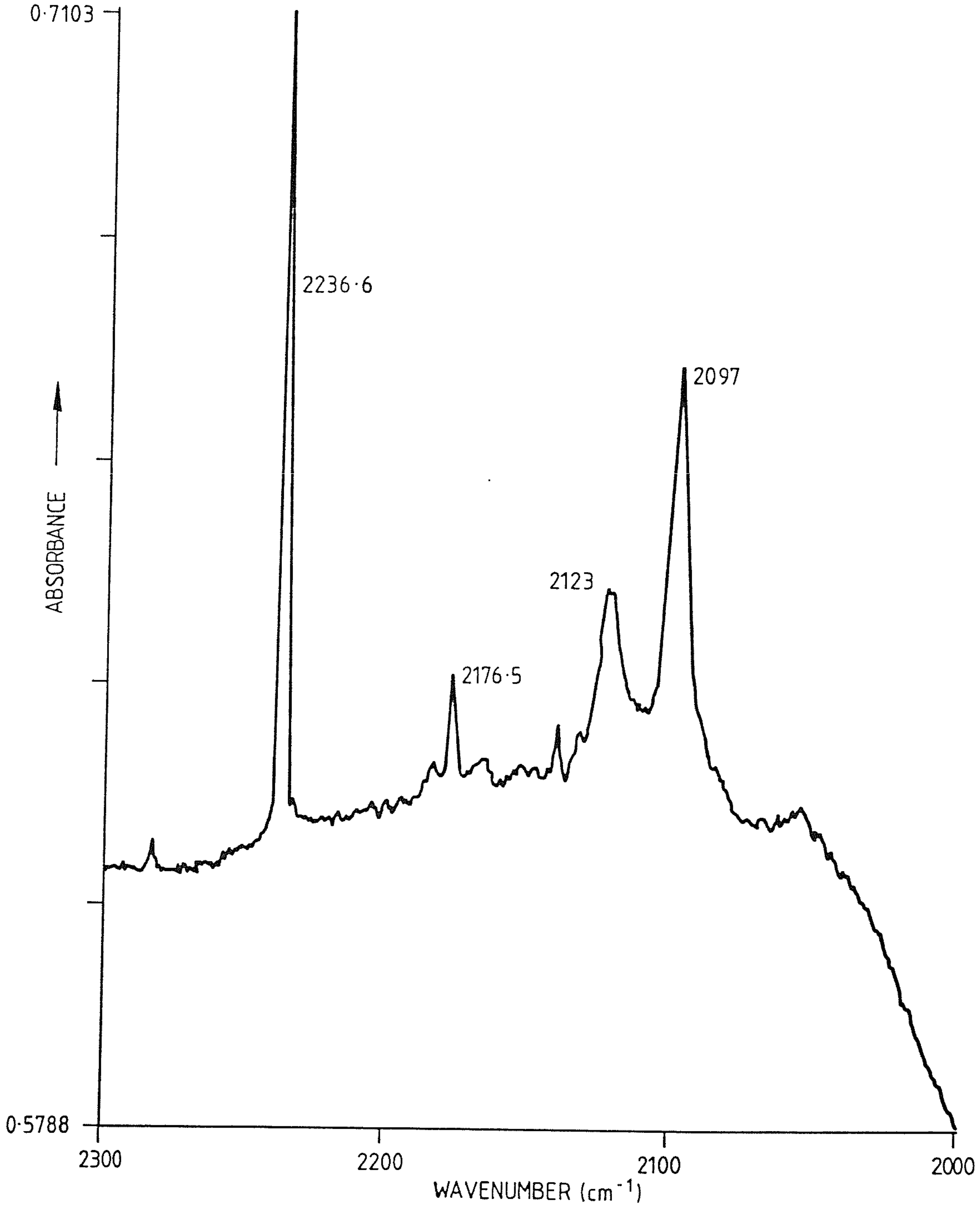

FIG. 21 NITROGEN MATRIX INFRARED SPECTRUM OBSERVED FOR THE CsI/B_2O_3 SYSTEM HEATED TO 450 - 500 °C

TABLE 6

Summary of Results of Quantitative Experiments

system	log (I_o/I)	mole HI	% I transfer
1.71 mmol $B(OH)_3$ 1.71 mmol CsI	0.046	7.2 μmol	0.42
1.99 mmol $B(OH)_3^+$ 2.2 mmol CsI	0.085	13.4 μmol	0.6
1.25 mmol $B(OH)_3^+$ 1.22 mmol CsI	0.041	6.5 μmol	0.53
1.3 mmol $B(OH)_3^+$ 1.22 mmol CsI	0.021	3.3 μmol	0.27
2.17 mmol $B_20_3^+$ 2.41 mmol CsI	0.098	15.6 μmol	0.65

HI, there will also be a quantity of molecular iodine and hydrogen due to thermal decomposition.

7. Discussion

It can be concluded from the above data that when caesium iodide reacts with boric acid, the iodine is released as hydrogen iodide under the experimental conditions in these studies. Molecular iodine and hydrogen are also detected as a result of the thermal decomposition of the hydrogen iodide. The hydrogen iodide/hydrogen/iodine system was one of the first gas phase systems to be investigated and Bodenstein(73-76) concluded that the reaction between hydrogen and iodine was bimolecular,

$$2HI \underset{k_1}{\overset{k_2}{\rightleftharpoons}} H_2 + I_2$$

with the equilibrium constant K, (k_1/k_2) expressed as

$$\log_{10}K = a + b \log_{10} T - (c/T)$$

where a = -2.45, b = 0.45, c = 508.3, and T in °K

At 450°C this gives a value of K = 0.013. The decomposition increases with temperature and Vogel von Falckenstein(77) has reported that at 1022°C hydrogen iodide is 32.9% dissociated whilst at 1217°C it is 37.55% dissociated.

More recent studies by Taylor and Crist(78) have calculated the equilibrium constant (K) and the rate constants k_1 and k_2 to be as shown in Table 7 below.

The equilibrium constants were measured by the change in concentration of the appropriate gases either for

TABLE 7

Equilibrium and Rate Constant Data for the HI/I_2/H_2 System

T°C	K_{synth}	K_{dec}	K_{av}	k_2	k_1	x%
490.0	0.02192	0.02172	0.02182			22.81
457.0	0.02018	0.02007	0.02013			22.10
425.0	0.01812	0.01811	0.01815	1.242	67.0	21.21
393.0	0.01639	0.01645	0.01642	0.259	15.59	20.40

combination or decomposition of HI. The rate constants were calculated using the equilibrium constants achieved above. The value in the last column, x% is the percentage decomposition of the hydrogen iodide calculated using the following equation.

$$x\% = \frac{100}{\frac{1}{2\sqrt{K_{av}}} + 1}$$

Zeise(79) claims that the rate constants may be too high and the work of Craven(80) indicates that the value of k_1 is slightly higher in the presence of hydrogen. Several workers(81,82) claim that at higher temperatures a radical or unimolecular pathway is significant.

Therefore at the temperatures employed (400-500°C) in these studies about 20-23% of the hydrogen iodide will be dissociated from the above considerations. The actual extent of decomposition will be less than this because the hydrogen iodide will be rapidly cryopumped away from the hot reaction zone although there is obviously some decomposition because of the detection of molecular hydrogen and iodine ions in the mass spectrometric experiments.

The reaction products of the interaction of caesium iodide and boron oxide or boric acid have been identified as $CsBO_2$ and HI. However the reactive B-O-H species has as yet not been identified although boric acid has been detected in both ir and mass spectrometric experiments. White et al(36) have found that the vapour above heated boron oxide in the presence of water is a complex system. Evans et al(83) have shown by thermodynamic arguments that orthoboric acid is not important in the boron oxide/water systems at high temperatures and low water vapour pressures. Chupka and Berkowitz(31) have passed water over heated B_2O_3 (1100K) and found from mass spectrometric experiments that the vapour in addition to water consists of almost entirely metaboric acid (HBO_2) and small amounts of its trimer and orthoboric acid (H_3BO_3). Linevsky(37) has carried out similar matrix ir experiments and has assigned his spectrum to HBO_2. It has recently been shown(35) that at room temperature, orthoboric acid has a finite vapour pressure and at about 50°C is the predominant gas phase boron containing species above heated boric acid.

The decomposition and dehydration of orthoboric acid has been studied using ir sepctroscopy by Broadhead and Newman(23,24). They found that it dehydrates at about 175°C into metaboric acid (HBO_2) which then dehydrates further, so that by about 440°C boron oxide is the predominant form. (They also report that pure orthoboric acid can be prepared by sublimation at 180°C). The decomposition can be detected at 85°C and metaboric acid is formed by 110°C. From x-ray powder pattern data they suggest that by 120°C the material is in the form of orthorhombic metaboric acid, ($B_3O_3(OH)_3$), which has the same empirical formula as the trimer of metaboric acid $(HBO_2)_3$, and that even at 100°C the metaboric acid phase is dominant. The phase diagram for the B_2O_3:H_2O system is shown in Figure 22 (84), and from this and the above arguments it can be seen that the only viable species above 400°C is B_2O_3.

However this cannot be the whole picture because orthoboric acid $B(OH)_3$ has been detected both in the matrix ir and mass spectrometric experiments. It is known that to dry B_2O_3 completely is a very laborious task(85) and arguably impossible, because of the equilibrium between the water vapour and the melt(38), and once dry it is very hygroscopic. Therefore, in general there will be OH or H_2O units within the internal structure. A structural

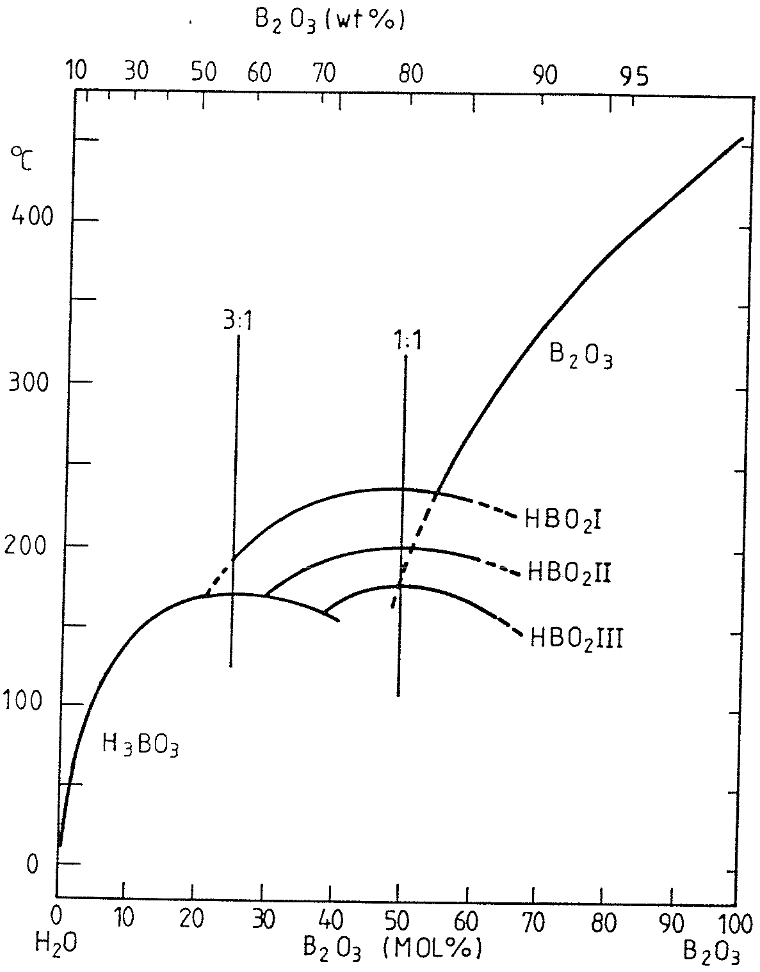

FIG. 22 PHASE DIAGRAM FOR THE B_2O_3/H_2O SYSTEM. (FROM REF.84)

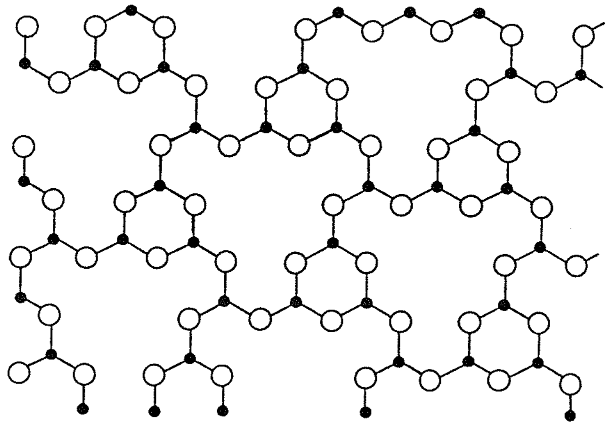

FIG. 23 SCHEMATIC ILLUSTRATION OF THE STRUCTURE OF MOLTEN B_2O_3. FILLED AND OPEN CIRCLES REPRESENT B AND O ATOMS RESPECTIVELY. (FROM REF. 86.)

analysis(86) of molten boron oxide using an x-ray radial distribution method (Fig 23) reveals that there is probably room for OH and H_2O groups to be accommodated within the structure. These groups will not be lost on heating until the boron oxide becomes molten, and thus it can be concluded that this is probably the source of the boric acid.

From these arguments it would appear that the B-O-H reactive species has to be in the gas phase (and is probably boric acid) as no HI is detected until CsI begins to sublime, and therefore the reaction is a gas phase reaction. Alternatively the presence of the caesium iodide sublimate, boric acid in the vapour and the production of hydrogen iodide could all be coincidental.

Transpiration experiments conducted at AEE Winfrith by Bowsher and Dickinson(22,87,90) and by Beattie et al(21) at Southampton indicate that substantial decomposition of caesium iodide occurs in the range 600-1000°C with the formation of caesium metaborate and a volatile iodine species, which reacted with stainless steel foil. This implied the formation of hydrogen iodide, whose dissociation into molecular iodine was enhanced significantly in more oxidising conditions(21,88). The decomposition of the caesium iodide and the boric acid was found to be greater than 70% when both were in the vapour phase(87). Hydrogen iodide was evolved when both boric acid vapour reacted with condensed caesium iodide and when caesium iodide reacted with a boric acid coated surface(87).

DTA and TGA studies(90) indicated that in the solid phase the reaction is diffusion controlled. By using isothermal TGA experiments Bowsher et al(90) were able to show that the reaction obeyed the Arrhenius equation with an activation energy of 190 ± 30 kJ/mole.

A revaluation of the thermodynamic parameters for the caesium iodide boric acid reaction is currently underway(89) using the matrix boric acid vibrational frequencies. This indicates that the equilibrium constant may be as much as an order of magnitude higher than originally thought for the vapour phase reaction.

8. Conclusions

The reaction of caesium iodide with boric acid or boron oxide has been studied by matrix isolation infrared spectrometry and mass spectrometry over the range 100-600°C. This work has shown conclusively that the volatile iodine product from this reaction is hydrogen iodide thus:

$$CsI + H_3BO_3 \rightarrow HI + CsBO_2 + H_2O.$$

Molecular iodine and hydrogen are also observed and these arise from the partial decomposition of hydrogen iodide, but the presence of iodine will also be favoured by the presence of adventitious oxygen(88).

The reaction occurs at temperatures as low as 100°C but not to such an extent as it is controlled by solid state diffusion kinetics(87, 90). At higher temperatures ($\approx$ 450-500°C) the reaction is significant, and this is probably because the reaction is now a vapour phase reaction between the caesium iodide and boric acid. This conclusion is confirmed by recent thermodynamic calculations(89) indicating that the equilibrium constant may be an order of magnitude higher than that previously thought using the recently acquired boric acid vibrational data.

A semi-quantitative study has shown that at least 1% of the iodine in caesium iodide/boric acid mixtures is transported as hydrogen iodide to the cryogenically cooled window. In practice the value should probably be considered to be at least 10% and under certain conditions may be quantitative.

Therefore it can be concluded that it is incorrect to assume that fission product iodine will be transported wholly as caesium iodide under the conditions of a severe reactor accident.

9. References

1. Bowsher B.R.
AEEW - R 1982, 1985.

2. Reactor Safety Study: An Assessment of Accident Risks in US Commercial Nuclear Power Plants.
WASH-1400, NUREG-75/014, 1975.

3. Cubicciotti D. and Sanecki J.E.
J. Nucl. Mat., 78, 96, 1978.

4. Lorenz R.A., Collins J.L., Malinauskas A.P., Kirkland O.L. and Towns R.L.
NUREG/CR-0772, 1980.

5. Garisto F.
AECL-7782, 1982.

6. Kohli R.
Trans. Am. Nucl. Soc., 39, 384, 1981.

7. Lemine R.J., Paquette J., Torgerson D.F., Wren D.J. and Fletcher J.W.
AECL-6812, 1981.

8. Levenson M.
Nucl. Technol., 53, 97, 1981.

9. Levenson M. and Rahn F.
Nucl. Technol., 53, 99, 1981.

10. Choppin G.R. and Rydberg J.
"Nuclear Chemistry", Pergamon, London. 1980.

11. Elrick R.M. and Sallach R.A.
Proc. Int. Mtg. on LWR Severe Accident Evaluation, Camb, Mass. 28 - 1 September 1983.

12. Levi M.G. and Garavini O.
Gazz. Chim. Ital., 41, 756, 1911.
Chem. Abs., 5, 3882, 1911.

13. Hackspill L., Rollet A.P. and Andrés L.
Compt. Rend., 192, 48, 1931.
Chem. Abs., 25, 1178, 1931.

14. Rollet A.P. and Andrés L.
Bull. Soc. Chim., 49, 1065, 1931.
Chem. Abs., 26, 21, 1932.

15. Schulek E. and Koros E.
Acta Chim. Acad. Sci. Hung., 3, 301, 1953.
Chem. Abs., 48, 6897g, 1954.

16. Gode H., Klavina L. and Kuka L.
Chem. Abs., 72, 59709c, 1970.

17. Gode H. and Klavina L.
Russ. J. Inorg. Chem., 16, 1794, 1971.

18. Gode G.K. and Klyavinya L.
Russ. J. Inorg. Chem., 17, 1495, 1972.

19. Zul'Fuyanly Yu. S.
Azenb. Khim. Zh., 6, 106, 1982.
Chem. Abs., 99, 94477e, 1983.

20. Bowsher B.R., Nichols A.L., Gomme R.A.,
Ogden J.S. and Young N.A.
"Speciation of Fission and Activation Products in the Environment". p 27-37.
Eds Bulman R.A. and Cooper J.R., Elsevier. 1986.

21. Beattie I.R., Bowsher B.R., Gilson T.R. and
Jones P.J.
AERE - R 11974, 253, 1985.

22. Bowsher B.R., Bruce D.M. and Dickinson S.
AERE - R 11974, 275, 1985.

23. Broadhead P. and Newman G.A.
J. Mol. Struct., 10, 157, 1971.

24. Broadhead P. and Newman G.A.
Spect. Chim. Acta , 28A, 1915, 1972.

25. White D., Mann D.E., Walsh P.N. and Sommer A.
J. Chem. Phys., 28, 508, 1958.

26. White D., Mann D.E., Walsh P.N. and Sommer A.
J. Chem. Phys., 32, 481, 1960.

27. Weltner W. and Warn J.R.W.
J. Chem. Phys., 37, 292, 1962.

28. Sommer A. and White D.
J. Chem. Phys., 38, 87, 1963.

29. Serebnnikov L.W., Sekachev Yu.N. and Maltsev A.A.
High Temp. Sci, 16, 23, 1983.

30. Ingham M.G., Porter R.F. and Chupka W.A.
J. Chem. Phys., 25, 498, 1956.

31. Meschi D.J., Chupka W.A. and Berkowitz J.
J. Chem. Phys., 33, 530, 1960.

32. Spirodonov A.P., Gershikov A.G., Zasorin E.Z.,
Ivanov A.A. and Ermolayeva L.I.
High Temp. Sci., 16, 325, 1983.

33. See for example the references in the previous chapter.

34. Mack J.L. and Wilmot G.B.
Proc. Mtg. Interagency Chem. Rocket Propulsion Gp. Thermo. Chem., 6th Calif., 1, 59, 1968.

35. Ogden J.S. and Young N.A.
J. Chem. Soc. Dalton Trans., 1988, 1645.

36. White D., Mann D.E., Walsh P.N. and Sommer A.
J. Chem. Phys., 32, 488, 1960.

37. Linevsky M.J.
US. Clearinghouse Fed. Sci. Tech. Inform., AD 1968 AD 670626. Available as: CFSTI US Govt. Res. Develop. Rept. 1968, 68(16), 63.

38. Sprague R.W.
In "A Comprehensive Treatise of Inorganic and Theoretical Chemistry". Vol 5. Supp 1. Part A. Ed Mellor J. W. Longmans. London. 1980.

39. Buchler A. and Marram E.D.
J. Chem. Phys., 39, 292, 1963.

40. Seshadri K.S., Nimon L.A. and White D.
J. Mol. Spect., 30, 128, 1969.

41. Hisatsune I.C. and Suarez N.H.
Inorg. Chem., 2, 168, 1964.

42. Buchler A. and Berkowitz-Mattuck J.B.
J. Chem. Phys., 39, 286, 1963.

43. Dickinson S.
AEEW - R 2227, 1988.

44. Emons H.H., Horlbeck W. and Kiessling D.
Z. Anorg. Allg. Chem., 488, 212, 1982.

45. Timm D.
Acta Chem. Scand., 16, 1455, 1962.

46. Bowers M.T. and Flygare W.H.
J. Chem. Phys., 44, 1389, 1966.

47. Bowers M.T. and Flygare W.H.
J. Mol. Spect., 19, 325, 1966.

48. Hughes A.N. and Purnell J.H.
Trans. Farad. Soc., 62, 1561, 1966.

49. Robinson D.W.
Chem. Abs., 69, 14299r, 1968.

50. Barnes A.J., Davies J.B., Hallam H.E.,
Scrimshaw G.F., Hayward G.C. and Milward R.C.
J. Chem. Soc. Dalton Trans., 1969, 1089.

51. Barker P.B., Halstead M.D., Purnell J.H.
Trans. Farad. Soc., 65, 2389, 1969.

52. Barnes A.J., Hallam H.E., Scrimshaw G.F.
Trans. Farad. Soc., 65, 3150, 1969.

53. Barnes A.J., Hallam H.E., Scrimshaw G.F.
Trans. Farad. Soc., 65, 3159, 1969.

54. Nobel P.N.
J. Chem. Phys., 56, 1957, 1972.

55. Barnes A.J., Davies J.B., Hallam H.E. and
Howells J.D.R.
J. Chem. Soc. Farad. Trans. II, 69, 246, 1973.

56. Walker N., Tevault D.E., Smardzevskii R.R.
J. Chem. Phys., 69, 564, 1978.

57. Bernadet P. and Schriver L.
J. Mol. Struct, 130, 193, 1985.

58. Schriver L., Schriver A. and Perchard J.P.
J. Chem. Soc. Farad. Trans. II, 81, 1407, 1985.

59. Schriver L., Schriver A. and Perchard J.P.
J. Chem. Phys., 84, 5553, 1986.

60. Perchard J.P., Schriver A. and Schriver L.
J. Mol. Struct., 156, 75, 1987.

61. Engdahl A. and Nelander B.
J. Phys. Chem, 90, 6118, 1986.

62. Schriver L., Schriver A., Hannachi Y. and Perchard J.P.
Ber. Bunsen. Chem. Phys. in Press. Private Communication from Schriver L. September 1987.

63. "C.R.C. Handbook of Chemistry and Physics" 62 ed. 1981.

64. Acquista N., Abramowitz S. and Lide D.R.
J. Chem. Phys., 49, 780, 1968.

65. Hoffman C.J.
Inorg. Synth., 7, 180, 1963.

66. Partington J.R.
"General and Inorganic Chemistry". Macmillan. London. 1946.

67. Strazhesko D.N. and Yankavskoya G.F.
Ukrain. Khim. Zhur., 25, 471, 1959.
Chem. Abs., 84 96866V, 1976.

68. Perutz R.N. and Turner J.J.
J. Chem. Soc. Farad. Trans. II, 69, 452, 1973.

69. Bowsher B.R.
Prog. Nucl. Energy, 20, 199, 1987.

70. See discussion in previous chapter.

71. Bartholemé E.
Z. Phys. Chem., B23, 131, 1933.

72. Ameer G. and Benesch W.
J. Chem. Phys., 37, 2699, 1962.

73. Bodenstein M.
Ber, 26, 2603, 1893.

74. Bodenstein M.
Z. Phys. Chem., 13, 56, 1894.

75. Bodenstein M.
Z. Phys. Chem., 22, 1, 1897.

76. Bodenstein M.
Z. Phys. Chem., 29, 295, 1899.

77. Vogel Von Falckenstein K.
Z. Phys. Chem., 68, 270, 1910.

78. Taylor A.H. and Crist R.H.
J. Am. Chem. Soc., 63, 1377, 1941.

79. Zeise H.
Z. Phys. Chem., A190, 56, 1941.

80. Craven W.M.
J. Am. Chem. Soc., 78, 3297, 1956.

81. Benson S.W. and Srinivasan R.
J. Chem. Phys., 23, 200, 1955.

82. Horie O., Ishii Y. and Amara A.
J. Phys. Chem., 68, 1264, 1964.

83. Evans W.H., Prosen E.J. and Wagman D.D.
N.B.S. Report No 6252, 1958.

84. Kracek F.C., Morey G.W. and Merwin H.E.
Am. J. Sci. 5th Series 35A, 148, 1938. from "Phase Diagrams for Ceramists" Ed Lewin and Murdle. NBS 1975.

85. See for eg Stern K.H.
J. Res. N.B.S., 69A, 281, 1965.

86. Miyake M., Suzuki T., Morikawa H., Takagi Y. and Marumo F.
J. Chem. Soc. Farad. Trans. I, 80, 1925, 1984.

87. Bowsher B.R., Dickinson S., Grubb S.R., Ogden J.S. and Young N.A.
Paper Presented at "IAEA/ACS Symposium on Chemical Phenomena Associated with Radioactivity Releases During Severe Nuclear Plant Accidents". Anaheim, California, 9-12 September 1986. NUREG/CP-00-78, 6-45, 1987.

88. Beattie I.R., Bowsher B.R., Gilson T.R. and Jones P.J.
AEEW - R 1974, 1985.

89. Bowsher B.R., Dickinson S., Ogden J.S. and Young N.A.
Thermochimica Acta, in press.
and Paper Presented at 'Third Chemical Congress of North America.' Toronto, June 1988.

90. Bowsher B.R. and Nichols A.L.
AEEW - R 1973, 1985.

CHAPTER EIGHT

CONCLUDING REMARKS

The work described in this thesis has shown the general applicability of matrix isolation infrared spectroscopy and mass spectrometry to the study of high temperature and unstable vapours. It has also shown that it is capable of providing direct experimental evidence to compare with the predictions of computer models.

Specifically the identification and partial characterisation of Cs_2WS_4 as the first ternary sulphide stable in the vapour has shown the utility of this approach to determining the vapour compositon above heated solids. The ir study of hydrogen telluride shows how the sharp absorption bands characteristic of matrix isolated species can be used to assign bands that are too close to each other to be resolved in the gas phase. The identification of $K^+TeO^-_2$ indicates how matrix isolation can be used to synthesise and stabilise highly unstable species.

The confirmation that orthoboric acid is volatile and that the molecular species have C_{3h} symmetry reveals the potential of the combined techniques of mass spectrometry and matrix isolation infrared spectroscopy. In particular it reveals that although no direct structural information is available, the molecular shape and often even the geometry can be inferred by the use of isotopic enrichment and vibrational analysis.

The study of the caesium iodide boric acid system has shown that the volatile form of iodine produced is hydrogen iodide. This indicates that provided the individual components of a system are characterised then complex systems can be studied using this method.

Therefore mass spectrometry and matrix isolation infrared spectroscopy are very valuable tools in the study of severe reactor accidents and often it is one of the only ways to study the chemistry. It should be noted however that the conditions of the experiment are radically different to those during a severe accident, especially with respect to pressure. For example, the experiments are usually carried out under high vacuum conditions (10^{-6} torr) whereas during a severe accident the pressure will be above atmospheric and contain large quantities of steam and hydrogen. Currently, the experiments described in this thesis are carried out in conjunction with small scale simulant tests, where the conditions are closer to those during a severe accident. These problems can also be partially overcome by using high pressure experiments, and a development rig is under construction at Southampton in order to mimic the accident conditions more exactly using matrix isolation and mass spectrometry. The more pernicious problems are as a result of the presence of up to thirty elements distributed amongst a hundred compounds making identification and characterisation awkward and the high neutron, beta and gamma flux within the core which may result in some very unexpected and novel chemistry, but about which little is presently understood.

APPENDIX A

THE CHARACTERISATION OF HIGH TEMPERATURE, UNSTABLE AND REACTIVE VAPOUR PHASE SPECIES

In this Appendix we shall deal in some detail with the various means of characterising vapour phase species. The term "vapour" is used to describe the vapours above solids or liquids, whilst the term "gas" implies that the compound is only found as a vapour at the conditions of interest. The term "high temperature" has been used extensively, but the same considerations apply to unstable species and often reactive ones.

The difficulties of characterising high temperature vapours can be separated into three areas;

(i) their production,

(ii) their detection,

(iii) the interpretation of the resultant spectra (if any).

The production and containment of reactive high temperature vapours in closed cell systems can severely limit the choice of materials that can be used for container and windows. These problems can be partially overcome by the use of molecular beams where only the furnace/cell have to withstand the elevated temperatures. The price one has to pay for this is reduced sample concentrations which may lead to detection problems. The spectroscopic detection of high temperature vapours is, on the whole not too difficult provided the above problems have been overcome and that the appropriate spectroscopically transparent "windows" are used. It is usually the interpretation of any observed spectra that can present the most difficulties. This, paradoxically is due to the over-abundance of information that is contained in the spectra. This over-abundance is due to the molecule not being in its molecular ground state because of the temperature required to vaporise it. This population of excited levels then leads to the possibility of a multiplicity of transitions being observed. Studies at lower resolution usually result in broad, ill defined features that yield little information.

The traditional non-spectroscopic methods for probing high temperature systems are by transpiration (1,2) and molecular effusion (Knudsen(3,4,5), Langmuir(4,5) or torsion(5)). These can be used to determine the vapour pressures and thermodynamic properties of the vapour under study. Alternatively the vapour can be condensed onto a suitable substrate and analysed by conventional methods or by techniques such as scanning electron microscopy and energy dispersive analysis of x-rays. (SEM/EDAX). In order to maximise the information obtained and its reliability, one really needs to know the chemical composition of the vapour under study. Vapour pressure measurements can usually infer how many species are present and the probable stoichiometry of a reaction(6). The analytical methods yield the elemental composition but rarely any data on the molecular formulae.

The most widely used technique for the interrogation of high temperature vapours and gases is mass spectrometry(7). The sample is vaporised by a variety of means, then ionised and the mass/charge ratios for the various ions produced are determined by either a magnetic field, the time of flight of the ions, or their oscillations in a quadrupolar field. Therefore mass spectrometry yields information about the molecular weight and hence molecular formula of the vapour(s) under study. It is often used in conjunction with the effusion and transpiration experiments to calculate the thermodynamic parameters but it is unable to give much structural information.

In the solid state the definitive methods for structural determination use single crystal diffraction. However in the gas phase this is not appropriate and one has to use other methods.

The diffraction technique available is that of electron diffraction ([8],[9],[10]). This can give details of both bonded and non bonded inter-atomic distances and hence bond angles. The technique records, by means of photographic plates, the scattering of a beam of electrons that is incident upon a molecular beam of the vapour under study. The resultant concentric rings are then analysed with a densitometer, and fourier transformed to yield a radial distribution function. These patterns are compared with the calculated patterns of a number of model compound structures and the model with the best fit to the observed is assumed to be the structure of the vapour under study.

The main objection to the results of electron difraction (ED) is that at the temperatures required (up to 2000K) to get 0.1 to 1 torr of the sample into the electron beam there is a possibility that excited vibrational and rotational energy levels will be appreciably populated. This therefore results in the inter-nuclear distances being averaged over all the vibrations of the molecule. The result of this is that linear molecules usually appear bent([11]) and planar molecules pyramidal([12]).

Even if the system has been examined mass spectrometrically and the vapour characterised, this does not necessarily imply that the same species are present with the same concentrations in the ED experiment. This discrepancy is due to the different vapour pressures of samples required in each experiment, (for mass spectrometry ~ 10^{-5} torr and ED ~1 torr). Recent examples of this are where the matrix ir data for $CrCl_2$([13]) and VCl_2([14]) indicate that these molecules are both linear whilst electron diffraction([15]) data indicates that they are severely bent with bond angles of ~ 110°. The discrepancy is assumed to be that in addition to MCl_2 there is also MCl_3 and/or MCl_4 in the vapour that can be identified and separated by ir but not by electron diffraction.

To try to surmount these problems people have used high pressure mass spectrometry ([10,16]) or low pressure electron diffraction([8]). However, until the mass spectrometric and electron diffraction measurements are carried out on the sample with identical conditions this problem will be not completely overcome. The actual interpretation of the raw data can also pose problems([17,18]).

In order to determine whether a molecule has a permanent dipole, electric deflection([19]) measurements on molecular beams can be used, one however has to be wary of vibrationally induced dipoles([20]). The method is essentially that of mass spectometry except that a quadrupole electric lens is inserted between the sample and ionisation chamber of the mass spectrometer. If a molecule has a permanent dipole moment then when the lens is acting the ion intensity will be less because the beam has been deflected.

Having ascertained that a molecule possesses a permanent dipole it may then be possible to carry out microwave spectroscopy ([21,23]). This will give data on moments of inertia and hence bond lengths and angles as well as the magnitude of the dipole moment. The sensitivity is however inversely proportional to temperature and the problems of interpreting spectra of anything except diatomics at high temperature is a formidable, and usually impossible task.

Raman rotational spectroscopy([24]) can be used if the molecule possesses no dipole, but suffers even further from detection problems because of the inherent lack of sensitivity of the Raman effect.

The use of photoelectron spectroscopy (PES)(25-29) is a relatively recent addition to the armoury of the high temperature spectroscopist. Its main advantage is that it provides electronic and bonding information expressed in molecular orbital terms. In the experiments a monochromatic beam of electromagnetic radiation (uv for UPS and x-rays for XPS) is allowed to interact with the molecular beam of the sample under study. If the energy of the incident light is greater than one or more of the ionisation potentials of the target vapour, then photoelectrons are ejected. The kinetic energies of these electrons are determined and these give the ionisation energies of the sample. The observed values are then compared to those calculated for model compounds, and when the best fit is arrived at, it is assumed that the sample and model compound are one and the same.

The sensitivity of the above techniques are sufficiently high to allow the study of the sample in a molecular beam. However, because of the inherent insensitivity of the vibrational (ir and especially Raman) techniques one needs to use other approaches if they are to be applied to high temperature vapour phase species.

Closed cells are usually used because they allow one to get a high enough vapour pressure of the sample into the spectrometer beam so that a sufficiently good signal to noise ratio can be achieved. It is also possible to study the effects of pressure and temperature on the spectra using such closed cells. However, the closed cells are the main source of problems in as much that the cell container must be unreactive towards the vapour under study and also withstand the elevated temperatures required. These problems are aggravated when one considers the window materials, and in addition to being unreactive must also be transparent to either the infrared or visible radiation used.

This problem is more acute in ir than in Raman gas phase studies (30,31) where glass or silica can be used both as cell and window because both the exiting and scattered light can be in the visible region. In either case the sensitivity at high temperatures is limited by the problem of emission from the hot cells.

The use of coherent Raman techniques such as coherent anti Stokes Raman spectroscopy (CARS)(32) is especially useful for gases at high temperatures because it can discriminate the coherent sample signal from the background radiation.

It is arguably the case that the most difficult and awkward part of high temperature gas phase spectroscopy (eg microwave, ir, Raman etc) is not the actual recording and storage of the data but the interpretation of it. This is because at the elevated temperatures there will be appreciable population of energy levels other than those of the ground state. Therefore the spectrum will consist of many more transitions than just the fundamentals because of hot bands, overtones and combination bands etc.

To try to overcome this problem of an over-abundance of data, gas phase molecules have been "cooled" so that only the ground state, or a very few energy levels are populated. There are two main ways of doing this, namely supersonic expansion of molecular beams or matrix isolation.

In a supersonic expanded molecular beam the sample is seeded in an excess of helium or argon, and then expanded through a small nozzle into a high vacuum. After further treatment (such as skimming and collimating) the beam is investigated, usually by laser induced fluorescence (LIF)(33). The molecules in the supersonic beam have rotational temperatures of about 10K and vibrational temperatures of approximately 100K. Therefore if the molecule fluoresces, the spectrum will contain information about the electronic, vibrational and rotational states. The advantage this has over matrix isolation is that the molecules are "free" and therefore not constrained by the rigid matrix which will perturb the energy levels and may distort the geometry. However, matrix isolation is a much easier experiment to perform, both experimentally and financially.

Matrix isolation lowers the complexity of the spectra for two main reasons. Firstly it keeps the molecules from rotating, so no rotational transitions are observed. Secondly, because the sample is maintained at cryogenic (10K) temperatures the molecule will almost certainly be in its ground state. The maintenance of the sample at these temperatures in a rigid matrix also enables one to study species that would normally only have a transient existence.

Matrix isolation is essentially about keeping the moeities of interest sufficiently far apart so that they can be regarded as being free and <u>not</u> in the condensed phase. This can be partially achieved in solution, but in addition to the interaction with the solvent, the solute molecules are free to move and react, even at very high dilutions. If the solution is frozen, then this movement is severely restricted and one has species that could be considered to be matrix isolated. Indeed this was how the first matrix experiments were carried out by Lewis in 1941(34) who used rigid glassy media to study the phosphorescence of aromatic molecules. Many experiments, (especially esr and epr) still use this method but they are not usually considered to be matrix experiments by today's criteria.

Porter(35) and Pimentel(36) suggested independently in 1954 that the rare gases at cryogenic temperatures could be used to study reactive, unstable radicals in the form of matrix isolated species.

It has recently been reported ([37]) that Pimentel and Whittle first conceived of the idea of matrix isolation one lunchtime in 1951 whilst eating sandwiches in Pimentel's office. This suggestion was vigorously pursued by Pimentel and his group([38]) who introduced chemically inert matrices to the world for the ir study of reactive species.

The application of matrix isolation to high temperature systems was suggested by Pimentel([39]) and pioneered by Linevsky([40]) in his work on lithium fluoride vaporised at 900°C and trapped in nitrogen and noble gas matrices.

As a result of its advantages over other methods, matrix isolation techniques have become common place and almost a routine spectroscopic tool and therefore reviewed extensively([41], [42], [43]). This popularity is evident by the bulk of literature reports (3326 papers up to 1985) in a recent review([44]).

The most widely used spectroscopic technique to characterise matrix isolated species is infra red (ir) vibrational spectroscopy.([45]) This is employed in this work and has been considered in detail in Chapter 2. However we will consider briefly the results obtainable. Because the rotational features in the spectrum have been removed, no moment of inertia data is directly available. The other side of the coin is that the transitions are sharp (~ $1 cm^{-1}$ fwhm) and therefore isotopic data can be resolved and used to generate a force field which in turn can lead to structural information.

Raman vibrational spectroscopy([46]) allows one to measure the Raman active fundamentals. This may confirm whether the molecule has an inversion centre and is especially valuable when only limited isotope data (eg fluorine compounds) is available from the corresponding matrix ir experiments. Raman matrix experiments are generally harder to carry out than their ir counter parts because of the inherent weakness of the Raman effect and the problem of scattering by the matrices. The resolution is usually lower because larger slit widths are required due to the weakness of the signal. The introduction of tunable lasers and fibre optics will ease these problems, but matrix Raman will probably never be as routine as matrix ir. A further point to note is that the concentration of the species of interest in the matrix is conventionally an order of magnitude higher in the Raman experiments than the ir, so confusion may arise over the assignment of monomeric and polymeric features between the two experiments.

Uv-Vis spectroscopy(47) can be used to identify the electronic transitions in the isolated species, but because of the broadness of the bands it is not a very good way of characterising unknown species. This can be surmounted by more accurate MO-calculations(47). However, when the experiments are carried out in conjunction with mass spectrometry and matrix ir(47) the features can be assigned and the vibrational progressions may give an indication of the value of the symmetric stretching fundamentals.

The use of magnetic circular dichroism (MCD)(49) and magnetic linear dichroism (MLD)(50) can ease the problems of broad featureless absorption bands. In MCD one records the difference in absorbance of light circularly polarised in the left and right directions in the presence of a magnetic field, whereas with MLD it is light polarised parallel and perpendicularly that is resolved. Therefore it is much easier to detect the presence of overlapping bands and their centres.

Matrix photoacoustic(51) spectroscopy can be used to interrogate the non-radiative release of electronic exitation energy and this is particularly advantageous for the study of non-luminescent polyaromatics.

Electron spin or electron paramagnetic resonance (esr or epr) is a very sensitive technique for detecting low concentrations of species containing unpaired electrons. These species can range from organic radicals to paramagnetic metal complexes. Although the technique is limited by its very nature, it has proved very useful in characterising high temperature species(52). The interaction of the unpaired electron with the nuclear spin of an atom with which it is associated leads to the hyperfine coupling(A). From this it is possible to identify which atoms the unpaired electron is associated with, and hence gives an indication of the atoms in the species of interest. The value of A can also give information about spin densities and thus bonding properties. The principal information from esr/epr experiments is the value of the g tensor. Because this is orientation dependent and the trapped species cannot rotate, information about the orientation of the species in the matrix can thus be obtained. If the molecules are randomly orientated then there will be no change in the relative intensities of g_x, g_y or g_z on rotating the sapphire or copper cold support. However if they are orientated then the relative intensities will vary.

The magnetic resonance technique used most widely in the liquid and solid state, namely nuclear magnetic resonance (nmr) has much less applicability to matrix isolated species. Indeed there are only two published reports of work involving matrix nmr, one using natural abundance ^{13}C nmr of matrix isolated ethylene(53) and the other a proton nmr spectrum of HCl monomers and dimers(54).

Mössbauer spectroscopy(55) of matrix isolated species can yield information on their oxidation state, co-ordination number and the symmetry of the environment of the Mössbauer active nuclei. This information is available from the isomer shift, the electric quadrupole interactions and magnetic interactions.

Whenever one carries out matrix isolation experiments, the dichotomy of having enough sample to detect above the background yet it being sufficiently well isolated has to be faced. Under "normal" laboratory conditions this precludes the use of some methods, however with the advent of synchrotron storage rings several, including UVPES and EXAFS have become possible.

The UVPES(56) experiments allow one to probe the bonding and electronic parameters in the species of interest in molecular orbital terms in a similar manner to gas phase PES.

Extended x-ray absorption fine structure (EXAFS) spectroscopy is a powerful way of investigating the local environment of a particular atom by studying either its K or L absorption edges. Thus in matrix isolation work this should allow the determination of bond lengths and angles directly, rather than via calculations and assumptions. Presently, it is used predominantly to study small metal clusters(57) and rare gases(58) although it is proposed to use it for the characterisation of high temperature inorganic species and in particular to try and resolve the problems over whether dihalides and dioxides are linear or bent.(59)

Although the rare gases themselves have been studied by x-ray diffraction at low temperatures it is only a recent suggestion(59) to study matrix isolated species by x-ray and neutron diffraction.

Knözinger et al (60) also suggest that inelastic neutron scattering could be used to gain valuable information on the low frequency vibrational modes that are either beyond the range of ir and Raman instruments, or, more importantly are non-active.

Another recent development is the use of spatially resolved matrix isolation (61) which utilises a photodiode array as a detector. Therefore it is possible to observe the effects of photolysis by only irradiating a small part of the matrix. At present it is limited to visible spectroscopy but one anticipates its rapid expansion into other spectral regions.

The identity of the trapped species usually has to be inferred from the spectroscopic data achieved by the above techniques. If however the species in the matrix can be characterised mass spectrometrically, then the spectral intepretation will be more accurate. There are essentially two ways of carrying this out:

a) the species can be sampled prior to or during deposition or boil off,

b) they can be sampled directly from the matrix environment.

We presently use a variation of the first method, where the sampling is carried out on two different instruments but there is a minimum of contamination. It is planned(62) in the near future to construct a combined matrix ir, mass spectrometry system to sample the molecular beam by both techniques simultaneously.

The second method makes use of secondary ion mass spectrometry (SIMS). A beam of energetic primary ions strikes the matrix and sputters and ionises the solid particles off the surface. It can also be used for depth profiling of the matrix. The only apparent report of this(63) is a SIMS study of a propane:argon 1:150 matrix at 10K.

References

1. Merten U. and Bell W.E.
Chapter 4 in "The Characterisation of High Temperature Vapours", ed Margrave, Wiley, 1967.

2. Sanders D.M., Haller W.K.
NBS Special Report, 561/1, 111, 1978.

3. Carlson K.D. Chapter 5 in reference 1.

4. Paule R.C. and Margrave J.L.
Chapter 6 in reference 1.

5. Cater E.D.
NBS Special Report, 561/1, 3, 1978.

6a. Margrave J.L. and Randall S.P.
J. Chem. Phys., 60, 715, 1956.

b. Randall S.P. and Margrave J.L.
J. Inorg. Nucl. Chem., 16, 29, 1960.

7. Grimley R.T.
Chapter 8 in reference 1.

8. Spiridonov V.P. and Zasorin E.Z.
NBS Special Report, 561/1, 711, 1978.

9. Akishin P.K., Rambidi N.G. and Spiridonov V.P.
Chapter 12 in reference 1.

10a. Hargittai I., Tremmel J. and Kalonits M.
Hung. Sci. Inst., 1980/50, 31.

b. Tremmel J. and Hargittai I.
Hung. Sci. Inst., 1980/50, 43.

c. Hargittai I., Bohatka S., Tremmel J. and Berez I.
Hung. Sci. Inst., 1980/50, 51.

11. Hargittai I. and Tremmel J.
Coord. Chem. Revs., 18, 257, 1976.

12. Zasorin E.Z., Rambidi N.G.
Zh. Strukt. Khim., 8, 931, 1967.

13. Odgen J.S. and Wyatt R.S.
J. Chem. Soc. Dalton Trans., 1987, 859.

14. Beattie I.R., Jones P.J., Willson A.D. and Young N.A.
J. Chem. Soc. Dalton Trans. in Press.

15. Hargittai M., Dorofeeva O.V. and Tremmel J.
Inorg. Chem., 24, 3963, 1985.

16. Stearns C.A., Kohl F.J., Fryburg G.G. and Miller R.A.
NBS Special Report, 561/1, 303, 1978.

17. Kuchitsu K.
p148 in "Molecular Structures and Vibrations".
ed S J Cyvin, Elsevier 1972.

18. Kuchitsu K.
P183 in ref 17.

19a. Buchler A., Stauffer J.L., Klemperer W. and Wharton L.
J. Chem. Phys., 56, 5392, 1972.

b. Milne T.A. and Greene F.T.
Adv. High Temp. Chem., 2, 107, 1969.

20a. Muenter A.A., Dyke T.R., Falconer W.E. and Klemperer W.
J. Chem. Phys., 63, 1231, 1975.

b. Mills I.M., Watson J.K.G. and Smith W.L.
Mol. Phys., 16, 329, 1969.

21. Barrett A.H. and Curl R.F.
Chapter 11 in ref 1.

22. Lovas F.J. and Lide D.R.
Adv. High Temp. Chem., 3, 177, 1971.

23. Torring T. and Tiemann E.
NBS Special Report, 561/1, 695, 1978.

24. Brassington N.J., Edwards H.G.M., Long D.A. and Skinner M.
J. Raman Spect., 7, 158, 1978.

25. Berkowitz J.
NBS Special Report, 561/1, 757, 1978.

26. Bowling R.A., Lassiter T.W., Vick D.O. and Schweitzer G.K.
NBS Special Report, 561/1, 771, 1978.

27. Berkowitz J.
Adv. High Temp. Chem., 3, 123, 1971.

28. Dyke J.M., Fayad N.K., Jossland G.D. and Morris A.
J. Chem. Soc. Farad. Trans. II, 76, 1672, 1980.

29. Dyke J.M.
J. Chem. Soc. Farad. Trans. II, 83, 69, 1987.

30. Drake M.C. and Rosenblatt G.M.
NBS Special Report, 561/1, 609, 1978.

31. Beattie I.R.
p111 "Essays in Structural Chem.".
Eds. Downs A.J., Long D.A. and Staveley L.A.K.
Macmillan, 1971.

32. Beattie I.R. and Greenhalgh D.A.
NBS Special Report, 561/1, 597, 1978.

33. Millington K.R.
PhD Thesis, Southampton University, 1987.

34. Lewis G.N. and Lipkin D.
J. Am. Chem. Soc., 64, 2801, 1942.

35. Norman I. and Porter G.
Nature, 174, 508, 1954.

36. Whittle E., Dows D.A. and Pimentel G.C.
J. Chem. Phys., 22, 1943, 1954.

37. Chemistry in Britain, 24, 201, 1988.

38. Becker E.D. and Pimentel G.C.
J. Chem. Phys., 25, 224, 1956.

39. Pimentel G.C.
p109 in "Formulation and Trapping of Free Radicals" ed
A. M. Bass and H. P. Broida. Academic Press NY 1960.

40. Linevsky M.J.
J. Chem. Phys., 34, 587, 1961.

41. Downs A.J. and Peake S.C.
Mol. Spect., 1, 523, 1973.

42. Chadwick B.M.
Mol. Spect., 3, 281, 1975.

43. Chadwick B.M.
Mol. Spect., 6, 72, 1979.

44. Ball D.M., Kafafi Z., Hauge R.H. and Margrave J.L.
"The Bibliography of Matrix Isolation". Rice University Press. December 1987.

45. "Vibrational Spectroscopy of Trapped Species".
Ed H. E. Hallam, Wiley 1973.

46. Andrews L.
Conf. Int. Spect. Raman 7th., 1980, p160.

47. Rest A.J.
Nato Adv. Study Ser., C76, 27, 1981.

48. Hope E.G., Levason W. and Ogden J.S.
J. Chem. Dalton Trans. 1988, 61 and 1988, 997.

49. Grinter R.
Nato Adv. Study Ser., C76, 49, 1981.

50. Vala M., Revoal J.C., Grisolia G. and Pyka J.
J. Chem. Phys., 82, 4376, 1985.

51a. Howell H.E., Mamantor G., Wehry E.L. and Shaw R.W.
Anal. Chem., 56, 821, 1984.

b. Bozlec B.J. and Nibler J.W.
J. Chem. Phys., 84, 783, 1986.

52a. Weltner W.
Ber. Bunsen., 82, 80, 1978.

b. Symons M.C.R.
Nato Adv. Study Ser., C76, 69, 1981.

53. Zilm K.W., Conlin R.T., Grant D.M. and Michl J.
J. Am. Chem. Soc., 100, 8038, 1978.

54. Kohl J.E., Semack M.G. and White D.
J. Chem. Phys., 69, 5378, 1978.

55. Micklitz H.
NATO Adv. Study Ser., C76, 91, 1981.

56. Rotermund H.H. and Kolb D.M.
Surf. Sci., 156, 785, 1985.

57a. Montano P.A. and Shenoy G.K.
Solid State. Comm., 35, 53, 1980.

b. Purdman H., Montano P.A., Shenoy G.K. and Morrison T.
Phys. Rev., 25B, 4412, 1982.

c. Montano P.A., Schulze W., Tesche B., Shenoy G.K. and Morrison T.
Phys. Rev., 30B, 672, 1984.

d. Niemann W., Malzfeldt W., Rabe P., Haensel R. and Lubcke M.
Phys. Rev., 35B, 1099, 1987.

58a. Malzfeldt W., Niemann W., Rabe P. and Schwenter N.
Springer Series in Chem. Phys., 27, 203, 1983.

b. Malzfeldt W., Niemann W. and Haensel R.
Springer Proc. Phys., 2, 445, 1984.

59. Beattie I.R. and Young N.A.
Unpublished Observations 1988.

60. Langel W., Kollhoff H., Knözinger E. and Prayer M.
Ber. Bungsen. Physik. Chem., 91, 1257, 1987.

61. Lang V.I. and Winn J.S.
Rev. Sci. Inst., 56, 2209, 1985.

62. Brisdon A.K. and Ogden J.S.
University of Southampton, Personal Comm. 1987.

63. Jonkman H.T. and Michl J.
J. Chem. Soc. Chem. Comm., 1978, 751.

APPENDIX B

EXAMPLE CONSTRUCTION OF G MATRIX AND F MATRIX

In Chapter 3 it was shown how $\underline{F}$ and $\underline{G}$ matrices are used in the analysis of data from vibrational spectroscopy. In this Appendix the "mechanics" of their derivation will be outlined in order to illuminate the principles in Chapter 3. The example, as previously will be the bent XY_2 molecule as defined in Figure 1. Recalling equations 37 and 39 in Chapter 3 we can see that

$$\underline{G} = \underline{B}\ \underline{M}^{-1}\ \underline{\tilde{B}}$$

and $\underline{R} = \underline{BX}$

Therefore in order to calculate $\underline{B}$ we need to know how the cartesian displacement co-ordinates (Figure 1(b)) are transformed into internal co-ordinate displacements (Figure 1(a)). That is we need to express Δr_1, Δr_2 and $\Delta\alpha$ in terms of Δx_1, Δx_2, Δz_1 etc. In this example we do not need to consider Δy_i as any displacement in this direction is perpendicular to the internal co-ordinates, and will hence not result in any change of them.

The method employed in this thesis is illustrated in Fig 1(b) where the effect of Δx_1 is shown upon Δr_1. In this case $\Delta r_1 = - \Delta x_1 \sin(\alpha/_2)$. If this procedure is applied to all the internal co-ordinates then the following result.

$$\Delta r_1 = - \Delta x_1 \sin\alpha/_2 - \Delta z_1 \cos\alpha/_2 + \Delta x_2 \sin\alpha/_2 + \Delta z_2 \cos\alpha/_2$$

$$\Delta r_2 = - \Delta x_2 \sin\alpha/_2 + \Delta z_2 \cos\alpha/_2 + \Delta x_3 \sin\alpha/_2 - \Delta z_3 \cos\alpha/_2$$

$$\Delta\alpha = - \frac{\Delta x_1 \cos\alpha/_2}{r_1} + \frac{\Delta z_1 \sin\alpha/_2}{r_1} + \frac{\Delta x_3 \cos\alpha/_2}{r_2} + \frac{\Delta z_3 \sin\alpha/_2}{r_2}$$
$$- \frac{\Delta x_2 \cos\alpha/_2}{r_1} + \frac{\Delta x_2 \cos\alpha/_2}{r_2} - \frac{\Delta z_2 \sin\alpha/_2}{r_1} - \frac{\Delta z_2 \sin\alpha/_2}{r_2}$$

Having calculated the elements of the $\underline{B}$ matrix we are now in a position to calculate the $\underline{G}$ matrix using

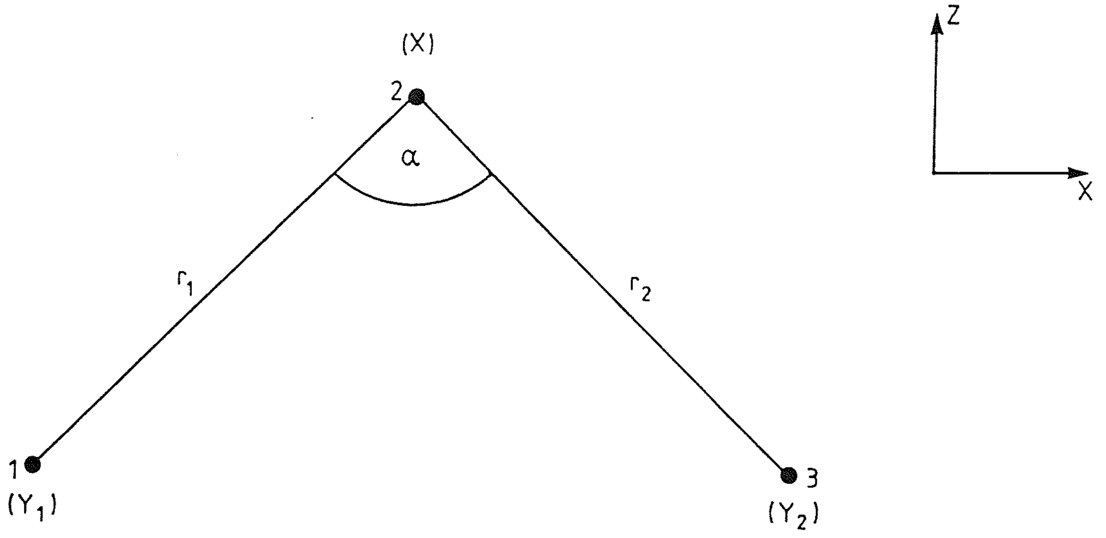

(a) INTERNAL CO-ORDINATES

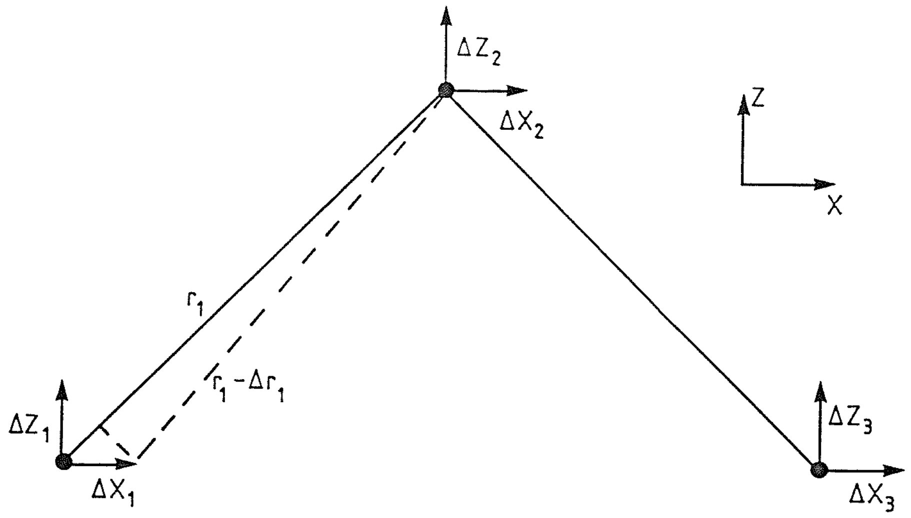

(b) CARTESIAN DISPLACEMENT CO-ORDINATES

FIG. 1 DEFINITIONS OF CO-ORDINATES USED IN THE FG ANALYSIS OF XY_2 MOLECULES

$$\underline{G} = \underline{B}\ \underline{M}^{-1}\ \underline{\tilde{B}}$$

this however is more conveniently done by constructing column matrices and using equation 40

$$G_{tt'} = \sum_{i=1}^{3N} ({}^{1}/_{M_i})\ B_{ti}\ B_{t'i}$$

This can be done for both the C_s case ($Y_1 \neq Y_2$) and the C_{2v} case ($Y_1 = Y_2$). In the former case the column matrices are made up of the cartesian displacements of Δr_1, Δr_2 and $\Delta\alpha$, whereas in the latter the column matrices are comprised of the cartesian displacements for the symmetry co-ordinates. We shall consider the case for the $C_s, Y_1 - X - Y_2$, molecule first and then use the symmetry co-ordinates available to simplify the calculations. The $\underline{G}$ matrix elements for C_s can obviously be used for the C_{2v} species but not vice versa.

	Δr_1	Δr_2	$\Delta\alpha$
Δx_1	$-\sin\alpha/_2$	0	$-(\cos\alpha/_2)/r_1$
Δz_1	$-\cos\alpha/_2$	0	$(\sin\alpha/_2)/r_1$
Δx_2	$\sin\alpha/_2$	$-\sin\alpha/_2$	$-\dfrac{\cos\alpha/_2}{r_1} + \dfrac{\cos\alpha/_2}{r_2}$
Δz_2	$\cos\alpha/_2$	$\cos\alpha/_2$	$-\dfrac{\sin\alpha/_2}{r_1} - \dfrac{\sin\alpha/_2}{r_2}$
Δx_3	0	$\sin\alpha/_2$	$(\cos\alpha/_2)/r_2$
Δz_3	0	$-\cos\alpha/_2$	$(\sin\alpha/_2)r_2$

The individual $\underline{G}$ matrix elements are then defined as:

$$G_{11} = \mu_{Y_1}\ (\sin^2\alpha/_2 + \cos^2\alpha/_2) + \mu_X\ (\sin^2\alpha/_2 + \cos^2\alpha/_2)$$

$$= \mu_{Y_1} + \mu_X$$

$$G_{22} = \mu_X\ (\sin^2\alpha/_2 + \cos^2\alpha/_2) + \mu_{Y_2}(\sin^2\alpha/_2 + \cos^2\alpha/_2)$$

$$= \mu_X + \mu_{Y_2}$$

$$G_{33} = \frac{\mu_{Y_1}}{{r_1}^2}\ (\cos^2\alpha/_2 + \sin^2\alpha/_2) + \frac{\mu_{Y_2}}{{r_2}^2}\ (\cos^2\alpha/_2 + \sin^2\alpha/_2)$$

$$+ \mu_X\left(\left\{\frac{-\cos\alpha/_2}{r_1} + \frac{\cos\alpha/_2}{r_2}\right\}^2 + \left\{\frac{-\sin\alpha/_2}{r_1} - \frac{\sin\alpha/_2}{r_2}\right\}^2\right)$$

$$= \frac{\mu_{Y_1}}{{r_1}^2} + \frac{\mu_{Y_2}}{{r_2}^2} + \mu_X\left\{\frac{1}{{r_1}^2} + \frac{1}{{r_2}^2} - \frac{2\cos\alpha}{r_1 r_2}\right\}$$

$$G_{12} = G_{21} = \mu_X\ (\cos^2\alpha/_2 - \sin^2\alpha/_2)$$

$$= \mu_X\ \cos\alpha$$

$$G_{13} = G_{31} = -\ \frac{\mu_X\ \sin\alpha}{r_1}$$

$$G_{23} = G_{32} = -\ \frac{\mu_X\ \sin\alpha}{r_2}$$

$$\underline{G} = \begin{bmatrix} \mu_x + \mu_{y_1} & \mu_x \cos\alpha & \dfrac{-\mu_x \sin\alpha}{r_1} \\ \mu_x \cos\alpha & \mu_x + \mu_{y_2} & \dfrac{-\mu_x \sin\alpha}{r_2} \\ \dfrac{-\mu_x \sin\alpha}{r_1} & \dfrac{\mu_x \sin\alpha}{r_2} & \mu_x \left(\dfrac{1}{r_1^2} + \dfrac{1}{r_2^2} - \dfrac{2\cos\alpha}{r_1 r_2}\right) \\ & & + \dfrac{\mu_{y_1}}{r_1^2} + \dfrac{\mu_{y_2}}{r_2^2} \end{bmatrix}$$

if $r_1 = r_2$ then the $\underline{G}$ matrix is given by:

$$\underline{G} = \begin{bmatrix} \mu_x + \mu_{y_1} & \mu_x \cos\alpha & -\dfrac{\mu_x \sin\alpha}{r} \\ \mu_x \cos\alpha & \mu_x + \mu_{y_2} & -\dfrac{\mu_x \sin\alpha}{r} \\ -\dfrac{\mu_x \sin\alpha}{r} & \dfrac{-\mu_x \sin\alpha}{r} & \dfrac{2\mu_x}{r^2}(1-\cos\alpha) + \dfrac{\mu_{y_1} + \mu_{y_2}}{r^2} \end{bmatrix}$$

If the molecule possess C_{2v} symmetry then $r_1 = r_2$ and $y_1 = y_2$ and we can make use of the symmetry co-ordinates to simplify the problem. The symmetrised $\underline{F}$ and $\underline{G}$ matrices are denoted as $\underline{F}_s$ and $\underline{G}_s$

$$S_1 = \frac{1}{\sqrt{2}} (\Delta r_1 + \Delta r_2)$$

$$S_2 = \Delta\alpha$$

$$S_3 = \frac{1}{\sqrt{2}} (\Delta r_1 - \Delta r_2)$$

ie:

	S_1	S_2	S_3
Δx_1	$-\sin\alpha/_2$	$(-\cos\alpha/_2)/r$	$-\sin\alpha/_2$
Δz_1	$-\cos\alpha/_2$	$(\sin\alpha/_2)/r$	$-\cos\alpha/_2$
Δx_2	0	0	$2\sin\alpha/_2$
Δz_2	$2\cos\alpha/_2$	$(-2\sin\alpha/_2)/r$	0
Δx_3	$\sin\alpha/_2$	$(\cos\alpha/_2)/r$	$-\sin\alpha/_2$
Δz_3	$-\cos\alpha/_2$	$(\sin\alpha/_2)/r$	$\cos\alpha/_2$

The individual G matrix elements are constructed as before to give:

$$G_{11} = \frac{1}{2}\left[\mu_y\,(\sin^2\alpha/_2 + \cos^2\alpha/_2) + \mu_x\,4\cos^2\alpha/_2\right.$$

$$\left. + \mu_y\,(\sin^2\alpha/_2 + \cos^2\alpha/_2)\right]$$

$$= \mu_y + \mu_x(1 + \cos\alpha)$$

$$G_{22} = \frac{2\mu_y}{r^2} + \frac{2\mu_x}{r^2}\,(1 - \cos\alpha)$$

$$G_{33} = \mu_y + \mu_x\,(1 - \cos\alpha)$$

$$G_{12} = \frac{1}{\sqrt{2}}\left\{\frac{2\mu_y}{r}\,(\sin\alpha/_2\,\cos\alpha/_2 - \sin\alpha/_2\,\cos\alpha/_2)\right.$$

$$\left. - \frac{4\mu_x}{r}\,\cos\alpha/_2\,\sin\alpha/_2\right\}$$

$$= \frac{-\sqrt{2}}{r}\,\mu_x\,\sin\alpha = G_{21}$$

$$G_{13} = \frac{1}{2}\,[\mu_y\,(\sin^2\alpha/_2 + \cos^2\alpha/_2) - \mu_y\,(\sin^2\alpha/_2 + \cos^2\alpha/_2)]$$

$$= 0 = G_{31}$$

$$G_{23} = \frac{1}{2}\,[\mu_y\,(\sin\alpha/_2\,\cos\alpha/_2 - \sin\alpha/_2\,\cos\alpha/_2)$$

$$+ \mu_y\,(-\cos\alpha/_2\,\sin\alpha/_2 + \sin\alpha/_2\,\cos\alpha/_2)]$$

$$= 0 = G_{32}$$

$$\underline{G}_s = \begin{bmatrix} \mu_y+\mu_x\,(1+\cos\alpha) & \frac{-\sqrt{2}}{r}\,\mu_x\,\sin\alpha & 0 \\ \frac{-\sqrt{2}}{r}\,\mu_x\,\sin\alpha & \frac{2\mu_y}{r^2} + \frac{2\mu_x}{r^2}\,(1-\cos\alpha) & 0 \\ 0 & 0 & \mu_y+\mu_x\,(1-\cos\alpha) \end{bmatrix}$$

In this format we can see how the original 3 x 3 $\underline{G}$ matrix in C_s symmetry has been reduced to a 2 x 2 and a 1 x 1 matrix for C_{2v} symmetry.

In order to carry out a Wilson FG analysis we need to define the $\underline{F}$ matrices for each case. For the C_s examples this is relatively straight forward and they are given below as quoted in Chapter 3.

$$\underline{F} = \quad (\text{for } r_1 \neq r_2) \quad \begin{bmatrix} f_{r_1} & f_{r_1 r_2} & r_1 f_{r_1 \alpha} \\ f_{r_1 r_2} & f_{r_2} & r_2 f_{r_2 \alpha} \\ r_1 f_{r_1 \alpha} & r_2 f_{r_2} & r_1 r_2 f_{\alpha} \end{bmatrix}$$

$$\underline{F} = \quad (\text{for } r_1 = r_2) \quad \begin{bmatrix} f_r & f_{rr} & r f_{r\alpha} \\ f_{rr} & f_r & r f_{r\alpha} \\ r f_{r\alpha} & r f_{r\alpha} & r^2 f_{\alpha} \end{bmatrix}$$

for the C_{2v} case we need to use the same $\underline{U}$ matrix that gives $\underline{G}_s = \underline{U}\ \underline{G}\ \underline{\tilde{U}}$ and $\underline{F}_s = \underline{U}\ \underline{F}\ \underline{\tilde{U}}$

$F_s = \underline{U F \tilde{U}}$

$$\underline{U} = \begin{bmatrix} 1/\sqrt{2} & 0 & 1/\sqrt{2} \\ 0 & 1 & 0 \\ 1/\sqrt{2} & 0 & -1/\sqrt{2} \end{bmatrix} = \underline{\tilde{U}}$$

$$\therefore \quad \underline{F_s} = \begin{bmatrix} f_r + f_{rr} & r\sqrt{2}f_{r\alpha} & 0 \\ r\sqrt{2}f_{r\alpha} & r^2 f_{\alpha} & 0 \\ 0 & 0 & f_r - f_{rr} \end{bmatrix}$$

APPENDIX C

DERIVATION OF THE F AND G MATRICES FOR THE TORSIONAL MODES IN BORIC ACID

In Chapter 6 use was made of F and G matrices to confirm the torsional frequency assignments in boric acid. The derivation of these is presented in this Appendix.

If we define the general case as illustrated in Figure 1 then the torsional angle $\tau = \phi_1 + \phi_2$

and $\Delta\tau = \Delta\phi_1 + \Delta\phi_2$

Therefore we need to determine the effect on τ of the displacements in the x and z directions of the atoms A, B, C and D. The displacements in the y direction do not need to be considered because they are perpendicular to the torsion angles and will thus not result in any change in this internal co-ordinate.

For the case of the terminal atoms A and D determining the effect of the cartesian displacements on $\Delta\phi_1$ and $\Delta\phi_2$ is relatively simple and by using the methods outlined in the previous appendix we can arrive at

$$\Delta\phi_1 = -\left\{\frac{z_A \sin\phi_1}{a\sin\beta} + \frac{x_A \cos\phi_1}{a\sin\beta}\right\}$$

$$\text{and } \Delta\phi_2 = -\left\{\frac{z_D \sin\phi_2}{c\sin\alpha} - \frac{x_D \cos\phi_2}{c\sin\alpha}\right\}$$

The case for the central atoms B and C is more complicated but by careful application of the procedures outlined one can arrive at

$$\Delta\phi_1 = \frac{z_B \sin\phi_1 (b - a\cos\beta) + x_B \cos\phi_1 (b - a\cos\beta)}{ab\sin\beta} + \frac{z_C \sin\phi_1 + x_C \cos\phi_1}{b\tan\beta}$$

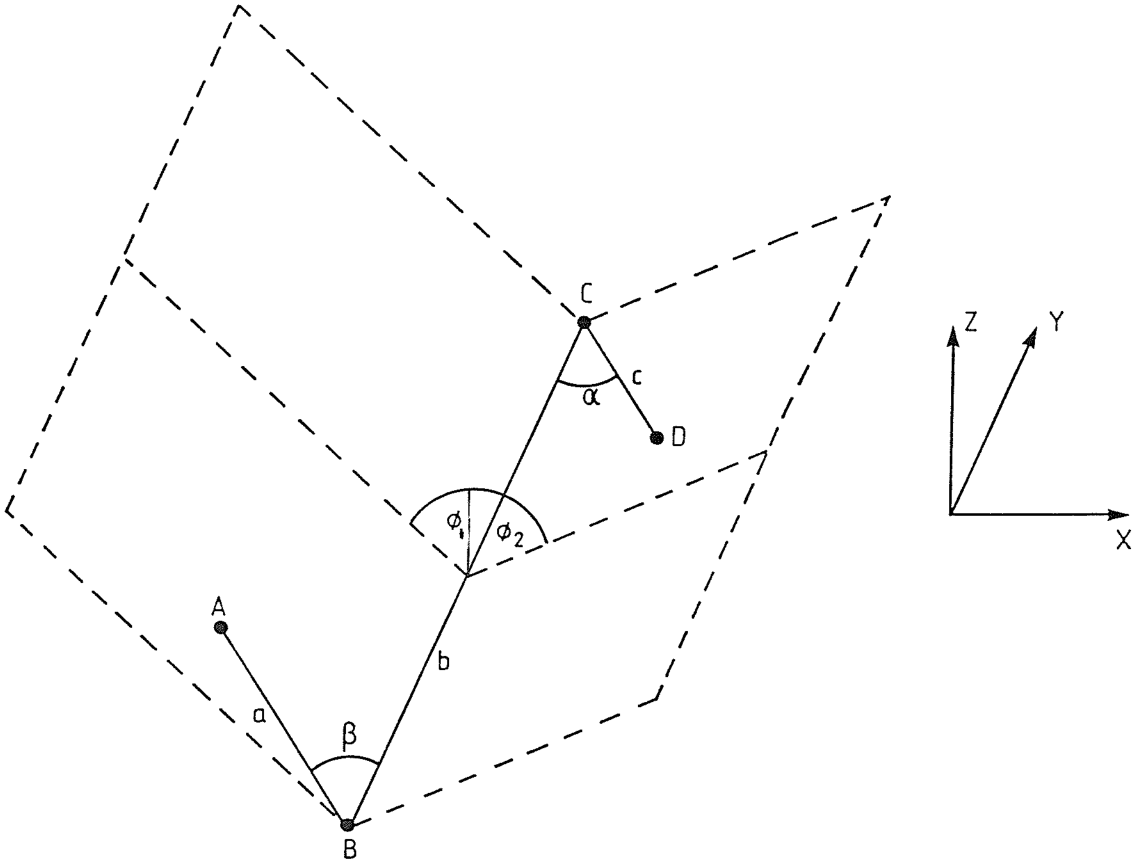

FIG. 1 DEFINITION OF CO-ORDINATES USED IN THE ANALYSIS OF TORSION MODES

$$\Delta\phi_2 = \left\{\frac{b - c\cos\alpha}{b}\right\} \times \left\{\frac{z_C \sin\phi_2 - x_C \cos\phi_2}{c\sin\alpha}\right\} + \frac{z_B \sin\phi_2 - x_B \cos\phi_2}{b \tan\alpha}$$

Therefore the total $\Delta\phi$'s are given by.

$$\Delta\phi_1 = -\frac{(z_A \sin\phi_1 + x_A \cos\phi_1)}{a\sin\beta} + \frac{b - a\cos\beta}{ab\sin\beta}\left(z_B\sin\phi_1 + x_B \cos\phi_1\right) + \frac{z_C \sin\phi_1 + x_C \cos\phi}{b \tan\beta}$$

$$\Delta\phi_2 = -\left(\frac{z_D \sin\phi_2 - x_D \cos\phi_2}{c\sin\alpha}\right) + \frac{b - c\cos\alpha}{bc\sin\alpha}\left(z_C\sin\phi_2 - x_C \cos\phi_2\right) + \frac{z_B \sin\phi_2 - x_B \cos\phi_2}{b\tan\alpha}$$

Therefore $\Delta\tau$ is expressed as

$$\Delta\phi_1 + \Delta\phi_2$$

$$= -\frac{x_A\cos\phi_1 - z_A\sin\phi_1}{a\sin\beta} + \frac{b - a\cos\beta}{ab\sin\beta}\left(z_B\sin\phi_1 + x_B\cos\phi_1\right) + \frac{z_C\sin\phi_1 + x_C\cos\phi_1}{b\tan\beta} + \frac{x_D\cos\phi_2 - z_D\sin\phi_2}{c\sin\alpha} + \frac{z_B\sin\phi_2 - x_B\cos\phi_2}{b\tan\alpha} + \frac{b - c\cos\alpha}{bc\sin\alpha}\left(z_C\sin\phi_2 - x_C\cos\phi_2\right)$$

This then is the general equation for expressing $\Delta\tau$ in terms of the displacements of the atoms. For boric acid however it can be simplified because both ϕ_1 and ϕ_2 are

90° as a result of the molecule being planar. Hence all the $\cos\phi_1$ and $\cos\phi_2$ terms are zero and $\Delta\tau$ now becomes,

$$\Delta\tau = \frac{-z_A}{a\sin\beta} + z_B\left\{\frac{b-a\cos\beta}{ab\sin\beta}\right\} + \frac{z_C}{b\tan\beta} - \frac{z_D}{c\sin\alpha} + \frac{z_B}{b\tan\alpha} + \left\{\frac{b-c\cos\alpha}{bc\sin\alpha}\right\}z_C$$

This is now the general expression for a torsion mode in a planar molecule. It will be noticed that all the x displacement components have been removed and this is because these can now be regarded as perpendicular to $\Delta\tau$.

If we define boric acid as in Figure 2, we can see that there are in fact three torsion modes $\Delta\tau_1$, $\Delta\tau_2$ and $\Delta\tau_3$ and by comparison with the definitions given earlier one can see that

	A	B	C	D	α	b	a	b	c
$\Delta\tau_1$	1	4	7	6	α	β	d	r	r
$\Delta\tau_2$	2	5	7	4	α	β	d	r	r
$\Delta\tau_3$	3	6	7	5	α	β	d	r	r

and

$$\Delta\tau_1 = \frac{-z_1}{a\sin\beta} + \frac{z_4}{b\tan\alpha} + z_4\left\{\frac{b-a\cos\beta}{ab\sin\beta}\right\} + \frac{z_7}{b\tan\beta} + z_7\left\{\frac{b-c\cos\alpha}{bc\sin\alpha}\right\} - \frac{z_6}{c\sin\alpha}$$

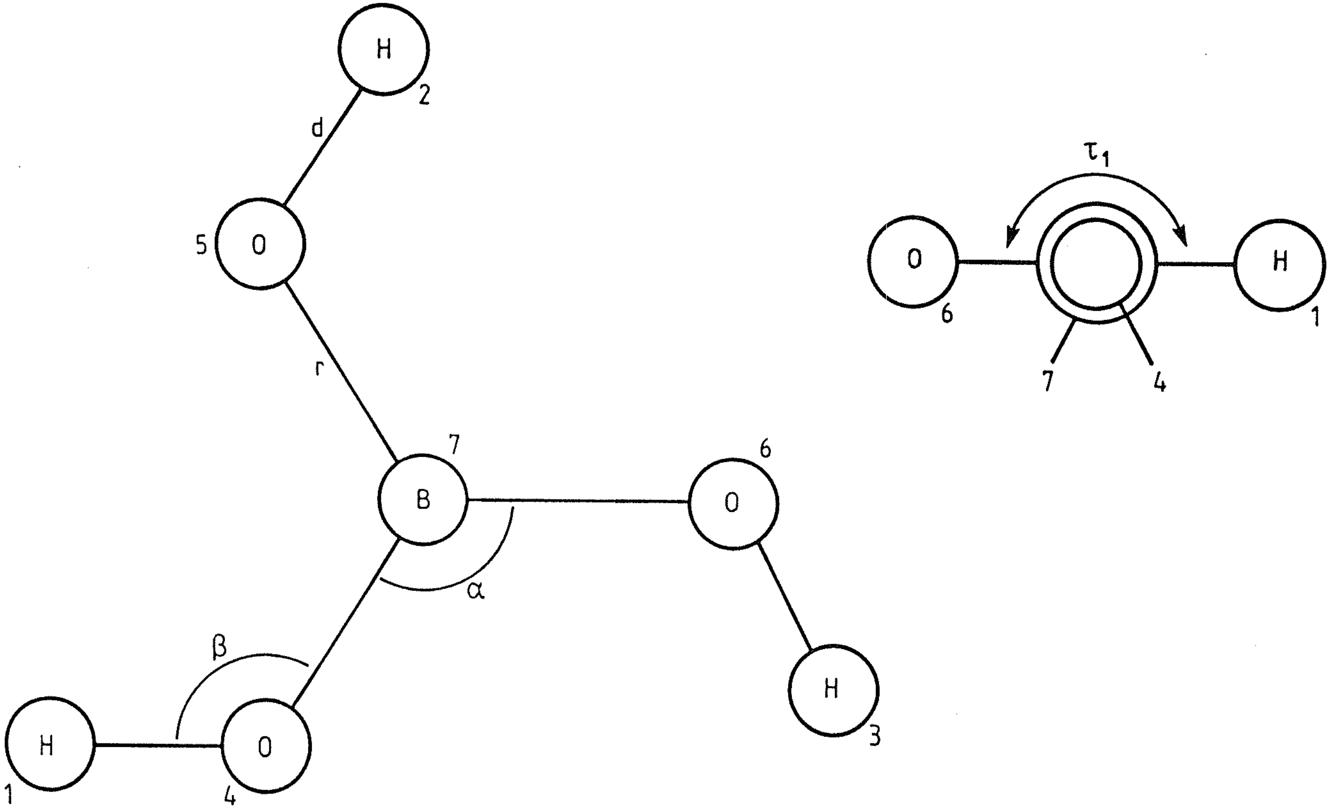

FIG.2 DEFINITION OF BORIC ACID USED IN THE FG ANALYSIS OF THE TORSION MODE

$$\Delta\tau_2 = \frac{-\ z_2}{a\sin\beta} + \frac{z_5}{b\tan\alpha} + z_5\left\{\frac{b-a\cos\beta}{ab\sin\beta}\right\} + \frac{z_7}{b\tan\beta}$$

$$+\ z_7\left\{\frac{b-c\cos\alpha}{bc\sin\alpha}\right\} - \frac{z_4}{c\sin\alpha}$$

$$\Delta\tau_3 = \frac{-\ z_3}{a\sin\beta} \quad \frac{+\ z_6}{b\tan\alpha} + z_6\left\{\frac{b-a\cos\beta}{ab\sin\beta}\right\} + \frac{z_7}{b\tan\beta}$$

$$+\ z_7\left\{\frac{b-c\cos\alpha}{b.c\sin\alpha}\right\} \frac{-\ z_5}{c\sin\alpha}$$

If the molecule possesses C_{3h} symetry, eg H_3BO_3, then symmetry co-ordinates can be used, but if the point group is C_s, eg H_2DBO_3 then these cannot be employed and the $\Delta\tau$'s have to be used. The symmetry co-ordinates can be derived in the usual way and are of the form.

$$S_1 = \frac{\sqrt{rd}}{\sqrt{3}}\,(\Delta\tau_1 + \Delta\tau_2 + \Delta\tau_3) \qquad \text{A}''$$

$$S_2 = \frac{\sqrt{rd}}{\sqrt{2}}\,(\Delta\tau_1 - \Delta\tau_2)$$

$$\text{E}''$$

$$S_3 = \frac{\sqrt{rd}}{\sqrt{6}}\,(2\Delta\tau_3 - \Delta\tau_1 - \Delta\tau_2)$$

Although the purpose of calculating the $\Delta\tau$'s for boric acid was to carry out calculations for isotopically enriched molecules, the $\underline{G}$ matrix elements were calculated for the C_{3h} species so that they could be compared with Cyvin's(1), and hence provide a check on our calculations.

In tabular form the symmetry co-ordinates are:

	$\sqrt{rd}S_1/\sqrt{3}$	$\sqrt{rd}S_2/\sqrt{2}$	$\sqrt{rd}S_3/\sqrt{6}$
z_1	$-1/a\sin\beta$	$-1/a\sin\beta$	$1/a\sin\beta$
z_2	$-1/a\sin\beta$	$1/a\sin\beta$	$1/a\sin\beta$
z_3	$-1/a\sin\beta$	0	$-2/a\sin\beta$
z_4	$\left(\frac{b-a\cos\beta}{ab\sin\beta}\right)+\frac{1}{b\tan\alpha}$ $-1/c\sin\alpha$	$\left(\frac{b-a\cos\beta}{ab\sin\beta}\right)+\frac{1}{b\tan\alpha}$ $+1/c\sin\alpha$	$(1/c\sin\alpha)-\left(\frac{b-a\cos\beta}{ab\sin\beta}+\frac{1}{b\tan\alpha}\right)$
z_5	$\frac{b-a\cos\beta}{ab\sin\beta}+1/b\tan\alpha$ $-1/c\sin\alpha$	$-\left(\frac{b-a\cos\beta}{ab\sin\beta}+\frac{1}{b\tan\alpha}\right)$	$\frac{-2}{c\sin\alpha}-\left(\frac{b-a\cos\beta}{ab\sin\beta}+\frac{1}{b\tan\alpha}\right)$
z_6	$\frac{b-a\cos\beta}{ab\sin\beta}+\frac{1}{b\tan\alpha}$ $-1/c\sin\beta$	$-1/c\sin\alpha$	$2\left(\frac{b-a\cos\beta}{ab\sin\beta}+\frac{1}{b\tan\alpha}\right)$ $+1/c\sin\alpha$
z_7	$3\left(\frac{b-c\cos\alpha}{bc\sin\alpha}+\frac{1}{b\tan\beta}\right)$	0	0

$G_{11} = S_1 \times S_1$ etc

$G_{12} = S_1 \times S_2$ etc

$$\therefore G_{11} = \frac{rd}{3}\left(\frac{3\mu_H}{a^2\sin^2\beta} + 3\mu_O\left\{\frac{b-a\cos\beta}{ab\sin\beta} + \frac{1}{b\tan\alpha} - \frac{1}{c\sin\alpha}\right\}^2 + 9\mu\beta\left\{\frac{b-c\cos\alpha}{bc\sin\alpha} + \frac{1}{b\tan\beta}\right\}^2\right)$$

This can be simplified because α = O-B-O = 120° and a = d and b = c = r

$$\therefore\ G_{11} = rd\left(\frac{\mu_H}{d^2\sin^2\beta} + \frac{\mu_0}{r^2}\left\{\frac{r}{d\sin\beta} - \cot\beta - \sqrt{3}\right\}^2 + \frac{3\mu_B}{r^2}\left\{\sqrt{3} + \cot\beta\right\}^2\right)$$

$$\rightarrow G_{11}\ \frac{r\mu_H}{d\sin^2\beta} + \frac{d\mu_0}{r}\left(\frac{r}{d\sin\beta} - \cot\beta - \sqrt{3}\right)^2 + \frac{3d}{r}\mu_B\left(\sqrt{3} + \cot\beta\right)^2$$

$$\therefore\ G_{22} = rd\left(\frac{\mu_H}{d^2\sin^2\beta} + \frac{\mu_0}{\sin^2\beta}\left\{\frac{1}{d^2} - \frac{2\cos\beta}{rd} + \frac{1}{r^2}\right\}\right)$$

$$\rightarrow G_{22} = \frac{r}{d}\,\frac{\mu_H}{\sin^2\beta} + \frac{\mu_0}{\sin^2\beta}\left\{\frac{r}{d} - 2\cos\beta + \frac{d}{r}\right\}$$

$G_{33} = G_{22}$

$G_{ij} = 0$ where $i \neq j$

the fact that $G_{22} = G_{33}$ and $G_{ij} = 0$ implies that we have carried out the calculations correctly but the further check is by comparison with those of Cyvin(1) et al.

The corresponding G matrix element to our G_{11} in Cyvin's paper is G_{55} and this is expressed as:

$$G_{55} = \frac{3D}{R}\left(\sqrt{3} + \cot B\right)^2\mu_B + \frac{R\mu_H}{D\sin^2 B}$$

$$+ \frac{\mu_0}{\sin^2 B}\left\{\frac{R}{D} + \frac{D}{R} + \frac{2D}{R}\sin B\left(\sqrt{3}\cos B + \sin B\right) - 2\left(\cos B + \sqrt{3}\sin B\right)\right\}$$

where $D = d$, $R = r$ and $B = \beta$

from inspection of the μ_H and μ_B terms it is clear that the two are identical, it therefore only remains to check the μ_0 term.

$$G_{11} = X\mu_H + Y\mu_B + \frac{d}{r}\mu_0\left(\frac{r}{d\sin\beta} - \cot\beta - \sqrt{3}\right)^2$$

$$= \frac{d}{r}\mu_0\left\{\frac{r^2}{d^2\sin^2\beta} - \frac{2r\cos\beta}{d\sin^2\beta} - \frac{2r\sqrt{3}}{d\sin\beta} + \cot^2\beta + 2\sqrt{3}\cot\beta + 3\right\}$$

$$= \frac{\mu_0}{\sin^2\beta}\left\{\frac{r}{d} - 2\cos\beta - 2\sqrt{3}\sin\beta + \frac{d\cos^2\beta}{r} + \frac{2d}{r}\sqrt{3}\cos\beta\sin\beta + \frac{3d}{r}\sin^2\beta\right\}$$

$$= \frac{\mu_0}{\sin^2\beta}\left\{\frac{r}{d} - 2(\cos\beta + \sqrt{3}\sin\beta) + \frac{2d\sqrt{3}}{r}\cos\beta\sin\beta + \frac{d}{r}\left(\cos^2\beta + 3\sin^2\beta\right)\right\}$$

$$= \frac{\mu_0}{\sin^2\beta}\left\{\frac{r}{d} - 2(\cos\beta + \sqrt{3}\sin\beta) + \frac{2d\sqrt{3}}{r}\cos\beta\sin\beta + \frac{d}{r} + \frac{2d}{r}\sin^2\beta\right\}$$

$$= \frac{\mu_0}{\sin^2\beta}\left\{\frac{r}{d} + \frac{d}{r} + \frac{2d}{r}\sin\beta(\sqrt{3}\cos\beta + \sin\beta) - 2(\cos\beta + \sqrt{3}\sin\beta)\right\}$$

and the μ_0 terms are now also shown to be equivalent.

By a similar approach it has been shown that our G_{22} is equivalent to Cyvins $G_{10,10}$.

Having confirmed that the C_{3h} G matrix elements were the same as those derived by Cyvin, those for the C_s species were then calculated using

$$G_{tt'} = \sum_{i=1}^{3N} (1/m_i)\, B_{ti}\, B_{t'i}$$

and are given as

$$G_{11} = \frac{\mu_{H_1}}{d^2\sin^2\beta} + \mu_{O_4}\left\{\frac{r-d\cos\beta}{rd\sin\beta} - \frac{1}{r\sqrt{3}}\right\}^2 + \mu_{O_6}\frac{4}{3r^2}$$

$$+ \frac{\mu_B}{r^2}\left(\sqrt{3} + \cot\beta\right)^2$$

$$G_{22} = \frac{\mu_{H_2}}{d^2\sin^2\beta} + \mu_{O_5}\left\{\frac{r-d\cos\beta}{rd\sin\beta} - \frac{1}{r\sqrt{3}}\right\}^2 + \mu_{O_4}\frac{4}{3r^2} +$$

$$\frac{\mu_B}{r^2}\left(\sqrt{3} + \cot\beta\right)^2$$

$$G_{33} = \frac{\mu_{H_3}}{d^2\sin^2\beta} + \mu_{O_6}\left\{\frac{r-d\cos\beta}{rd\sin\beta} - \frac{1}{r\sqrt{3}}\right\}^2 + \mu_{O_5}\frac{4}{3r^2} +$$

$$\frac{\mu_B}{r^2}\left(\sqrt{3} + \cot\beta\right)^2$$

$$G_{12} = \mu_{O_4}\left\{\frac{r-d\cos\beta}{rd\sin\beta} - \frac{1}{r\sqrt{3}}\right\}\left\{\frac{-2}{r\sqrt{3}}\right\} + \frac{\mu_B}{r^2}\left(\sqrt{3} + \cot\beta\right)^2 = G_{21}$$

$$G_{13} = \mu_{O_6}\left\{\frac{r-d\cos\beta}{rd\sin\beta} - \frac{1}{r\sqrt{3}}\right\}\left\{\frac{-2}{r\sqrt{3}}\right\} + \frac{\mu_B}{r^2}\left(\sqrt{3} + \cot\beta\right)^2 = G_{31}$$

$$G_{23} = \mu_{O_5} \left\{ \frac{r - d\cos\beta}{rd\sin\beta} - \frac{1}{r\surd 3} \right\} \left\{ \frac{-2}{r\surd 3} \right\} + \frac{\mu_B}{r^2} (\surd 3 + \cot\beta)^2 = G_{32}$$

where μ is the reciprocal mass and the labels are as in Figure 2.

In order that the force constants for both the C_{3h} and C_s species are in the same units, these $\underset{\sim}{G}$ matrix elements need to be multiplied by rd. These are shown below.

$$G_{11} = A\mu_{H_1} + B\mu_{O_4} + C\mu_B + D\mu_{O_6}$$

$$G_{22} = A\mu_{H_2} + B\mu_{O_5} + C\mu_B + D\mu_{O_4}$$

$$G_{33} = A\mu_{H_3} + B\mu_{O_6} + C\mu_B + D\mu_{O_5}$$

$$G_{12} = G_{21} = C\mu_B + E\mu_{O_4}$$

$$G_{13} = G_{31} = C\mu_B + E\mu_{O_6}$$

$$G_{23} = G_{32} = C\mu_B + E\mu_{O_5}$$

where $A = \left(\frac{r}{d}\right) \operatorname{cosec}^2\beta$

$$B = \left(\frac{r}{d}\right) \operatorname{cosec}^2\beta - 2\operatorname{cosec}\beta \left(\cot\beta + \frac{1}{\surd 3}\right) +$$

$$\frac{d}{r} (\cot\beta + 1/\surd 3)^2$$

$$C = \left(\frac{d}{r}\right) (\surd 3 + \cot\beta)^2$$

$$D = \frac{4}{3} \frac{d}{r}$$

$$E = \frac{2}{\surd 3} \left[(\cot\beta + 1/\surd 3) \left(\frac{d}{r}\right) - \operatorname{cosec}\beta \right]$$

The $\underline{F}$ matrix for the C_{3h} species is given by Cyvin(1) as

$$\underline{F} = \begin{bmatrix} F_\tau+2F_{\tau\tau} & 0 & 0 \\ 0 & F_\tau - F_{\tau\tau} & 0 \\ 0 & 0 & F_\tau - F_{\tau\tau} \end{bmatrix}$$

whilst that for the C_s species is simply

$$\underline{F} = \begin{bmatrix} F_\tau & F_{\tau\tau} & F_{\tau\tau} \\ F_{\tau\tau} & F_\tau & F_{\tau\tau} \\ F_{\tau\tau} & F_{\tau\tau} & F_\tau \end{bmatrix}$$

Reference

1. Cyvin S.J., Mooney R.W., Brunvoll J. and Kristiansen L.A.
Acta Chem. Scand., 19, 1031, 1965.

APPENDIX D

METHOD OF SOLVING CUBIC SECULAR DETERMINANTS

1. INTRODUCTION

From the previous appendix we can see that the secular determinant for the ir active torsion mode is a one line equation for the C_{3h} species whereas it is cubic for the isotopically enriched C_s species. Therefore from the H_3BO_3 and D_3BO_3 frequencies a value of $(F_\tau + 2F_{\tau\tau})$ can be obtained but information as to the magnitude of F_τ or $F_{\tau\tau}$ can only be obtained by solving the cubic determinant of the isotopically mixed species.

Although it is possible to solve cubic equations analytically a different approach was adopted in the study of the vibrational modes of boric acid. This was principally because of the problem of defining the torsion mode and the isotopic data satisfactorily in the SOTONVIBP program. The method used swept through the frequency range desired and located the roots of the cubic determinant for inputted values of the force constants, bond lengths, angles, masses etc.

The program 'TORSION' works by first calculating $(F_\tau + 2F_{\tau\tau})$ for the C_{3h} A" mode. If we use the assumption that this is uncoupled from the other A" mode (BO_3 out of plane bend) then this calculation is expressed as a one line equation thus:

$$G_{A''}\,(F_\tau + 2F_{\tau\tau}) = \lambda \qquad\qquad \lambda = (\nu/1302.83)^2$$

In order to get the values of $F_{\tau\tau}$ and F_τ from the isotopically mixed species the value of $F_{\tau\tau}$ was varied in a loop. Within this loop the masses of the isotopomers were read in and the G matrix values calculated. In order to obtain the roots of $|FG-E\lambda|$ the value of λ was varied in a loop and its value recorded when the determinant equalled zero. Having found all the roots for a particular isotopomer their intensities were calculated as described in Chapter 6 and the set of masses for the next isotopomer were then read in and the sequence repeated. Once all the isotopomers had been considered the value of $F_{\tau\tau}$ was incremented and the process repeated.

Although this can be a lengthy procedure it does enable one to see where the solution lies if it is not exact.

This procedure was also used for the O-H stretches in boric acid using $(F_d - F_{dd})$ for the E' O-H stretch in the C_{3h} case. The calculated frequencies were identical to those produced by SOTONVIBP using the same force constants.

The remainder of this appendix consists of a flow diagram for the program 'TORSION', together with its listing in BBC BASIC and a representative section of the output in the region of the solution.

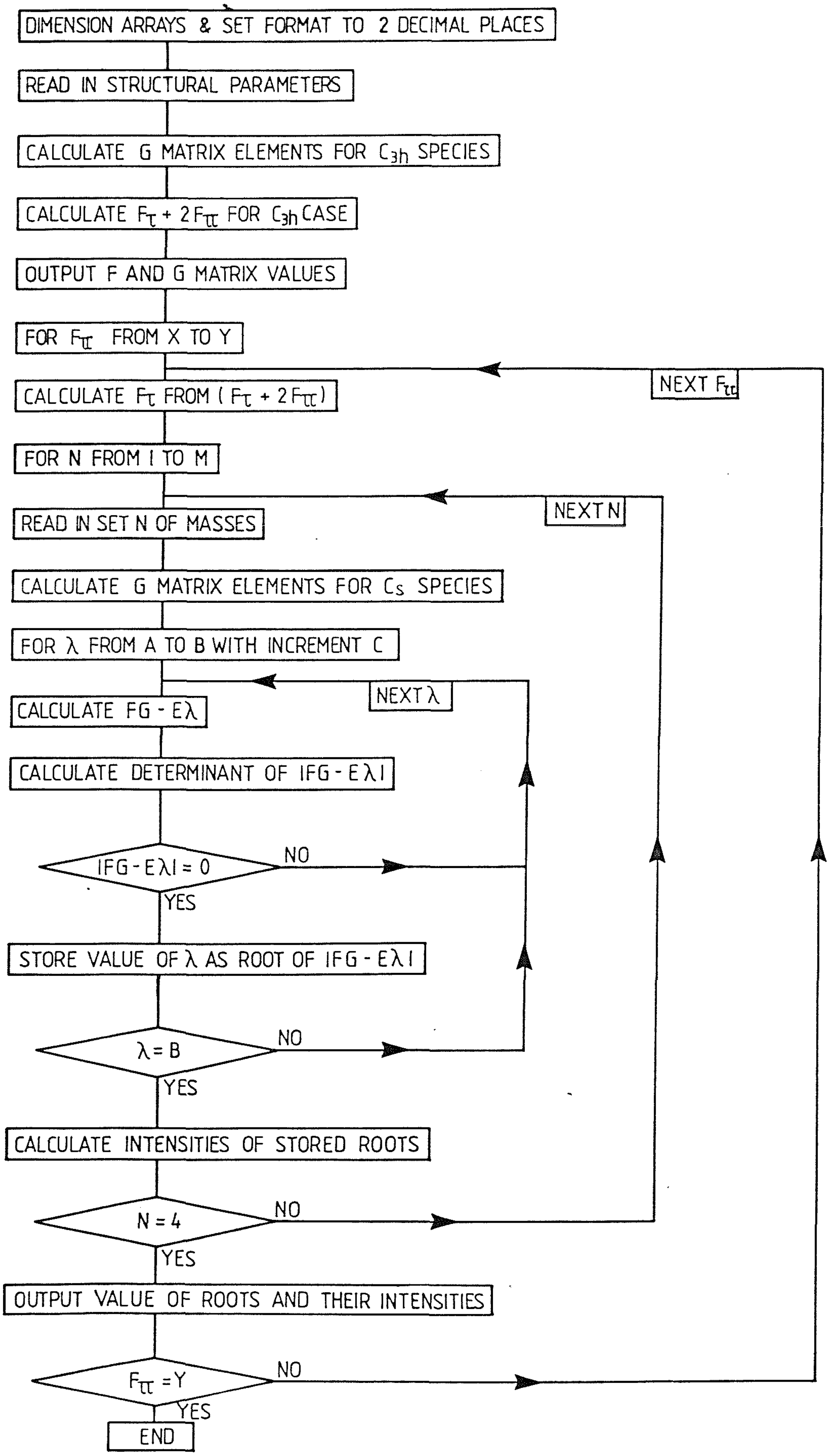

FIG. 1 FLOW CHART FOR PROGRAM `TORSION´

```
 10  REM Program to Calculate Frequencies and Intensities of the Torsion Mode of
 20  REM Boric Acid Using Wilson's FG Analysis.
 30  REM Written by NA Young. January 1987
 40 REM
 50 REM Setting up Monitor Colour, No of Decimal Places , Enabling Printer
 60 REM
 70  VDU 19,0,4,0,0,0
 80  VDU 19,1,6,0,0,0
 90  CLS
100  @%=&20510
110  VDU2
120  VDU15
130 REM
140 REM Dimensioning Arrays and Inputting Structural Data etc.
150 REM
160  PRINT" "
170  DIM G(3,3),F(3,3),FG(3,3),FFG(3,3),NU(4,3),LA(4,3),I(4,3)
180  BETA=RAD(131.0):ALPHA=RAD(120.):A=0.95:B=1.362:C=1.362
190  MUO=1/15.99491:MUB=1/11.00931:MUH=1/1.007825:MUD=1/2.01410
200 REM
210 REM Defining the C3h G matrix elements
220 REM
230  AB=(B-(A*COS(BETA)))/(A*B*SIN(BETA))
240  BC=1/(B*TAN(ALPHA))
250  CD=-1/(C*SIN(ALPHA))
260  DE=(B-(C*COS(ALPHA)))/(B*C*SIN(ALPHA))
270  EF=1/(B*TAN(BETA))
280  GH=((1/A^2)-(2*(COS(BETA))/(A*B))+(1/B^2))*(1/((SIN(BETA))^2))
290  HI=1/(A^2*(SIN(BETA)^2))
300  GSYM=(((AB+BC+CD)^2)*MUO)+(((DE+EF)^2)*3*MUB)
310  GSYMD=(GSYM+(MUD*HI))*(A*B)
320  GSYM=(GSYM+(MUH*HI))*(A*B)
330 REM
340 REM Calculating and Displaying Ft+2Ftt, G matrix elements for C3h species
350 REM
360  LA=(513.8/1302.83)^2
370 F=(LA/GSYM)
380  PRINT" PROGRAM TO CALCULATE ROOTS OF CUBIC FG EQUATIONS BY VARYING THE "
390  PRINT"            TORSIONAL FORCE CONSTANTS FT and FTT "
400  PRINT"                WRITTEN by N.A. Young Jan 87"
410  PRINT
420  PRINT
430  PRINT"    O-H BOND LENGTH  ";"   B-O BOND LENGTH  ";"     B-O-H ANGLE  ";"      O-B-O ANGLE"
440  PRINT"       ";A;"            ";B;"             ";BETA*180/PI;"          ";ALPHA*180/PI
450  PRINT
460  PRINT"  ";"G(A'') H3BO3 ";"    G(A'') D3BO3  ";"     G(E'') H3BO3"; "    G(E'') D3BO3";"       FT+2FTT"
470  PRINT "    ";GSYM;"         ";GSYMD;"            ";(MUH*HI)+(MUO*GH);"        ";(MUD*HI)+(MUO*GH);"        ";F
480  DT=0
```

```
490 REM
500 REM Interaction Force Constant Ftt Increment Loop
510 REM
520  PRINT"________________________________________"
530   FOR FTT=-0.005 TO -0.004  STEP 0.0001
540    DT=1
550   REM
560   REM Calculating values for Ft and Ftt
570   REM
580    FT=F-(2*FTT)
590    PRINT
600    PRINT
610    PRINT"    FT";"               FTT       "
620    PRINT"  ";FT;"       ";FTT
630   REM
640   REM Read in sets of masses
650   REM
660    FOR N=1 TO 4
670      DT=1
680      M=1
690      READ N,H1,H2,H3
700      MUH1=1/H1:MUH2=1/H2:MUH3=1/H3
710     REM
720     REM Calculate G and F matrix values for the Cs species
730     REM
740      G(1,1)=(((AB+BC)^2)*MUO)+((CD^2)*MUO)+(((DE+EF)^2)*MUB)
750      G(2,2)=G(1,1):G(3,3)=G(1,1)
760      G(1,1)=(G(1,1)+(MUH1/(A^2*(SIN(BETA)^2))))*(A*B)
770      G(2,2)=(G(2,2)+(MUH2/(A^2*(SIN(BETA)^2))))*(A*B)
780      G(3,3)=(G(3,3)+(MUH3/(A^2*(SIN(BETA)^2))))*(A*B)
790      G(1,2)=((((AB+BC)*CD)*MUO)+(((DE+EF)^2)*MUB))*(A*B)
800      G(1,3)=G(1,2):G(2,3)=G(1,3)
810      G(2,1)=G(1,2):G(3,2)=G(2,3):G(3,1)=G(1,3)
820      F(1,1)=FT:F(2,2)=F(1,1):F(3,3)=F(1,1)
830      F(1,2)=FTT:F(1,3)=FTT:F(2,1)=FTT:F(2,3)=FTT:F(3,1)=FTT:F(3,2)=FTT
840     REM
850     REM Set Matrix FG equal to zero
860     REM
870      FOR P=1 TO 3
880        FOR Q=1 TO 3
890          FG(P,Q)=0
900        NEXT Q
910      NEXT P
920     REM
930     REM Calculate FxG
940     REM
950      REM MATRIX MULT
960      FOR P=1 TO 3
```

```
 970    FOR Q=1 TO 3
 980      FOR R=1 TO 3
 990        FG(P,Q)=FG(P,Q)+F(P,R)*G(R,Q)
1000      NEXT R
1010    NEXT Q
1020  NEXT P
1030 REM
1040 REM Calculate FG-E.lambda
1050 REM
1060  FOR NU=320 TO 600 STEP 0.1
1070    LAMBDA=(NU/1302.83)^2
1080    FFG(1,1)=FG(1,1)-LAMBDA
1090    FFG(2,2)=FG(2,2)-LAMBDA
1100    FFG(3,3)=FG(3,3)-LAMBDA
1110   REM
1120   REM Calculate Determinant of (FG-El)
1130   REM
1140   DET=(FFG(1,1)*FFG(2,2)*FFG(3,3))-(FFG(1,1)*FG(3,2)*FG(2,3))
       +(FG(2,1)*FG(3,2)*FG(1,3))-(FG(2,1)*FG(1,2)*FFG(3,3))
       +(FG(3,1)*FG(1,2)*FG(2,3))-(FG(3,1)*FFG(2,2)*FG(1,3))
1150    DET=DET*5E6
1160   REM
1170   REM If Determinant equals zero then store root else next lambda
1180   REM
1190    IF DT*DET <0.0 THEN 1200 ELSE 1220
1200    NU(N,M)=NU:LA(N,M)=(NU(N,M)/1302.83)^2
1210    M=M+1
1220    DT=DET
1230   REM
1240   REM Next frequency value
1250   REM
1260  NEXT NU
1270  M=1
1280 REM
1290 REM Calculate the Intensities for the stored roots
1300 REM
1310  IF N=1 THEN 1320 ELSE 1330
1320  I(N,1)=3:GOTO 1420
1330  IF N=4 THEN 1340 ELSE 1350
1340  I(N,1)=(3*GSYMD/GSYM): GOTO 1420
1350  ABC=3/LA
1360  BCD=(G(1,1)+G(2,2)+G(3,3)+(6*G(1,2)))/GSYM
1370  I(N,N)=LA(N,N)*((ABC*LA(N,1))-BCD)/(LA(N,1)-LA(N,N))
1380  I(N,1)=BCD-I(N,N)
1390 REM
1400 REM Next set of masses
1410 REM
1420 NEXT N
```

```
1430  RESTORE
1440 REM
1450 REM Output Roots and Calculated Intensities for various isotopic enrichements
1460 REM
1470  PRINT
1480  PRINT" ROOTS FOR FT =";FT;" AND FTT= ";FTT;" ARE"
1490  FOR Y=1 TO 4
1500    FOR Z=1 TO 3
1510      IF NU(Y,Z)=0.0 THEN PRINT"  ";
1520      PRINT "       ";NU(Y,Z);
1530    NEXT Z
1540    IF Y=1 THEN 1580 ELSE 1550
1550    IF Y=2 THEN 1590 ELSE 1560
1560    IF Y=3 THEN 1600 ELSE 1570
1570    IF Y=4 THEN 1610 ELSE 1620
1580    PRINT"       H3BO3":GOTO 1630
1590    PRINT"       H2DBO3":GOTO 1630
1600    PRINT"       HD2BO3":GOTO 1630
1610    PRINT"       D3BO3":GOTO 1630
1620    PRINT" SOMETHING IS WRONG HERE !!!!":GOTO END
1630  NEXT Y
1640  PRINT
1650  PRINT" INTENSITIES OF THESE ROOTS "
1660  FOR PQR = 0.0 TO 1.05 STEP 0.1
1670    PRINT" AT DEUTERIUM  ENRICHMENT OF  ";PQR*100;"%"
1680    PRINT
1690    FOR Y=1 TO 4
1700      FOR Z=1 TO 3
1710        IF Y=1 THEN 1750
1720        IF Y=2 THEN 1760
1730        IF Y=3 THEN 1770
1740        IF Y=4 THEN 1780
1750        PRINT "          ";I(Y,Z)*((1-PQR)^3);:GOTO 1790
1760        PRINT "          ";I(Y,Z)*3*((1-PQR)^2)*PQR;:GOTO 1790
1770        PRINT "          ";I(Y,Z)*3*(1-PQR)*(PQR^2);:GOTO 1790
1780        PRINT "          ";I(Y,Z)*(PQR^3);:GOTO 1790
1790      NEXT Z
1800      IF Y=1 THEN 1840 ELSE 1810
1810      IF Y=2 THEN 1850 ELSE 1820
1820      IF Y=3 THEN 1860 ELSE 1830
1830      IF Y=4 THEN 1870 ELSE 1880
1840      PRINT"       H3BO3":GOTO 1890
1850      PRINT"       H2DBO3":GOTO 1890
1860      PRINT"       HD2BO3":GOTO 1890
1870      PRINT"       D3BO3":GOTO 1890
1880      PRINT" SOMETHING IS WRONG HERE !!!!":GOTO END
1890      GOTO 1900
1900    NEXT Y
```

```
1910    NEXT POR
1920    PRINT
1930    PRINT"  THE VALUES OF (FT-FTT)*G(E'') FOR "
1940    PRINT"     H3BO3       and        D3BO3   ARE "
1950    PRINT"  ";SQR((FT-FTT)*(((MUH*HI)+(MUO*GH))*(A*B)))*1302.83;"cm-1";"
                ";SQR((FT-FTT)*(((MUD*HI)+(MUO*GH))*(A*B)))*1302.83;"cm-1";
1960    PRINT
1970    PRINT"________________________________________"
1980   REM
1990   REM Next value of Ftt
2000   REM
2010  NEXT FTT
2020  PRINT
2030 REM
2040 REM Masses Data Sets
2050 REM
2060  DATA 1,1.007825,1.007825,1.007825
2070  DATA 2,1.007825,1.007825,2.01410
2080  DATA 3,1.007825,2.01410,2.01410
2090  DATA 4,2.01410,2.01410,2.01410
2100  VDU3
2110 REM
2120 REM Disable Printer
2130 REM
2140  VDU14
2150  END
```

```
 PROGRAM TO CALCULATE ROOTS OF CUBIC FG EQUATIONS BY VARYING THE
         TORSIONAL FORCE CONSTANTS FT and FTT
             WRITTEN by N.A. Young Jan 87


    O-H BOND LENGTH     B-O BOND LENGTH       B-O-H ANGLE        O-B-O ANGLE
       0.95000             1.36200          131.00000          120.00000

  G(A'') H3BO3     G(A'') D3BO3       G(E'') H3BO3    G(E'') D3BO3      FT+2FTT
    2.68588          1.43808            2.22233         1.25796         0.05791
_______________________________________


     FT               FTT
  0.06491        -0.00350

 ROOTS FOR FT =0.06491 AND FTT= -0.00350 ARE
        513.80004         0.00000         0.00000        H3BO3
        408.70002       541.70002       577.89998        H2DBO3
        390.60002       434.80003       561.50000        HD2BO3
        376.00001         0.00000         0.00000        D3BO3

 INTENSITIES OF THESE ROOTS
 AT DEUTERIUM  ENRICHMENT OF  0.00000%

          3.00000         0.00000         0.00000        H3BO3
          0.00000         0.00000         0.00000        H2DBO3
          0.00000         0.00000         0.00000        HD2BO3
          0.00000         0.00000         0.00000        D3BO3
 AT DEUTERIUM  ENRICHMENT OF  10.00000%

          2.18700         0.00000         0.00000        H3BO3
          0.25664         0.35946         0.00000        H2DBO3
          0.03828         0.00000         0.01763        HD2BO3
          0.00161         0.00000         0.00000        D3BO3
 AT DEUTERIUM  ENRICHMENT OF  20.00000%

          1.53600         0.00000         0.00000        H3BO3
          0.40556         0.56804         0.00000        H2DBO3
          0.13610         0.00000         0.06270        HD2BO3
          0.01285         0.00000         0.00000        D3BO3
 AT DEUTERIUM  ENRICHMENT OF  30.00000%

          1.02900         0.00000         0.00000        H3BO3
          0.46576         0.65236         0.00000        H2DBO3
          0.26796         0.00000         0.12343        HD2BO3
          0.04337         0.00000         0.00000        D3BO3
 AT DEUTERIUM  ENRICHMENT OF  40.00000%

          0.64800         0.00000         0.00000        H3BO3
          0.45625         0.63905         0.00000        H2DBO3
          0.40831         0.00000         0.18809        HD2BO3
          0.10280         0.00000         0.00000        D3BO3
 AT DEUTERIUM  ENRICHMENT OF  50.00000%

          0.37500         0.00000         0.00000        H3BO3
          0.39605         0.55473         0.00000        H2DBO3
```

```
          0.53166          0.00000          0.24491          HD2B03
          0.20078          0.00000          0.00000          D3B03
 AT DEUTERIUM  ENRICHMENT OF  60.00000%

          0.19200          0.00000          0.00000          H3B03
          0.30417          0.42603          0.00000          H2DB03
          0.61247          0.00000          0.28213          HD2B03
          0.34695          0.00000          0.00000          D3B03
 AT DEUTERIUM  ENRICHMENT OF  70.00000%

          0.08100          0.00000          0.00000          H3B03
          0.19961          0.27958          0.00000          H2DB03
          0.62523          0.00000          0.28801          HD2B03
          0.55095          0.00000          0.00000          D3B03
 AT DEUTERIUM  ENRICHMENT OF  80.00000%

          0.02400          0.00000          0.00000          H3B03
          0.10139          0.14201          0.00000          H2DB03
          0.54442          0.00000          0.25079          HD2B03
          0.82241          0.00000          0.00000          D3B03
 AT DEUTERIUM  ENRICHMENT OF  90.00000%

          0.00300          0.00000          0.00000          H3B03
          0.02852          0.03994          0.00000          H2DB03
          0.34452          0.00000          0.15870          HD2B03
          1.17097          0.00000          0.00000          D3B03
 AT DEUTERIUM  ENRICHMENT OF  100.00000%

          -0.00000          0.00000          0.00000          H3B03
          0.00000          0.00000          0.00000          H2DB03
          -0.00000          0.00000          -0.00000          HD2B03
          1.60627          0.00000          0.00000          D3B03

  THE VALUES OF (FT-FTT)*G(E'') FOR
     H3B03        and         D3B03   ARE
  577.81670cm-1            434.72938cm-1
```